

Impact of alkali salts on the kinetics and microstructural development of cementitious systems

THÈSE N° 6763 (2015)

PRÉSENTÉE LE 11 DÉCEMBRE 2015

À LA FACULTÉ DES SCIENCES ET TECHNIQUES DE L'INGÉNIEUR
LABORATOIRE DES MATÉRIAUX DE CONSTRUCTION
PROGRAMME DOCTORAL EN SCIENCE ET GÉNIE DES MATÉRIAUX

ÉCOLE POLYTECHNIQUE FÉDÉRALE DE LAUSANNE

POUR L'OBTENTION DU GRADE DE DOCTEUR ÈS SCIENCES

PAR

Berta MOTA GASSÓ

acceptée sur proposition du jury:

Prof. V. Michaud, présidente du jury
Prof. K. Scrivener, Dr T. Matschei, directeurs de thèse
Dr R. Barbarulo, rapporteur
Prof. R. Flatt, rapporteur
Prof. P. Bowen, rapporteur



ÉCOLE POLYTECHNIQUE
FÉDÉRALE DE LAUSANNE

Suisse
2015

The veracity of construction materials: concrete, brick and stone,
will remain in all buildings, constructed or to be constructed.

– Le Corbusier

Acknowledgements

Special thanks to Prof. Karen Scrivener, for giving me the opportunity to do this thesis in her laboratory and dive in the universe of cement. I am most grateful for her advices and discussions, which contributed to the quality of this work, and for the opportunity to present my research in several international conferences. Thank you, Karen!

I would like to thank Dr. Thomas Matschei, my co-supervisor in LafargeHolcim, for his enthusiastic support and all the constructive comments throughout these years. It has been great working with him.

This thesis has been financially supported by LafargeHolcim. Thank you for giving me the opportunity to work on the fascinating world of cement and alkalis.

I would like to acknowledge Prof. Robert Flatt, Dr. Rémi Barbarulo and Prof. Paul Bowen to be members of my Jury. I highly appreciate their critical review of the thesis and constructive advices. I am also thankful to Prof. Veronique Michaud, president of this Jury.

Thanks to Dr. Barbara Lothenbach, who has always been there for my alkali questions. I enjoyed the discussions and moments shared with her. Thank you also to Dr. Dimitrii Kulik for his advices on GEMS calculations.

Thanks to Danièle Laub from CIME and Carlos Morais from LTP in EPFL for their help on the preparation and characterization of the samples, and to Helmut Kolb from LafargeHolcim for his help on the production of alite.

A big acknowledgement goes to the undergraduate EPFL students, Léo, Betty and Vincent, for their great work and contribution on this thesis.

Nothing would have been the same without the amazing *crew* at the Laboratory of Construction Materials. How lucky I am for sharing these PhD years with you! I deeply thank you all for the hard-working, friendly and funny moments we spent together. A special thank you to Mo and Julien with whom I shared the office during most of my PhD, I am blessed to have you as my *friends*, and for sharing my everyday life (and trips!) with you for so long. I warmly thank Julien Ston and Alexandre, my current office mates, for all your constant support and laughs during the end of my thesis; Elise and Amélie for your fruitful discussions and good moments inside and outside the laboratory; Maude and Anne-Sandra for your support and the organization of trips, ski seminars and lab-hikes; Pawel for your *jeux de mots*; John for all the *fou rire* we had together and to be (more than once) the surgeon of my computer; Mathieu for being always ready-to-help and for your jokes; Aslam for having so much positive energy (and transmit it); Arnaud for all the good discussions and your help with ^1H NMR; Ashley, for your everyday joy and the music we shared; Lily for your kindness and because you deserve the “best guide in Beijing” prize; François for your good spirit attitude. I would like to thank all the Post-doc: Ruben, Hadi, Cyrille (thank you for the corrections on the thesis), Aurélie, Xuerun, Hamed and

Adrien. I also thank Lionel for being an excellent teacher on mechanics, et un énorme merci à Tonio et Jean pour m'avoir toujours aidé très efficacement quand j'en ai eu besoin.

A big thank you to Luis, Sandra, Ellina, Frank, Émilie, Marta, Delphine and Elizaveta for all the meetings, conferences, drinks and trips we spent together around the *cement world*.

I would like to thank all my friends who always supported me either being in Switzerland or outside: Merci Maléna and Aurelia, pour tous les repas et pauses café qu'on a partagé pour se raconter les aventures avec la thèse ou simplement pour discuter de *la vie* (Maléna, c'était cool de faire des compétitions entre mes micro-échantillons de ciment et tes méga-échantillons de béton!). Nos soirées vont me manquer!

Thank you Nariye for your attentions during all these years and being with me since the beginning.

Thank you Luis for being my friend. Y tenemos unas barbacoas pendientes!

Thank you Mònica, Anna, Txell and Danae (my friends in Girona) for making me feel like there is no distance between us (just a few km...!) and always being there when I need it.

Thank you TEDxLausanne colleagues for the extraordinary team we build up and all the excitement/stress we shared to organize each *ideas worth spreading* event.

Merci Maude pour être toujours prête à un café, pour tes conseils et tout ton encouragement.

Merci (infini!) Elise, simplement pour tout. Tu as été ma coloc, ma collègue du labo, mais surtout tu es une méga copine; un des meilleurs cadeaux que la Suisse m'a offert. Et on a encore tellement des moments à partager ensemble...!

An enormous thank you goes to my parents, my sister and my brother for all your love and support; for always being there no matter what, for your advices and for being such a good adventures team! *Un enorme gràcies als meus pares, la meva germana i el meu germà pel seu amor i suport; per estar sempre allà passi el que passi, pels vostres consells i per a formar un gran equip d'aventures!*

Last but not least, thank you, Martí! Thank you for all your energy, support, for making life so exciting and... for your curiosity on cement!

Lausanne, 16th November 2015

Berta Mota Gassó

Abstract

Supplementary cementitious materials (SCM) lower the environmental impact of cement and concrete but react more slowly than Portland cement, which therefore limits the levels of substitution possible as reasonable early strengths are necessary. One of the main factors affecting the reaction of the SCMs is the alkalinity of the pore solution. However, alkalis do not only affect SCMs, but also the clinker phases. It is generally accepted that alkalis accelerate the hydration of Portland cement but may have a detrimental impact on strength at later ages.

The aim of this work is to clarify the impact of alkali salts (NaOH and Na₂SO₄) on the kinetics and microstructural development of cementitious systems to better understand their effect on the mechanical properties. The study of many different systems, from models such as alite to more realistic cement-slag systems, allows a general overview of the trends in each parameter. The novelty of this thesis is the study of the relationship between the development of the porosity over time, as well as the evolution of the phase assemblage, and the resulting mechanical strength in the presence of alkalis. Moreover, the use of ¹H NMR brings new insights on the impact of alkalis on the amount of water and density of C-S-H in non-dried samples.

For a same degree of hydration of cement, the addition of Na₂SO₄ leads to the same compressive strength as the alkali-free system while NaOH clearly lowers it. Ettringite is suggested as responsible for the differences. While Na₂SO₄ promotes the precipitation of ettringite, NaOH clearly inhibits it. Therefore, a higher volume of hydrates can better fill the space, the porosity decreases and consequently the strength is increased. Moreover, the addition of sodium gluconate to the cement-slag systems with Na₂SO₄ improves the strength development which seems to be related to the formation of a less dense C-S-H that better fills the space and lowers the porosity.

The presence of Na₂SO₄ or NaOH does not affect the bulk density of C-S-H but major differences are observed in the morphology of C-S-H. Sulfate uptake leads to a divergent needle-like C-S-H while NaOH promotes a C-S-H that tends towards a foil-like morphology. Also, alkalis lead to a lower and more stable Ca/Si in C-S-H. However, the mechanical strength appears to be independent on the morphology and chemical composition of C-S-H.

Alkali salts clearly accelerate the hydration rate at early ages but decrease the degree of hydration at later ages. From the studies on alite, white cement and white cement-slag systems, it has been observed that a slowdown in hydration kinetics could not be explained by changes in the relative humidity, i.e. the water activity. The increased concentration of aluminate ions could explain some of the slowdown but it appears there are other effects.

Key words: alkali, kinetics, microstructure, mechanical properties, C-S-H.

Resumé

Les matériaux cimentaires de substitution (MCS) sont une aide importante dans la diminution de l'impact environnemental du ciment et du béton, mais réagissent plus lentement que le ciment Portland, ce qui limite les taux effectifs de substitution atteignables, une résistance à jeune âge suffisante étant requise. L'un des principaux facteurs affectant la réaction des MCS est l'alcalinité de la solution de pore. Toutefois, les alcalins n'affectent pas seulement les MCS, mais aussi le clinker. Il est généralement admis que les alcalins sont des accélérateurs de l'hydratation mais peuvent réduire la résistance à long terme.

L'objectif de ce travail est de clarifier l'impact des sels alcalins sur la cinétique et le développement de la microstructure des systèmes cimentaires, afin d'expliquer leur impact sur les propriétés mécaniques. L'étude de nombreux systèmes, partant de phases pures comme l'alite jusqu'à des mélanges cimentaires avec laitiers, permet d'avoir une vue globale des effets sur les différents paramètres. La nouveauté de cette thèse est la meilleure compréhension du rôle de la porosité ainsi que de la distribution des phases sur la résistance mécanique finale en présence des alcalins. Les résultats de la NMR du proton sur des échantillons en cours d'hydratation apporte de nouvelles connaissances quant à l'effet des alcalins sur le C-S-H en termes de quantité d'eau et de densité.

À degré d'hydratation identique, l'addition de Na_2SO_4 conduit à la même résistance à la compression que dans les systèmes sans alcalins, tandis que le NaOH la réduit nettement. Il est suggéré que l'ettringite est responsable de cette différence. Le Na_2SO_4 favorise la précipitation de l'ettringite, conduisant à un plus grand volume d'hydrates formé, mais par contre en présence de NaOH la précipitation d'ettringite est inhibée et en conséquence le volume rempli par les hydrates est inférieur. Ainsi, un volume plus important d'hydrates promeut une diminution de la porosité et, en conséquence, une résistance mécanique plus élevée. En outre, l'addition de gluconate de sodium au système ciment-laitier avec du Na_2SO_4 accélère le développement de la résistance à la suite de la formation d'un type de C-S-H moins dense qui favorise le remplissage de l'espace ainsi que la réduction de la porosité.

La présence de Na_2SO_4 ou NaOH n'a pas un effet sur la densité du gel C-S-H mais par contre des différences majeures dans la morphologie du C-S-H et de la portlandite sont observées. L'adsorption de sulfates à la surface du C-S-H conduit à la formation de structures de C-S-H en aiguilles divergentes, alors qu'en présence de NaOH le C-S-H forme des feuillets. Toutefois, la résistance mécanique est indépendante de la morphologie du C-S-H.

Les sels alcalins accélèrent le taux d'hydratation à jeune âge, mais diminuent le degré d'hydratation pour des âges plus tardifs. A partir des études sur l'alite, le ciment blanc et systèmes avec laitier, il a été observé que un ralentissement de la cinétique d'hydratation ne pourrait être expliqué par des changements liés à l'humidité relative, autrement dit l'activité de l'eau. La concentration croissante d'ions aluminate pourrait expliquer une partie du ralentissement, mais il semble qu'il y a d'autres effets.

Mots-clefs: alcalins, cinétique, microstructure, propriétés mécaniques, C-S-H.

Resum

Els materials cementicis suplementaris redueixen l'impacte ambiental del ciment i el formigó però reaccionen més lentament que el ciment Portland, limitant per tant els nivells de substitució possibles ja que es necessita una resistència inicial raonable. Un dels principals factors que determina la reacció dels materials cementicis suplementaris és l'alcalinitat de la solució porosa. No obstant, els àlcalis no sols afecten aquests materials alternatius, sinó també a les fases del clínquer. En general s'accepta que els àlcalis acceleren la hidratació del ciment Portland però que poden impactar negativament la resistència en etapes posteriors.

L'objectiu d'aquest treball és aclarir l'impacte de sals alcalines (NaOH i Na_2SO_4) a la cinètica i el desenvolupament microestructural dels sistemes cementicis per entendre millor el seu efecte sobre les propietats mecàniques. L'estudi de diversos sistemes, des de models com l'alita fins a sistemes més realistes com ciment-escòries, permet obtenir una visió general de les tendències de cada paràmetre. La novetat d'aquesta tesi és l'estudi de la relació entre el desenvolupament de la porositat al llarg del temps, així com l'evolució de la distribució de fases, i la resistència mecànica resultant en presència d'àlcalis. D'altra banda, l'ús de la tècnica ^1H NMR aporta nous coneixements sobre l'impacte dels àlcalis sobre la quantitat d'aigua i la densitat del C-S-H en mostres on no s'ha parat la hidratació.

A mateix grau d'hidratació del ciment, s'observa que l'addició de Na_2SO_4 obté el mateix nivell de resistència a la compressió que el sistema sense àlcalis, mentre que l'addició de NaOH la redueix clarament. L'etringita sembla ser el factor responsable d'aquestes diferències. Mentre el Na_2SO_4 promou la precipitació d'etringita, el NaOH la inhibeix clarament. En conseqüència, un major volum d'hidrats poden omplir millor l'espai, la porositat disminueix i per tant la resistència augmenta. D'altra banda, l'addició de gluconat de sodi als sistemes de ciment-escòries amb Na_2SO_4 millora el desenvolupament de la resistència, fet que sembla estar relacionat amb la formació d'un C-S-H menys dens, el qual omple millor l'espai, reduint així la porositat.

La presència de Na_2SO_4 o NaOH no afecta la densitat del gel C-S-H però s'observen diferències importants en la morfologia del C-S-H. L'adsorció de sulfats dona lloc a un C-S-H divergent, en forma d'agulles, mentre que el NaOH promou un C-S-H que tendeix a una morfologia més aplanada, sense agulles i més aviat amb làmines. Així mateix, els àlcalis promouen un C-S-H amb un Ca/Si més baix i estable. No obstant, la resistència mecànica sembla ser independent de la morfologia i la composició química del C-S-H.

Les sals alcalines acceleren clarament la velocitat d'hidratació en etapes inicials però disminueixen el grau d'hidratació en etapes posteriors. Mitjançant l'estudi de sistemes d'alita, ciment blanc i sistemes amb escòries, s'ha observat que una desacceleració en la cinètica d'hidratació no podria explicar-se per canvis en la humitat relativa del sistema, és a dir, en l'activitat d'aigua. L'augment de la concentració d'aluminats podria explicar part d'aquesta desacceleració, però sembla que hi ha altres efectes.

Paraules clau: àlcalis, cinètica, microestructura, propietats mecàniques, C-S-H.

Resumen

Los materiales cementicios suplementarios reducen el impacto ambiental del cemento y el hormigón pero reaccionan más lentamente que el cemento Portland, limitando así los niveles de sustitución posibles ya que es necesaria una resistencia inicial razonable. Uno de los principales factores que afecta la reacción de los materiales cementicios suplementarios es la alcalinidad de la solución porosa. Sin embargo, los álcalis no afectan solamente estos materiales alternativos, sino también a las fases del clínker. En general es aceptado que los álcalis aceleran la hidratación del cemento Portland pero también pueden tener un impacto perjudicial sobre la resistencia en etapas posteriores.

El objetivo de este trabajo es clarificar el impacto de sales alcalinas (NaOH i Na_2SO_4) sobre la cinética y el desarrollo microestructural de los sistemas cementicios para entender mejor su efecto sobre las propiedades mecánicas. El estudio de sistemas variados, desde modelos como la alita hasta sistemas más realistas como cemento-escoria, permite obtener una visión general de las tendencias de cada parámetro. La novedad de esta tesis es el estudio de la relación entre el desarrollo de la porosidad a través del tiempo, así como la evolución de la distribución de fases, y la resistencia mecánica resultante en presencia de álcalis. Además, el uso de la técnica ^1H NMR aporta nuevos conocimientos en relación al impacto de los álcalis sobre la cantidad de agua y a densidad del C-S-H en muestras donde no se ha parado la hidratación.

Para el mismo grado de hidratación del cemento, la adición de Na_2SO_4 lleva al mismo nivel de resistencia a la compresión que el sistema sin álcalis, mientras que la adición de NaOH la reduce claramente. La etringita parece ser el factor responsable de estas diferencias. Mientras el Na_2SO_4 promueve la precipitación de etringita, el NaOH la inhibe claramente. En consecuencia, un mayor volumen de hidratos permiten rellenar mejor el espacio, la porosidad disminuye y por tanto la resistencia aumenta. Por otro lado, la adición de gluconato de sodio a los sistemas de cemento-escoria con Na_2SO_4 mejora el desarrollo de la resistencia, hecho que parece estar relacionado con la formación de un C-S-H menos denso, que llena mejor el espacio y reduce la porosidad.

La presencia de Na_2SO_4 o NaOH no afecta a la densidad de gel C-S-H pero se observan diferencias importantes en la morfología del C-S-H. La adsorción de sulfato da lugar a un C-S-H divergente, en forma de agujas, mientras que el NaOH promueve un C-S-H que tiende a una morfología más aplanada, sin agujas y más bien laminado. Asimismo, los álcalis promueven un C-S-H con un Ca/Si menor y más estable. No obstante, la resistencia mecánica parece ser independiente de la morfología y la composición química del C-S-H.

Las sales alcalinas aceleran claramente la velocidad de hidratación en etapas iniciales pero disminuyen el grado de hidratación en etapas posteriores. Mediante el estudio de sistemas de alita, cemento blanco y sistemas con escorias, se ha observado que una desaceleración en la cinética de hidratación no podría explicarse por cambios en la humedad relativa, es decir, en la actividad de agua. El aumento de la concentración de los iones aluminato podría explicar parte de esta deceleración, pero parece que hay otros efectos.

Palabras clave: álcalis, cinética, microestructura, propiedades mecánicas, C-S-H.

Table of Contents

Acknowledgements	v
Abstract.....	vii
Resumé	ix
Resum	xi
Resumen	xiii
Table of Contents	xv
List of Figures	xix
List of Tables.....	xxiii
Glossary	xxv
CHAPTER 1. Introduction	1
1. Introduction	1
1.1. Use of SCMs and alkali.....	1
2. Motivation and objectives of the thesis	2
3. Chapter overview	2
CHAPTER 2. Literature review	5
1. Cement hydration.....	5
1.1. Kinetics of hydration	5
1.2. C-S-H	7
1.3. Microstructural development and hardening of cement pastes.....	10
1.4. Outlook.....	12
2. Influence of alkalis on cement hydration	12
2.1. Acceleration effect	12
2.2. Strength development.....	13
2.3. Porosity.....	15
2.4. Morphology of hydrates.....	16
2.5. Chemical composition and structure of C-S-H	17
3. The impact of sulfate in cement hydration	19
4. Sodium gluconate	20
5. Summary	21

CHAPTER 3. Materials and methods	23
1. Materials	23
1.1. Alite	23
1.2. White Portland cement.....	25
1.3. Slag	27
2. Experimental methods	28
2.1. Preparation of alkali solutions	28
2.2. Preparation of pastes	28
2.3. Preparation of mortars	29
2.4. Methods to monitor the kinetics of reaction	30
2.5. Methods to assess the microstructural development	31
 CHAPTER 4. The impact of NaOH, Na₂SO₄ and gypsum on alite hydration	 39
1. Introduction.....	39
2. Systems studied	39
3. Results	40
3.1. Heat release and degree of hydration	40
3.2. Morphology of hydrates	44
3.3. Chemical composition of hydrates	50
3.4. Mechanical strength of alite mortars	53
4. Summary.....	57
 CHAPTER 5. The impact of NaOH and Na₂SO₄ on white cement hydration	 59
1. Introduction.....	59
2. Systems studied	60
3. Compressive and flexural strength	60
4. Kinetics.....	61
5. Porosity and relation to mechanical strength	65
6. Hydrates precipitated	67
6.1. Type of hydrates precipitated	67
6.2. Characteristics of C-S-H.....	70
7. Summary.....	78
 CHAPTER 6. The impact of NaOH and Na₂SO₄ on white cement-slag systems	 81
1. Introduction.....	81
2. The impact of NaOH and Na ₂ SO ₄ on white cement-slag systems	82
2.1. Systems studied.....	82
2.2. Mechanical strength	82
2.3. Kinetics	84
2.4. Composition of pore solution.....	88
2.5. Phase assemblages.....	90
2.6. Distribution of hydrates in the matrix	93
2.7. Porosity	95

3.	Impact of sodium gluconate on white cement-slag systems with Na ₂ SO ₄	98
3.1.	Reason to study the impact of sodium gluconate	98
3.2.	Systems studied	98
3.3.	Mechanical strength.....	99
3.4.	Kinetics	100
3.5.	Phase assemblages	101
3.6.	Distribution of hydrates and morphology of C-S-H.....	102
3.7.	Chemical composition of C-S-H	105
3.8.	Water distribution in capillary and C-S-H porosity.....	107
3.9.	Discussion on the effect of sodium gluconate	110
4.	Summary	112
CHAPTER 7.	Conclusions and perspectives	115
Appendix A.	Comparison between alite and cement	121
Appendix B.	C-S-H characteristics in white cement-slag systems	123
Appendix C.	Calculations for the analysis of ¹H NMR data.....	127
Bibliography.....		129
Curriculum Vitae		137

List of Figures

Figure 2.1. Typical isothermal calorimetry curves of a) alite and b) Portland cement	6
Figure 2.2. Schematic diagram showing dreierkette chains present in a) 1.4 nm Tobermorite and b) for the C-S-H with Ca/Si ratio 1.5, more representative of hydrated cement pastes.....	7
Figure 2.3. Morphology of C-S-H product in a) a cement paste and b) a C ₃ S paste, both during the nucleation and growth period.....	8
Figure 2.4. SFEG micrographs of C-S-H needles and graphical representation of C-S-H as seen by ¹ H NMR.....	9
Figure 2.5. Evolution of ¹ H NMR signal fractions with time (white cement paste, w/c=0.4)	9
Figure 2.6. Microstructural development of a white cement paste at 7 days of hydration.....	10
Figure 2.7. Measured heat evolution profiles up to 50 hours and DoH of alite hydrating in different alkali hydroxide solutions.....	13
Figure 2.8. Measured heat evolution profiles up to 50 hours and DoH of alite hydrating in different alkali sulfate solutions.....	13
Figure 2.9. A higher content in alkali (Na ₂ O _{eq}) in concrete lowers the compressive strength	14
Figure 2.10. Data collection of the compressive strength values for different clinker systems containing alkali sulfates at early (2 days) and later age (28 days)	14
Figure 2.11. Influence of NaOH and KOH on the porosity of a cement paste.	15
Figure 2.12. Microstructural characteristics, as observed under the SEM, of a) low-alkali cement paste with w/c of 0.4 (7 days) and b) high-alkali paste with w/c of 0.4 (7 days)	15
Figure 2.13. Fracture surface images of C-S-H at the ages of 11 h (top) and 24 h (bottom) for alite samples with a) DI-water and b) 0.5 M NaOH.....	16
Figure 2.14. Morphology of CH at 1 day a) in C ₃ S plain paste and b) with gypsum and 0.1 M KOH	17
Figure 2.15. EDS for alite samples at 30 hours hydrated with different solutions of NaOH or KOH	17
Figure 2.16. Data collection of Na/Si or K/Si for synthetic C-S-H in equilibrium with NaOH or KOH	18
Figure 2.17. a) Relative fraction of signals observed by Renaudin et al [58] but plotted by Lothenbach and Nonat [22] as a function of the Ca/Si ratio of synthetic C-S-H. b) ²³ Na NMR spectra from samples belonging to the C-A-S-H series with Na [58]	18
Figure 2.18. Morphology of CH at 1 day in a) C ₃ S plain paste and b) with 5 wt.% gypsum	20
Figure 2.19. Effect of different dosages of sodium gluconate on early hydration of a cement paste.....	21
Figure 3.1. a) Differential and b) cumulative PSD of alite and gypsum.....	24
Figure 3.2. Calorimetry curve of the two batches of synthesized alite	24
Figure 3.3. a) Alite grain and b) detail of the surface.	25
Figure 3.4. a) Grain of white cement and b) detail of the surface of a white cement grain.	26
Figure 3.5. a) Differential and b) cumulative PSD of alite compared to white cement.....	26
Figure 3.6. a) Differential and b) cumulative PSD of slag compared to white cement	27
Figure 3.7. a) Slag grain and b) detail of the surface.....	28
Figure 3.8. Tests with standard grey cement (on mortars and cement pastes of 10 × 10 × 40 mm)	29
Figure 3.9. Schematic description of the preparation of samples at early ages with SFEG	32
Figure 3.10. Determination of C-S-H composition from atomic ratio scatter plots.....	33
Figure 3.11. Relaxation time of each water population in a white cement paste at 1, 6 and 28 days.	35
Figure 4.1. Composition of the alite-based mixes studied, in wt.%	40
Figure 4.2. Effect of Na-salts and gypsum on the heat evolution rate of alite.....	41
Figure 4.3. Al content in pore solution calculated by GEMS at a) 7% DoH and b) 25 days of hydration..	42

Figure 4.4. Ca and Si content in pore solution calculated by GEMS at a) 7% DoH and b) 25 days	42
Figure 4.5. Effect of Na-salts and gypsum on the DoH of alite up to 25 days.	43
Figure 4.6. Times (dots) when hydration was stopped.....	44
Figure 4.7. 4% DoH, corresponding to the beginning of the N+G period	45
Figure 4.8. C-S-H and portlandite solubility curves	46
Figure 4.9. 10% DoH (minutes after the main peak).....	47
Figure 4.10. 2% DoH for the system with 5wt.% gypsum and NaOH	48
Figure 4.11. Polished sections of alite systems at 72 hours	49
Figure 4.12. Polished section at 28 days for the system with 5 wt.% gypsum.	50
Figure 4.13. Quantification of portlandite as a function of DoH alite.....	50
Figure 4.14. EDS analyses at 7 days of hydration: a) Al/(Ca-S) vs S/(Ca-S) ratio and b) (Si+Al)/(Ca-S) vs Al/(Ca-S) ratio	51
Figure 4.15. EDS analyses at 28 days of hydration: a) Al/(Ca-S) vs S/(Ca-S) ratio and b) (Si+Al)/(Ca-S) vs Al/(Ca-S) ratio	51
Figure 4.16. Hypothetical scheme of the impact of sulfate ions on the orientation of C-S-H subcritical nucleation sites when they nucleate in the surface of alite	52
Figure 4.17. a) Compressive and b) flexural strength for alite mortars as a function of time	53
Figure 4.18. a) Compressive and b) flexural strength for alite mortars as a function of DoH.....	54
Figure 4.19. Total porosity as a function of the pore radius for alite systems at a) 7 and b) 28 days.....	55
Figure 4.20. Total porosity as a function of the compressive strength for alite systems	55
Figure 4.21. Polished sections at 28 days	56
Figure 4.22. Schematic morphologies of C-S-H and other hydrates depending on solution chemistry ..	57
Figure 5.1. Composition of the white cement systems studied	60
Figure 5.2. a) Compressive and b) flexural strength results over time (up to 90 days) for each system of white cement mortars	61
Figure 5.3. Effect of Na ₂ SO ₄ and NaOH on the heat evolution rate of white Portland cement during the first 24 hours.....	61
Figure 5.4. Effect of Na ₂ SO ₄ and NaOH on the cumulative heat release up to 28 days	62
Figure 5.5. Effect of Na ₂ SO ₄ and NaOH on the degree of hydration of cement up to 28 days	62
Figure 5.6. Impact of Na ₂ SO ₄ and NaOH on the reaction of C ₃ S and C ₃ A during the first 24 hours with in-situ XRD-Rietveld.....	63
Figure 5.7. Effect of Na ₂ SO ₄ and NaOH on the consumption of a) C ₃ S and b) C ₃ A up to 28 days	64
Figure 5.8. Effect of Na ₂ SO ₄ and NaOH on a) the relative humidity over time and b) the concentration of Al in the pore solution estimated with GEMS at 28 days.....	65
Figure 5.9. Compressive strength results for white cement mortars as a function of the DoH cement ...	65
Figure 5.10. Total porosity as a function of the pore radius and derivative They correspond to 24 hours, 7 days and 28 days	66
Figure 5.11. a) Relationship between compressive strength and total porosity (measured by MIP) and b) relationship between the total porosity and the DoH of cement	67
Figure 5.12. Estimation of the phase assemblage over time	68
Figure 5.13. Relationship between the porosity measured with MIP and estimated with GEMS	69
Figure 5.14. Effect of gypsum addition on the compressive strength as a function of DoH cement	70
Figure 5.15. Comparison of the phase assemblages (GEMS) over time in the system with NaOH and in the system with NaOH plus gypsum.....	70
Figure 5.16. Images on the left column show the surface of the cement grains at the end of the nucleation and growth period for each system. Images on the right column show SEM-BSE micrographs at 28 days.....	71
Figure 5.17. Impact of Na ₂ SO ₄ and NaOH on a) (Ca-S)/(Si+Al) and b) S/(Ca-S) ratio of C-S-H at 7d.....	72
Figure 5.18. The impact of Na ₂ SO ₄ and NaOH on the Na/(Si+Al) ratio at 28 days.....	73

Figure 5.19. Impact of Na_2SO_4 and NaOH on the evolution of each population of water from the mixing time until 28 days, measured by ^1H NMR	74
Figure 5.20. Solid signal from ^1H NMR compared to that from XRD	75
Figure 5.21. Impact of NaOH and Na_2SO_4 on the relationship between RH and gel/sheet ratio at 28d ..	76
Figure 5.22. Impact of NaOH and Na_2SO_4 on the solid density and gel density of C-S-H at 28 days.....	76
Figure 5.23. Schematic representation of the impact of Na_2SO_4 and NaOH in the chemical structure of C-S-H	77
Figure 5.24. Schematic representation of the impact of Na_2SO_4 and NaOH in the C-S-H	78
Figure 6.1. Composition of the slag mixes studied, in wt.%.	82
Figure 6.2. Evolution of the compressive and flexural strength in the presence of Na_2SO_4 and NaOH for slag 1 and slag 8 systems.....	83
Figure 6.3. Effect of Na_2SO_4 and NaOH on the cumulative heat release up to 28 days for a) slag 1 and b) slag 8 systems.....	84
Figure 6.4. Effect of Na_2SO_4 and NaOH on the degree of hydration of cement up to 28 days for a) slag 1 systems and b) slag 8 systems	85
Figure 6.5. Impact of Na_2SO_4 and NaOH on the DoH C_3S over time for a) slag1 and b) slag 8 systems... ..	85
Figure 6.6. Impact of Na_2SO_4 and NaOH on the DoH C_3A over time for a) slag1 and b) slag 8 systems ..	86
Figure 6.7. Contribution of a) slag 1 and b) slag 8 on the total heat release	87
Figure 6.8. Sulfate concentration in pore solution extracted for a) slag 1 and b) slag 8 systems	89
Figure 6.9. Concentration of aluminate in pore solution extracted for a) slag 1 and b) slag 8 systems....	89
Figure 6.10. Effect of NaOH and Na_2SO_4 on the relative humidity of slag 1 systems over time.	90
Figure 6.11. Comparison between GEMS and mass balance calculations for the slag system with Na_2SO_4 at 28 days.....	91
Figure 6.12. Estimation of the phase assemblage for slag 1 systems at 28 days	92
Figure 6.13. Estimation of the phase assemblage for slag 8 systems at 28 days	92
Figure 6.14. Polished sections of slag 1 systems at 28 days of hydration.....	94
Figure 6.15. $\text{S}/(\text{Ca-S})$ versus $\text{Al}/(\text{Ca-S})$ for the small plates in slag 1 system with NaOH at 28 days.	95
Figure 6.16. Impact of Na_2SO_4 and NaOH on the total porosity of b) slag 1 and d) slag 8 samples at 28 days.....	96
Figure 6.17. Relationship between compressive strength and total porosity (measured by MIP) for slag systems.	96
Figure 6.18. Impact of NaOH and Na_2SO_4 on the critical entry radius of a) slag 1 and b) slag 8 samples at 28 days compared to c) the non-blended systems at 28 days.	97
Figure 6.19. Composition of the slag systems studied, with and without gluconate, in wt.%.	98
Figure 6.20. Evolution of the compressive and flexural strength in the presence and absence of GL for the slag 1 and slag 8 systems	99
Figure 6.21. Effect of sodium gluconate on the heat evolution rate up to 40 hours for slag systems in the presence of Na_2SO_4 with a) slag 1 and b) slag 8.	100
Figure 6.22. Effect of sodium gluconate on the cumulative heat release up to 28 days for slag systems in the presence of Na_2SO_4 with a) slag 1 and b) slag 8.	100
Figure 6.23. Effect of sodium gluconate on the $\text{DoH}_{\text{cement}}$ up to 28 days for for slag systems in the presence of Na_2SO_4 with a) slag 1 and b) slag 8.	101
Figure 6.24. XRD-Rietveld quantification of portlandite (CH), ettringite (Ett) and hydrotalcite (Ht) for slag 1 and slag 8 systems with Na_2SO_4 at 28 days, in the absence and presence of sodium gluconate ..	102
Figure 6.25. Polished sections of slag 1 and slag 8 systems with Na_2SO_4 at 24 hours in the absence and presence of sodium gluconate	103
Figure 6.26. Polished sections of slag 1 and slag 8 systems with Na_2SO_4 at 28 days in the absence and presence of sodium gluconate at 28 days.....	104

Figure 6.27. C-S-H morphology at the end of acceleration period in systems with slag 1 and Na ₂ SO ₄ , without and with sodium gluconate.	105
Figure 6.28. Impact of sodium gluconate on the (Ca-S)/Si ratio (left column) and the uptake of sulfate (right column) in C-S-H in slag 1 systems at 24 hours, 7 days and 28 days	106
Figure 6.29. Impact of sodium gluconate on the uptake of sodium in C-S-H at 7 days in slag 1 systems with Na ₂ SO ₄	107
Figure 6.30. Impact of sodium gluconate on the amount of mass loss in slag systems with Na ₂ SO ₄ at 28 days between 30 and 600°C.....	108
Figure 6.31. Impact of sodium gluconate on the distribution of the water among the different populations of water at 28 days for the systems with slag 1.....	108
Figure 6.32. Identification of anhydrous phases taken as reference grey levels (belite and slag) and each type of C-S-H to analyse	109
Figure 6.33. Impact of sodium gluconate on the density of inner and outer C-S-H (qualitative comparison) at 28 days for the systems a) with slag 1 and b) with slag 8.	110
Figure 6.34. Schematic C-S-H representation a) without and b) with sodium gluconate	110
Figure 6.35. Impact of sodium gluconate on the compressive strength of slag systems as a function of the total porosity from MIP.....	111
Figure 6.36. Impact of sodium gluconate on the total porosity of slag systems at 28d	111
Figure 6.37. Ettringite crystals growing in the capillary pores and helping to reduce the total porosity of slag 8 systems with Na ₂ SO ₄ at a) 24 hours and b) 7 days.....	113
Figure 7.1. a) Total porosity related to the compressive strength and b) evolution of the compressive strength related to the critical entry radius from MIP for all the systems studied in this work.....	116
Figure 7.2. Cumulative heat release related to the compressive strength for all the systems.....	117
Figure 7.3. Experimental measurements of calcium and silicon concentrations in the pore solution extracted over time for white cement systems with slag 1	119
Figure A.1. a) Cumulative heat and b) total porosity (7 days) for alite and white cement pastes.	121
Figure A.2. Polished sections at 24 hours of a) alite and b) cement pastes (lower magnification).....	122
Figure A.3. Polished sections at 24 hours of a) alite and b) cement pastes (higher magnification)	122
Figure B.1. Times when hydration was stopped to analyse the surface of cement/slag grains.....	123
Figure B.2. Hydrates in the surface of the cement/slag grains of slag systems (at the end of the nucleation and growth period). Lower magnification (left side images) and higher magnification (right side images)	124
Figure B.3. Al/(Ca-S) ratio against Si/(Ca-S) ratio for slag systems at 28 days.	125

List of Tables

Table 3.1. d(10), d(50) and d(90) for each batch of alite and gypsum.....	24
Table 3.2. Mineralogical composition of white Portland cement by X-ray diffraction and Rietveld.....	25
Table 3.3. Oxides composition of white Portland cement by X-ray Fluorescence (in wt.%)	25
Table 3.4. d(10), d(50) and d(90) for each batch of alite and white cement	26
Table 3.5. Oxides composition of slag 1 and 8 by X-ray Fluorescence (in wt.%)	27
Table 3.6. d(10), d(50) and d(90) for white cement, slag 1 and slag 8	27
Table 4.1. Formulations of the alite-based systems studied	40
Table 5.1. Formulations of the white cement systems studied	60
Table 5.2. Quantification of the (Ca-S)/(Si+Al) ratio of C-S-H product at 7 and 28 days.....	72
Table 6.1. Formulations of the slag mixes studied	82
Table 6.2. Enthalpies of the three major reactions in cement hydration [16]	87
Table 6.3. Degree of reaction of slag ($\pm 2\%$) for each system at 28 days	88
Table 6.4. Formulations of slag systems studied with and without gluconate	98
Table 6.5. Quantification of the (Ca-S)/Si ratio of C-S-H in slag 1 systems in the presence and absence of sodium gluconate at 24 hours (a and b), 7 days (c and d) and 28 days (e and f).....	107
Table B.1. (Ca-S)/Si ratio for white cement-slag systems at 28 days, calculated from EDX analysis	125

Glossary

Abbreviation Definitions

Cement notation

C	Calcium oxide – CaO
S	Silicon dioxide – SiO ₂
A	Aluminium oxide – Al ₂ O ₃
F	Iron oxide – Fe ₂ O ₃
H	Water – H ₂ O
\$	Sulfate – SO ₃

Anhydrous

C ₃ S	Tricalcium silicate – 3 CaO · SiO ₂
Impure C ₃ S	Alite – 3 CaO · SiO ₂
C ₂ S	Dicalcium silicate (belite) – 2 CaO · SiO ₂
C ₃ A	Tricalcium aluminate (aluminate) – 2 CaO · Al ₂ O ₃
C ₄ AF	Ferrite – 4 CaO · Al ₂ O ₃ · Fe ₂ O ₃
C\$H ₂	Gypsum – CaSO ₄ · 2 H ₂ O
PC	Portland cement

Hydrates

CH	Portlandite (calcium hydroxide) – Ca(OH) ₂
C-S-H	Calcium silicate hydrate – CaO - SiO ₂ - H ₂ O
C-A-S-H	Calcium silicate hydrate with alumina – CaO - Al ₂ O ₃ - SiO ₂ - H ₂ O
C-(N)-A-S-H	Calcium silicate hydrate with sodium and alumina – CaO-Na ₂ O-Al ₂ O ₃ -SiO ₂ -H ₂ O
Aft or C ₆ A\$ ₃ H ₃₂	Ettringite – 3 CaO · Al ₂ O ₃ · 3 CaSO ₄ · 32H ₂ O
AFm	Monosulfoaluminate – 3 CaO · Al ₂ O ₃ · CaSO ₄ · 12 H ₂ O
	Monocarboaluminate – 3 CaO · Al ₂ O ₃ · CaCO ₃ · 11 H ₂ O
	Hemicarboaluminate – 3 CaO · Al ₂ O ₃ · 0.5Ca(OH) ₂ · 0.5CaCO ₃ · 11.5 H ₂ O
C ₂ ASH ₈	Strätlingite – 2 CaO · Al ₂ O ₃ · SiO ₂ · 8 H ₂ O

Acronyms

SCM	Supplementary Cementitious Materials
DoH	Degree of hydration
DoR	Degree of reaction
w/c or w/s	Water-to-cement ratio
w/s	Water-to-solids ratio
SEM	Scanning Electron Microscopy
TEM	Transission Electron Microscopy
SFEG	Scanning Field Emission Gun
BSE	Backscatter Electron
SE	Secondary Electron
EDX or EDS	Energy-Dispersive X-ray Spectroscopy
Ip	Inner Product C-S-H
Op	Outer Product C-S-H
XRD	X-Ray Diffraction
MIP	Mercury Intrusion Porosimetry
IA	Image Analysis
¹ H NMR	Proton Nuclear Magnetic Resonance
TGA	Thermogravimetry Analysis
PSD	Particle Size Distribution
XRF	X-Ray Fluorescence
PSE	Pore Soluiton Extraction

CHAPTER 1. Introduction

1. Introduction	1
1.1. Use of SCMs and alkali	1
2. Motivation and objectives of the thesis	2
3. Chapter overview	2

1. Introduction

Concrete is so widely used around the world that cement production represents 5 per cent of annual anthropogenic global CO₂ [1]. One cubic meter of concrete per year is produced for each person on earth, making concrete the most widely used substance apart from water. The demand for cement and concrete is expected to double by 2050 [2], due to the increase in the world population and increasing urbanisation [3,4].

1.1. Use of SCMs and alkali

Research into more sustainable concrete manufacturing and construction is essential as worldwide demand of concrete increases. One of the most promising ways to reduce emissions from the Portland cement calcination process, as well as to avoid the depletion of limestone quarries, is the use of supplementary cementitious materials (SCMs). SCMs are used as a partial replacement for clinker leading to so-called blended cements. SCMs can compensate the dilution of clinker by themselves producing hydrates. However their reactions involve changes in the clinker hydration.

SCMs are secondary products of a manufacturing process for a primary product. Instead of going to landfill they are recycled for cementitious systems and contribute to the hydration process next to cement. Slag (from iron industry) and fly ash (from the burning of coal in power plants) are some of the commonly used SCMs. The chemical composition of SCMs is very wide. For instance, slag is homogeneous and with a similar composition to Portland cement, while fly ash is a highly heterogeneous material with an important amorphous fraction compared to crystalline phases.

The development and application of cementitious systems with SCMs is promising from a sustainability point of view. SCMs increase the resistance to chloride penetration, sulfate attack and they lower the heat of hydration compared to non-blended systems [5]. On the contrary, the levels of replacement are limited as SCMs react more slowly than Portland cement and it is important to obtain reasonable early strengths.

The addition of alkali can increase the reactivity of SCMs. Consequently, alkalis accelerate the initial hydration of cement and lead to higher early strength development. However, they may have a detrimental impact on strength at later ages [6,7] as alkalis do not only affect SCMs, but also the reaction of the clinker phases. At present there is no clear explanation of the impact of alkalis. It is also possible that alkalis affect the structure and the intrinsic properties of the hydrates in addition to the rate of hydration. However, this has not been systemically confirmed and findings in the literature are often contradictory [8–10].

2. Motivation and objectives of the thesis

The present work studies the impact of alkali salts, as well as gypsum, on the hydration kinetics and microstructural development of cementitious systems and the mechanisms behind this; to explain their influence on the strength development. It starts with the study of the alkali influence on the hydration of alite, as a model system, before moving to white cement and cement-slag systems.

This work focuses not only on early ages but tries to clarify if the changes induced by alkalis at the first hours of hydration have an impact on the properties of the systems at later ages. NaOH and Na₂SO₄ are the two sodium-based alkali salts are used in this work.

The **main questions** to elucidate in this thesis are the following:

- How do Na₂SO₄ and NaOH affect the hydration kinetics of alite, white cement and cement-slag systems?
- Is there a difference between the impact of NaOH and Na₂SO₄ on the strength development?
What could explain such differences?
 - Changes in the morphology of the main hydrates?
 - Changes in the density of C-S-H?
 - Changes in porosity?
 - Changes in the phase assemblage?

3. Chapter overview

Chapter 2 presents the state of the art about the impact of alkali salts and gypsum on the hydration of cementitious systems. It includes an overview of the influence on several parameters individually including kinetics, morphology and chemical composition of the main hydrates, mechanical properties.

Chapter 3 describes the materials and methods used in this work.

Chapter 4 focuses on the impact of NaOH, Na₂SO₄ and gypsum on the hydration of alite. The effect on the kinetics and the microstructure is studied, as well as the impact of alkali on the mechanical properties of alite micromortars. A factor that could control the kinetics in alite systems with alkalis is identified, as well as those related to the strength development. The differences in the morphology of C-S-H are discussed, and its further relationship with the final mechanical properties is clarified.

Chapter 5 reports on the effect of NaOH and Na₂SO₄ on the hydration of white cement. It specially focuses on the impact on the kinetics, the phase assemblage and the porosity. The main responsible mechanism behind the impact of alkalis on the mechanical strength is identified. It brings new insights on the impact of alkalis on the amount of water, density and structure of C-S-H in non-dried samples based on ¹H NMR measurements.

Chapter 6 studied the effect of NaOH and Na₂SO₄ on slag-white cement systems. Not only the results are compared to those obtained mainly in Chapter 5 but also the reaction of slag is studied. Moreover, it focuses on the impact of sodium gluconate to identify which parameter is responsible for the higher strength development when combined with Na₂SO₄.

Chapter 7 presents and discusses the main conclusions of this work as well as the perspectives.

CHAPTER 2. Literature review

1. Cement hydration.....	5
1.1. Kinetics of hydration	5
1.2. C-S-H	7
1.3. Microstructural development and hardening of cement pastes.....	10
1.4. Outlook.....	12
2. Influence of alkalis on cement hydration	12
2.1. Acceleration effect	12
2.2. Strength development.....	13
2.3. Porosity.....	15
2.4. Morphology of hydrates.....	16
2.5. Chemical composition and structure of C-S-H	17
3. The impact of sulfate in cement hydration	19
4. Sodium gluconate	20
5. Summary	21

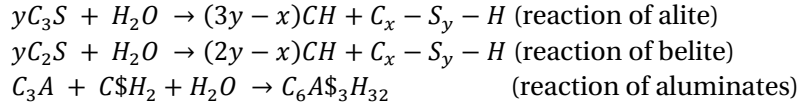
The first section of this chapter focuses on the hydration of cement in a general context. It presents the kinetics of cementitious systems, what leads to the precipitation of hydrates, how do hydrates contribute to the development of a microstructure and what are the main parameters reported to be linked to strength development. It is clear from the literature that the final mechanical properties are related to several parameters such as the degree of hydration, the distribution of phases, the type of hydrates, the total porosity and its distribution, among others. The second section reviews the current knowledge about the impact of alkali salts on the above mentioned parameters during the hydration of cementitious systems in order to define the starting point of this work.

1. Cement hydration

1.1. Kinetics of hydration

The hydration of cement starts as soon as it comes into contact with water. Cement grains start to dissolve and calcium, silicate, aluminate, sulfate, hydroxide and alkali ions enter the aqueous solution. The precipitation of hydrates from combinations of these ions leads to the transformation from a paste to a hardened solid. The hydration of silicate phases lead to the formation of calcium silicate hydrate

(C-S-H) and portlandite or calcium hydroxide (CH) while the hydration of aluminate phases leads to the formation of ettringite (AFt) and other aluminate phases (AFm). The main reactions with cement notation are (see Glossary):



Most of these reactions are exothermic. Although the hydration of cement may continue over months and years, the reactions with the most significant heat release take place within the first 24 hours. The heat release can be monitored with a calorimetric device. Typical calorimetry curves of Portland cement and alite are shown in Figure 2.1.

As C_3S and C_3A dissolve, the solution is quickly supersaturated with respect to C-S-H and ettringite, which precipitate. It is the precipitation of portlandite that determines the beginning of the acceleration period, or also called “nucleation and growth period” (when C-S-H precipitates and grows in the surface of the anhydrous cement grains [11]). The dissolution-precipitation continues over time but all the time the concentrations of silica and alumina in the solution are quite low. The precipitation of hydrates contributes to the filling of the empty space.

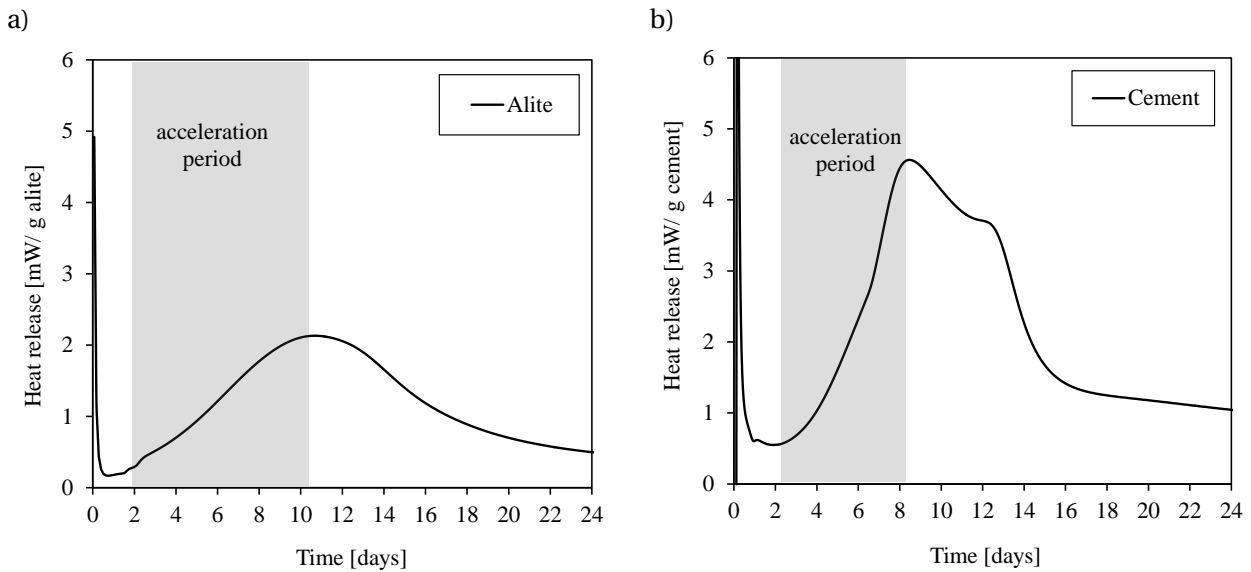


Figure 2.1. Typical isothermal calorimetry curves of a) alite and b) Portland cement.

C-S-H is the main hydration product as it represents approximately half of the solid phases by mass in a mature cement paste [12]. Due to the importance of C-S-H as the main binding phase, it has received special attention and has been a subject of study for many decades [12–14]. However, its chemical composition, morphology and density continue to be debated in the literature. The first reason is the diversity of morphologies and composition that the structure of C-S-H can adopt. The second reason is that it was not until very recently that Muller and coworkers have been able to characterize the C-S-H without removing the water (and consequently without damaging nano-scale structures), thanks to the use of 1H NMR relaxometry [12,15]. The following sections describe the main characteristics of C-S-H.

1.2. C-S-H

The structure and chemical composition of C-S-H

C-S-H is a poorly crystalline phase which forms in cement pastes and concrete [15]. It has a low crystallinity as it has short range order or regions of “nanocrystalline” material [16]. The characterization of the nano-crystalline structure of C-S-H in hydrated cement pastes is a difficult task because it does not show very distinct reflections in XRD but a broad hump. Consequently, C-S-H is often called “gel”.

The C-S-H structure is based on chains of attached silicate tetrahedra with a repeating pattern of three (called “dreierketten”) that are coordinated to a central layer of octahedrally coordinated Ca^{2+} ions. Two of the three tetrahedra are linked by sharing O-O edges with the central Ca-O part of the layer, often referred to as “paired” tetrahedra (P). The third tetrahedron, which connects the two P tetrahedra is termed “bridging” (B) (Figure 2.2a). Each layer of Ca^{2+} ions has silicate chains either side and the distance between two Ca^{2+} layers is defined as the layer spacing. The interlayer can contain variable amounts of water, calcium ions and other type of ions such as alkalis. Experiments and atomistic simulation have indicated that the 14Å Tobermorite is a good model for the C-S-H structure [17,18].

One of the most characteristic parameters concerning the chemical composition of C-S-H is its calcium-to-silicon ratio (Ca/Si). The normal ratios in hydrated cement pastes are around Ca/Si~1.5-2. The increase of Ca/Si ratios above 0.8 result from three main types of modification to the structure: a) omission of some bridging tetrahedra, b) replacement of terminal protons on $\equiv\text{SiOH}$ by extra Ca^{2+} ions, and c) the additional incorporation of Ca^{2+} ions balanced by OH^- in the interlayer [13,19] (see Figure 2.2b).

The chemical composition of C-S-H influences its surface charge. The silicate tetrahedra end with an oxygen atom that forms a silanol group $\equiv\text{SiOH}$. Under most circumstances, the pH will be high in cement pastes and thus the silanol groups in the surface of cement grains will deprotonate according to $\equiv\text{SiOH} + \text{OH}^- \rightarrow \equiv\text{SiO}^- + \text{H}_2\text{O}$. Thus, the surface of C-S-H is negatively charged. However, calcium ions compensate the $\equiv\text{SiO}^-$ sites resulting in a charge reversal (apparent positive surface charge with $\equiv\text{SiOCa}^+$) [20–23].

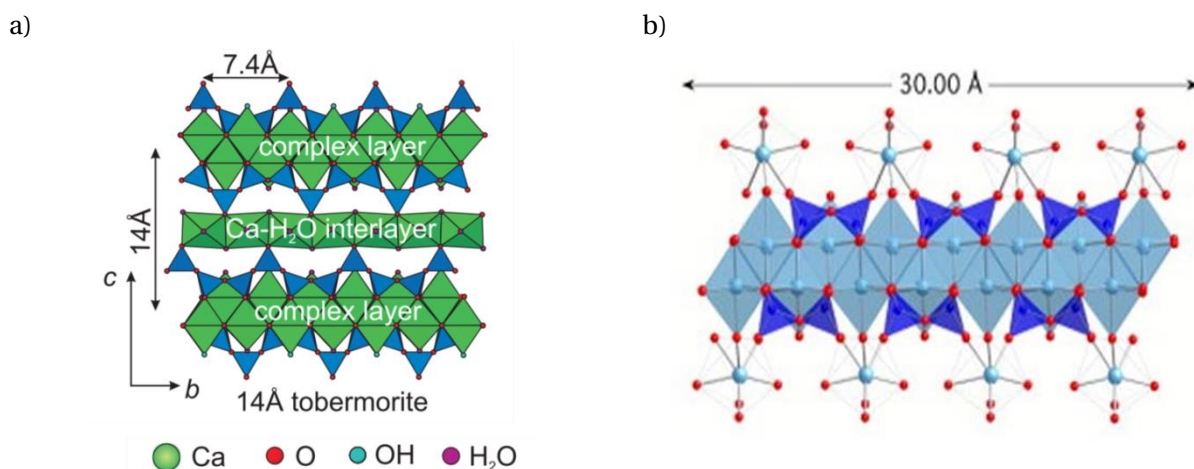


Figure 2.2. Schematic diagram showing dreierkette chains present in a) 1.4 nm Tobermorite, adapted from Garbev et al. [24] and b) for the C-S-H with Ca/Si ratio 1.5, more representative of hydrated cement pastes, adapted from Richardson [13].

The morphology of C-S-H

Electron microscopy indicates that during the main heat evolution peak C-S-H grows as clusters of needles termed “fibrillary morphology” [25], comparable to a sea-anemone structure. Although C-S-H is fibrillar in both cases, in a cement system the fibrils (i.e. needled structures) adopt a divergent morphology while in the case of C_3S or alite they are more convergent as they merge in the top [17]) as shown in Figure 2.3.

One familiar problem with electron microscopy is that the specimen preparation is often harsh or damaging during the drying and coating process. This can consequently lead to problems of misinterpretation of the results due to artifacts. However, the preparation methodology to characterize the morphology of C-S-H with electron microscopy has been optimized and the damage is considered minor at the level of resolution of the electron microscope [17,26–28]. The needles of C-S-H observed on a carbon coated sample are equivalent to the observations on non-coated samples [17],.

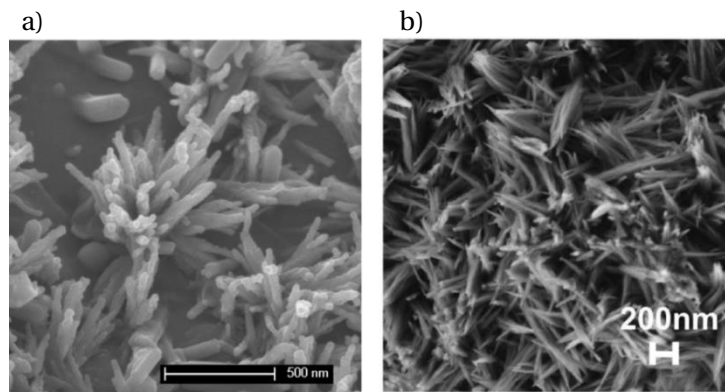


Figure 2.3. Morphology of C-S-H product in a) a cement paste (from Berodier [27]) and b) a C_3S paste (from Bazzoni [17]), both during the nucleation and growth period.

The distribution of water and density of C-S-H

Recent experiments on white cement pastes with 1H NMR [12] indicate two different populations of water in C-S-H (see Figure 2.4):

- *Interlayer or sheet* ($\varnothing \sim 1$ nm): Water between the layers of C-S-H.
- *Gel* ($\varnothing > 1$ nm to 5 nm): Interlayer together with the water in the pores created among different nanocrystalline regions.

Both populations increase with hydration during the first two days. From then on, gel water reaches a plateau, as shown in Figure 2.5. On the contrary, interlayer water continues to increase as the number of aggregated layers increases as C-S-H continues to form.

1H NMR analyses allow the calculation of the density of C-S-H. Two types of density can be differentiated: the density of C-S-H exclusive (called “solid density”) and inclusive (called “bulk density”) of the gel water, as indicated in Figure 2.4. The bulk density gradually increases with time (densification of C-S-H) since the number of aggregated layers increases (bulk density at 28 days ~ 1.96 g/cm³). On the contrary, the solid density is mostly independent on the DoH and remains fairly constant all the time (2.69 g/cm³).

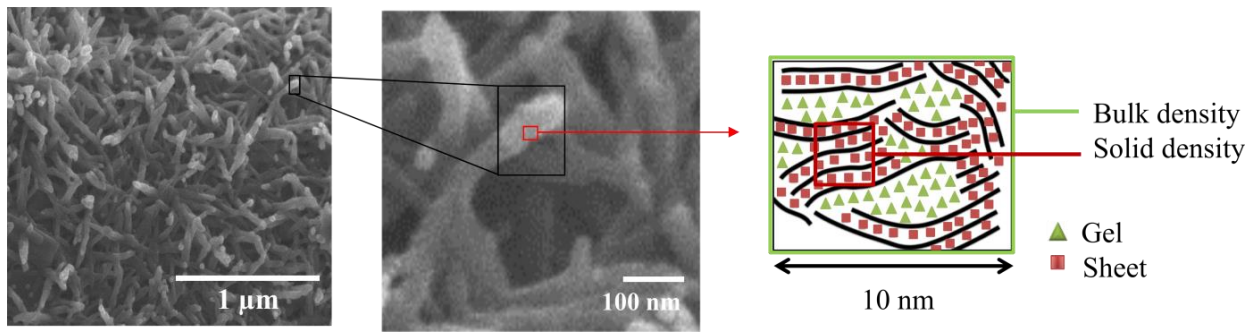


Figure 2.4. SFEG micrographs of C-S-H needles and graphical representation of C-S-H as seen by ^1H NMR. The black lines of the schema are the calcium oxide layers with silicate tetrahedral; the red squares are the interlayer water and the green triangles represent the gel water (adapted from Muller [12]).

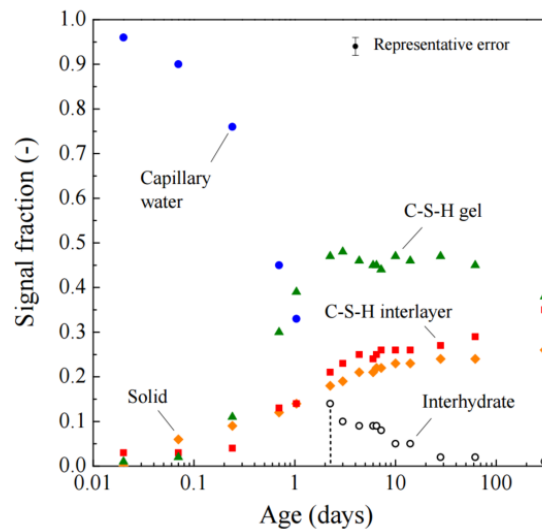


Figure 2.5. Evolution of ^1H NMR signal fractions with time (white cement paste, $w/c=0.4$). Capillary water becomes interhydrate water beyond 2 days of hydration. When interhydrate water is fully consumed (~ 2 months, $\text{DoH} = 0.8$) hydrates grow at the expense of gel water. From Muller [15].

The addition of SCMs further complicates the characterisation of C-S-H. SCM can change the composition of the pore solution and therefore the characteristics of C-S-H [13,29]. For example, the use of aluminate-rich SCM can lead to higher levels of Al substitution for Si in C-S-H in the bridging tetrahedra of dreierkette chains or the presence of slag or fly ash in cement systems can promote a more foil-like morphology of C-S-H.

Despite the fact that C-S-H is the main binding phase, the remaining hydrates cannot be disregarded. It is the precipitation and growth of C-S-H along with other hydrates such as portlandite and ettringite which promotes the microstructural development and contributes to the hardening of cement pastes.

1.3. Microstructural development and hardening of cement pastes

Microstructural development

The cohesion of the paste increases with the hydration time due to the filling of the space. The molecular mechanisms of the cohesion in cement are not well understood yet mainly due to i) lack of structural data for C-S-H and ii) the wide variation on cement compositions. Jönsson and coworkers [30] reported that the two main factors contributing to the cohesion of a cement paste are:

- *Surface charge density:*

The surface charge density of the C-S-H and C_3S particles is determined by the alkalinity of the solution. Both the surface of C_3S and C-S-H are negatively charged (SiO^- groups) due to high pH. In a solution with $pH > 12$, C-S-H particles attract each other at short range (~ 2 nm).

- *Presence of mono (Na^+) or divalent (Ca^{2+}) cations:*

The interaction between a) C-S-H particles, b) C_3S particles or c) between C_3S and C-S-H becomes more attractive at higher concentration of divalent calcium ions, contrary to monovalent sodium ions. Therefore, the cohesion will be higher in the presence of Ca^{2+} ions. Anions are reported to participate less to the cohesion.

The amount of hydrates increases with time of hydration and so there is more space filled by hydrates. The result is a network of solids within the paste, as shown in Figure 2.6. The formation of a connected solid skeleton (microscopic scale) gradually increases the strength of the cement paste (macroscopic scale). A higher strength development is linked to a decrease of the porosity with progressing hydration as the water gets bound within the hydrates. Consequently, the characteristics of the microstructure will directly influence the strength development.

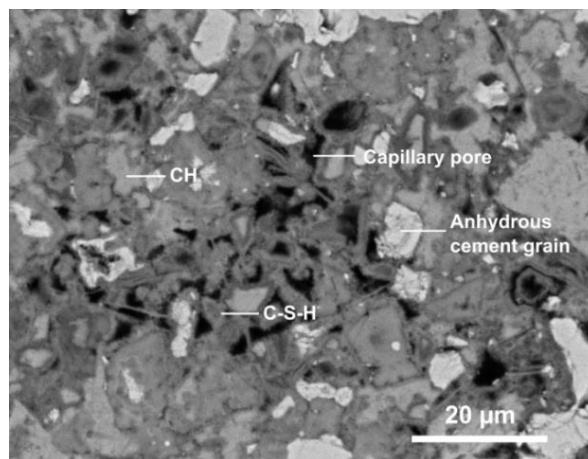


Figure 2.6. Microstructural development of a white cement paste at 7 days of hydration.

Mechanical properties

It is much discussed in literature which are the main components that determine the strength of a hardened cement paste. It is a complex issue since it does not depend on one single parameter but on several. The main components reported to be related to the mechanical properties are presented below, being difficult to isolate the effect of each one:

- a. *Pores*: generally, coarser pores are more detrimental than finer pores [31,32] (the type of pores in hydrated ordinary cement pastes are described in the next section).
- b. *Gel-space ratio (GSR)*: This relationship is based on the ratio between the amount of hydrates (related to the degree of hydration) and the total porosity in the system [33–36]. It is defined as $\frac{V_{hydrates}}{V_{hydrates} + V_{cap pores}}$, where $V_{hydrates}$ is the volume fraction of hydrates and $V_{cap pores}$ is the volume fraction of capillary porosity (gel pores count as part of solid).
- c. *Residual anhydrous cement grains*: act as filler and exhibits the capacity to resist external stresses due to its high hardness [35].
- d. *Nature and morphology of hydrates*: the morphology and density of hydrates could impact the mechanical strength of the matrix [6,37]. The type and nature of hydrates may influence the links between the different phases as well as the cohesive bonds (physical attraction between solid surfaces and chemical bonds).

Porosity

Although the precipitation of hydrates in the matrix contributes to form a solid skeleton, a system of pores remains between different phases. A cement paste is a porous material with a system of pores of variable sizes. Not only a lower but also a finer porosity promotes a higher strength development. There are mainly three categories of pores in hydrated ordinary cement pastes. From biggest to smallest [15]:

- *Air/compaction voids* (\emptyset from a few μm to a few nm)

They are created during the mixing.

- *Capillary porosity* ($\emptyset \sim 10 \text{ nm}$ to few μm)

These are the spaces between the hydrates. They can be interconnected channels or, if the structure is dense enough, cavities interconnected only by gel pores. The capillary porosity decreases as hydration advances. It is generally considered as the category of porosity that better correlates to the strength results.

- *Gel pores* (\emptyset from 1 to 5 nm)

It is the intrinsic porosity of C-S-H and it is considered to be a part of it. This category is fully saturated with water at relative humidities above about 50% (detailed in previous section).

1.4. Outlook

In the last decade, there have been important insights to understand the mechanisms behind the hydration of cement. However, the wider use of SCMs increases the complexity of cementitious systems. For high replacements of SCMs, since they are less reactive than cement, accelerators such as alkali may be helpful. However, alkali will alter the mechanisms of hydration even further. There is a need to understand which parameters are affected during cement hydration in the presence of alkali salts for an optimized design of blended systems and an improved performance. For such purpose, it is interesting to understand their impact on the main parameters that could be related to the final mechanical properties, such as the characteristics of the main hydrates, the porosity, the kinetics of reaction, the phase assemblage, among others.

2. Influence of alkalis on cement hydration

This section reviews the knowledge on the impact of alkali on the kinetics, the porosity, the morphology of C-S-H and Portlandite, as well as the chemical composition and structure of C-S-H. The objective is to identify which points require clarification in order to define the starting point of the present work.

2.1. Acceleration effect

Lerch was probably one of the first to note that the presence of alkali accelerated the hydration process [38]. Some years later, Jawed and Skalny [6] reviewed the main work done on the effect of alkali on cement hydration and reported an acceleration effect with alkalis. An early acceleration of hydration by alkalis has been attributed to an enhancement of the rate of dissolution of the calcium silicate phases and precipitation of the hydrated phases [37,39–42], although no clear evidence has been presented. A recent study [42] shows that sodium hydroxide and sulfate (between 0.2-0.5M) lead to a shorter induction period, a higher rate of hydration during the acceleration regime, an increase in the intensity of the main heat peak and a faster rate of deceleration (Figure 2.7 and Figure 2.8). From modelling, an increase in the alkalinity of the solution was found to promote a faster precipitation of portlandite as the amount of calcium ions needed in solution to achieve the critical supersaturation level for portlandite precipitation is lower. In addition, the silica concentration in solution increases, which may lead to an earlier (and maybe more abundant) precipitation of C-S-H product.

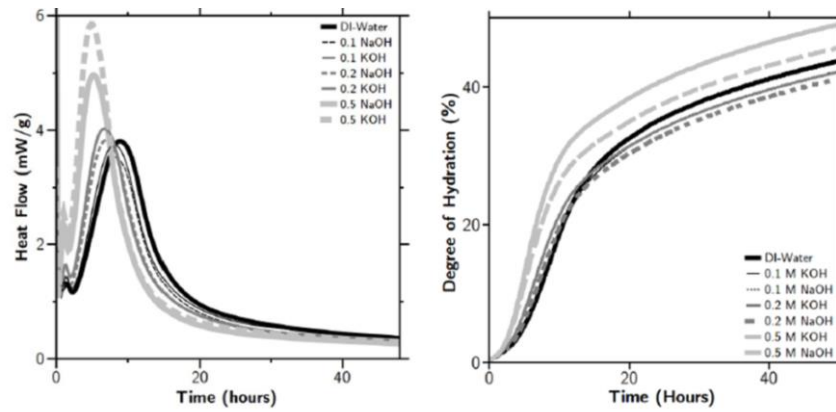


Figure 2.7. Measured heat evolution profiles up to 50 hours and DoH of alite hydrating in different alkali hydroxide solutions, adapted from [42].

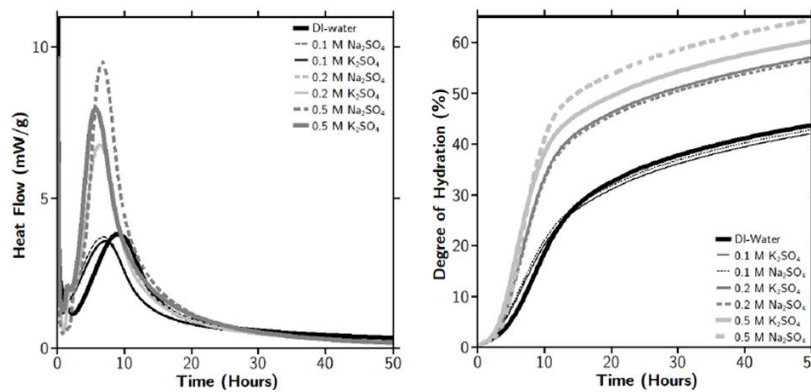


Figure 2.8. Measured heat evolution profiles up to 50 hours and DoH of alite hydrating in different alkali sulfate solutions, adapted from [42].

2.2. Strength development

It is generally accepted that the acceleration of the hydration of cement promoted by alkalis (at least initially) usually leads to a higher strength development at early ages. However, alkalis are usually found to have a detrimental impact on strength at later ages [6]. Some authors [32,43] reported a detrimental effect on compressive strength also at early ages (Figure 2.9). From an extensive data collection of the compressive strength values for different clinker systems (ground to the same fineness and adjusted to the same gypsum content) containing alkali sulfate, based on available data from Holcim, it was noted that an increasing content of alkali sulfate promoted a higher compressive strength at early ages but lower at later ages (Figure 2.10). They also observed that the addition of NaOH not only does not increase the compressive strength at early age but also the lowering of the compressive strength at later ages is more pronounced than with the addition of alkali sulfates [44]. Kumar and coworkers [45] found a lower rate and extend of strength development in presence of 0.5 M NaOH and 0.5 M KOH at later ages and Shayan and Ivanusec [46] observed that an increasing addition of NaOH from 0.5 M to 4.5 M gradually lowered the compressive strength of cement mortars at 7, 28 and 90 days.

Unfortunately, in most studies on the effect of alkalis on the mechanical properties the alkali content is not the only parameter involved, e.g., the results are based on cements that already contain high levels of alkali or cements with different alkali contents. For instance, Shayan and Ivanousec [46] made additions to a cement with a high alkali content of 0.8 %Na₂O_{eq}¹. This makes the understanding of the mechanism behind the lower strength development in the presence of alkali salts more complicated. Moreover, strength development does not only depend on one single parameter but it can depend on many, such as the total porosity and its distribution, the type of hydrates, the degree of hydration, among others, and alkalis may have an effect on each parameter as detailed in the following sections.

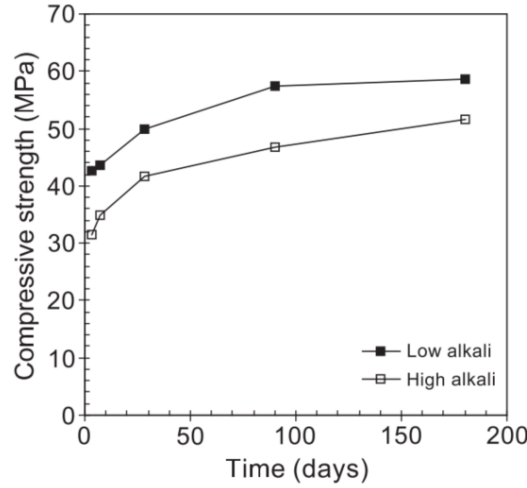


Figure 2.9. A higher content in alkali (Na₂O_{eq}) in concrete lowers the compressive strength, adapted from Smaoui et al [32].

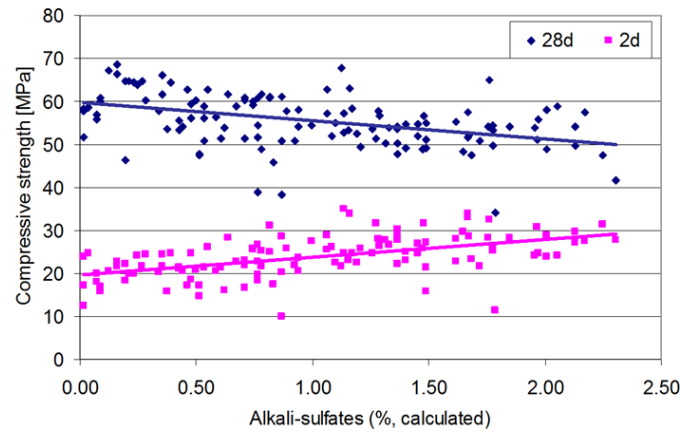


Figure 2.10. Data collection of the compressive strength values for different clinker systems containing alkali sulfates at early (2 days) and later age (28 days), based on EN 196 standard mortars at w/c = 0.5 (internal data from Holcim [44]).

¹ Na₂O equivalent defined as %Na₂O + 0.658 × %K₂O.

2.3. Porosity

To understand why the addition of alkali salts may have a detrimental impact on strength at later ages it is necessary to look at their effect of the total porosity and its distribution. Kumar and coworkers [45] observed that 0.5M NaOH promoted a coarser porosity in cement pastes (Figure 2.11). Smaoui and coworkers [32] and Shayan and Ivanusec [46] attributed lower strength to a more porous and less dense cement paste based on SEM observations in secondary electron mode at 7 days (Figure 2.12). However, it is subjective to judge or analyse the porosity of a cement sample from micrographs of fractured surfaces. The authors did not use other more appropriate techniques (like MIP, for instance) to characterize the porosity.

Bentz [41] reported that the combined addition of 0.43 wt.% NaOH and 0.60 wt.% KOH (per mass of cement) in cement pastes resulted in only gel pores while the cement paste without the addition of alkali exhibited percolated capillary and gel pores (measured by low temperature calorimetry, LTC). The author suggested that, for equal w/c ratios and degree of hydration, the depercolation of capillary and larger open gel pores in the pastes with alkali could be linked to a more voluminous C-S-H. However, these observations seem to suggest that the strength development would be improved, which is actually the contrary to what is mostly observed in literature.

A limited number of studies have been done to characterize the porosity in the presence of alkalis. Although it is found in literature that porosity seems to be affected by the addition of alkalis, a detailed characterization of those changes and the mechanisms behind them are still missing. It is important to study these changes since it is known that the porosity (and its distribution) is strongly related to the strength development. Many authors (detailed in the following section) propose/hypothesize that a change in the porosity, and thus in the strength results, could be related to a change in the morphology of C-S-H and their ability to fill the space, but do not investigate this hypothesis further.

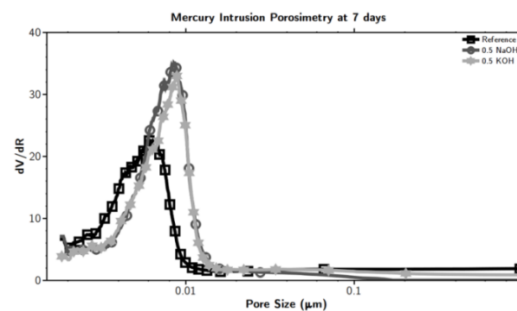


Figure 2.11. Influence of NaOH and KOH on the porosity of a cement paste, from Kumar et al [45].

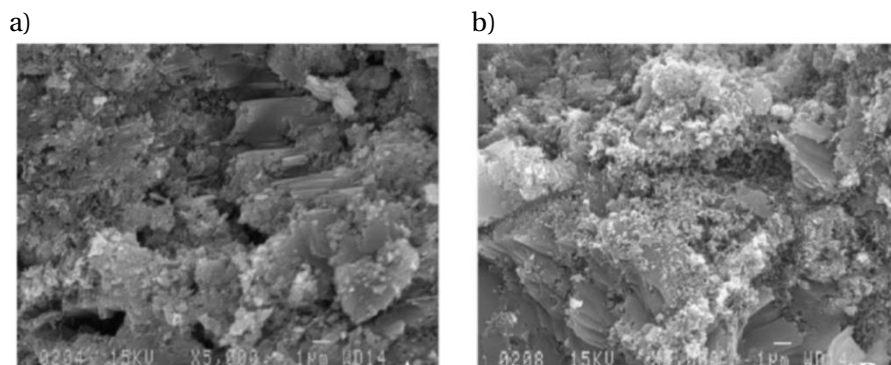


Figure 2.12. Microstructural characteristics, as observed under the SEM, of a) low-alkali cement paste with w/c of 0.4 (7 days) and b) high-alkali paste with w/c of 0.4 (7 days), adapted from Smaoui et al [32].

2.4. Morphology of hydrates

It has been hypothesized in the literature that changes in the morphology and the composition of hydrates (especially C-S-H but also portlandite) in the presence of alkali may explain the lower strength development, and probably a change in the porosity. A change in the morphology could be related to a change in the ability to fill the porosity.

The morphology of C-S-H

Mori and coworkers [37] reported that the addition of NaOH to C_3S favoured the growth of a “coarser” C-S-H and Na_2SO_4 favoured fine “acicular” C-S-H. The authors considered that the C-S-H was more “heterogeneous” in both cases compared to the C-S-H in cementitious systems without the addition of alkali. These changes in the morphology of C-S-H were speculated to be linked to differences in the pore structure. The microscopy images are not shown in the present work because, unfortunately, these studies are quite old and the quality of the images is not good enough. Alkalis were found to decrease the specific surface area of C-S-H (measured by N_2 adsorption) and the authors suggested that this was because C-S-H was not growing into the void spaces. Jawed and Skalny [6] reported in their review that the presence of alkalis in cement promoted the growth of long “straw-like” crystals starting after a few hours and persisting even after many weeks, proposing the formation of a better crystallized C-S-H with the addition of alkalis.

On the contrary, it has also been reported that the addition of alkali hydroxide to alite does not seem to induce any changes in the morphology of C-S-H [8]. In summary the descriptions found in literature regarding the impact of alkali salts on the morphology of C-S-H are rather vague and ambiguous.

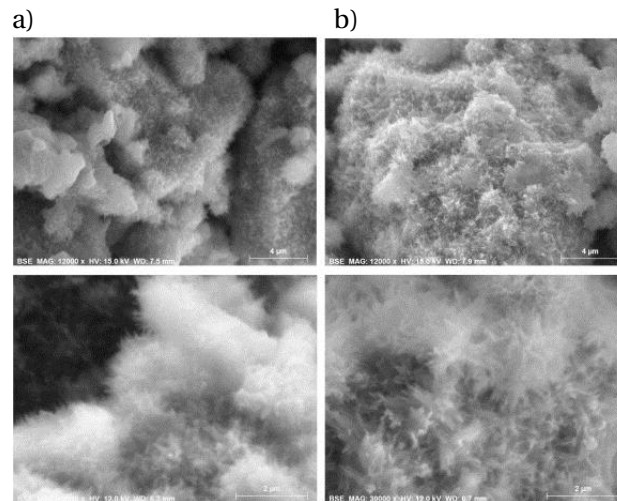


Figure 2.13. Fracture surface images of C-S-H at the ages of 11 h (top) and 24 h (bottom) for alite samples with a) DI-water and b) 0.5 M NaOH, adapted from Kumar et al [8].

The morphology of portlandite

Changes in the morphology of portlandite have also been reported. Berger and McGregor [47] observed that a platelet-like morphology with a c/a crystallographic axis ratio below 0.5 was dominant when C_3S hydrated in the presence of alkali hydroxides [47]. At equal degrees of hydration, alkali hydroxides were reported to induce the formation of smaller and more numerous particles. Way and Shayan [9] noted an increase in the rate of formation of portlandite when increasing the concentration of NaOH in mixing water. Gallucci and Scrivener [48] also reported that cement pastes with alkalis seem to promote

portlandite nucleation with a hexagonal platelet morphology which grows onto already existing clusters. Recently, Galmarini et al. [49,50] studied the morphology of portlandite particles formed by coprecipitation with the addition of different ions. From experimental and atomistic simulations the authors observed that the presence of alkali hydroxides can promote the formation of particles with a thinner, hexagonal platelet shape in which the relative growth speed in $[10.0]$ direction of the plate edges is higher with respect to the other directions ($[00.1]$ and $[10.1]$), agreeing with previous findings in [47,48,51].

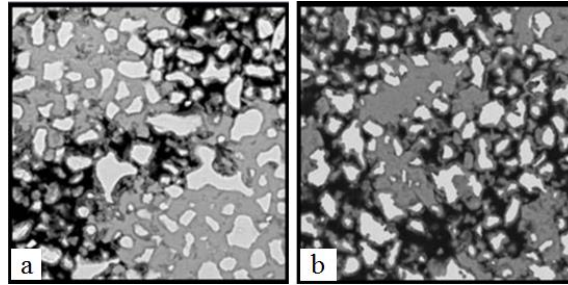


Figure 2.14. Morphology of CH at 1 day a) in C_3S plain paste and b) with gypsum and 0.1 M KOH, adapted from Gallucci and Scrivener [48].

2.5. Chemical composition and structure of C-S-H

The interest of understanding the influence of alkali salts on the chemical composition and structure of C-S-H arises from the fact that alkali salts will increase the pH of the pore solution, lower the calcium and increase the silicon dissolved concentrations [22,52–54]. Thus, alkalis tend to lower the Ca/Si ratio in the liquid [22] and so the structure of the gel could change, probably having an impact on the final mechanical properties. However, Kumar and coworkers [8] found that the stoichiometry of C-S-H did not change significantly in alite pastes with NaOH (0.1, 0.2 and 0.5M) in the mixing solution. All the pastes had a Ca/Si~1.7 at 30 hours of hydration.

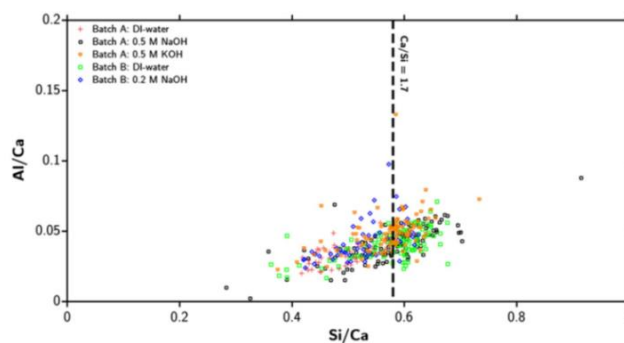


Figure 2.15. EDS for alite samples at 30 hours hydrated with different solutions of NaOH or KOH [8].

The impact of alkali salts on the structure of C-S-H product is complex and not fully understood. The uptake of alkalis in C-S-H depends of the concentration of alkalis in solution. L'Hôpital [55] recently reported an extensive study on the effect of alkali ions on the chemical composition of synthetic C-S-H from Ca/Si 0.6 to 1.6. An increase of the alkali uptake in C-S-H for lower Ca/Si was observed, as previously reported by Stade [56] and Hong and Glasser [53].

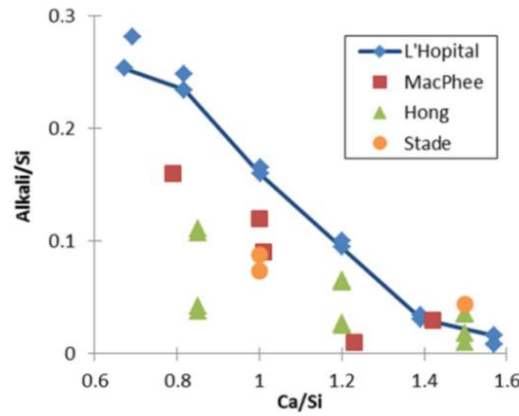


Figure 2.16. Data collection of Na/Si or K/Si for synthetic C-S-H in equilibrium with NaOH or KOH (for different Ca/Si ratios) [22].

It is generally agreed that sodium ions are not chemically bound in C-S-H. However, the uptake of sodium can take place in the interlayer space in the nano-crystalline region of C-S-H (less mobile and so not easily removed) or adsorbed on the surface of C-S-H (more mobile and easy to remove) [53,56–58]. The data obtained by Renaudin and coworkers [58] about the distribution of more and less mobile sodium ions measured with ^{23}Na NMR as a function of the Ca/Si ratio were recently plotted by Lothenbach and Nonat [22] (Figure 2.17a).

On the one hand, if sodium ions are adsorbed on C-S-H surface they substitute a proton charge balancing the deprotonated silanol sites² ($\equiv\text{SiO}^-$). On the other hand, if they are adsorbed in the interlayer space of C-S-H, the two most plausible uptake mechanisms proposed in literature are [55] (i) substitution of a Ca^{2+} in the interlayer and (ii) occupation of vacant sites. However, Lognot and coworkers [59] reported that the substitution of Ca^{2+} in the interlayer would be the dominant mechanism for C-S-H with Ca/Si ratios around 1.5 (commonly found in cement pastes).

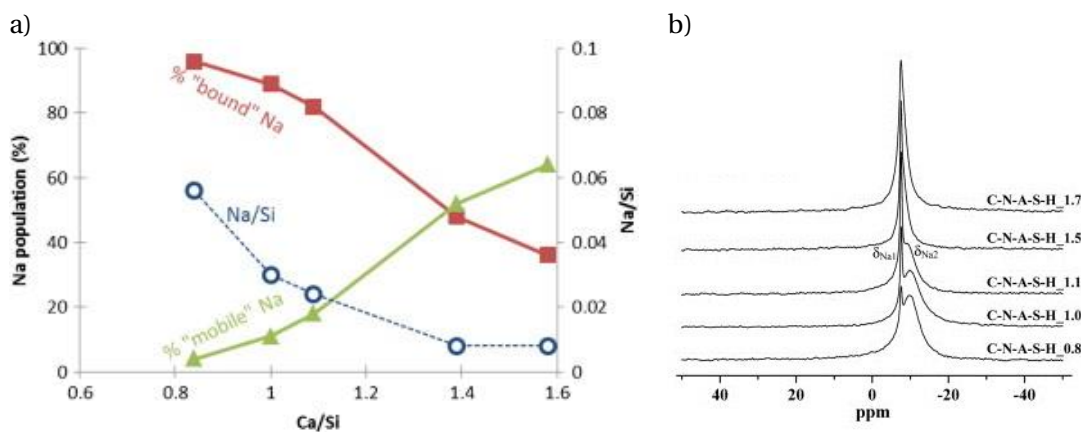


Figure 2.17. a) Relative fraction of signals observed by Renaudin et al [58] but plotted by Lothenbach and Nonat [22] as a function of the Ca/Si ratio of synthetic C-S-H. b) ^{23}Na NMR spectra from samples belonging to the C-A-S-H series with Na [58], where the sharp resonance is assigned to Na in the surface and the broader signal Na in the interlayer.

² Alkali ions compete with calcium ions to compensate the negative charge of C-S-H, although bivalent cations such as calcium are preferred compared to monovalent sodium [22].

Most of studies reported in literature about the uptake of alkalis on C-S-H are based on synthetic C-S-H with low Ca/Si ratios, but in cement pastes the Ca/Si ratio is high (≥ 1.5), corresponding to a type of C-S-H where the dreiketten chains are mainly dimers as there is a complete omission of all bridging tetrahedra [24]. At such high concentrations of calcium ions the uptake of alkali is reported to be suppressed and the changes in the structure of C-S-H are negligible [22,53,56]. However, García-Lodeiro and coworkers [60] found that C-S-H synthesised with Ca/Si ratio 1.9 in the presence of NaOH favoured the formation of Na-containing C-S-H (detected with Fourier Transform Infrared Spectroscopy). The interaction mechanisms between alkali and C-S-H with high Ca/Si ratios are not well understood yet, as assumed in some studies [61].

At the same time, it is worth noting that the comparison between results obtained on synthetic systems and on more realistic systems like cement pastes is not straightforward. For instance, in cement pastes there is the influence of other ionic species and the effect of alkali could be modified depending on the other ions in the pore solution.

3. The impact of sulfate in cement hydration

Sulfate ions control the dissolution of C_3A and they may come from different sulfate sources: gypsum, anhydrite, basanite, sodium sulfate and other sulfated salts, among others. It is important that the aluminate reaction occurs during the deceleration period to contribute to the strength development by one day [62]. Sulfate ions can change the ionic concentrations in the pore solution, the properties of C-S-H surface, the morphology of different hydrates and can also negatively affect the mechanical properties when the sulfate content is beyond the optimum content. For this reason, and to better understand the combined effect of alkali combined with sulfate, this section focuses on the impact of sulfate ions on C-S-H and Portlandite.

The effect of sulfate on C-S-H

Zeta potential experiments on C-S-H with increasing sulfate concentration in solution have shown that sulfate are adsorbed on the surface of C-S-H [63]. This is a surface phenomenon as the sulfate uptake does not modify the structure of C-S-H. Sulfate ions can be physically adsorbed as a result of the charges affinity. The negative surface of C-S-H attracts the positive divalent Ca^{2+} ions leading to a charge reversal in the surface of C-S-H (apparent positive surface charge) [20,64]. This “apparent” positive surface then attracts SO_4^{2-} ions from the solution. It has been shown that there is a coupled adsorption of sulfate and calcium ions [65,66]. The amount of sulfate uptake in C-S-H increases with the Ca/Si ratio of the C-S-H [66]. Microanalysis on the C-S-H showed that the sulfate content measured as S/Ca ratio decreases during the deceleration period [67], confirming that sulfate ions desorb when the sulfate concentration in solution drops, due to the depletion of gypsum, and can form ettringite. Thus, ettringite continues to precipitate despite the calcium sulfate being depleted [27,67,68]. However, there is no clear study in the literature about the impact of sulfate ions in the morphology of C-S-H.

The effect of sulfate on the morphology of portlandite

Several authors [47–49] reported that sulfate promote the same effect as alkali but to a lesser extent, leading to smaller but more abundant particles of portlandite but less significant as in the presence of alkali. Galmarini and coworkers [49,50] recently observed that the presence of sulfate promotes the formation of hexagonal platelets, indicating a speed-up of growth in [10.0] direction and slow-down in [00.1] direction, which agrees with previous results from Berger and McGregor [47]. Also, sulfate promote a preferential growth of portlandite in the neighbourhood of gypsum crystals [48].

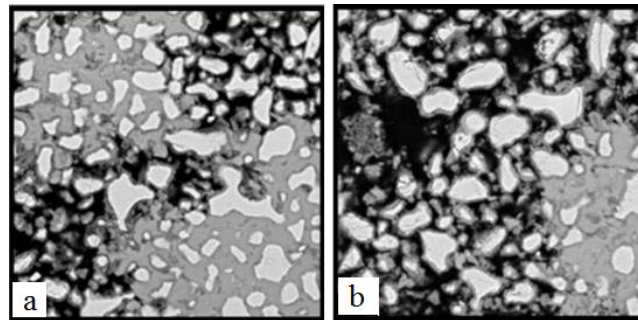


Figure 2.18. Morphology of CH at 1 day in a) C_3S plain paste and b) with 5 wt.% gypsum [48].

Besides sulfate, there are other components that can be added in cement systems and alter the effect of alkali salts. For instance, the addition of retarders is known to retard the early reaction of cement, and this could interfere with the previously mentioned acceleration effect induced by alkali salts also at early ages. In the present work, the impact of sodium gluconate combined with Na_2SO_4 is studied. Therefore, the next section focuses on the impact of sodium gluconate on cement hydration.

4. Sodium gluconate

While alkali salts are commonly found to accelerate the hydration of cement, retarding admixtures are commonly used to control the setting time of cement. Sodium gluconate ($NaC_6H_{11}O_7$) belongs to the group of hydroxycarboxylic acids. It is very soluble in water and leads to a greater retardation compared to other gluconates such as potassium gluconate, magnesium gluconate or calcium gluconate [69]. Sodium gluconate allows better workability of cementitious systems. The induction period can be controlled between 4 and 55 hours with 0.05 to 0.15% of sodium gluconate. The exact retarding effect is dependent on temperature, w/c ratio, cement type, among others [70]. Hydroxycarboxylic acids are commonly used as retarders but have secondary effects as water reducers (bifunctional) [71].

It has been observed that sodium gluconate retards the hydration at early ages. The higher the dosage of sodium gluconate, the more the early retardation in cement (as shown in Figure 2.19). Also, the reaction of C_3A in presence of sulfate was significantly retarded with the addition of sodium gluconate [69,72]. Due to the retardation effect, the setting time is delayed [73,74]. There is a lack of knowledge of the impact of sodium gluconate at later ages and on the mechanical strength.

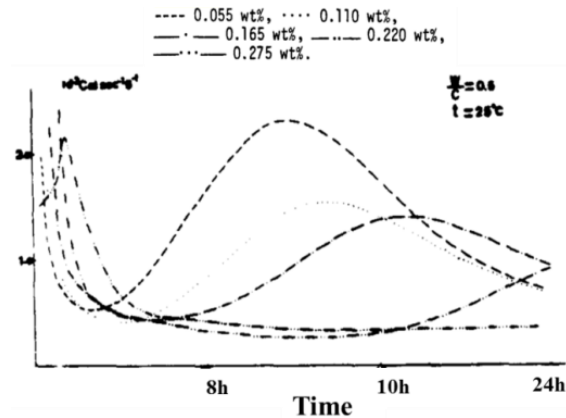


Figure 2.19. Effect of different dosages of sodium gluconate on the early hydration of a cement paste, adapted from Singh [69].

Although retarders have been extensively studied to explain the how they interact with cement, there are still many open questions as one retarding admixture can act by more than one type of interaction. The main reaction mechanisms between retarders and cement can be found in [72,75,76]. The most referred to are complexation, adsorption on the surface of cement grains and poisoning of the nucleation and/or growth of C-S-H and/or portlandite. A complete understanding of the mechanisms that take place with the addition of sodium gluconate is out of the scope of this project.

5. Summary

The present literature review demonstrates that, notwithstanding extensive effort, the effect of alkalis on the kinetics, microstructural development and strength is not fully explained. The open questions that require more in-depth research and that justify this work are the following:

- Although it is generally reported that the mechanical strength decreases in the presence of alkali salts, the mechanisms behind this effect are not clear and most hypotheses in the literature are purely speculative.
- The impact of alkalis on the porosity and the final mechanical properties has not been systematically studied.
- A change in the morphology of C-S-H in the presence of alkalis is suggested to explain differences in the porosity and thus on the strength development, but there has been no systematic study to prove it. The impact of alkali combined with sulfate should be considered.
- Most of studies on the characterization of C-S-H in the presence of alkalis have been done on diluted systems. Although they provide an extensive knowledge on the composition and structure of C-S-H, as well as suggestions to make progress in this area, further research on cement pastes is needed.
- There is a need to work on systems in which the effect of alkalis is an isolated parameter, i.e. doing experiments on cements that have a very low content of alkali.

CHAPTER 3. Materials and methods

1. Materials	23
1.1. Alite	23
1.2. White Portland cement	25
1.3. Slag.....	27
2. Experimental methods	28
2.1. Preparation of alkali solutions.....	28
2.2. Preparation of pastes.....	28
2.3. Preparation of mortars.....	29
2.4. Methods to monitor the kinetics of reaction	30
2.5. Methods to assess the microstructural development	31

This chapter includes the characterization of raw materials and the description of the methods used in this work.

1. Materials

1.1. Alite

Two batches of alite (impure C_3S , monoclinic) were synthesized in the laboratory by mixing 81.4 wt.% calcium carbonate (precipitated GR for analysis, Merk), 16.6 wt.% silica (highly dispersed extra pure, Merk), 1.3 wt.% magnesium oxide (GR for analysis, Merk) and 0.6 wt.% aluminium oxide (anhydrous, Merk). Powders were homogenized for 24 hours in a ball mill with deionized water and the blend was dried at 90°C for 24 hours. The dried mass was pressed into pellets and burned at 1500°C for 8 hours. The pellets were quenched in air, ground using a ring grinder and sieved at 100 μ m.

The capacity of the crucible of the furnace used for this work was 1.5 kg. Therefore, as the total amount of alite needed for all the experiments was bigger than 1.5 kg, two batches of alite had to be synthesized separately. Batch A was used for calorimetry, TGA and microscopy analysis. Batch B was used for the mechanical strength tests and MIP experiments. The PSD (Figure 3.1) of both batches are very similar. The morphology of alite particles is shown in Figure 3.3. Small particles resulting from the grinding process are apparent on the surface of the larger grains.

The calorimetry curves (Figure 3.2) show that the hydration rate of the Batch A is slightly higher than the Batch B. However, these differences at early ages have a minor impact on the DoH at later ages. Therefore, the two batches of alite were considered to be comparable. Free lime was not detected in the XRD patterns for either Batch A and B, it may be considered to be under the detection limit in both cases (<0.5wt.%).

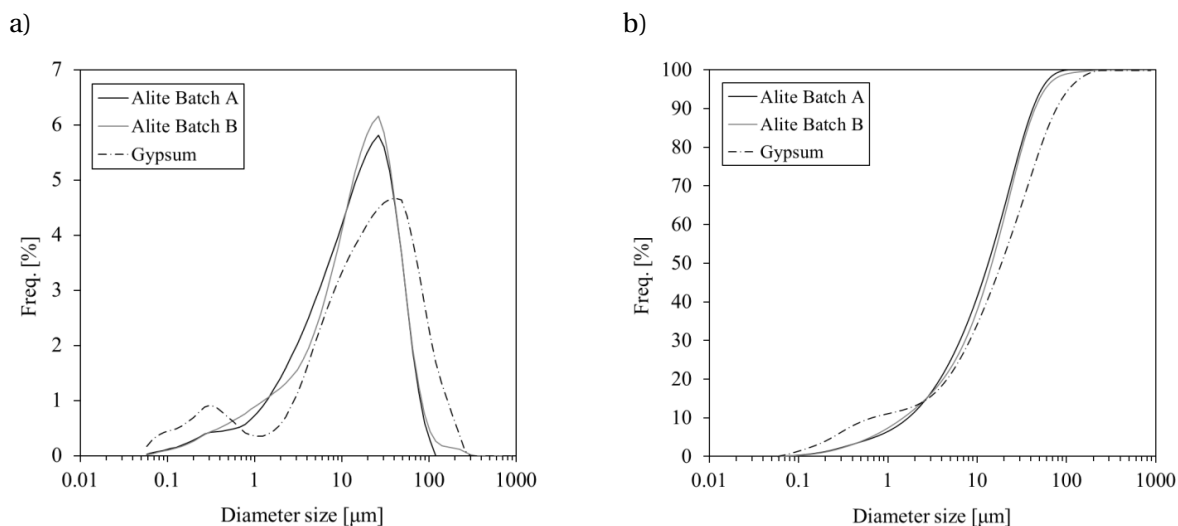


Figure 3.1. a) Differential and b) cumulative PSD of alite and gypsum.

Table 3.1. $d(10)$, $d(50)$ and $d(90)$ for each batch of alite and gypsum.

	Diameter size [μm]		
	Alite Batch A	Alite Batch B	Gypsum
$dv(10)$	1.7	1.5	0.7
$dv(50)$	13.2	15.2	19.3
$dv(90)$	42.4	44.8	76.5

Note: $dv(x)$, size where x % of the volume of the particles are less than this size.

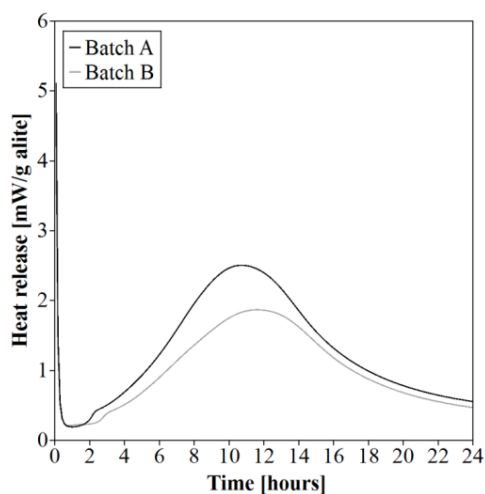


Figure 3.2. Calorimetry curve of the two batches of synthesized alite.

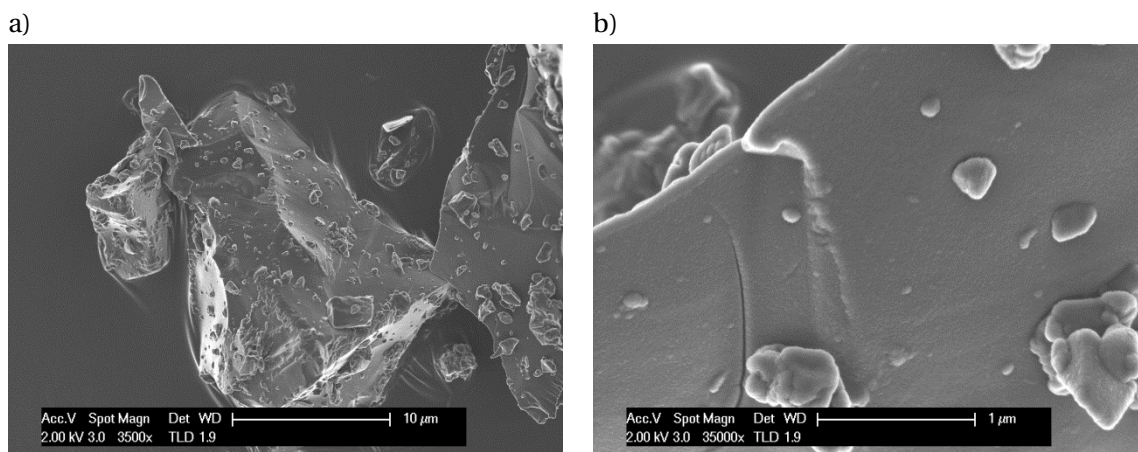


Figure 3.3. a) Alite grain and b) detail of the surface. Small particles result from the grinding process.

1.2. White Portland cement

White Portland cement was used in this study to minimise the excess of paramagnetic species (e.g. Fe^{3+} ions) that can enhance relaxation in ^1H NMR experiments. It only contains 0.32 wt.% of Fe_2O_3 . Moreover it contains a low amount of alkali oxides, which is an advantage to study the impact of alkali salts on the hydration of cement. Table 3.2 shows the mineralogical composition (by XRD-Rietveld) of the white Portland cement used and Table 3.3 shows the oxide composition (by XRF) of the cement.

Table 3.2. Mineralogical composition of white Portland cement by X-ray diffraction and Rietveld.

Anhydrous phase	Content [wt.%]
C_3S	72.4
C_2S	18.6
C_3A	3.5
Gypsum	1.2
Basanite	2.3
Other species	1.7

Table 3.3. Oxides composition of white Portland cement by X-ray Fluorescence (in wt.%). Total alkali content ($\text{Na}_2\text{O}_{\text{eq}}$) calculated as $\text{Na}_2\text{O}_{\text{eq}} = \text{Na}_2\text{O} + 0.658 \times \text{K}_2\text{O}$.

Oxide	White cement
SiO_2	24.40
Al_2O_3	2.16
Fe_2O_3	0.32
CaO	68.12
MgO	0.56
SO_3	1.94
Na_2O	0.05
K_2O	0.06
$\text{Na}_2\text{O}_{\text{eq}}$	0.09

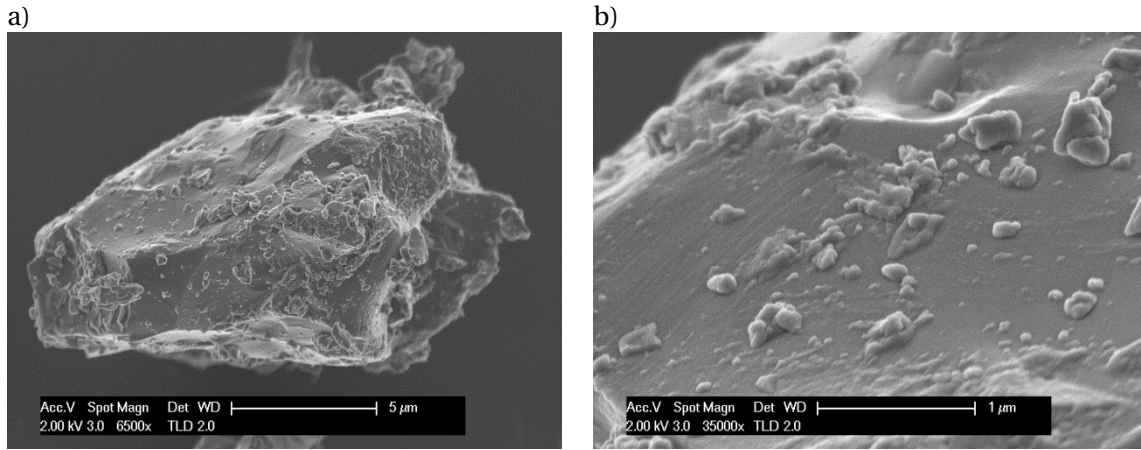


Figure 3.4. a) Grain of white cement and b) detail of the surface of a white cement grain.

Alite and cement: difference in particle size distribution

Alite has a coarser particle size distribution than cement. It results from the synthesis and grinding in the laboratory. The main difference is the amount of very fine material, which is not well estimated by the $d(50)$. Considering $d(10)$ as a representation of the finer particles it is lower for the white cement compared to alite: $d(10)_{\text{white cement}} = 1.0 \mu\text{m}$, $d(10)_{\text{alite}} = 1.7 \mu\text{m}$.

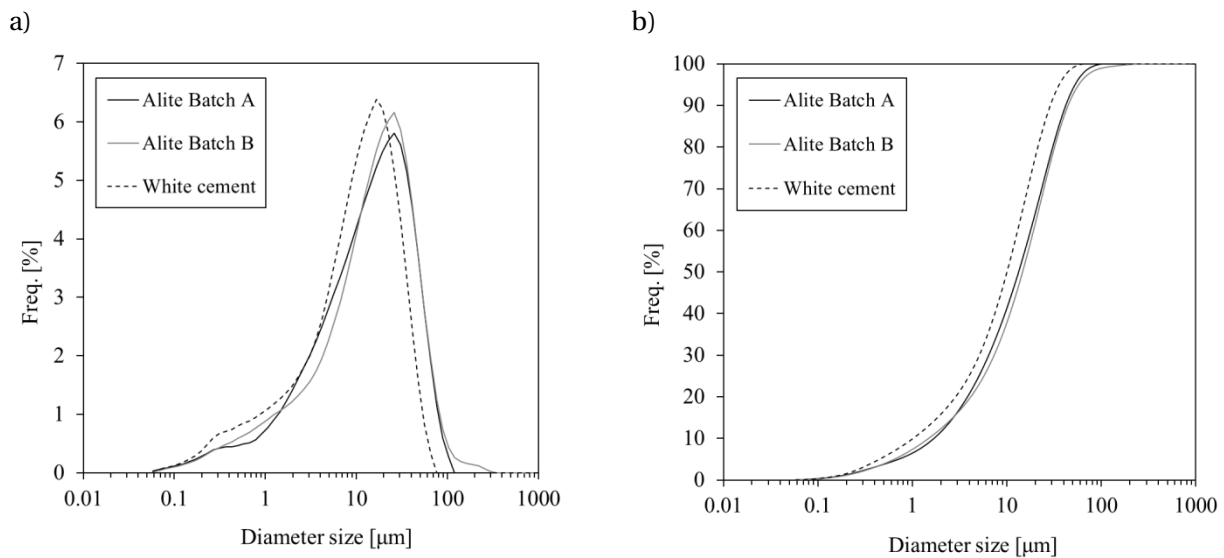


Figure 3.5. a) Differential and b) cumulative PSD of alite (batches A and B) compared to white cement.

Table 3.4. $d(10)$, $d(50)$ and $d(90)$ for each batch of alite and white cement.

	Diameter size [μm]		
	Alite Batch A	Alite Batch B	White cement
$dv(10)$	1.7	1.5	1.0
$dv(50)$	13.2	15.2	9.8
$dv(90)$	42.4	44.8	29.1

Note: $dv(x)$, size where x % of the volume of the particles are less than this size.

1.3. Slag

For the white cement blended systems, two types of slag were used as the replacement SCM. The slags were chosen to have different aluminium oxide contents. The PSD is comparable to the PSD of cement.

Table 3.5. Oxides composition of slag 1 and 8 by X-ray Fluorescence (in wt.%).

Oxide	Slag 1	Slag 8
SiO ₂	35.72	34.09
Al ₂ O ₃	11.94	19.87
Fe ₂ O ₃	0.84	0.45
CaO	41.38	33.01
MgO	7.45	9.73
SO ₃	1.38	0.75
Na ₂ O	0.26	0.25
K ₂ O	0.27	0.84
Na ₂ O _{eq}	0.43	0.80

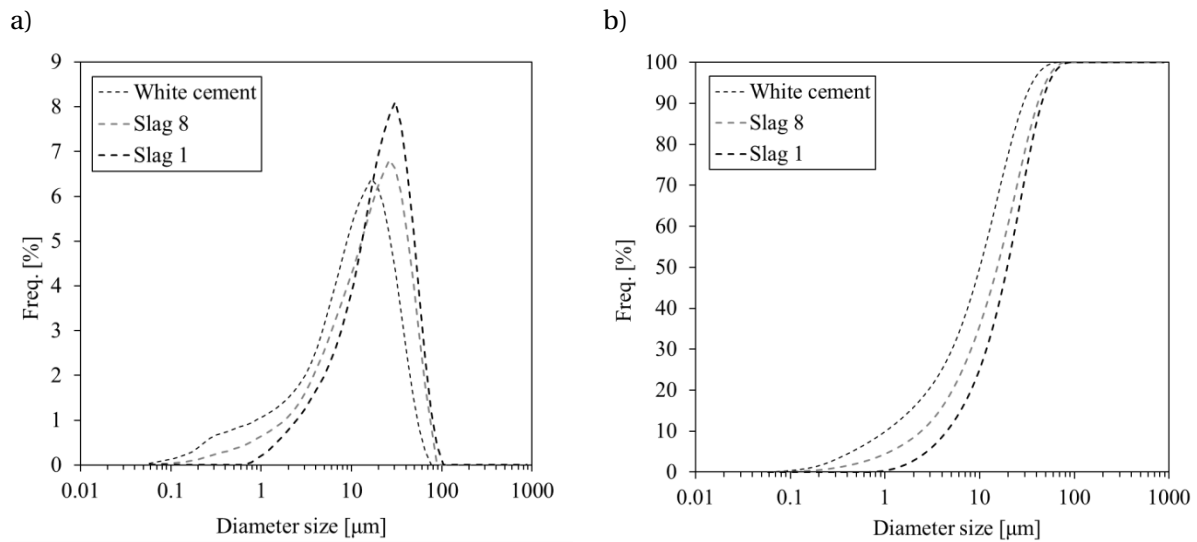


Figure 3.6. a) Differential and b) cumulative PSD of slag compared to white cement.

Table 3.6. $d(10)$, $d(50)$ and $d(90)$ for white cement, slag 1 and slag 8.

	Diameter size [μm]		
	White cement	Slag 1	Slag 8
dv(10)	1.0	2.46	4.1
dv(50)	9.8	15.4	20.2
dv(90)	29.1	39.5	45.1

Note: dv(x), size where x % of the volume of the particles are less than this size.

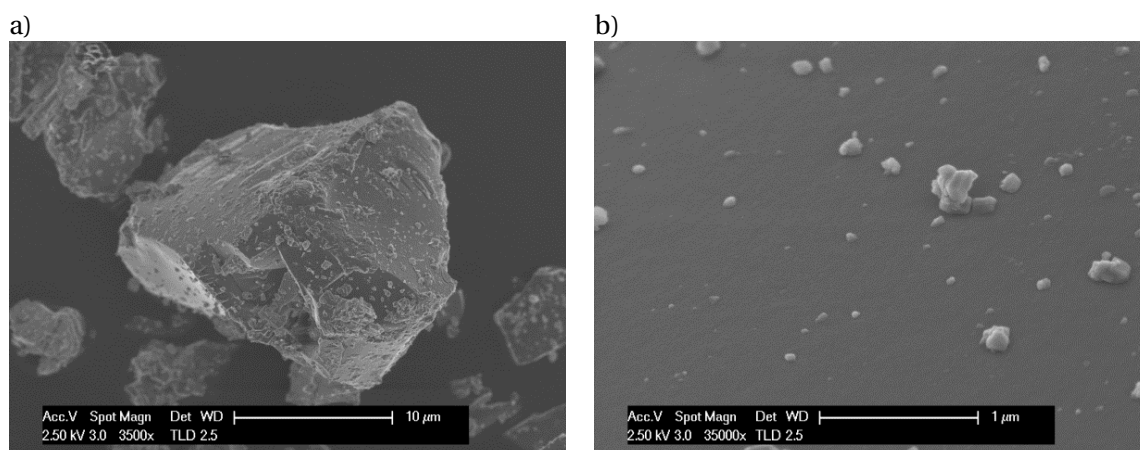


Figure 3.7. a) Slag grain and b) detail of the surface.

2. Experimental methods

2.1. Preparation of alkali solutions

NaOH (>98%, Reagent grade, Sigma-Aldrich) and/or Na₂SO₄ (>99%, ReagentPlus, Sigma-Aldrich) were dissolved in water prior to the mixing to ensure a homogeneous distribution. The compositions were selected to be equivalent in sodium content. They were freshly prepared before each experiment.

2.2. Preparation of pastes

Alite pastes

These were prepared at constant water to solid ratio (w/s) of 0.35 using de-ionized water (DI-water) or the appropriate aqueous solution. When required, 5 wt.% (of alite mass) of gypsum (>98%, AcrosOrganics) was added. The pastes were mixed 2 minutes by hand due to small amounts available. The samples were stored at 20°C in sealed conditions in individual plastic containers (well-sealed with parafilm) for each testing time to be analyzed to minimize exposure to the air and limit carbonation.

White cement pastes

Both cement or cement-slag pastes were prepared at constant water to solid ratio (w/s) of 0.4 using de-ionized water (DI-water) or the appropriate aqueous solution. The pastes were mixed for 2 minutes at 1600 rpm. They were stored at 20°C in sealed conditions in individual plastic containers (well-sealed with parafilm) for each testing time to be analyzed to minimize exposure to the air and limit carbonation.

2.3. Preparation of mortars

Alite mortars

As the production of alite is time-consuming mechanical tests were made on small $10 \times 10 \times 40$ mm mortars prisms. Tests were done with a standard grey cement to determine the number of specimens needed to give a reasonable coefficient of variation (Figure 3.8 shows that with 12 prisms the variation is reasonable).

12 prisms were cast for each testing time with sand:alite ratio = 3:1. 12 prisms of $10 \times 10 \times 40$ mm were tested for the flexural strength and 24 prisms of 10×10 mm section for the compressive strength. The water to solid ratio was 0.5 (due to the ITZ this is roughly equivalent to $w/s=0.4$ in pastes). The sand size was limited to $\varnothing < 2$ mm to avoid segregation. Compressive and flexural strength measurements were carried out at 1, 2, 3, 7, 14, 28 and 90 days. The error bars in the graphs with compressive and flexural strength tests of this work represent one standard deviation on the average of several measurements.

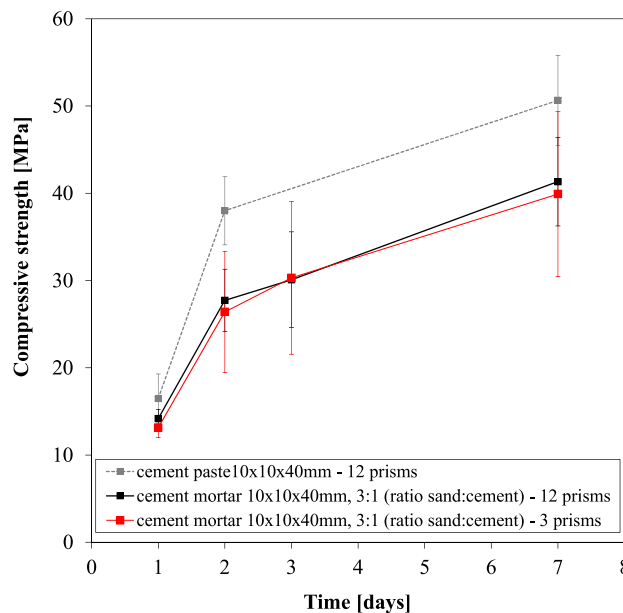


Figure 3.8. Tests with standard grey cement (on mortars and cement pastes of $10 \times 10 \times 40$ mm) to determine a reasonable coefficient of variation. With 3 prisms the error was still too large.

White cement mortars and white cement-slag mortars

Mortar prisms were prepared according to EN-196. 2 prisms of $160 \times 40 \times 40$ mm were tested for the flexural strength and 4 prisms of 40×40 mm section for the compressive strength. Flexural and compressive strength measurements were carried out at 1, 2, 3, 7, 14, 28 and 90 days. The error bars in the graphs with compressive and flexural strength tests of this work represent the standard deviation of the results.

2.4. Methods to monitor the kinetics of reaction

2.4.1. Isothermal calorimetry

The heat release was recorded with an isothermal calorimeter (TAM Air, Thermometrics). This technique records the heat released by the exothermic reactions of cement hydration and compares it to a reference sample. The reference sample should have a constant heat capacity similar to the measured sample. For this study the reference sample is deionized water. The amount required is determined as

$$m_{water\ ref} = \frac{C_{p\ paste} \times m_{paste}}{C_{p\ water}} \quad [Eq. 3.1]$$

Where C_p is the mass heat capacity of the material ($C_{p\ water} = 4.18 \text{ J} \cdot \text{g}^{-1} \cdot \text{K}^{-1}$)

The heat release at early ages can provide information about the dissolution of each anhydrous phase and the overall heat flow provides information about the degree of hydration of the system.

Sample preparation

10 grams of paste were placed in glass vessel and then into the calorimeter. The ambient temperature was 20°C to ensure the stability of the baseline. The measurements were carried out for 28 days. Beyond this time the heat released by the exothermic reactions is too low to be reliable.

2.4.2. Chemical composition of the pore solution

Cations (X^+)

The cation concentrations in the extracted pore solution was analysed with inductively coupled plasma/ optical emission spectroscopy (ICP/OES, Shimadzu ICPE 9000) at the Central Environmental Laboratory of EPFL. The solution is nebulized into a plasma source of Argon. The elements of the solution are released as free atoms which convert to excited ions. Their relaxation emits a photon at a characteristic wavelength that can be used to identify the elements from the initial solution. The standard error of this technique is ~10%.

Anions (X^-)

The concentration of anions (here just sulfate ions) was analysed with anion-exchange chromatography (IC, Dionex ICS-3000) at the Central Environmental Laboratory of EPFL. Substances from the solution can be separated based on their charges using an ion-exchange resin containing positively charged groups. Each type of anion is associated to a release time. The standard error of measurement of this technique is ~10%.

Sample preparation

The same procedure is valid for the analysis of cation and anions. Cement paste was cast into plastic bottles (35 mm Ø, 50 mm height) and stored in sealed conditions at 20°C. The pore solution was extracted at the desired time using a steel die device. 70 kN of pressure was applied for early age samples and 1200 kN for later age samples. The liquid extracted was filtered with a 0.2 µm filter and 3.3 mL were diluted in a solution acidified with HNO₃ to prevent precipitation.

2.4.3. Chemical shrinkage

Chemical shrinkage is related to the volume changes during the hydration process. The volume of the hydrates is lower than the initial volume of the reactants (i.e. water, cement, SCM). This effect is due to the water binding in the hydrates which decreases the total volume.

Sample preparation

About 3 grams of mixed paste was placed into a plastic cylindrical bottle (2 cm of diameter, 5 cm height). The thickness of the paste was kept constant and thin enough to ensure the complete percolation (<1cm)[77]. To remove all the entrapped bubbles in the paste, the bottle was tapped manually and placed in an ultrasonic bath for 30 seconds. Then water was added drop by drop to minimize the disturbance of the top layer of the paste. Once the bottle was completely filled with water, it was sealed with a rubber stopper with a 10 mL pipette passing through it. The sealed system was maintained straight for a couple of minutes. On the top of the water level, few drops of coloured oil were added with a syringe. The bottles were placed in a water bath at 20°C. The level of the colored oil was recorded automatically over 28 days. Three replicates for each system were prepared. The level of water in the pipette was similar for all the samples.

2.5. Methods to assess the microstructural development

2.5.1. Microstructure at early age

The surface of the grains was observed at different times during hydration, with a FEI XLF-30 SFEG-SEM in secondary electron mode. The microscope parameters are shown on the micrographs. For both techniques, the hydration was stopped by solvent exchange with isopropanol.

Sample preparation

For the SEM-SFEG specimens, 0.5 g of the paste was taken out from the sealed sample at the required times and put in a filtrating funnel with two filter papers (retention $\varnothing \geq 5 \mu\text{m}$). The funnel was immediately filled with isopropanol and the sample was continuously stirred in the funnel for 3 minutes. This procedure was repeated 4 times to ensure the maximum removal of water. The powder from the filter was collected and further stored for 1 day under vacuum to remove the isopropanol. The dried powder was dispersed on an adhesive carbon tab and coated with a carbon layer of 10-15 nm. This procedure is summarized in Figure 3.9.

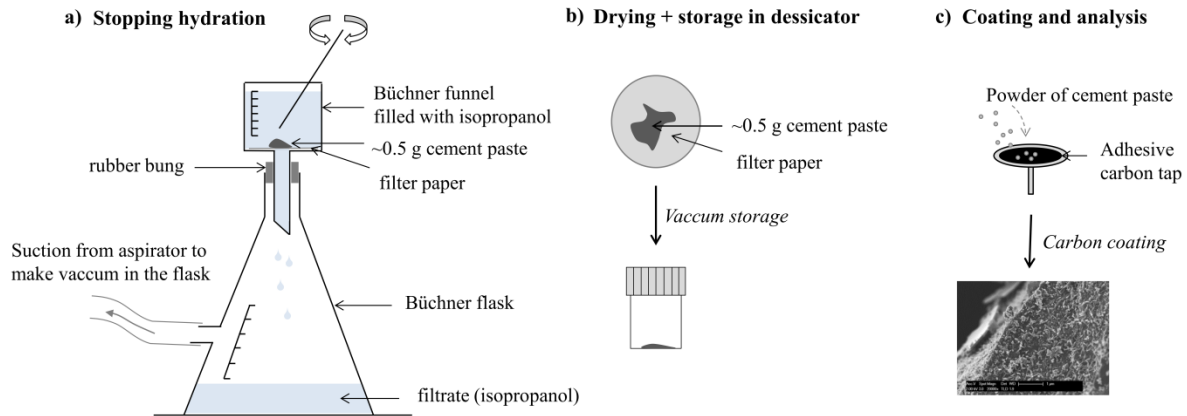


Figure 3.9. Schematic description of the preparation of samples to be analysed at early ages with SFEG.

2.5.2. Polished sections at later ages

The overall development of microstructures was observed on polished sections with a FEI quanta 200 SEM microscope in backscattered electron mode. EDX measurements were done with a Bruker AXS XFlash detector for Energy dispersive X-ray analysis.

Sample preparation

A slice was cut (~2 mm thick) at the required time and hydration was stopped by immersion in isopropanol for 7 days (exchanging the solvent twice during the first 24h), and further vacuum drying for 2 days. It was followed by impregnation in a low-viscosity epoxy resin, polishing with a diamond powder down to 1 μm and carbon coating.

2.5.3. Energy dispersive X-ray spectroscopy

Quantitative analysis of the chemistry of the sample can be achieved with the X-ray emitted from the interaction of the primary electrons and the sample. Each element produces an X-ray with a specific energy which allows the identification and quantification of each element. However as X-rays interact with the bulk sample, the volume of interaction has to be carefully considered. Basically the volume is about several μm in size. Nevertheless it has been demonstrated that EDS measurements done on SEM samples are in very good agreement with EDS on TEM sample where the volume of interaction is significantly limited [78].

EDS is widely used in hydrated cement to determine the composition of the C-S-H from atomic ratio scatter plots. C-S-H has a variable chemical composition and EDS provides information on the stoichiometry of the components. Figure 3.10 shows a typical atomic ratio scatter plot of Al/Ca versus Si/Ca. Each point represents one measurement. All the measurements give a cloud which represents the variability of the C-S-H composition in the sample. The extreme point of the cloud (for the highest Si/Ca) indicates the purest C-S-H composition (red point in Figure 3.10) [78]. In the present work, (Ca-S) is also used to focus on the Ca in the structure of C-S-H rather than the co-adsorbed with sulfate through ion-ion correlations [48,66,67] and (Si+Al) to consider the replacement of silicon per aluminate.

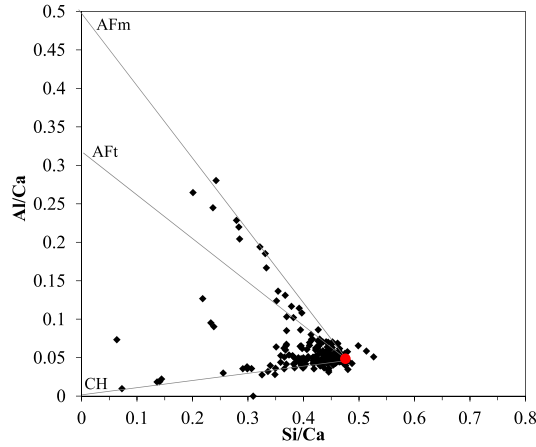


Figure 3.10. Determination of C-S-H composition from atomic ratio scatter plots.

2.5.4. Transmission electron microscopy (TEM)

TEM observations were carried out using a FEI Tecnai Osiris at an operating voltage of 80 kV in scanning TEM mode (STEM) with EDS mapping. Additional details in the procedure can be found in [78,79].

Sample preparation

Thin lamellae for transmission electron microscopy (TEM) were prepared by taking smaller pieces of dried paste and impregnating them using EMS Embed 812 resin. Each sample was then cut to a thin slice (of dimensions 1.7 mm × 1.7 mm × 0.7 mm) using a WELL diamond wire saw, thinned down mechanically to a bevel by mean of the Tripod method (supplied by ALLIED Tech) to yield a thickness of about 20–30 μm on the thick side. It was then glued to a copper ring, ion-thinned with an Argon PIPS (GATAN Precision Ion Polishing System Model 691) operated at maximum 1.5 keV to achieve electron transparency and coated with a 5 nm layer of carbon using a Cressington 208 high vacuum carbon coater. As a precaution, samples were coated only prior to observation in the TEM and were always stored in a high vacuum desiccator.

2.5.5. X-ray diffraction

Standard XRD measurements allow the identification of crystalline phases. Analysis were carried out with a Panalytical X'Pert Pro MPD diffractometer in a $\theta - \theta$ configuration using CuK α source with a fixed divergence slit size of 0.5°. The X-ray tube was operated at 45 kV and 40 mA. Phase identification and Rietveld quantitative phase analysis were carried out using the X'Pert High Score Plus software by PANalytical. The external standard method (rutile powder supplied by Kronos – 2300 Titanium dioxide) was used to quantify the phase content. The degree of hydration of the cement (DoH) was calculated as follows (the error bars of the DoH graphs in this thesis correspond to the instrumental error $\pm 3\%$):

$$DoH(t) = 1 - \frac{W_{anhydrous}(t)}{W_{anhydrous}(t_0)} \quad [Eq. 3.2]$$

Where, $W_{anhydrous}(t)$ is the weight fraction of the anhydrous clinker phases at the time of interest and $W_{anhydrous}(t_0)$ is the initial weight fraction of the anhydrous clinker phase. In the present study, the DoH was always calculated from fresh samples. Therefore, a correction of the dilution effect was not needed.

Sample preparation for fresh paste

The samples were cured at room temperature (20°C). Measurements were done on fresh paste samples (without stopping the hydration) to minimize damage/artifacts. One slice of the hardened paste was cut and slightly polished (to have a flat surface) at the required testing time and immediately inserted in the XRD holder. The slice was scanned on a rotating stage between 7 and 70 [°2 θ]. The X'Celerator detector had a step size of 0.0167°2 θ and a time per step of 30s. The measurement lasts about 15 min and the slice was near saturated after the test.

Sample preparation for insitu measurements

The paste was directly cast in the holder and carefully tapped to remove air bubbles. It was further protected with a kapton film to maintain the humidity during the hydration. The sample was placed in a chamber with temperature controlled at 20°C. XRD measurements were done each 15 minutes for 24 hours. The slice was scanned between 7 and 70 [°2 θ]. The X'Celerator detector had a step size of 0.0167°2 θ and a time per step of 30s.

2.5.6. Thermogravimetric analysis

Thermogravimetric analysis (TGA) were done using a Mettler Toledo TGA/SDTA851e using a 10°C/min ramp from 30 °C to 1000 °C under a 30 ml/min flow of N₂ to prevent carbonation. The tangent method was used to quantify portlandite from the dehydration peak between 450 and 600 °C in the derivative of the mass loss.

Sample preparation

After 7 days of immersion in isopropanol and further vacuum drying for 2 days, the sample was crushed to powder. 50 mg of powder were put in pure alumina crucibles covered with an aluminum lid to prevent carbonation.

2.5.7. ¹H NMR

¹H NMR measurements were made on a Bruker Minispec NMR spectrometer operating at 7.5 MHz. Both quadrature (solid) echo [80] and Carr–Purcell–Meiboom–Gill CPMG [81] (spin) echo measurements were carried out. The quadrature echo signals were deconvoluted into a Gaussian and an exponential decay part. The exponential fraction arises from the mobile water within the sample and is not pulse gap dependent. The Gaussian intensity decay is assigned to water in solid crystalline phases [12,82]. The amplitude of this component depends on the pulse gap. Pulse gaps were varied in the range 15–45 μ s and the amplitude was back extrapolated to zero pulse gap free from relaxation phenomena using Gaussian fitting. The mobile part of the signal was separately resolved into different T₂ components using the CPMG pulse sequence as in [12]. For this, the inverse Laplace transform (ILT) algorithm developed by Venkataramanan et al. [83] was applied to the CPMG echo intensity decay.

The combination of solid echo and CPMG pulse sequences allows the detection and quantification of all hydrogen protons within the cement paste, which are distributed among four water locations (as a function of their relaxation time): the chemically combined water in portlandite and ettringite ($I_{\text{solid}} = I_{\text{ett}} + I_{\text{CH}}$), C-S-H interlayer water ($I_{\text{C-S-H}}$), water in the C-S-H gel pores (I_{gel}) and water in larger capillary pores that become interhydrate spaces (I_{cap}). The resulting NMR signal fraction is the sum of all the mentioned intensities as $I_{\text{solid}} + I_{\text{C-S-H}} + I_{\text{gel}} + I_{\text{cap}}$. There are empty volumes created by the chemical shrinkage during the hydration because the paste is kept in sealed conditions, but those are not measure by ¹H NMR experiments.

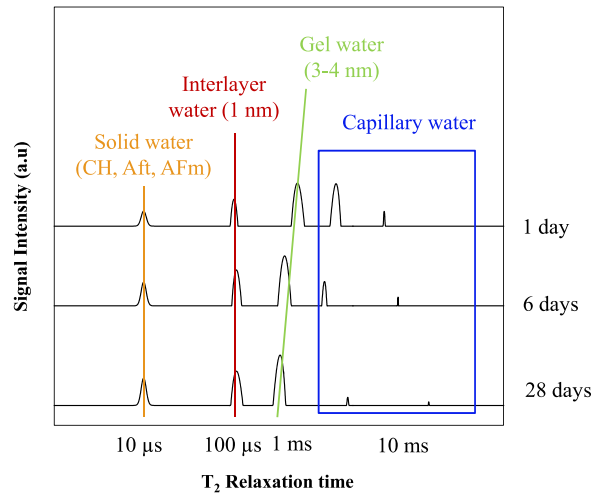


Figure 3.11. Relaxation time of each water population in a white cement paste at 1, 6 and 28 days. Adapted from [15].

For density calculation, the chemical shrinkage volume (normalised per gram of binder and expressed as the equivalent water fraction $I_{void} = \frac{V_{void}}{w/c}$; where I_{void} is the chemical shrinkage volume in cm^3 per gram of binder) and the DoH of cement calculated by XRD-Rietveld are required. The equations to calculate the mass balance and density of C-S-H as well as more details about the measurements, experimental parameters, analysis and interpretation of ^1H NMR are given in the work of Muller and coworkers [12].

Sample preparation

Aliquots about 0.35 cm^3 ($\sim 0.8 \text{ g}$ of paste) were deposited directly into NMR tubes and tightly sealed with parafilm to avoid any loss of water and keep a constant water to cement ratio of 0.4. Samples were stored in a temperature-controlled room at 20°C during hydration. Samples were measured at 28 days in a temperature-controlled NMR probe (without stopping hydration). Care was taken to ensure the reproducibility of the results across multiple repeated samples and repeated measurements.

2.5.8. Mercury intrusion porosimetry (MIP)

A mercury intrusion porosimeter from Thermoscience (Pascal 140/ 440) was used. MIP technique can measure the connected porosity. The pressure was increased up to 400 MPa which allows intrusion of pore entries down to nominally 2 nm radius (assuming a contact angle of 140°). From the resulting measurement two main values are used in this study: the cumulative pore volume curve and the pore entry size distribution. The first one is deduced from the intruded volume of mercury and gives the total connected pore volume in the entire specimen. This value can be read from the cumulative porosity for the smallest pore size. The differential distribution curve is calculated from the cumulative pore volume curve and clearly shows the “critical” radius of the sample (i.e. inflexion point in the cumulative curve [84]). The critical entry radius was used to characterize the pore entry size of the connected porosity.

Sample preparation

Fresh paste was cast into plastic containers (35 mm diameter, 50 mm height) and cured under sealed conditions at 20°C . At the required time of hydration, a slice was cut ($\sim 2 \text{ mm}$ thick) and the hydration was stopped by immersion in isopropanol for 7 days (exchanging the solvent twice during the first 24h), and further vacuum drying for 2 days. $\sim 0.7 \text{ g}$ of sample (cut into four small pieces) were used for MIP tests.

2.5.9. Humidity buffer method

This method was developed in the recent work of Baquerizo [85,86] under the principle of salt-hydrates pair which considers a thermodynamic equilibrium between hydrates and the water vapour pressure of the surrounding gas. However, for the purpose of using this method for the present study is to monitor the relative humidity of the pastes over time, which is mainly dependent on the concentration of ions in the pore solution (as shown below).

The relative humidity was monitored with a pen hygrometer (Testo 605-H1, accuracy $\pm 3\%$ RH, which corresponds to the error bars values of the RH graphs of this thesis). The device consists in a pen hygrometer tightly fitted a plastic container with the sample and fully sealed with parafilm and with insulating tape on top of it to avoid any leakage. The RH at which the combined system (water vapour and paste) reached equilibrium was recorded with the hygrometer. The system is closed and there is no exchange of water with the exterior; therefore, the relative humidity (RH) inside will be at equilibrium with the hydrated phases at the given temperature. Additional details in the procedure can be found in [85].

The RH of an air-water mixture is the ratio of the partial pressure of water vapour in the mixture to the equilibrium vapour pressure of water at a given temperature. When the RH of air is in equilibrium with a sample is called Equilibrium Relative Humidity (ERH). ERH is defined as follows:

$$ERH = a_w \times 100\%. \quad [Eq. 3.3]$$

And the water activity (a_w) is defined as the ratio between the actual contained water and the maximal water admissible by the fluid (up to the saturation limit) and ranges between 0 and 1 (0 being a fully dried fluid and 1 a saturated fluid). The water activity is directly related to the amount of ionic species in the fluid as expressed by the following equation:

$$a_w \equiv I_w \times x_w \quad [Eq. 3.4]$$

where I_w is the activity coefficient of water and x_w is the mole fraction of water in the aqueous fraction. Consequently, the higher the concentration of ions in the pore solution the lower the a_w .

Sample preparation

~10 grams of cement paste were placed inside a small container (20 ml glass bottles) and the hygrometer pen was tightened to the container with parafilm. The measurements were repeated twice for each sample to obtain a representative average value. A value of 100% RH at the very early age indicates a good calibration of the device.

2.5.10. Thermodynamic modelling

Gibbs Energy Minimization software (GEMS-PSI) [87–89] was used to estimate the concentration of aluminate ions in solution as well as the phase assemblage of different systems. The thermodynamic data for aqueous species and other solids is from the GEMS-PSI thermodynamic database [90] and the cemdata14 database for the solubility products of cementitious phases [91–93]. The extended Debye-Hueckel model was used for the calculations. The solid solution model for C-S-H recently suggested by Kulik [54] was considered. XRF analyses were used to create the new phases in GEMS corresponding to alite, white cement, slag 1 and slag 8. Further details of the input data for each calculation can be found in the corresponding experimental section.

The uptake of sulfate in C-S-H and the incorporation of alkali are not considered in the model. Due to the absence of alkalis in the thermodynamic model, the trends of the ionic concentrations in the pore solution calculated with GEMS are more reliable than the absolute amounts (which can differ from experimental measurements).

For alite and white cement systems (Chapters 4 and 5, respectively) GEMS was used as a proper thermodynamic calculation to calculate either the pore solution composition or the phase assemblage. On the contrary, in the case of white cement- slag systems (Chapter 6), the phase assemblage was not calculated using GEMS as a thermodynamic tool but rather a mass balance. The reason for this was that the amount of phases predicted with the simulation did not agree with XRD-Rietveld analysis. This strengthens the fact that GEMS is a very useful tool for thermodynamic predictions but the calculations (nature and amount of the phases) need to be validated by experimental analysis (e.g. XRD-Rietveld) to be sure that GEMS is representative of the real systems.

CHAPTER 4. The impact of NaOH, Na₂SO₄ and gypsum on alite hydration

1. Introduction	39
2. Systems studied	39
3. Results	40
3.1. Heat release and degree of hydration	40
3.2. Morphology of hydrates	44
3.3. Chemical composition of hydrates	50
3.4. Mechanical strength of alite mortars	53
4. Summary	57

1. Introduction

The effect of Na₂SO₄ and NaOH, as well as gypsum, on the degree of hydration (DoH) at later ages remains unclear as most studies are focused on the earlier stages of hydration. The study of a simplified system of cement such as alite may help to better understand the impact of alkali on more complex cementitious systems.

The present chapter aims to:

- Study the impact of Na₂SO₄ and NaOH, as well as gypsum, on the hydration kinetics of alite at early and also later ages and explain the mechanisms behind.
- Study the impact of Na₂SO₄ and NaOH, as well as gypsum, on the microstructural development of alite: the morphology of the main hydrates, the chemical composition of C-S-H and the strength development.

2. Systems studied

Table 4.1 shows the formulation of each studied system. The aim is to isolate the effect of gypsum, NaOH, Na₂SO₄ and to see the combined effect of gypsum and NaOH. The alkali free system is compared to alite systems with the addition of: i) gypsum, ii) Na₂SO₄, iii) NaOH plus gypsum and iv) NaOH.

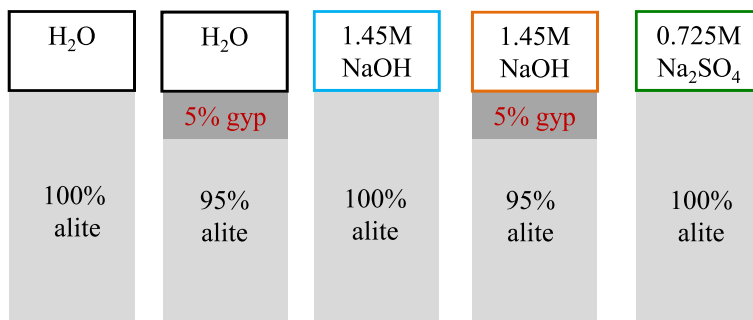


Figure 4.1. Composition of the alite-based mixes studied, in wt. %.

Table 4.1. Formulations of the alite-based systems studied.

Alite [wt.%]	Gypsum [wt.%]	Mixing solution	Nomenclature in figures
100	-	DI-water	alkali-free
95	5	DI-water	5G
100	-	1.45M NaOH	NaOH
95	5	1.45M NaOH	NaOH5G
100	-	0.725M Na ₂ SO ₄	Na ₂ SO ₄

3. Results

3.1. Heat release and degree of hydration

The addition of gypsum slightly lengthens the induction period compared to alkali free alite but it leads to a higher rate of hydration in the acceleration period and a higher peak (Figure 4.2) as previously reported by Quennoz and Scrivener [67]. The combined addition of NaOH and gypsum decreases the length of the induction period and leads to a higher main peak which occurs at an earlier time than in the alkali free systems. These effects are accentuated with the addition of Na₂SO₄. In the presence of NaOH, the induction period is almost non-existent. The time to reach the peak is much earlier but the peak is not as high as with a combination of sulfate and alkali. In previous papers [94,95] it was shown that the dissolution rate of alite could be understood in terms of the undersaturation of alite. Kumar and coworkers [95] showed that the results of Brown et al [96] on the kinetics in different solutions could be well captured by the fact that alkali ions (e.g. Na⁺) lower the concentration of Ca²⁺ ions in solution, thus the undersaturation with respect to alite is increased and so the dissolution rate. This effect outweighs the impact of increasing OH⁻ concentration on the undersaturation.

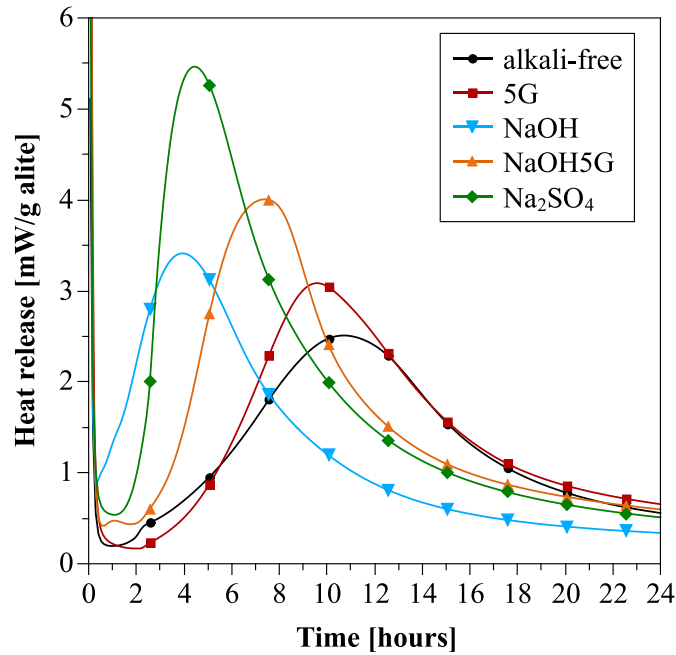


Figure 4.2. Effect of Na-salts and gypsum on the heat evolution rate of alite.

As it was impossible to measure the composition of the pore solution experimentally due to the small quantities of material, Gibbs Energy Minimization software (GEMS-PSI) [87–89] was used to estimate the pore solution composition in each system at early (during the nucleation and growth period) and later ages (25 days). The thermodynamic data for aqueous species and other solids is from the GEMS-PSI thermodynamic database [90] and the CEMDATA database for the solubility products of cementitious phases [91–93]. The ionic concentrations were calculated in order to know the concentrations of Ca, Si and Al (Figure 4.3 and Figure 4.4). For the early age, all the systems are simulated at 7% DoH, which corresponds to the end of the nucleation and growth (N+G) period. For later ages, at 25 days, the DoH of alite is calculated for each system from its cumulative heat evolution curve (shown in Figure 4.5): 58% DoH for the alkali free and NaOH5G systems, 54% DoH for the Na₂SO₄ and 5G systems, and 44% DoH for the NaOH system. For all the calculations the corresponding amount of unreacted alite is used as an input to calculate the composition of the pore solution at that DoH.

At both early (Figure 4.3a) and later (Figure 4.3b) ages, GEMS calculations indicate the highest aluminate ions concentration in the presence of only NaOH. In the systems containing sulfate the concentration of aluminate ions in solution is negligible. Phenomenologically it has been observed that the presence of aluminate ions in solution lowers the reaction rate of alite but the exact reasons for this are not known. On the one hand, it has been suggested by Begarin and coworkers [97] to be related to the poisoning of C-S-H in the presence of aluminate ions in solution but this does not agree with the present results because, as presented later (Figure 4.7 and Figure 4.9), we see an evidence of the growth of C-S-H over time during the N+G period (even if it contains Al, as shown later on in the EDS analysis in Figure 4.14 and Figure 4.15). On the other hand, it could be due to the inhibition of silica dissolution, as shown by Chappex and Scrivener [98]. Quennoz and Scrivener [67] also showed that the presence of aluminate ions in the alite suppresses the reaction of the alite in the absence of sulfate addition. This hypothesis seems to better agree with the present results: due to a higher solubility of aluminate ions in the presence of alkali, silica dissolution may be further inhibited. In the presence of sulfate (from gypsum and/or Na₂SO₄) and aluminate ions released from alite, aluminate precipitate as ettringite, which lowers the aluminate ions concentration of the pore solution. Recently, Suraneni and Flatt [99]

also suggested that the reduction on the dissolution should be due to an impact on the dissolution itself and not on the nucleation of C-S-H since the authors observed small particles of C-S-H when hydrating C_3S in the presence of aluminium in solution. Nicoleau and coworkers [100] reported that, as the pH increases, the inhibiting effect of aluminate is suppressed to a greater extent (through the addition of NaOH) in diluted systems based on C_3S as the formation of Si-O-Al bounds should not be favoured by increasing the pH. Differences between these observations and the present results could lie in the fact that the authors worked on diluted systems instead of pastes.

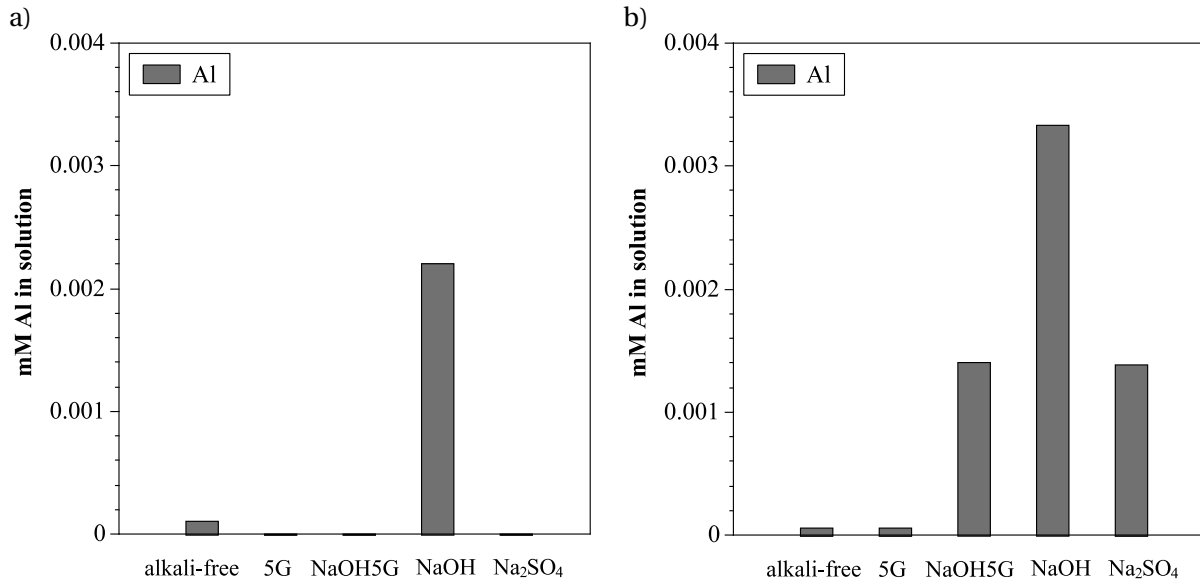


Figure 4.3. Al content in the pore solution calculated by GEMS at a) 7% DoH and b) 25 days of hydration.

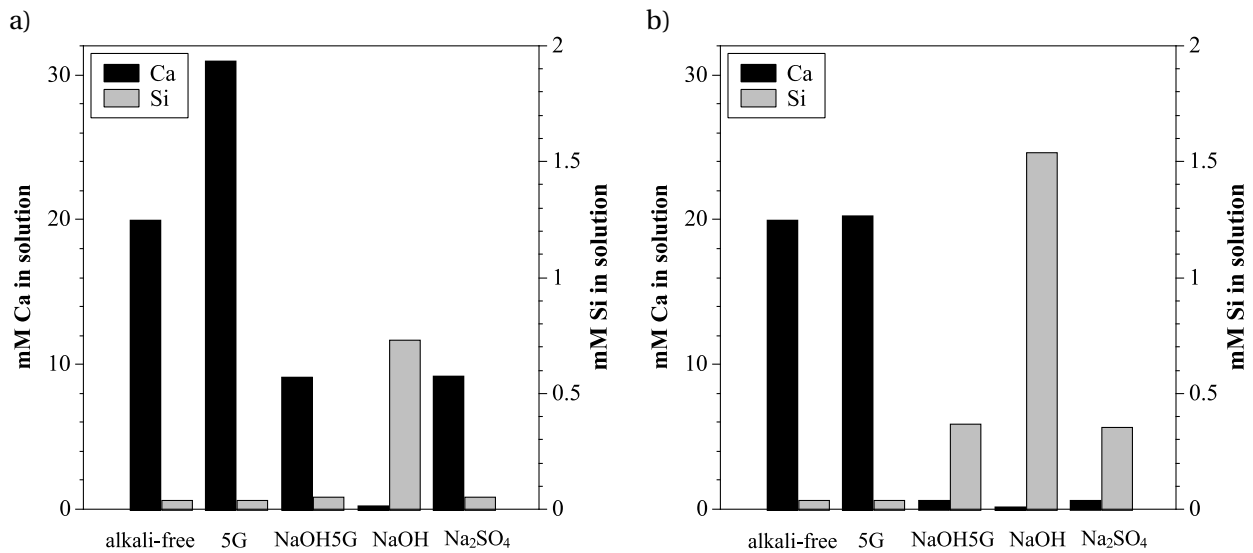


Figure 4.4. Ca and Si content in the pore solution calculated by GEMS at a) 7% DoH and b) 25 days of hydration.

Figure 4.5 shows the DoH calculated from the cumulative heat evolution curves. Compared to alkali free alite the addition of NaOH leads to a very fast initial reaction until ~20 hours of hydration. After ~20 hours the hydration of alite in presence of NaOH becomes significantly slower than the alkali free alite mixed with water. The presence of gypsum has a minor impact on the initial hydration kinetics but seems to further accelerate alite consumption at intermediate times between ~10 hours and 300 hours. The presence of Na₂SO₄ accelerates the hydration of alite significantly. Whereas alkali free alite samples or those with only gypsum need ~10 hours to reach a DoH of ~10%, the Na₂SO₄ sample achieved that in only 5 hours. In contrast to the pure NaOH sample, the hydration of alite in presence of Na₂SO₄ remained faster than alkali free alite until ~300 hours. The addition of gypsum to NaOH cancels out the negative impact of pure NaOH at later hydration stages. Nevertheless, with a combined addition of NaOH and gypsum, hydration was still slower compared to the Na₂SO₄ sample with equivalent amounts of sodium and sulfate. Highly soluble sulfate, e.g. Na₂SO₄, can accelerate ettringite formation which in turn would then lead to a faster removal of aluminate ions from the solution. This may explain the differences in heat release between the system with Na₂SO₄ and the one with NaOH plus gypsum. At later ages (from ~300 hours) all the systems progressively catch up and achieve similar DoHs at the end of the measurement period, except for the system with only NaOH.

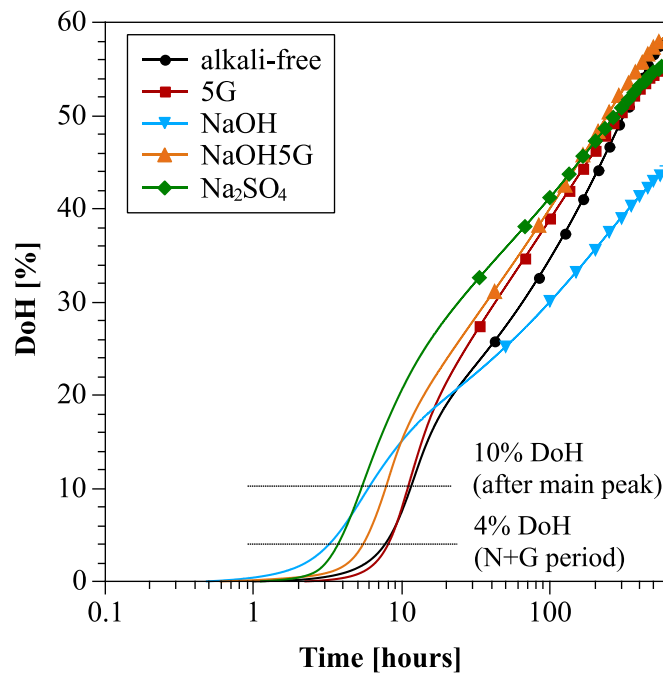


Figure 4.5. Effect of Na-salts and gypsum on the DoH of alite (calculated from calorimetry) up to 25 days. Dotted lines correspond to the DoH at which hydration was stopped to analyse the surface of the grains.

Note: It is worth noting that the DoH of alite is lower than in typical cement systems. Alite reaches ~10% DoH at the peak while in the case of cement it would be around 30%. The main difference is the amount of very fine material (for further details, see Appendix A and the characterization of both materials in Chapter 3). Differences in microstructure, heat release and porosity between alite and white cement are detailed in Appendix A.

3.2. Morphology of hydrates

The morphology of the hydrates was studied at two DoHs: 4 % corresponding to the nucleation and growth period of the calorimetry curve, and 10% corresponding to some minutes after the main hydration peak. The respective times of hydration are indicated in Figure 4.6.

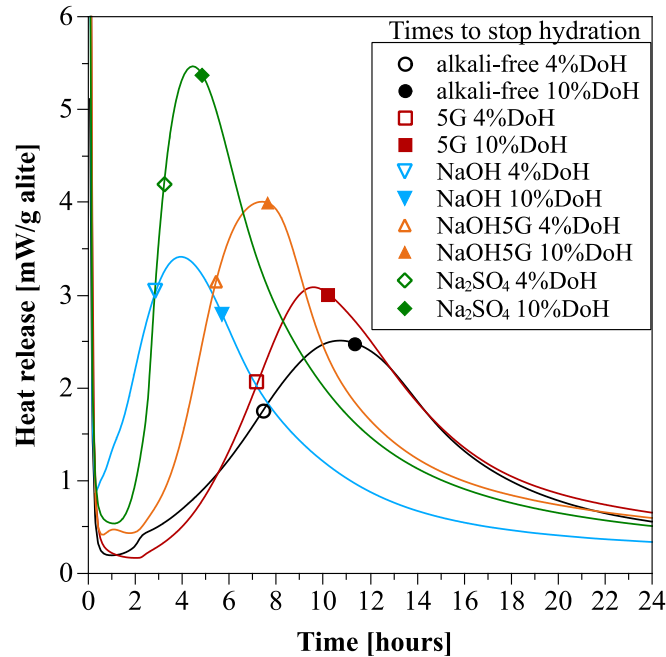


Figure 4.6. Times (dots) when hydration was stopped. Empty symbols, 4% DoH. Full symbols, 10% DoH.

Figure 4.7 shows the surface of the grains for each system at a degree of hydration of 4%. Needle-like growths of C-S-H (i.e. “fibrillar”) can be clearly seen in all cases. However, it is not possible to make a quantitative assessment of the nucleation density of C-S-H in the different cases.

In the alkali free system without any addition (Figure 4.7a), the C-S-H needles grow in isolated clusters, which seem to merge together to the same point as they grow out from the surface. Hexagonal crystals of portlandite can also be identified intermixed with the needles. With the addition of gypsum (Figure 4.7b), the morphology of C-S-H does not seem to be convergent as in the alkali free alite but they adopt a more divergent needle-structure. The C-S-H morphology is very similar when either Na_2SO_4 (Figure 4.7e) or NaOH plus gypsum (Figure 4.7c) are added. There are some small (~200-500nm) ettringite crystals (AFt) present in all sulfated systems. In the presence of NaOH plus gypsum it is easy to identify small hexagonal crystals of portlandite, contrary to the system with Na_2SO_4 in which it is not that obvious. For NaOH with no sulfate (Figure 4.7d) the morphology of C-S-H is a convergent needle-structure similar to the alkali free alite. However, the needles are less well defined tending towards a more foil-like morphology which does not grow much out from the surface. Numerous thin but large crystals of portlandite are intermixed with the C-S-H (much more numerous than in the system with NaOH plus gypsum). They do not always show a clear hexagonal morphology as they often seem to be broken probably due to the sample preparation methodology.

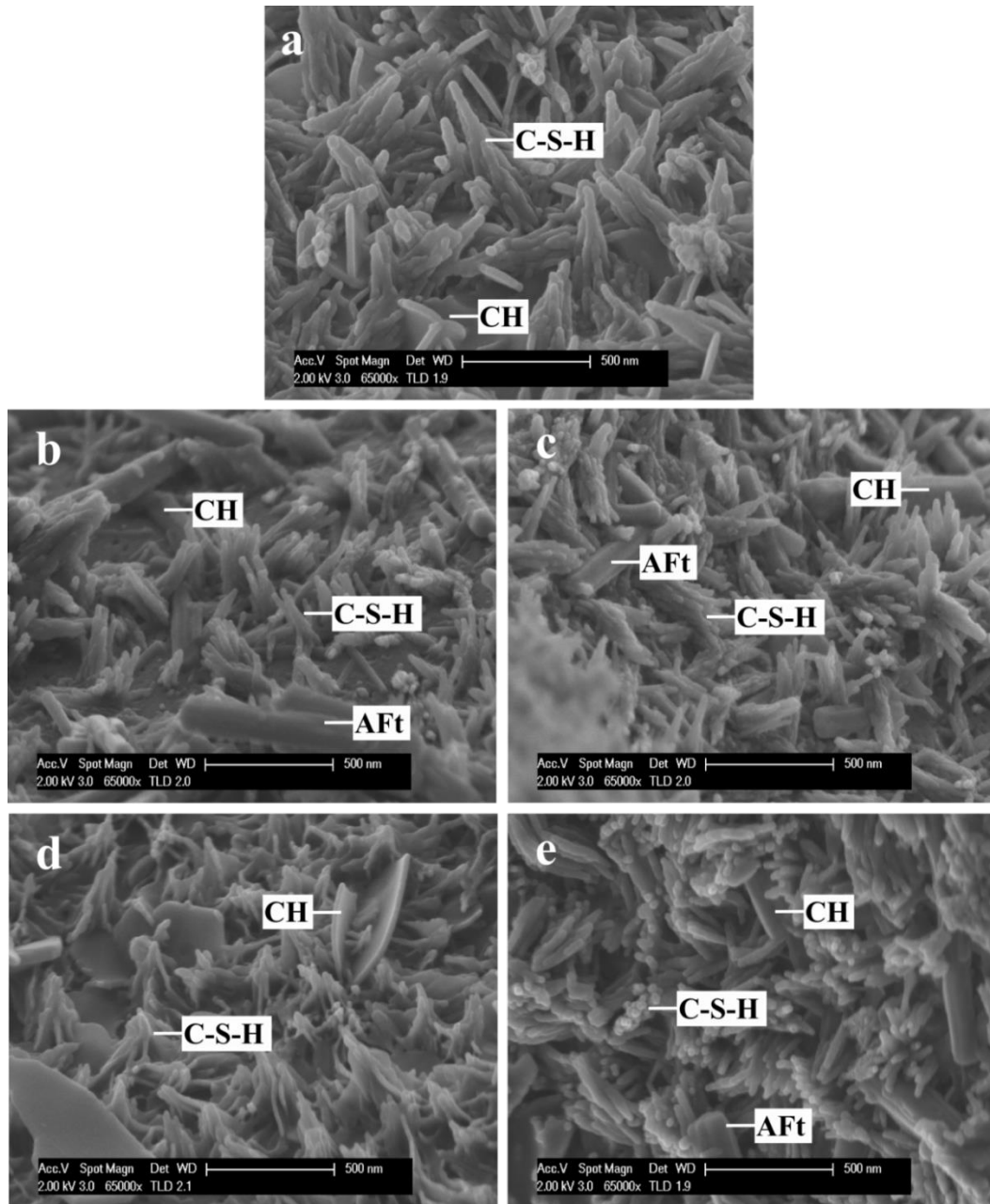


Figure 4.7. 4% DoH, corresponding to the beginning of the N+G period: a) alkali free alite and alite with b) 5wt.% gypsum, c) 5wt.% gypsum and NaOH, d) NaOH and e) Na₂SO₄.

Some insights into these differences can be obtained by looking at the effect of the different solutions on the solubility of C-S-H and portlandite and the expected evolution of the solution at the start of hydration. PHREEQC [101] was used to calculate the theoretical evolution of the pore solution during the first stages of hydration. The thermodynamic data for aqueous species and other solids is derived by Jacques [102] from the GEMS-PSI thermodynamic database [90] and the CEMDATA database for the solubility products of cementitious phases [91,92] using the ideal solid solution model for C-S-H. C-S-H was equilibrated in the relevant solution. The concentrations of calcium and silicon were increased assuming congruent dissolution of alite. Figure 4.8 shows the solubility curves for C-S-H and portlandite in the four systems with the line of congruent dissolution superposed.

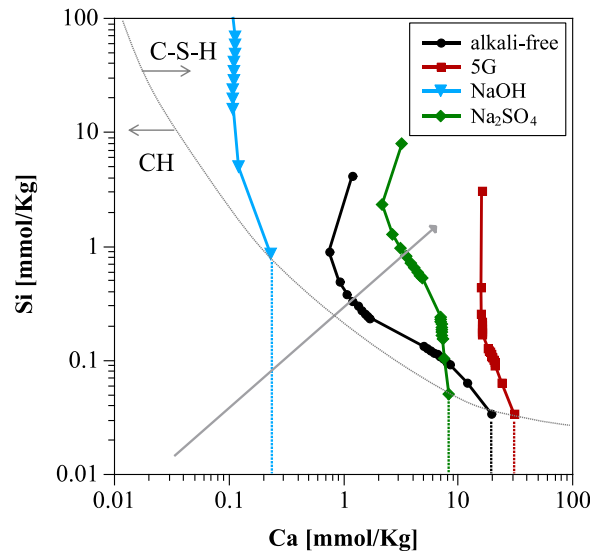


Figure 4.8. C-S-H and portlandite solubility curves. The arrow indicates the congruent C_3S dissolution.

The reference system with water has already been widely described [42][103]. C_3S will dissolve until the solution crosses the C-S-H solubility curve. At a critical degree of supersaturation C-S-H will precipitate and from that point the solution will become enriched in calcium relative to silicon as the Ca/Si ratio of C-S-H is much lower (~ 1.7) compared to that of alite (3). The solution concentration will then move towards the invariant point where portlandite is also saturated. It has been observed experimentally that a quite high supersaturation of portlandite must be reached ($SI_{\text{portlandite}}=0.4$) [42] before this phase precipitates at the end of the induction period. The addition of gypsum and Na_2SO_4 to the system shifts slightly the solubility curves of C-S-H towards higher calcium concentration due to the formation of calcium sulfate complex ions in solution. More dissolution of C_3S should occur before C-S-H precipitates, but since this stage is very short (few minutes) in pastes, these changes are unlikely to have much obvious impact in the calorimetry curves. The presence of NaOH alone, on the other hand, drastically changes the solubility curves such that it would be expected that the precipitation of calcium hydroxide occurs before that of C-S-H. This would explain the absence of any obvious induction period and also the fine intermixing of portlandite crystals with C-S-H on the surface of the cement grains.

Figure 4.9 shows the surface of the grains at 10% degree of hydration, which corresponds to some minutes after the main peak for all the samples. The C-S-H has grown further. These images confirm the observations at earlier ages. At 10% DoH it is possible to see that the presence of sulfate changes significantly the morphology of C-S-H from a convergent (Figure 4.9a) into a more divergent needle-structure (Figure 4.9b, c and e). In the system with only addition of NaOH the tendency towards a converging foil-like morphology is confirmed (Figure 4.9d) as well as the presence of numerous thin plates of portlandite. Similar to the 4% DoH, in the presence of NaOH together with gypsum there are many hexagonal portlandite crystals (Figure 4.9c) while these are not observed in the system with Na_2SO_4 (Figure 4.9e), (meaning that they are linked to the presence of OH^- ions).

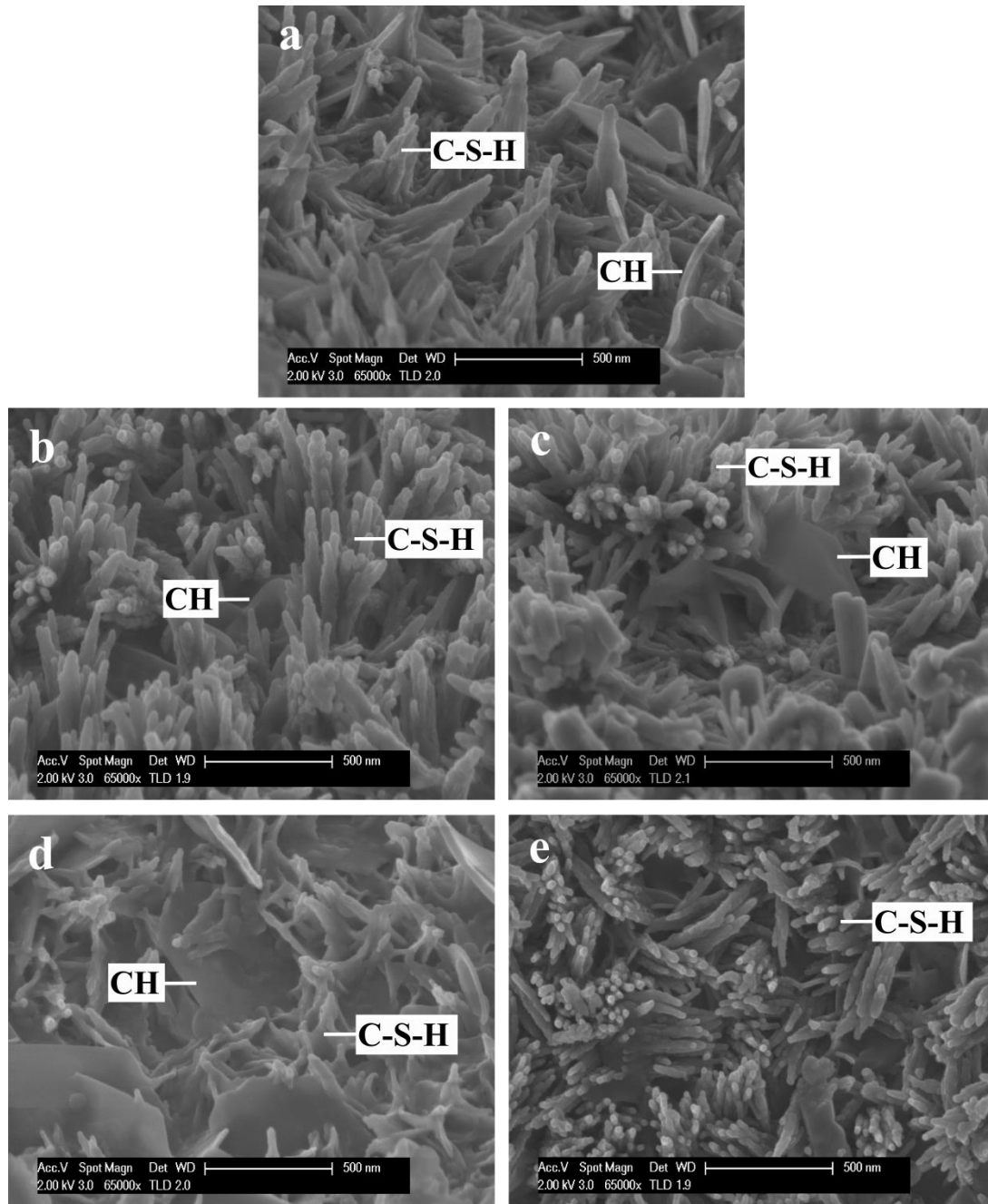


Figure 4.9. 10% DoH (minutes after the main peak): a) alkali free alite and alite with b) 5wt.% gypsum, c) 5wt.% gypsum and NaOH, d) NaOH and e) Na₂SO₄.

At the very beginning of the reaction in the system with NaOH plus gypsum, the alkali ions may have a higher impact than sulfate, as gypsum needs to dissolve. Figure 4.10 of the system with 5wt. % gypsum and NaOH seems to suggest this behaviour. Therefore, C-S-H could initially tend to form closer to the grain surface (with a foil-like morphology as in the NaOH case at 2% DoH, Figure 4.10) but it could evolve into a more divergent needle-like morphology when sulfate concentration in solution is high enough (as shown in Figure 4.9c).

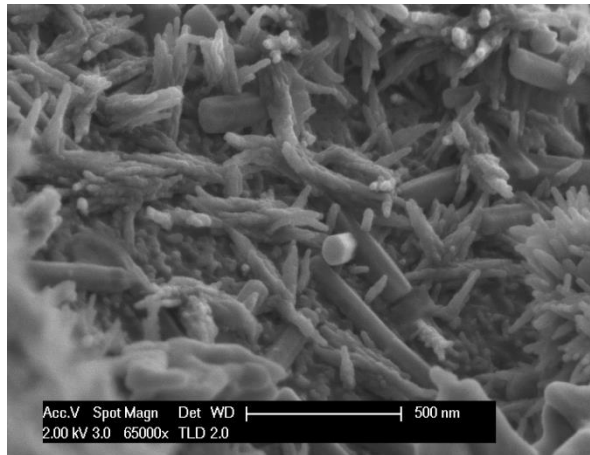


Figure 4.10. 2% DoH for the system with 5wt.% gypsum and NaOH.

Polished sections were examined at 3 days to see the distribution of the hydrates (Figure 4.11). It was not possible to look at samples at the same degree of hydration as this was too different after the first day or so.

In the alkali free system without additions equiaxed masses of portlandite are observed (Figure 4.11a). In the presence of gypsum, the portlandite masses become slightly more elongated and smaller but more abundant (Figure 4.11b and Figure 4.12). These changes are accentuated in the presence of Na_2SO_4 (Figure 4.11e) and in the presence of NaOH together with gypsum (Figure 4.11c). Portlandite precipitation seems to occur preferentially in the neighbourhood of gypsum crystals (Figure 4.12), as previously observed by Gallucci and Scrivener [48]. In the system with gypsum it is still possible to observe undissolved gypsum particles at 28 days (Figure 4.12). They are entrapped by portlandite masses and have not been able to dissolve. Any gypsum particles are observed in the system with NaOH plus gypsum. With NaOH but no sulfate (Figure 4.11d) the portlandite deposits are thin elongated plates much more numerous in quantity compared to the alkali free system. Portlandite adopts an elongated morphology (favouring hexagonal platelets). The results agree with recent work from Galmarini et al [49] based on experimental results as well as atomistic simulations. They reported that the presence of hydroxide can favour the formation of hexagonal platelets linked to the lower growth on the [00.1] and [10.1] surfaces compared to the speed up growth in the [10.0] direction. The authors also observed that sulfate promote the formation of hexagonal platelets, indicating a speed-up of growth in [10.0] direction and slow-down in [00.1] direction. Thus, they observed that sulfate lead to a similar effect as alkalis but to a lesser extent. It was suggested by Diamond [104] that portlandite precipitates in an elongated fashion if there are narrow spaces left between the unreacted grains. However, elongated precipitates of portlandite were observed at early ages when there are still big spaces between unreacted grains. In all the cases, portlandite masses encapsulate unreacted grains. This is less evident with addition of NaOH because the elongated portlandite precipitates are smaller than unreacted alite grains. TGA measurements in Figure 4.13 indicate that, although there are considerable differences in the morphology of portlandite, the amount remains almost the same between systems for a same DoH.

BSE images in Figure 4.11 indicate at 3 days slightly thicker C-S-H rims around alite grains in the systems with sulfate, since the degree of hydration is higher. It is worth noting that in the system with only NaOH (absence of sulfate) there is almost no outer product C-S-H.

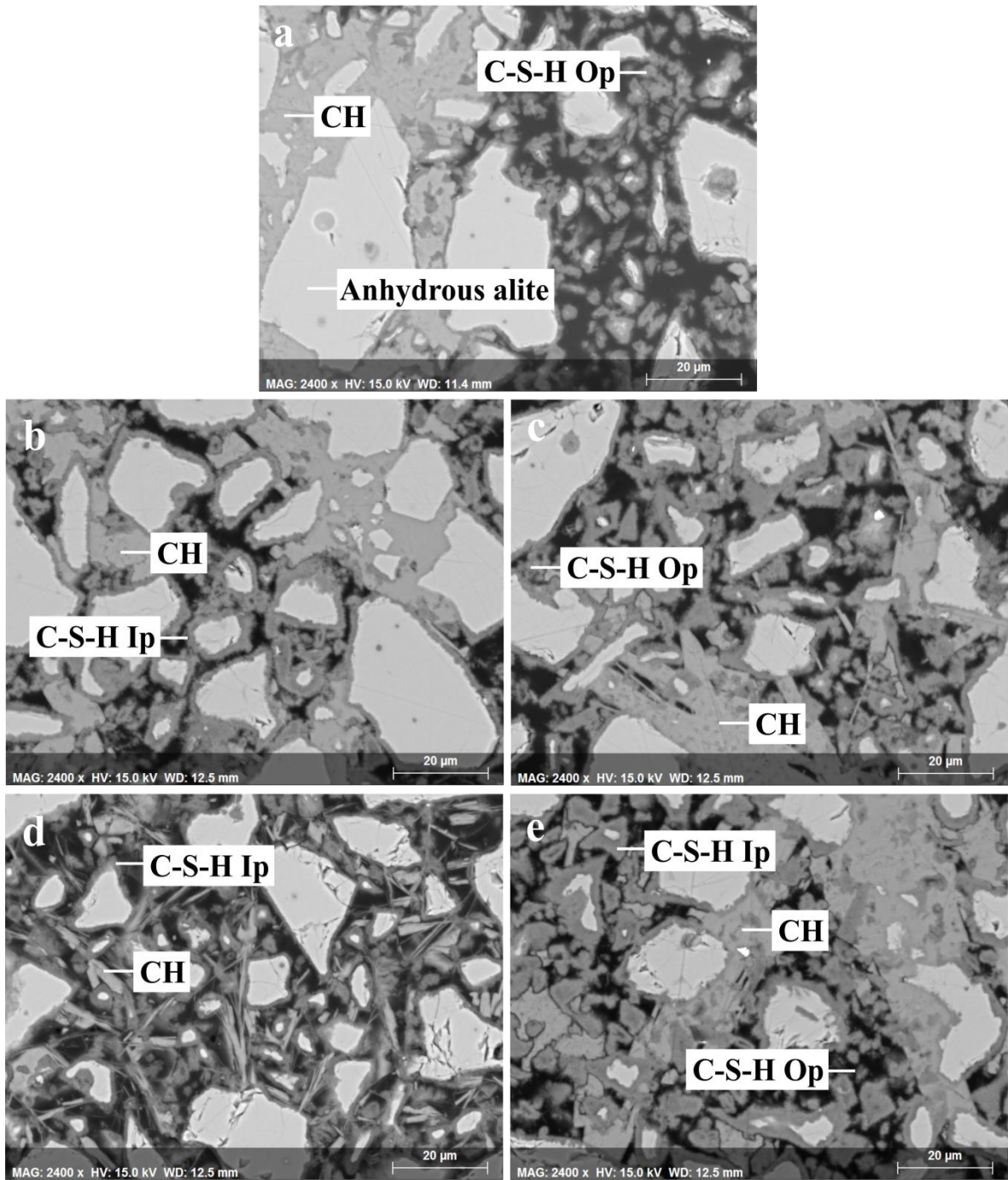


Figure 4.11. Polished sections of alite systems at 72 hours: a) alkali free alite and alite with b) 5wt.% gypsum, c) 5wt.% gypsum and NaOH, d) NaOH and e) Na₂SO₄.

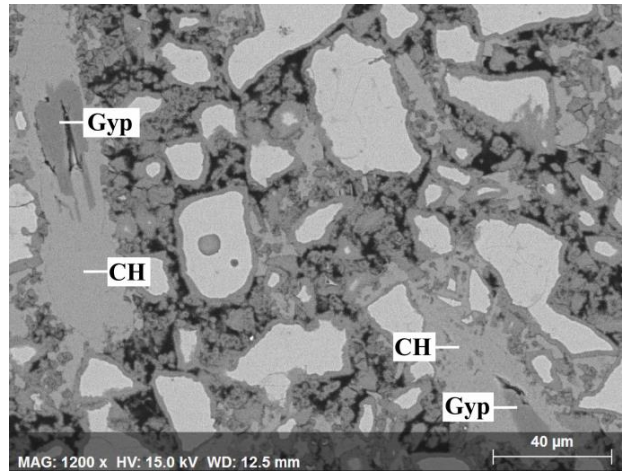


Figure 4.12. Polished section at 28 days for the system with 5 wt.% gypsum.

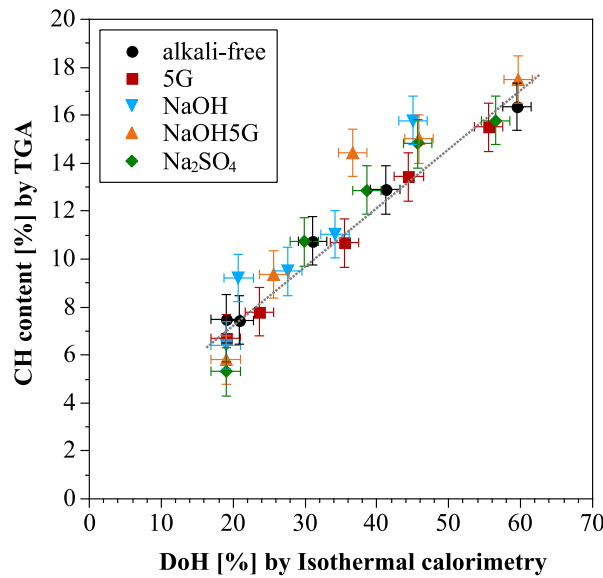


Figure 4.13. Quantification of portlandite as a function of DoH alite. The dotted line is an eye-guide. The error bars correspond to the instrumental error.

3.3. Chemical composition of hydrates

EDS microanalyses of the C-S-H for each system were done at 7 and 28 days (Figure 4.14 and Figure 4.15, respectively). At earlier ages the degree of hydration is not high enough to make reliable EDS analysis on alite systems due to the large interaction volume in the SEM. At 7 and 28 days the C-S-H product is bigger. The data obtained were sorted so that the analyses avoided intermixed products as much as possible and could be attributed to C-S-H product. Care was taken to avoid EDS analyses near undissolved gypsum crystals. Previous studies reported that sulfate ions are adsorbed on C-S-H structure [48,66,67]. As there is a coupled adsorption of Ca^{2+} with SO_4^{2-} through ion-ion correlations [66] in presence of gypsum, (Ca-S) is used in the analyses to focus on the Ca in the structure of the C-S-H rather than that co-absorbed with sulfate. To consider the replacement of silicon per aluminate, (Si+Al) is used for the ratios.

EDS microanalyses of the C-S-H in each system at 7 and 28 days are presented in Figure 4.14 and Figure 4.15, respectively. The results indicate that the sulfate content in C-S-H is higher in the systems where sulfate were initially added. The S/(Ca-S) ratio at 7 days is slightly higher than at 28 days. The addition of sulfate lowers the aluminate ions content in the C-S-H as it is removed from the solution to give ettringite (observed in SFEG images in Figure 4.7 and Figure 4.9). Figure 4.14b and Figure 4.15b show the evolution of the (Ca-S)/(Si+Al) ratio in each system at 7 and 28 days, respectively. When sulfate sorption takes place the (Ca-S)/(Si+Al) ratio is slightly higher. In the case of NaOH without sulfate there is a higher scatter in the measurements due to a higher intermixing with the small but abundant portlandite crystals and also due to the lower amount of C-S-H product in this system. The level of aluminate in the C-S-H appears to be slightly higher in the system with NaOH than in the alkali free system due to higher aluminate ions concentration in solution as indicated by the GEMS calculation (Figure 4.3). The incorporation of sodium in C-S-H could not be precisely quantified because the EDS analysis would include the sodium precipitated on the surface of C-S-H as an artefact of drying.

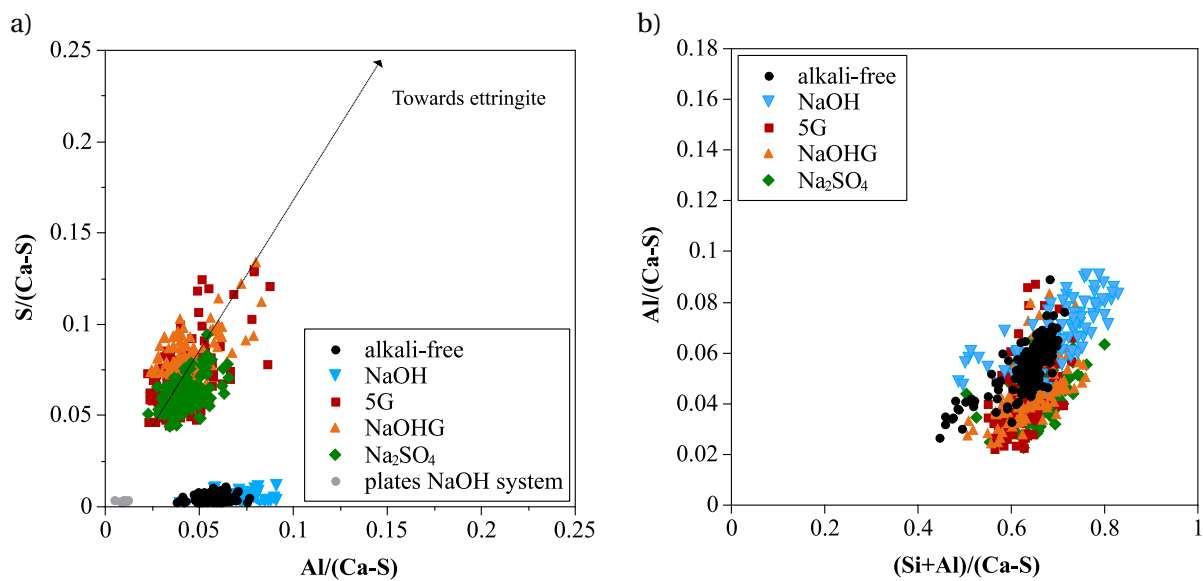


Figure 4.14. EDS analyses at 7 days of hydration: a) Al/(Ca-S) vs S/(Ca-S) ratio and b) (Si+Al)/(Ca-S) vs Al/(Ca-S) ratio. The arrow indicates the trend towards ettringite. The small elongated platelets observed in the system of alite with NaOH were verified to be portlandite (grey dots in a)).

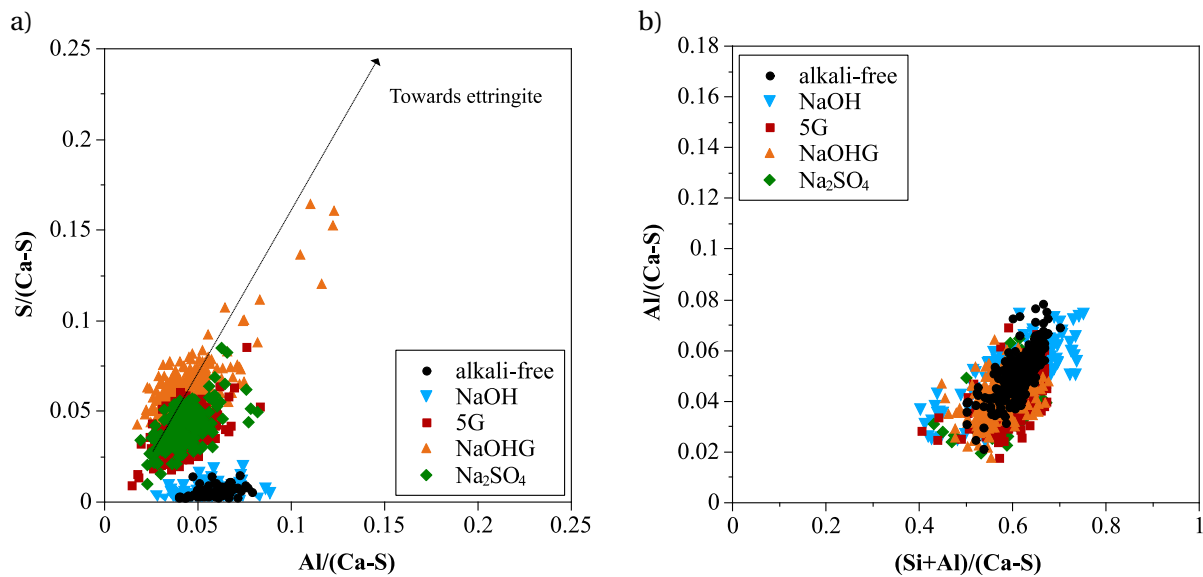


Figure 4.15. EDS analyses at 28 days of hydration: a) Al/(Ca-S) vs S/(Ca-S) ratio and b) (Si+Al)/(Ca-S) vs Al/(Ca-S) ratio. The arrow indicates the trend towards ettringite.

The impact of sulfate uptake on the morphology of C-S-H

EDS analyses suggest that the divergent morphology of C-S-H observed in the presence of sulfate could result from the sulfate sorption on C-S-H. Since electrostatic forces are fairly short range (few nm), here the influence is likely to occur during the very early nucleation and orientation of growth.

During the very first minutes of hydration, subcritical nucleation sites of C-S-H, which are not stable yet, remain in the solution. In the absence of sulfate (Figure 4.16a), Ca^{2+} ions in solution compensate the SiO^- sites in the C-S-H resulting in a charge reversal (apparent positive surface charge) [20,21]. In the presence of sulfate (Figure 4.16b), sulfate ions could be physically adsorbed by electronic interactions [105] to this apparent positively charged surface leading to a subcritical nucleation site with a negative surface charge. Afterwards, those subcritical nuclei could attach to a surface of alite (heterogeneous nucleation) or between themselves. Consequently, the interface energy decreases and the nucleation sites become stable. But due to a still unknown reason, the stable nucleation sites in the presence of sulfate could probably adopt a different orientation than those without sulfate: different composition of the nucleation sites, different interactions between the nucleation site and the surface of alite, partial inhibition of the growing sites of the nucleation sites due to the sorption of sulfate, etc. This would then promote a different growth orientation of the needles of C-S-H, in presence or absence of sulfate. Further work is needed to understand the reason for such orientation at a nucleation site level.

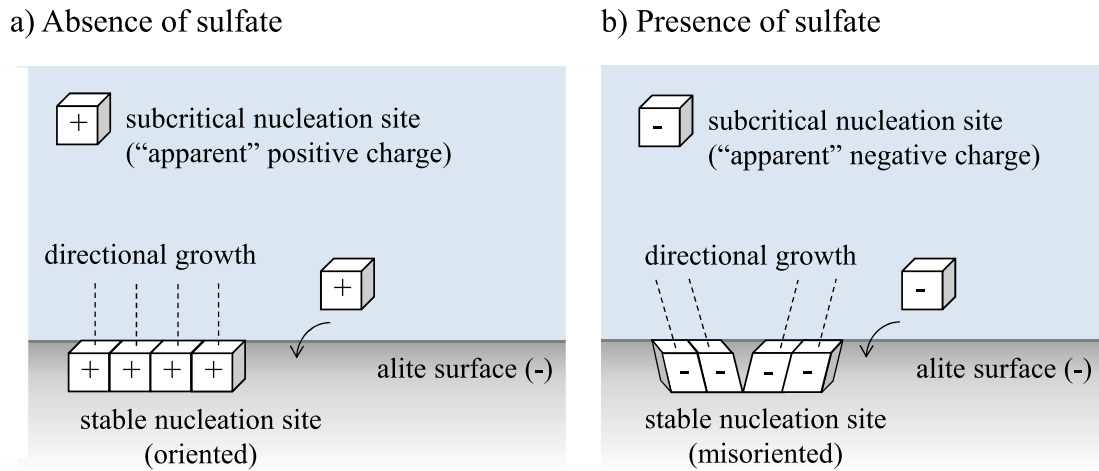


Figure 4.16. Hypothetical scheme of the impact of sulfate ions on the orientation of C-S-H subcritical nucleation sites when they nucleate in the surface of alite. Etch pits are not represented here.

3.4. Mechanical strength of alite mortars

The evolution of the compressive and flexural strength over time for the different systems is shown in Figure 4.17a and b, respectively. Strength results of alite systems are lower than for typical cement values mainly related to the already mentioned lower DoH of alite.

Over the whole period measured, the compressive strength of alite mortars is higher in presence of gypsum and is higher still in the two sulfated Na-systems. On the contrary, the hydration of alite in a NaOH solution (without sulfate) leads to lower strength values from 7 days in despite being higher than the alkali free system up to 7 days. It is worth noting that the alkali free alite system and the one with NaOH have almost the same compressive strength at 90 days although the latter appears to have a much lower DoH. The trends for the flexural strength are quite similar to those mentioned for the compressive strength except that the system with NaOH appears to have higher flexural strengths than the alkali free system and the one with gypsum in most of testing times. It presents similar values as the system with Na₂SO₄ up to seven days but further on the trend is reversed.

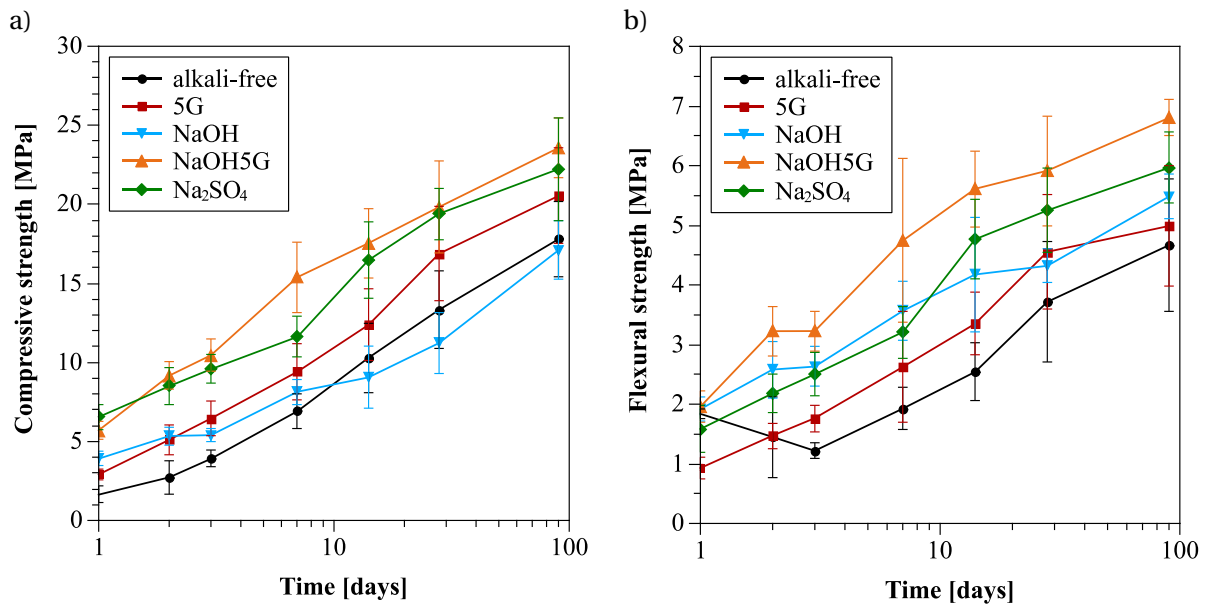


Figure 4.17. a) Compressive and b) flexural strength for alite mortars as a function of time. Time is plotted in logarithmic scale in order to better appreciate the results during the first days.

To see if the changes in the compressive and flexural strength are only due to the modification of the hydration rate and the degree of hydration, the strength values are plotted as a function of the DoH obtained from isothermal calorimetry (Figure 4.5 and Figure 4.18). For a given DoH, there is a clear increase in the compressive strength in the following order: alkali free system \approx gypsum < NaOH \approx Na₂SO₄ < NaOH + gypsum.

The compressive strength values for a same DoH do not change with the addition of gypsum. On the contrary, the compressive strength is higher in the presence of sodium. Although in the presence of only NaOH C-S-H doesn't seem to grow that much outwards to fill space (Figure 4.9d) and outer C-S-H product seems to be inhibited, probably the small platelets of portlandite have a better ability to fill the space compared to bigger masses (as seen in Figure 4.11d). The flexural strength is also higher with the addition of alkali (Figure 4.18b). The systems with only NaOH and with gypsum plus NaOH have similar flexural strength values for a same DoH.

The effect of alkali on the strength for a same DoH appears to be independent of the morphology of C-S-H. In the system with the addition of gypsum, for an equivalent DoH the compressive strength remains the same although the morphology of C-S-H differs significantly. It is reported in literature [20,21] that Na^+ monovalent ions lead to lower ion-ion interactions between the C-S-H surfaces than Ca^{2+} because the ionic radius of the latter is bigger and it is multicharged [105]. Weaker interactions would be expected to lead to lower compressive strength results, which is not the case here. Thus, the observed differences in the compressive strength cannot only be explained by ion-ion interactions.

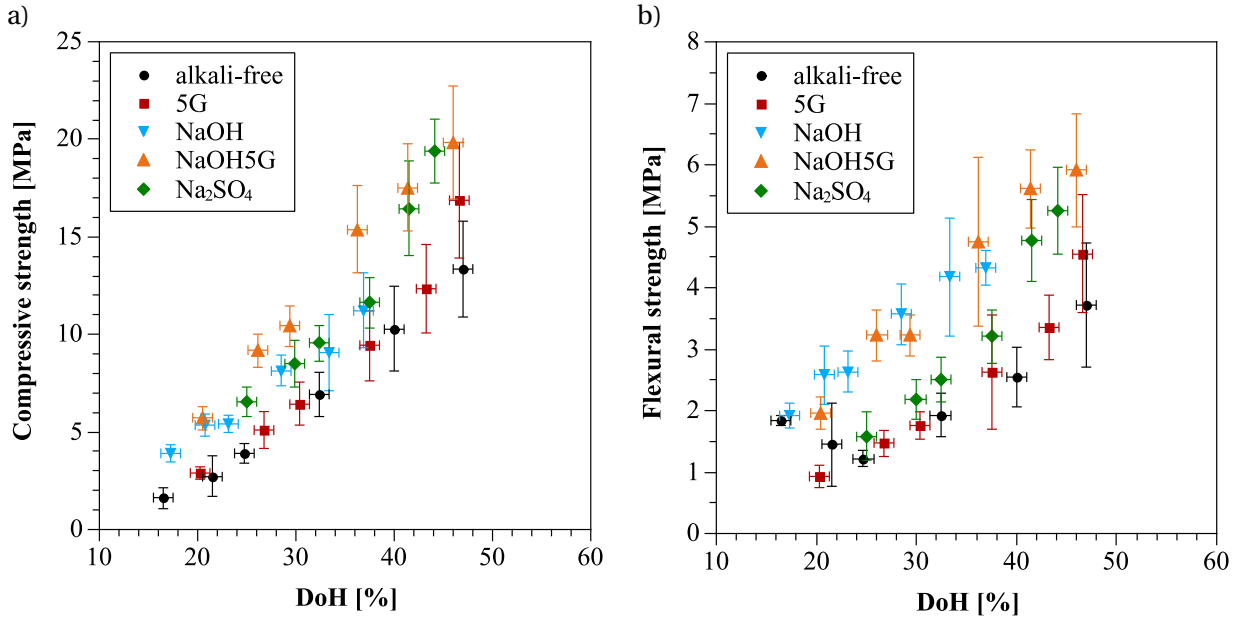


Figure 4.18. a) Compressive and b) flexural strength for alite mortars as a function of DoH.

Compressive strength can depend on many factors: degree of hydration, distribution of phases, number of contact points, type of hydrates, total porosity and its distribution, among others. However, we cannot evaluate most of these quantitatively. Here it can be commented about the porosity as well as the distribution of hydrates in the matrix.

Porosity

Figure 4.19 shows the total porosity MIP measurement of alite systems at 7 days (Figure 4.19a) and 28 days (Figure 4.19b). A system with better mechanical properties would be expected to have a lower total porosity. However, this is not observed here. At 7 days, the total porosity of the alkali free systems, with gypsum and with Na_2SO_4 is quite similar (~25%), NaOH reaches the highest porosity (~30%) and NaOH plus gypsum the lowest porosity (~20%). At 28 days the trends are the same, although the systems with Na_2SO_4 and NaOH have a more similar total porosity.

The system with NaOH plus gypsum reaches the lowest porosity measurements which agrees with the higher compressive and flexural strength tested. On the contrary, the Na_2SO_4 system has a much higher total porosity although the compressive strength at 28 days is the same as in the NaOH5G system. Figure 4.20 shows that the compressive strength is fairly related to the total porosity. However, to make further conclusions on the relationship between the total porosity and the compressive strength there is a need to study systems with a higher degree of hydration, such as cement.

The two systems with NaOH have a lower critical entry radius. This could be due to the precipitation of microcrystalline portlandite. As mentioned before, the presence of NaOH promotes more elongated and more numerous crystals of portlandite that could better fill the space instead of bigger crystals. The critical entry radius of the alite systems with the presence of NaOH is similar to that in cement systems presented in the next chapter (see Chapter 5).

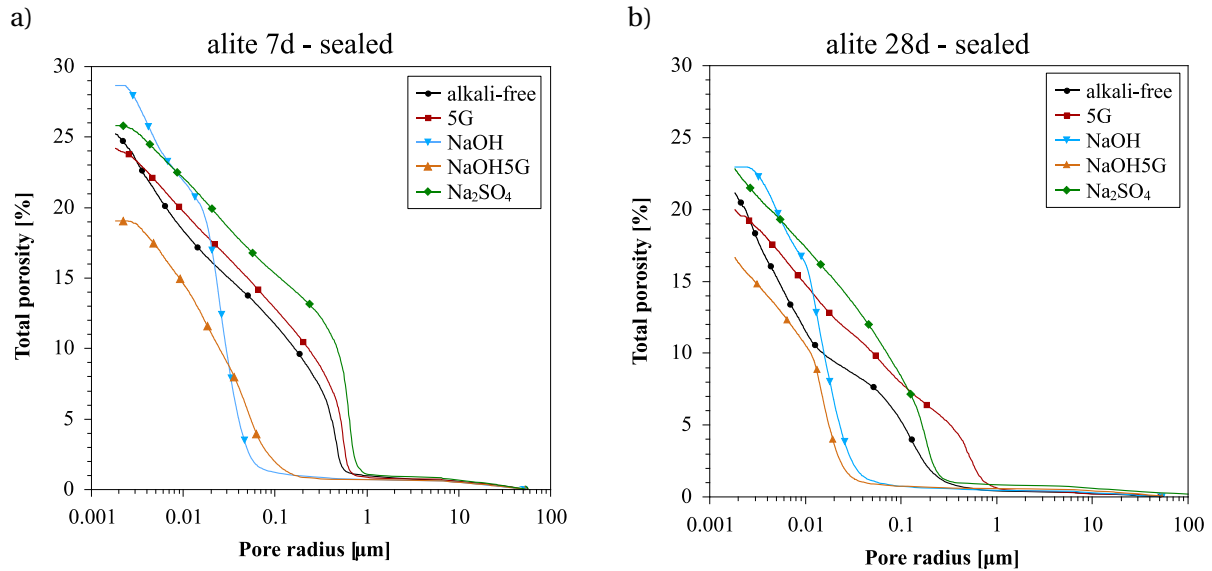


Figure 4.19. Total porosity as a function of the pore radius for alite systems at a) 7 days and b) 28 days.

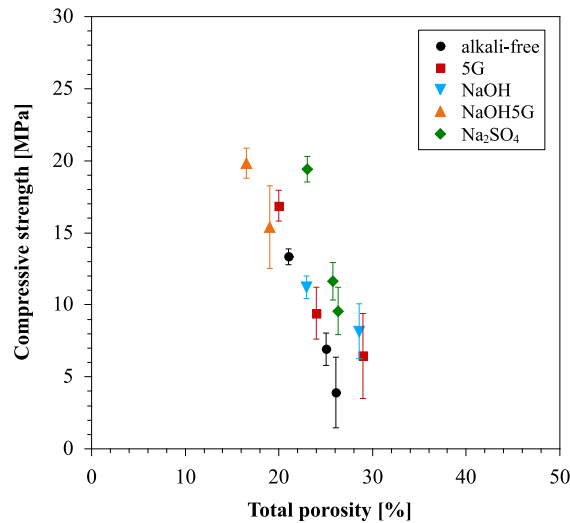


Figure 4.20. Total porosity as a function of the compressive strength for alite systems.

The distribution of hydrates

Figure 4.21 shows the BSE images of alite systems at 28 days. There are major differences in the homogeneity of the distribution of hydrates. The least homogeneous matrix corresponds to the alkali free system and with gypsum. This has very big masses of portlandite but also there are many areas where portlandite is absent. The system with Na₂SO₄ is more homogeneous, and it becomes more homogeneous with the addition of NaOH and gypsum and even more with only NaOH mainly due to a more uniform distribution of the smaller and more numerous portlandite crystals (see also Figure 4.11). In the case of NaOH without gypsum, although the outer C-S-H is not abundant, these small but

numerous platelets of portlandite could probably help to decrease the amount of capillary pores and the critical entry radius, and thus to increase the strength development despite a lower DoH. Smaller particles of portlandite in the presence of NaOH could be responsible of a lower critical entry radius and similar to that found in cement systems as mentioned above (see Chapter 5). At this stage it is not possible to analyse these effects in a more quantitative manner.

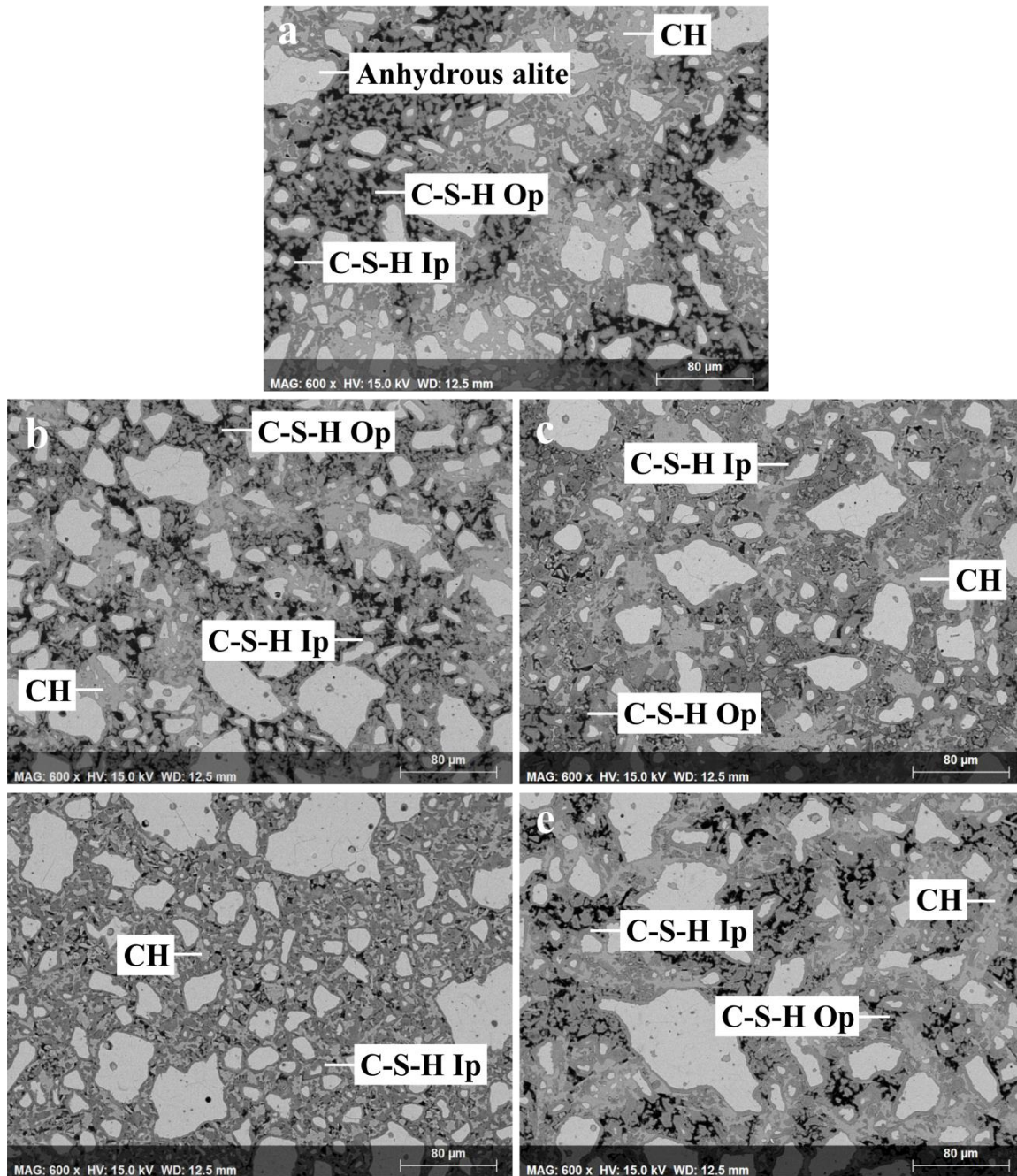


Figure 4.21. Polished sections at 28 days. a) alkali free alite and alite with b) 5wt.% gypsum, c) 5wt.% gypsum and NaOH, d) NaOH and e) Na_2SO_4 .

4. Summary

- The combination of alkali and sulfate accelerates the hydration at all times leading to a higher DoH. On the contrary, in the presence of only NaOH the DoH is lower compared to the alkali free alite after 20 hours. Alkalies increase the aluminate ions in solution and, unless there is a sulfate source, the reaction of alite is inhibited.
- The morphology of C-S-H clearly depends on the chemical composition of the surrounding solution. Sulfate promote a divergent needled structure (Figure 4.22c) instead of a convergent needled structure as observed in the alkali free system without additions (Figure 4.22b). The addition of alkali besides gypsum does not seem to induce any further change. The presence of NaOH alone (without sulfate) promotes the formation of C-S-H with a foil-like morphology (Figure 4.22a).

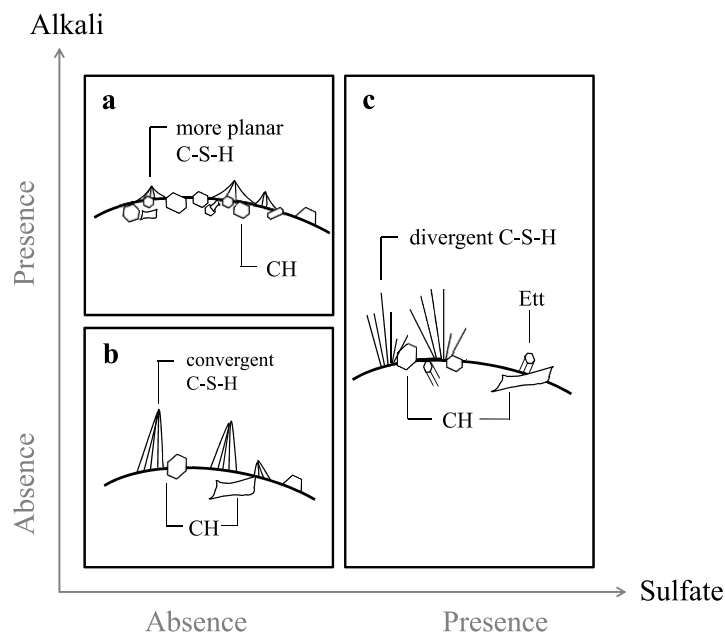


Figure 4.22. Schematic morphologies of C-S-H and other hydrates depending on the solution chemistry.

- The equiaxed masses of portlandite in alkali free alite become elongated and smaller but more abundant in all the systems with additions. This effect is extreme in the presence of only NaOH. Small platelets with high aspect ratio could explain a smaller critical entry radius in the systems with NaOH.
- Alkalies increase the compressive and flexural strength of alite micromortars at the same DoH. These changes do not correlate with the changes in the morphology of C-S-H. To better discuss and understand the influence of the porosity on the strength development, this needs to be studied further in systems with a higher DoH such as cement.
- It is important to note that alite is a simplified system of cement (as it represents up to ~75% of Portland cement) but the DoH, distribution of phases, porosity and strength development of both pastes may differ.

CHAPTER 5. The impact of NaOH and Na₂SO₄ on white cement hydration

1. Introduction	59
2. Systems studied	60
3. Compressive and flexural strength.....	60
4. Kinetics	61
5. Porosity and relation to mechanical strength	65
6. Hydrates precipitated	67
6.1. Type of hydrates precipitated.....	67
6.2. Characteristics of C-S-H	70
7. Summary	78

1. Introduction

In Chapter 4 it was observed that the differences in the strength development in the presence and absence of alkali in alite systems do not seem to depend on the morphology of C-S-H. So, the main reason for the differences in strength remains unclear. In order to be clarified, this chapter present the impact of Na₂SO₄ and NaOH on cement systems rather than alite. Chapter 5 aims are:

- To study the impact of Na₂SO₄ and NaOH on the whole phase assemblage on white cement systems.
- To bring new insights on the impact of alkalis on the amount of water, density and structure of C-S-H in non-dried samples with ¹H NMR.

2. Systems studied

Figure 5.1 shows the white cement systems studied and Table 5.1 shows further details of the used formulations. The concentration of each alkali solution was kept the same as in alite systems in order to be comparable.

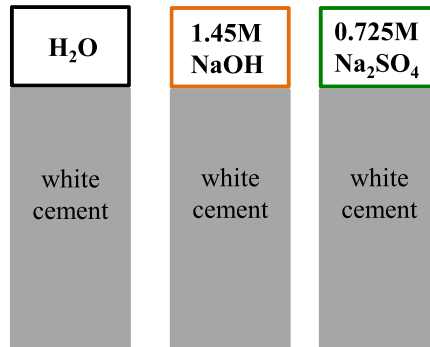


Figure 5.1. Composition of the white cement systems studied.

Table 5.1. Formulations of the white cement systems studied.

White cement [wt.%]	Mixing solution	Nomenclature in figures
100	DI-water	W alkali-free
100	1.45M NaOH	W NaOH
100	0.725M Na ₂ SO ₄	W Na ₂ SO ₄

3. Compressive and flexural strength

Figure 5.2 shows the impact of Na₂SO₄ and NaOH on compressive (Figure 5.2a) and flexural strength (Figure 5.2b) as a function of time. The addition of Na₂SO₄ leads to a slight increase of the compressive strength at 24 hours but at later ages, from 3 days on, the compressive strength is lower than in the alkali free system. The addition of NaOH significantly decreases the mechanical strength even at 24 hours compared to the alkali free system and also the system with Na₂SO₄. From 3 days up to 90 days there is a steady increase of the compressive strength of all systems, with almost constant differences between the highest alkali free system (71 MPa at 90 days), the system with Na₂SO₄ (64.5 MPa) and the lowest system with NaOH (47 MPa). This agrees with what is generally reported in literature, i.e. the addition of alkali decreases the compressive strength at later ages although it can increase the early strength.

The flexural strength of the three systems is much more similar. The Na₂SO₄ system seems to have slightly higher flexural strength at 1-3 days, but the differences are within the higher error range as typically seen for flexural strength results. The flexural strength does not appear to increase significantly after about 3-7 days.

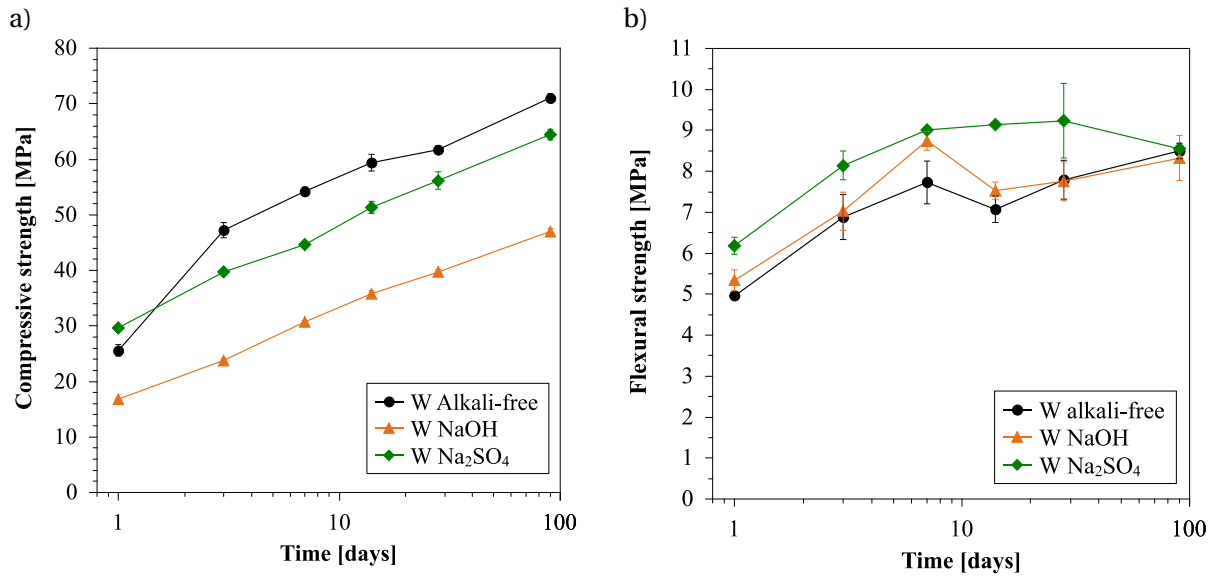


Figure 5.2. a) Compressive and b) flexural strength results over time (up to 90 days) for each system of white cement mortars. The time is plotted in logarithmic scale in order to better appreciate the results during the first days.

4. Kinetics

Figure 5.3 shows the isothermal calorimetry results for the systems. The addition of Na₂SO₄ decreases the length of the induction period and increases the hydration rate compared to the alkali free system. These effects are more accentuated in the presence of NaOH. In the presence of Na₂SO₄ and NaOH the silicate peak seems higher than in the alkali free system. The aluminate peak is very sharp in the alkali-free system. In the presence of Na₂SO₄ it becomes broader as well as lower. In the presence of NaOH no separate aluminate peak can be differentiated.

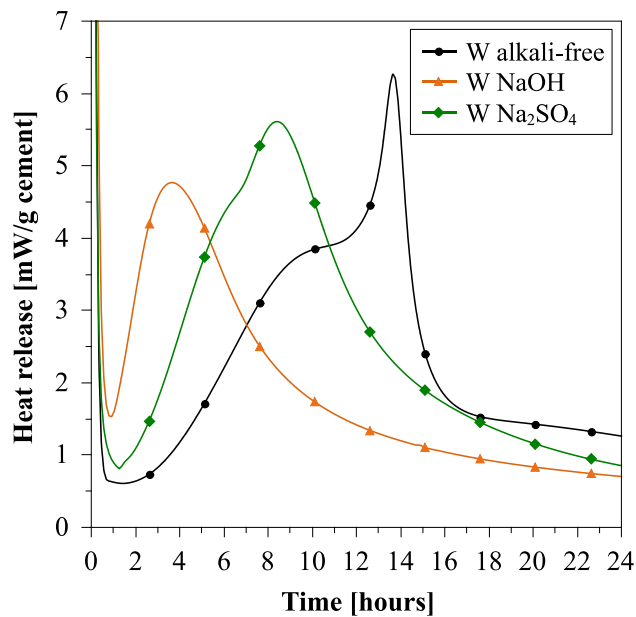


Figure 5.3. Effect of Na₂SO₄ and NaOH on the heat evolution rate of white Portland cement during the first 24 hours.

Figure 5.4 shows the cumulative heat release over 28 days for the different systems. During the first 35 hours, the presence of Na_2SO_4 leads to a higher cumulative heat release compared to the alkali free system. From there on, the trend is reversed. This change in the trend takes place even earlier in the presence of NaOH (at 15 hours). Thus, at 28 days of hydration the alkali free system reaches the highest cumulative heat release while the addition of NaOH leads to the lowest values, but reaching a very similar value to the system with Na_2SO_4 at 28 days.

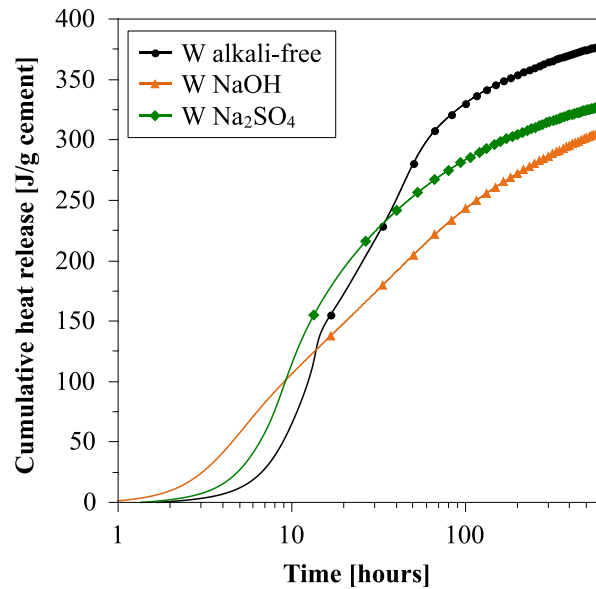


Figure 5.4. Effect of Na_2SO_4 and NaOH on the cumulative heat release up to 28 days.

Figure 5.5 shows the degree of hydration calculated with XRD-Rietveld as a function of time. At 1 day the DoH of cement in the alkali free system and the system with NaOH are very similar (~ 0.40 DoH) while in the presence of Na_2SO_4 it is higher (~ 0.45 DoH). Afterwards, from 7 days on, the alkali free system reaches the highest DoH, being 10% higher than the alkali systems (which are then similar). The DoH trends agree with the cumulative heat results in Figure 5.4.

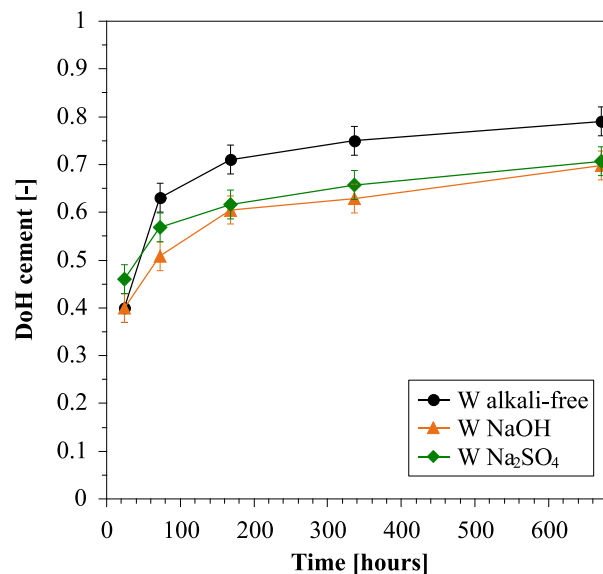


Figure 5.5. Effect of Na_2SO_4 and NaOH on the degree of hydration of cement up to 28 days.

Figure 5.6 shows the quantification of C₃S and C₃A with in-situ XRD-Rietveld during the first 24 hours of hydration. C₃S reaction is accelerated during the first hours in the presence of both alkali salts, which agrees with the acceleration of the reaction observed in the calorimetry results and a higher silicate peak (Figure 5.3). After a period of rapid reaction the reaction rate of C₃S slows down. This slow down occurs at about 13-14 hours in the alkali free system, at about 9 hours in the system with Na₂SO₄ and about 7 hours in the presence of NaOH. The very early slowdown in the NaOH system means that the DoH of alite is the lowest in this system at 24 hours. These observations agree with the cumulative heat release results in Figure 5.4.

The impact of alkalis on the hydration of C₃A is even more marked. C₃A is totally consumed at 24 hours in absence of alkalis, having its fastest reaction at about ~14 hours (when the aluminate peak takes place). In the presence of Na₂SO₄ only the half the amount of C₃A is reacted at 24 hours with its main dissolution at about 9 hours (which corresponds to the aluminate peak by calorimetry). The amount of C₃A reacted with NaOH is even lower and it is not possible to identify a significant period of rapid reaction, there is a progressive and slow reaction from the first hour until 24 hours. The low reaction of C₃A in the presence of NaOH agrees with the absence of a clear aluminate peak in the calorimetry curve (Figure 5.3). In both alkali systems the amount of C₃A is quantified to be lower than in the alkali free system at the very first hours, however this difference is less than 1% in absolute amount and is within the precision of measurement.

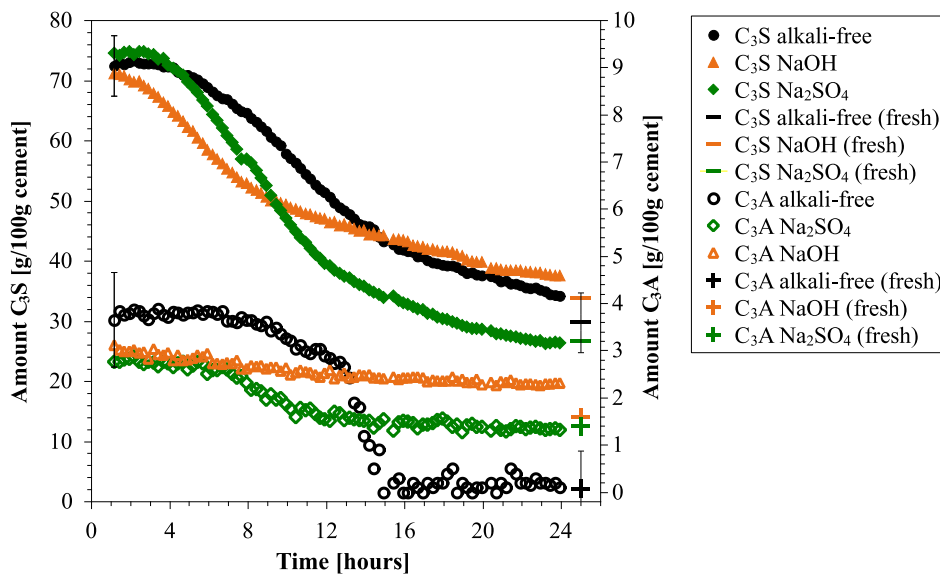


Figure 5.6. Impact of Na₂SO₄ and NaOH on the reaction of C₃S and C₃A during the first 24 hours with in-situ XRD-Rietveld. In-situ results at 24 hours are compared to C₃S quantification on fresh slices at 24 hours. Error bars are indicated at the beginning of each series of the alkali-free system, being the same error valid for each alkali system.

Figure 5.7 shows the evolution of C₃S and C₃A from 24 hours to 28 days, measured by XRD on undried slices. The trends observed agree with the trends of the XRD-Rietveld in-situ during the first 24 hours. Figure 5.7a shows that the degree of reaction of C₃S in the alkali-free system continues to increase until it is almost totally consumed at 28 days. On the contrary, the hydration rate of C₃S is lower in the presence of Na₂SO₄ and of NaOH, both having 10% of unhydrated C₃S at 28 days. The same trend is observed for the degree of hydration of C₃A at later ages in Figure 5.7b. While in the alkali-free system it is totally consumed at already 24 hours, C₃A continues to slowly dissolve from 24 hours on with the addition of Na₂SO₄ or NaOH although at 28 days there is still ~20% of the original C₃A remaining in both cases.

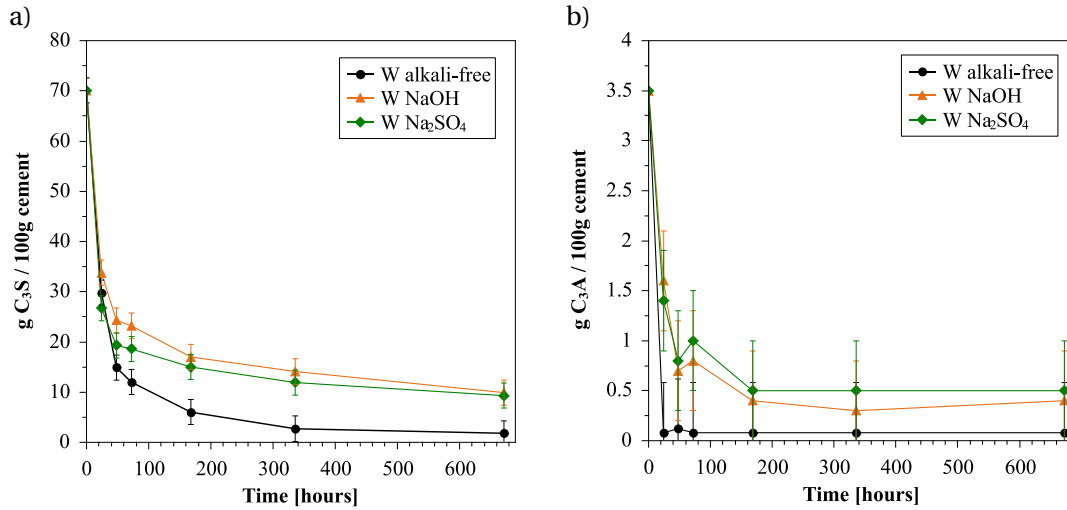


Figure 5.7. Effect of Na_2SO_4 and NaOH on the consumption of a) C_3S and b) C_3A up to 28 days.

Two potential mechanisms to explain the lower DoH of cement in the presence of alkali were investigated further. The first one concerns the relative humidity and the second one concerns the amount of aluminate ions in solution.

Figure 5.8a shows the evolution of the RH over time. In the alkali free system the RH remains close to 100% up to 28 days. However, in the presence of Na_2SO_4 or NaOH the RH is lower. They both show a continuous decrease of the RH up to ~7 days and stabilise at a value of ~85% in the system with Na_2SO_4 and ~90% RH in the system with NaOH . The lower equilibrium relative humidity confirms that the higher the concentration of ions in the pore solution the lower the water activity (a_w).

A second mechanism that could potentially contribute to the lower DoH of cement is a change in the aluminate ions concentration in the presence of alkali. It has been reported in literature that alkali increases the solubility of aluminate from cement and that this can inhibit the silica dissolution [26,67,98]. It was not possible to quantify the aluminate ions in the pore solution for these systems because the amount of Al_2O_3 in the pore solution of the white cement used for this study was too low for the detection limit of the ICP-OES instrument. Therefore GEMS was used to estimate the content of aluminate ions in the pore solution at 28 days. For each system, the DoH of each individual anhydrous phase mainly C_3S and C_3A as C_2S starts to react later than 28 days- measured from XRD-Rietveld analysis (Figure 5.7) was used as input to estimate the composition of the pore solution at 28 days³. Figure 5.8b indicates that in the presence of Na_2SO_4 or NaOH the concentration of aluminate ions in the pore solution is higher than in the alkali free system. This could inhibit the dissolution of silicate species and consequently the DoH of cement would be lower, as observed here. The fact that the concentration of aluminate ions in solution is lower in the presence of Na_2SO_4 compared to NaOH may be attributed to ettringite precipitation. The same trends in the concentration of aluminate ions in the presence of NaOH or Na_2SO_4 were estimated for alite systems in Chapter 4, i.e. higher concentrations in the presence of alkalis and especially with NaOH . Recently, Suraneni and Flatt [99] also suggested that the reduction on the dissolution should be due to an impact on the dissolution itself and not on the nucleation of C-S-H since the authors observed small particles of C-S-H when hydrating C_3S in the

³ GEMS calculations provide information about the trends of the ionic concentrations in the pore solution more than absolute amounts, which can differ from experimental values. For a more detailed explanation on GEMS see Chapter 3 (Materials and methods, thermodynamic modelling section).

presence of aluminium in solution. As mentioned in the previous chapter with alite systems, Nicoleau et al [100] reported that as the pH increases the inhibiting effect of aluminate ions is suppressed to a greater extent (through the addition of NaOH) in diluted systems based on C₃S since the formation of Si-O-Al bounds should not be favoured by increasing the pH. Differences between these observations and the present results could lie in the fact that the authors worked on diluted systems instead of pastes. However, the present results suggest that a lower DoH of cement could not only be explained by a single mechanism but rather through several of them.

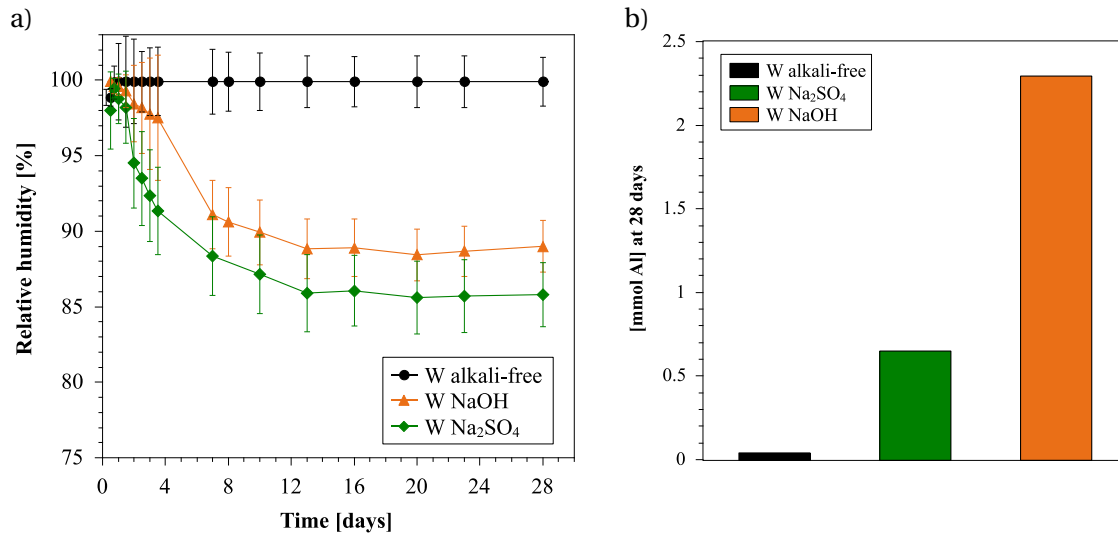


Figure 5.8. Effect of Na₂SO₄ and NaOH on a) the relative humidity over time and b) the concentration of Al in the pore solution estimated with GEMS at 28 days.

5. Porosity and relation to mechanical strength

Figure 5.9 shows compressive strength values as a function of the DoH of cement. For the same DoH, the addition of Na₂SO₄ has a similar compressive strength to the alkali free system while in the presence of NaOH it is lower.

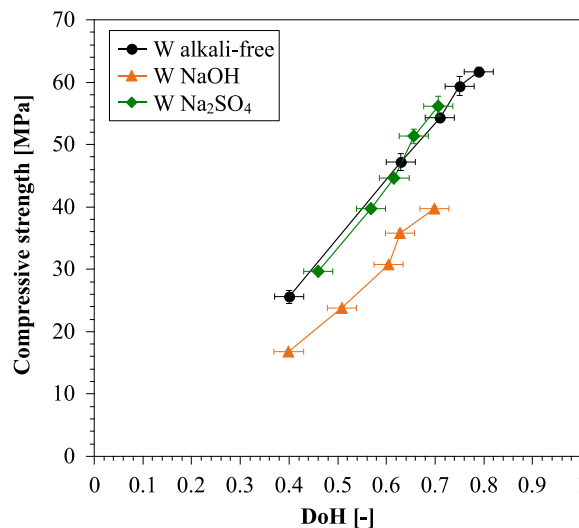


Figure 5.9. Compressive strength results for white cement mortars as a function of the DoH of cement.

In Figure 5.10, the graphs in the left column show the total porosity curves as a function of the pore radius at 1, 7 and 28 days. At 1 day the presence of Na_2SO_4 lowers the total amount of porosity in the sample (which agrees with a higher DoH of cement and higher compressive strength at early age) compared to the alkali free system and the system with NaOH (which both have the same total porosity). However, both sodium salts reduce the critical pore entry radius already at 1 day, especially in the case of Na_2SO_4 (Figure 5.10b). Later on at 7 and 28 days the total porosity (Figure 5.10c and e) is very similar for the alkali free system and in the presence of Na_2SO_4 but the porosity in the case of NaOH remains almost 10% higher. The derivative curves of the total porosity (Figure 5.10b, d and f – right column) show that the evolution of the critical entry radius over time does not follow the same trend as the total porosity. At 28 days, it is clear that alkalis increase the amount of capillary porosity but it is finer compared to the alkali free system as the critical entry radius is slightly reduced.

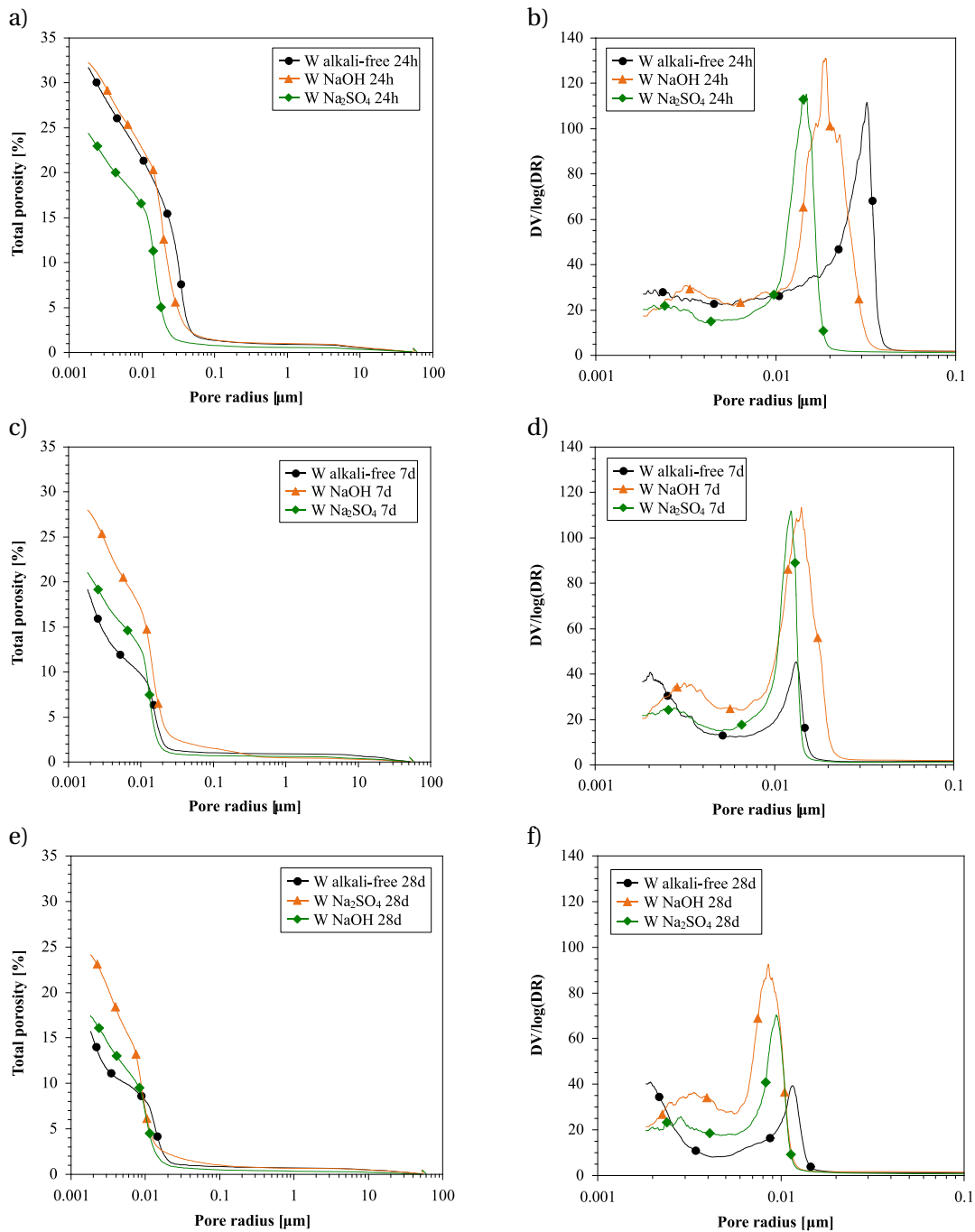


Figure 5.10. Total porosity as a function of the pore radius (left column - a, c, e) and derivative (right column - b, d, f). They correspond to 24 hours (a and b), 7 days (c and d) and 28 days (e and f).

Figure 5.11a shows the compressive strength against the total porosity measured by MIP. The linear relationship suggests that the compressive strength can be explained by the total amount of porosity in the sample. For the same DoH of cement the system with NaOH has a higher total porosity compared to the alkali free system and the system with Na₂SO₄ (Figure 5.11b). This agrees with what is observed in Figure 5.9 where for a same DoH the presence of NaOH leads to a lower mechanical strength.

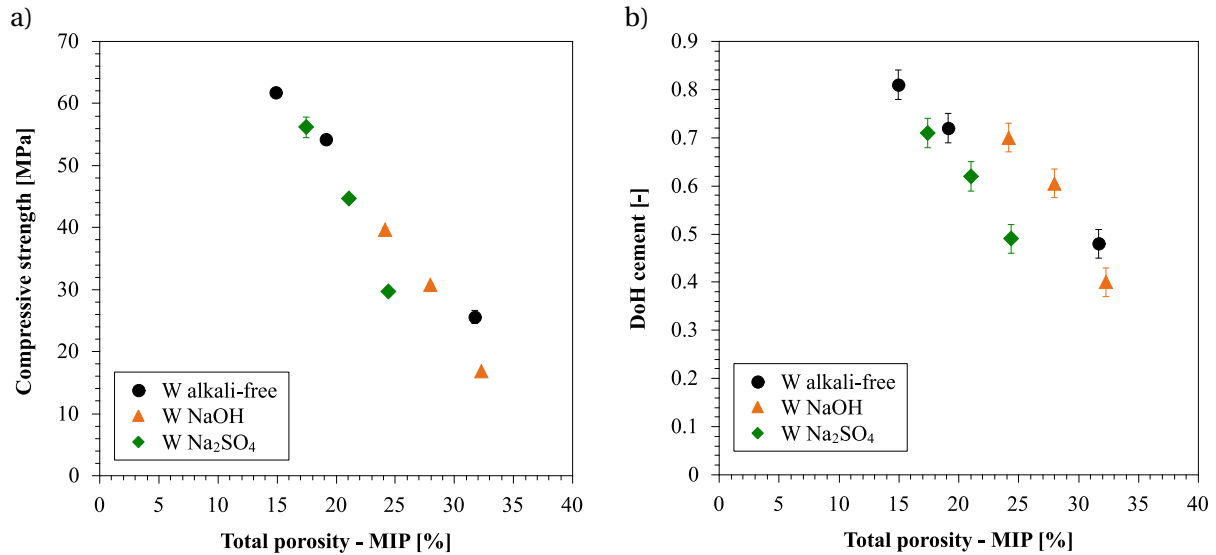


Figure 5.11. a) Relationship between compressive strength and total porosity (measured by MIP) and b) relationship between the total porosity and the DoH of cement.

6. Hydrates precipitated

The remaining question is to know where the differences in the porosities come from (almost similar for the alkali free system and with the addition of Na₂SO₄ but higher with NaOH for a same DoH of cement). The aspects studied to explain this phenomenon are:

- Type and amount of hydrates precipitated
- Characteristics of C-S-H (morphology, chemical composition and density)

6.1. Type of hydrates precipitated

GEMS was used to estimate the phase assemblage for each system over time and determine the nature of hydrates precipitating as well as their amount. For each system, the DoH of each individual anhydrous phase - mainly C₃S and C₃A, as C₂S starts to react from 28 days on- measured from XRD-Rietveld analysis (Figure 5.7) was used as input to estimate the phase assemblage at 1, 3, 7, 14 and 28 days. The volume of C-S-H was estimated based on the gel density value of 2 g/cm³ obtained from ¹H NMR analysis (detailed in the following section). Further details on the calculation parameters with GEMS can be found in Chapter 3 (Materials and methods, thermodynamic modelling section).

Figure 5.12 shows the evolution of each phase over time. The most important observation is that in the presence of Na_2SO_4 the amount of ettringite is significantly higher compared to the alkali free system while in the presence of NaOH it is lower. The addition of NaOH increases the pH of the pore solution which increases solubility of ettringite [106]. With the addition of Na_2SO_4 monosulfate will not precipitate as the sulfate in solution will never be totally consumed due to the high initial addition of Na_2SO_4 .

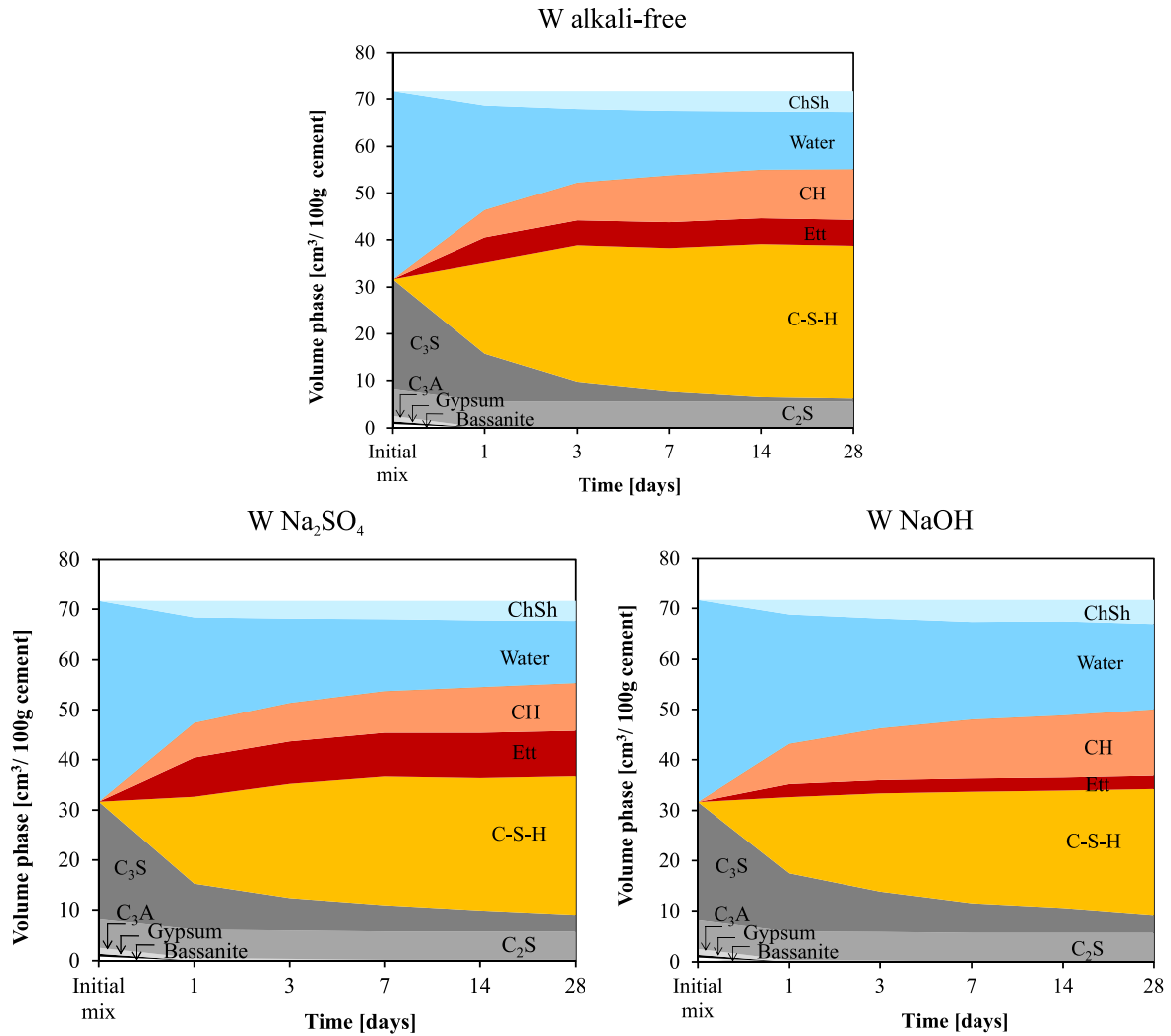


Figure 5.12. Estimation of the phase assemblage over time.

Figure 5.13 compares the capillary porosity estimated by the GEMS calculation to that measured by MIP. MIP technique can measure the connected porosity, mainly capillary porosity (pore radius $\geq 5\text{nm}$). However, recent work of Muller [15] reported that, for non-blended white cement pastes, MIP technique can potentially detect a fraction of the gel porosity in C-S-H (pore radius $<1.5\text{-}5\text{ nm}$) through the comparison of MIP and ^1H NMR porosity results. Therefore, for the present results on white cement pastes, MIP porosity down to a pore radius of 5 nm was taken as a measure of the capillary porosity (i.e. without the inclusion of the gel and interlayer porosity of C-S-H). Figure 5.13 shows a close agreement between the corrected MIP porosity and the GEMS porosity (i.e. remaining water). It is worth noting that the Young's modulus of ettringite (22.4 GPa) and C-S-H (22.55 GPa) are very comparable [107], suggesting that ettringite behaves similarly to C-S-H in its influence on mechanical properties.

Thus, considering the whole phase assemblage, the difference in the amount of ettringite can mainly explain the differences in compressive strength observed between Na₂SO₄ and NaOH for the same DoH of cement. The lower the amount of ettringite, the higher the capillary porosity and consequently, the lower the mechanical strength. For the same DoH of cement, there is a much higher amount of ettringite in the presence of Na₂SO₄ compared to the alkali free system. This agrees with the cumulative MIP curves at 7 and 28 days (Figure 5.10c and Figure 5.10e) because the capillary porosity is lower in the alkali free system and with the addition of Na₂SO₄ than in the presence of NaOH.

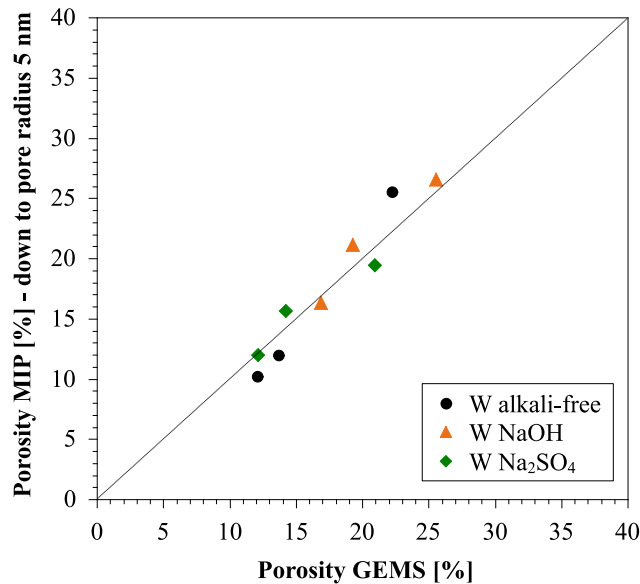


Figure 5.13. Relationship between the porosity measured with MIP (considering the porosity down to a pore radius of 5nm, i.e. the capillary porosity without the C-S-H porosity) and the estimated porosity with GEMS.

Influence of gypsum combined with NaOH on the strength development

Figure 5.14 shows the influence of gypsum combined with NaOH on the relationship between compressive strength and DoH of cement. It is shown that gypsum can mitigate the impact of NaOH. For a same DoH of cement, the system with NaOH plus gypsum has a higher compressive strength than the gypsum with only NaOH. GEMS calculations were done (following the same procedure as mentioned in section 6.1) in order to compare the phase assemblage of both systems. Figure 5.15 shows the calculations. The addition of gypsum promotes the precipitation of a higher volume of hydrates, especially ettringite (similar to the system with Na₂SO₄ in Figure 5.12). Therefore, more space is filled and the compressive strength is improved.

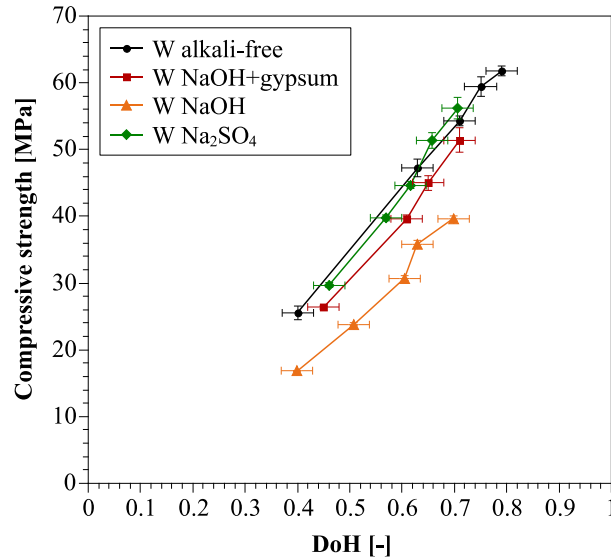


Figure 5.14. Effect of gypsum addition on the compressive strength as a function of the DoH of cement.

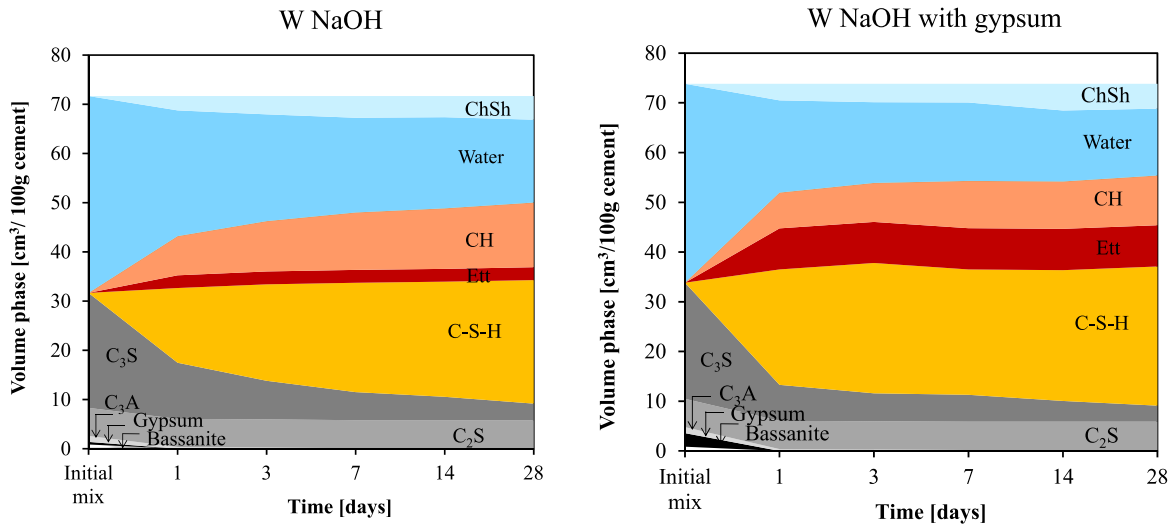


Figure 5.15. Comparison of the phase assemblages (GEMS) over time in the system with NaOH and in the system with NaOH plus gypsum.

6.2. Characteristics of C-S-H

Morphology of C-S-H

Although the difference in the amount of ettringite formed appear to be the reason for the differences in compressive strength, it is interesting to look at the impact of Na_2SO_4 and NaOH on the characteristics of C-S-H.

Figure 5.16 (left column) shows the morphology of C-S-H product on the surface of the grains for each system. In the alkali free system (Figure 5.16a), C-S-H adopts a needle-like divergent morphology (i.e. “fibrillar”) that grows outwards from the surface or sometimes the needles appear to grow in parallel with each other. Some crystals of CH can also be detected. The same C-S-H morphology is identified

with the addition of Na₂SO₄ (Figure 5.16c). The addition of NaOH (Figure 5.16b) leads to an abundant initial precipitation of CH and also a more planar, foil-like C-S-H. C-S-H is not growing outwards but closer to the surface resulting in a network of needles which cover the surface.

Figure 5.16 (right column) also shows the BSE images at 28 days. C-S-H in the presence of Na₂SO₄ (Figure 5.16e) is very similar to the C-S-H in the alkali free system (Figure 5.16d), while in the presence of NaOH (Figure 5.16f) there seems to be less outer C-S-H.

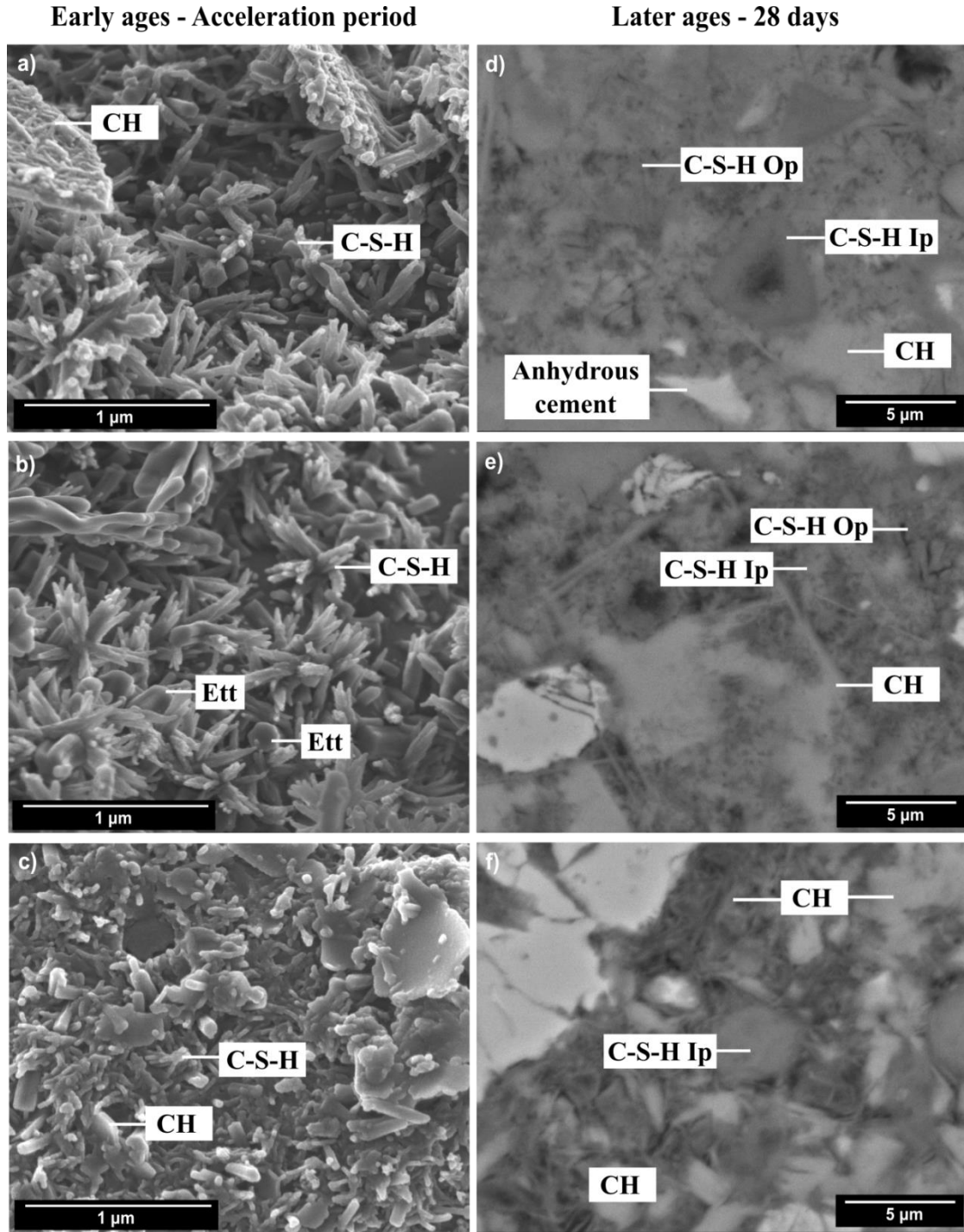


Figure 5.16. Images on the left column show the surface of the cement grains at the end of the nucleation and growth period for each system: a) alkali free system, b) with Na₂SO₄ and c) with NaOH. Images on the right column show SEM-BSE micrographs at 28 days for d) the alkali free system, e) with Na₂SO₄ and f) with NaOH.

BSE images show that in the presence of NaOH (Figure 5.16f) the morphology of CH changes from large and flat, big crystals to small and more homogeneously distributed crystals, as it was previously observed in alite systems in the presence of NaOH (see Chapter 4) or also observed in synthetic C-S-H systems [49]. The precipitation of small and more numerous crystals of portlandite promoted in the presence of NaOH could initially contribute to decrease the size of the largest pores. For instance, the cumulative MIP curve at 24 hours with NaOH (Figure 5.10a) shows a similar capillary porosity to the alkali free system but with a lower critical entry radius probably resulting from a better distribution of CH in the matrix.

Chemical composition of C-S-H

Figure 5.17 shows the composition of the C-S-H measured by EDS microanalyses in the SEM. The presence of Na₂SO₄ or NaOH clearly leads to a lower (Ca-S)/(Si+Al) ratio in C-S-H product (ratio around 1.5) compared to the alkali free system (ratio around 1.7) (Figure 5.17a and Table 5.2).

Figure 5.17a and b also show that the presence of alkali does not seem to increase the uptake of aluminate ions in C-S-H although GEMS simulations indicate a higher concentration of aluminate ions in the solution in the presence of alkali (Figure 5.8). Thus, the uptake of sodium does not seem to be related to a valence compensation mechanism with aluminate ions [108]. L'Hopital et al [109] found that the aluminate ions content of C-S-H was correlated with the concentration of aluminium in solution.

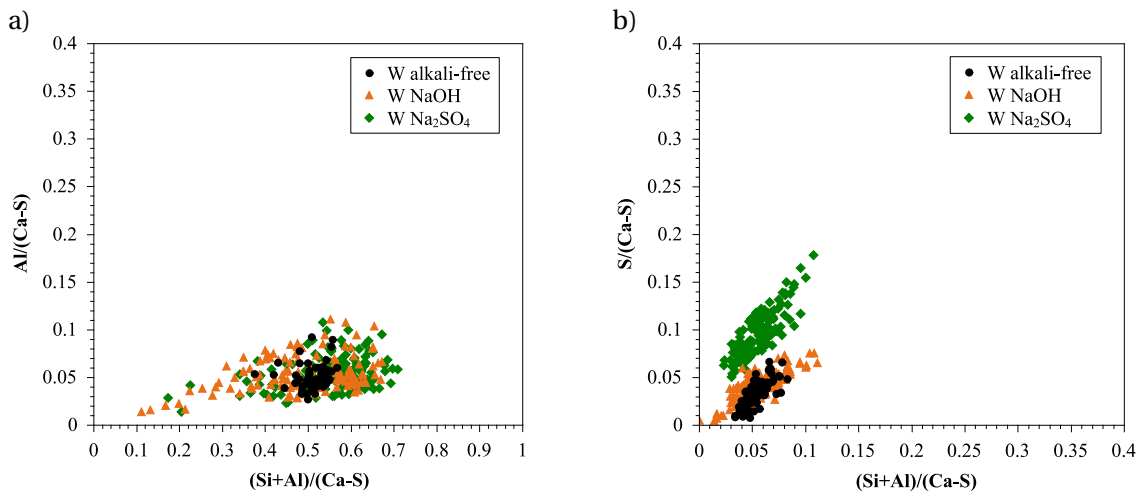


Figure 5.17. Impact of Na₂SO₄ and NaOH on a) (Ca-S)/(Si+Al) and b) S/(Ca-S) ratio of C-S-H at 7 days.

Table 5.2. Quantification of the (Ca-S)/(Si+Al) ratio of C-S-H product at 7 and 28 days.

	(Ca-S)/(Si+Al)	
	7 days	28 days
W alkali free	1.75	1.79
W Na ₂ SO ₄	1.49	1.52
W NaOH	1.52	1.56

Figure 5.18 compares SEM and TEM measurements of the Na/(Si+Al) ratio in C-S-H at 28 days in the alkali-free system and with Na₂SO₄ or NaOH. The addition of Na₂SO₄ or NaOH significantly increases the Na/(Si+Al) in C-S-H. The presence of alkali salts lowers the solubility of calcium and a lower amount of calcium ions in solution is likely to favour the formation of C-S-H with less calcium in the interlayer [22]. This suggests that more sodium ions could be incorporated in the interlayer space of C-S-H. Lognot and coworkers [59] reported that the substitution of Ca²⁺ in the interlayer would be the dominant mechanism for the uptake of alkali in C-S-H with Ca/Si ratios ~1.5. The fact that the ratio is the same for both alkali salts as well as the good agreement between TEM and SEM values suggests that the results are reliable as both alkali systems have been designed to be equivalent in sodium content. These results confirm that at high Ca/Si ratios (~1.5) there is still significant uptake of alkali, contrary to what was reported in [22,53,56], and therefore changes in the structure of C-S-H may be expected.

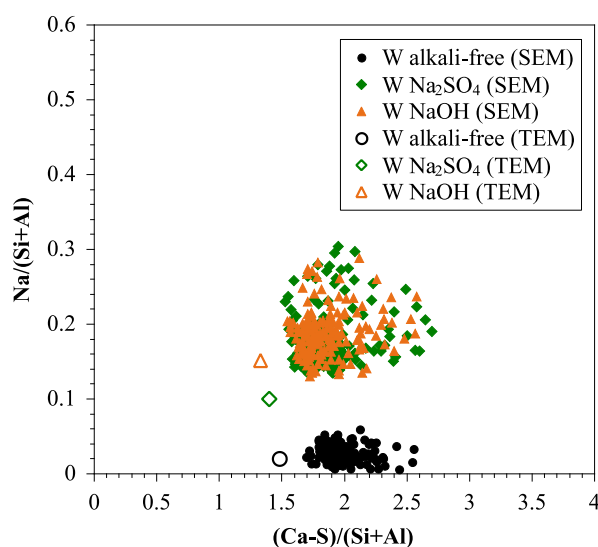


Figure 5.18. The impact of Na₂SO₄ and NaOH on the Na/(Si+Al) ratio at 28 days. Full symbols represent EDX analysis done with SEM and empty symbols represent EDX analysis done with TEM. This ratio represents the total amount of sodium quantified in C-S-H, and it is not possible to identify the less mobile fraction of sodium from the more mobile one.

Density of C-S-H

¹H NMR experiments on sealed samples allow the quantification of each population of water over time: capillary, gel, sheet and solid (see Chapter 2 and Appendix C for more details about this technique). The impact of Na₂SO₄ and NaOH on each population is shown in Figure 5.19. The addition of Na₂SO₄ or NaOH clearly leads to an initial fast reduction of the capillary water during the first hours but from 1 day on it remains higher than in the alkali-free system, especially in the presence of NaOH⁴. The solid signal is significantly higher in the presence of Na₂SO₄ at all ages compared to the alkali free system and with NaOH, which related to the higher amount of ettringite with addition of Na₂SO₄. An interesting observation is that although the evolution of the sheet water remains the same in the presence or absence of alkali, the gel water is significantly reduced in the presence of Na₂SO₄ or NaOH and it never reaches a plateau as it does in the alkali free system from 2 days on.

⁴ The comparison of the capillary porosity from MIP and ¹H NMR is not straightforward since MIP measurements are based on dried samples (hydration stopped) and ¹H NMR measurements are done on non-dried samples. See Chapter 3 (Materials and methods) for more details on each technique.

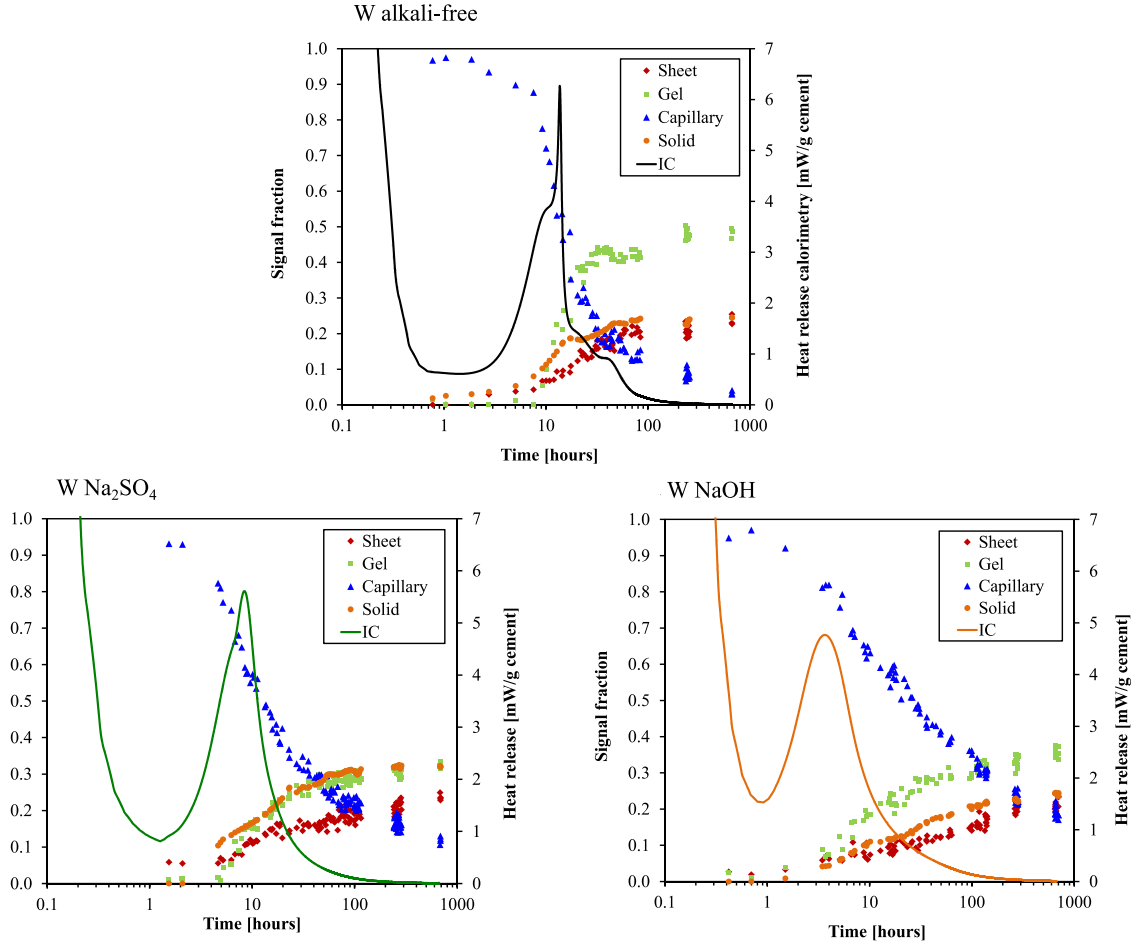


Figure 5.19. Impact of Na_2SO_4 and NaOH on the evolution of each population of water from the mixing time until 28 days, measured by ^1H NMR. Calorimetry curves are represented by the continuous curves.

In order to verify the results from ^1H NMR, the solid intensity was indirectly calculated from XRD measurement and compared to the solid signal from ^1H NMR measurements [15]. The intensity of the solid signal from XRD measurements was calculated based on the amount of ettringite and portlandite as follows,

$$I_{\text{solid from XRD}} = \frac{\frac{CH_{\text{XRD}}}{Mm_{\text{CH}}} \times CH_{\text{H}_2\text{O}} + \frac{Ett_{\text{XRD}}}{Mm_{\text{Ett}}} \times Ett_{\text{H}_2\text{O}}}{0.35} \quad [\text{Eq. 5.1}]$$

where CH_{XRD} is the amount of portlandite from XRD, Mm_{CH} is the molar mass of portlandite (74 g/mol), $CH_{\text{H}_2\text{O}}$ is the number of water molecules in portlandite (18 water molecules), Ett_{XRD} is the amount of ettringite from XRD, Mm_{Ett} is the molar mass of ettringite (1255 g/mol) and $Ett_{\text{H}_2\text{O}}$ is the number of water molecules in ettringite (576 water molecules).

Figure 5.20 shows the comparison of the solid signal between ^1H NMR and XRD for each studied system. The two techniques show a good agreement.

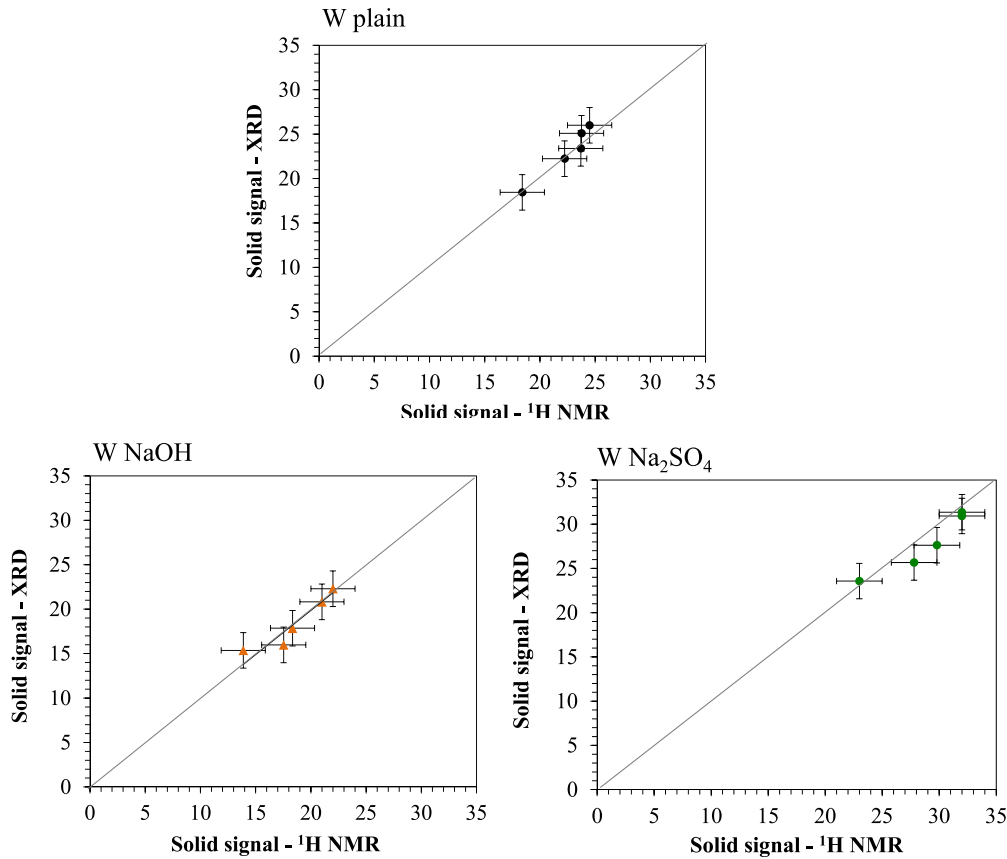


Figure 5.20. Solid signal from ¹H NMR compared to that from XRD. Error bars correspond to the instrumental errors.

The ratio between the gel water and the sheet water is an indication of the amount of the amount of water in C-S-H. Figure 5.21 shows the evolution of the relative humidity of the samples as a function of the gel/sheet ratio in C-S-H at 28 days calculated with ¹H NMR. The gel/sheet ratio appears to decrease with the presence of Na₂SO₄ or NaOH in the following order: alkali free > NaOH > Na₂SO₄. Lower gel/sheet values suggest a lower amount of water in the C-S-H product, and it corresponds also to the lower RH values (lower a_w). Therefore, the more ions in solution (i.e. the lower a_w), the less the water seems to be available for C-S-H to grow.

Figure 5.22 shows the impact of Na₂SO₄ and NaOH on the solid and gel density of C-S-H measured with ¹H NMR. Despite the lower water content in C-S-H with the presence of alkali salts, the density of the C-S-H 'gel' (including gel pores) is not measured to be higher. The solid density of C-S-H is lower in the presence of Na₂SO₄ or NaOH but the gel density remains the same as in the alkali free system (~2 g/cm³).

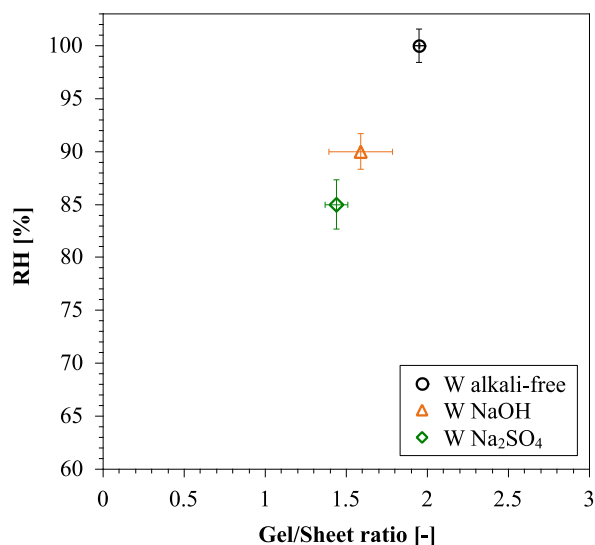


Figure 5.21. Impact of NaOH and Na₂SO₄ on the relationship between RH and gel/sheet ratio at 28 days (error bars for the gel/sheet ratio correspond to a standard deviation on the average of several measurements).

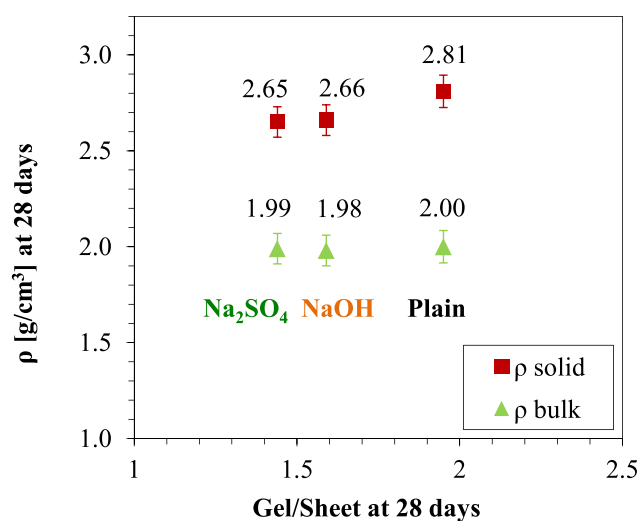


Figure 5.22. Impact of NaOH and Na₂SO₄ on the solid density (squares) and gel density (triangles) of C-S-H at 28 days measured with ¹H NMR.

The impact of alkali on the structure of C-S-H

Lothenbach and Nonat [22] recently reported that lower Ca/Si ratios lead to a higher Na/Si ratio with a higher incorporation of sodium in the interlayer space and less sodium adsorbed in the surface of C-S-H. In a range of Ca/Si ratios from 1.6 to 1.4, as for the present study, the authors reported that despite not changing significantly the Na/Si ratio, the distribution of Na population between the fraction in the interlayer space and the fraction adsorbed in the surface of C-S-H can change from ~35%/ 65% (Na interlayer/ Na adsorbed in C-S-H surface) for a Ca/Si ratio of 1.6 to almost 50% / 50% for a Ca/Si ratio of 1.4. Therefore, for Ca/Si ratios ~1.4 the incorporation of sodium in the interlayer space could be greater.

The solid density is quantified to be lower in the presence of Na₂SO₄ or NaOH (Figure 5.22). However, the amount of interlayer water at 28 days is the same whether in the presence or absence of alkali (~22-23%). A lower amount of calcium ions in solution due to high levels of alkali leads to less calcium ions in the interlayer according to Lothenbach and Nonat [22] which would mean that the Coulomb interactions (i.e. electrostatic force between the atoms) are weaker because the interactions with the monovalent Na⁺ are weaker than with the divalent Ca²⁺. This all indicates an increase of the interlayer space, as represented in Figure 5.23. A bigger distance between the layers would suggest a C-S-H with less layers/cm³ and more water (see the blue squared areas in Figure 5.24), meaning that the solid density of C-S-H would be lower⁵. Figure 5.24 shows schematically these effects.

The present observations agree with the work of L'Hôpital and coworkers [109] where they recently reported that KOH modifies the structure of synthetic C-S-H by increasing the interlayer distances as potassium ions can partially replace the calcium ions in the interlayer. Moreover, the author [55], as well as Stade [56], did not observe any difference between the uptake of sodium and potassium ions in synthetic C-S-H which suggests that sodium would cause the same effect.

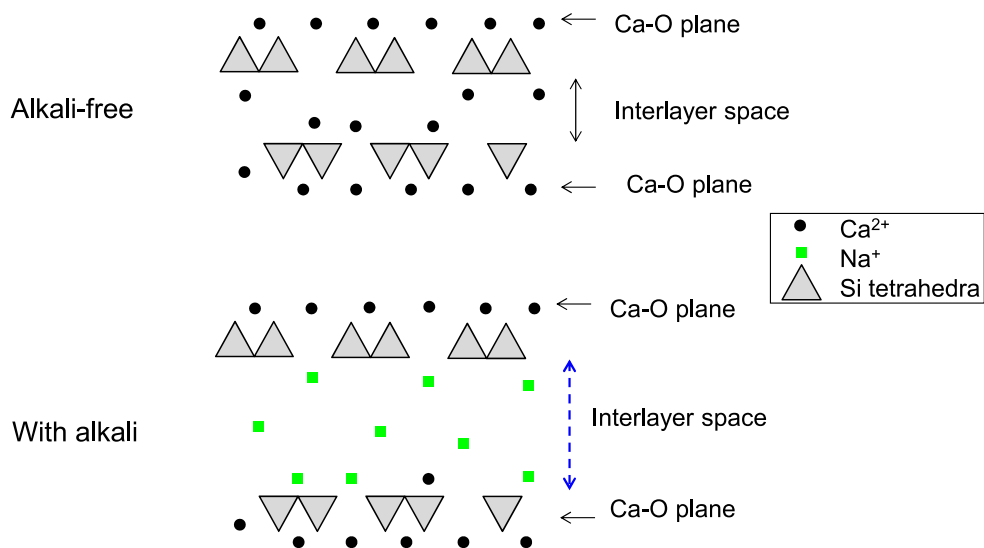


Figure 5.23. Schematic representation of the impact of Na₂SO₄ and NaOH in the chemical structure of C-S-H. At high Ca/Si ratios, C-S-H chains are dominated by dimers [24].

⁵ The potential influence of differences in the ionic size of Ca²⁺ and Na⁺ was not considered in this work due to the following drawbacks: a) the absence of consensus in the hydrated/solvated \varnothing of Na⁺ and b) the absence of consensus in the enthalpy of hydration (i.e. how easily the ion is de-solvated).

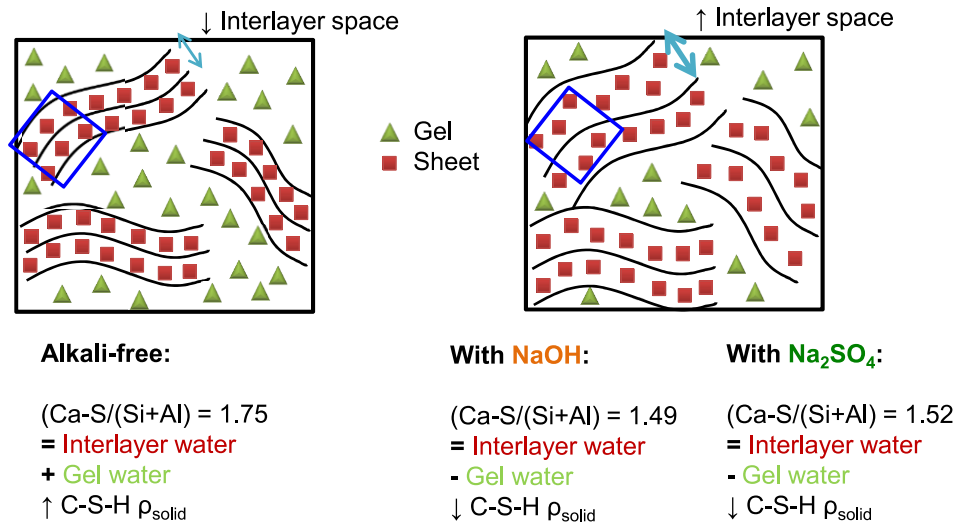


Figure 5.24. Schematic representation of the impact of Na_2SO_4 and NaOH in the C-S-H. The whole picture corresponds to the bulk C-S-H, including squares and triangles, while the solid C-S-H is represented by the blue squares.

7. Summary

- Na_2SO_4 and NaOH clearly accelerate the kinetics during the first hours, and so the DoH of cement is higher. However, at later ages the DoH of cement is lower compared to the alkali free system. The DoH of both C_3S and C_3A are lower.
- From alite systems it was suggested that a higher concentration of aluminate ions in solution in the presence of alkali could contribute to a lower DoH. The same trends are observed for white cement systems from GEMS calculations. However, the lower DoH of cement for white cement systems seems to be better related by a second potential mechanism: a lower RH (explained by a lower water activity) is observed in the presence of Na_2SO_4 or NaOH , and in both systems the RH decreases at the same time, leading to very similar RH at later ages for both alkali systems, which agrees with the same DoH in both cases at later ages. The present results suggest that a lower DoH of cement could not only be explained by a single mechanism but rather through several of them.
- The strength development is directly related to the amount of porosity.
- For the same DoH of cement, the compressive strength in the system with Na_2SO_4 is the same as in the alkali free system. Na_2SO_4 promotes a higher volume of hydrates that fill more space and lower the porosity. It favours the precipitation of ettringite. On the contrary, the addition of NaOH results in significantly lower compressive strengths. It inhibits the precipitation of ettringite and outer C-S-H so there is a lower volume of hydrates filling the space and consequently a higher porosity.
- The addition of Na_2SO_4 promotes a divergent morphology of C-S-H due to the adsorption of sulfate on C-S-H while NaOH leads to a more planar morphology. The same effect was observed in Chapter 4 with alite systems. However, the mechanical strength appears not to be

affected by these changes in the morphology of C-S-H. The addition of Na₂SO₄ or NaOH leads to a lower Ca/Si ratio, as well, but this also appears not to affect the mechanical strength.

- EDX analysis show that the presence of NaOH or Na₂SO₄ favours the uptake of sodium in C-S-H but it does not appear to be related to the uptake of aluminate as it was measured to be the same with and without alkali salts.
- The solid density of C-S-H is lower in the presence of Na₂SO₄ or NaOH and could be explained through the incorporation of sodium ions in the interlayer space replacing calcium ions. However, the gel (bulk) density is not affected by the addition of NaOH and Na₂SO₄.

CHAPTER 6. The impact of NaOH and Na₂SO₄ on white cement-slag systems

1. Introduction	81
2. The impact of NaOH and Na ₂ SO ₄ on white cement-slag systems.....	82
2.1. Systems studied	82
2.2. Mechanical strength.....	82
2.3. Kinetics	84
2.4. Composition of pore solution	88
2.5. Phase assemblages	90
2.6. Distribution of hydrates in the matrix.....	93
2.7. Porosity.....	95
3. Impact of sodium gluconate on white cement-slag systems with Na ₂ SO ₄	98
3.1. Reason to study the impact of sodium gluconate	98
3.2. Systems studied	98
3.3. Mechanical strength.....	99
3.4. Kinetics	100
3.5. Phase assemblages	101
3.6. Distribution of hydrates and morphology of C-S-H.....	102
3.7. Chemical composition of C-S-H.....	105
3.8. Water distribution in capillary and C-S-H porosity.....	107
3.9. Discussion on the effect of sodium gluconate	110
4. Summary	112

1. Introduction

In the previous chapters it was observed that a better strength development in the presence of Na₂SO₄ compared to NaOH is mainly related to a higher volume of hydrates and thus a lower porosity and independent on the morphology, chemical composition and density of C-S-H. The present chapter describes the effect of Na₂SO₄ and NaOH on white cement-slag systems. The two main goals are:

- To study the impact of Na₂SO₄ and NaOH on the phase assemblage of slag systems.
- To understand the impact of sodium gluconate combined with Na₂SO₄ on the strength development compared to the addition of only Na₂SO₄.

2. The impact of NaOH and Na₂SO₄ on white cement-slag systems

2.1. Systems studied

Figure 6.1 shows the white cement-slag systems studied and Table 6.1 shows further details of the used formulations, Two slags were used (slag 1 and slag 8) at high replacement levels. The concentrations of NaOH and Na₂SO₄ added in solution were kept the same as for the alite and white cement systems. It is worth noting that slag 8 has a higher content of aluminium oxide than slag 1 (see Chapter 3 for the chemical composition of slags).

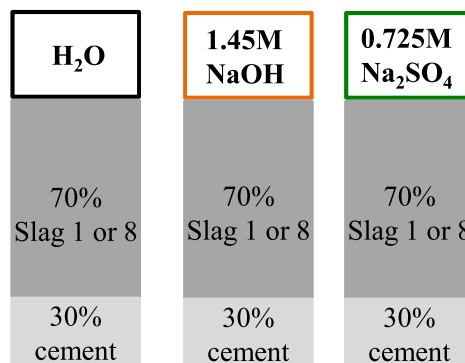


Figure 6.1. Composition of the slag mixes studied, in wt.%.

Table 6.1. Formulations of the slag mixes studied.

	White cement [wt.%]	Slag 1 or 8 [wt.%]	Mixing solution	Nomenclature in figures
	30	70	DI-water	W70S1
Slag 1	30	70	1.45M NaOH	W70S1 NaOH
	30	70	0.725M Na ₂ SO ₄	W70S1 Na ₂ SO ₄
	30	70	DI-water	W70S8
Slag 8	30	70	1.45M NaOH	W70S8 NaOH
	30	70	0.725M Na ₂ SO ₄	W70S8 Na ₂ SO ₄
	30	70	DI-water	W70S1

2.2. Mechanical strength

Figure 6.2 shows the impact of Na₂SO₄ and NaOH on the compressive (Figure 6.2a and b) and flexural strength (Figure 6.2c and d) of slag systems. In the presence of Na₂SO₄ the compressive strength is higher than in the alkali free system for a longer period compared to the non-blended systems: in the non-blended system, Na₂SO₄ led to a decrease of the compressive strength at all the testing times except at 1 day, while the addition of Na₂SO₄ in the slag 1 system increases the compressive strength

significantly up to 14 days. From then on the values are equivalent to the alkali free system. A very similar trend is observed in for the slag 8 system with Na₂SO₄ as the compressive strength is also increased up to 7 days but from there on is lower than in the alkali free system. The addition of NaOH clearly leads to a decrease of the compressive strength at all the ages tested compared to the alkali free systems, except at 1 day when the compressive strengths are comparable. This is the same effect as was observed with the addition of NaOH to non-blended systems.

On the contrary, the flexural strength of the three systems is fairly similar in both slag 1 and slag 8 systems. The systems with Na₂SO₄ seem to have slightly higher flexural strength until 28 days but the differences are not significant and no further conclusions can be done since only two specimens were tested at each time. The flexural strength does not appear to increase significantly after 7-14 days.

For the cement-slag systems, the relationship between the compressive strength and the DoH of cement is not very informative, because besides the DoH of cement there is also the degree of reaction of slag.

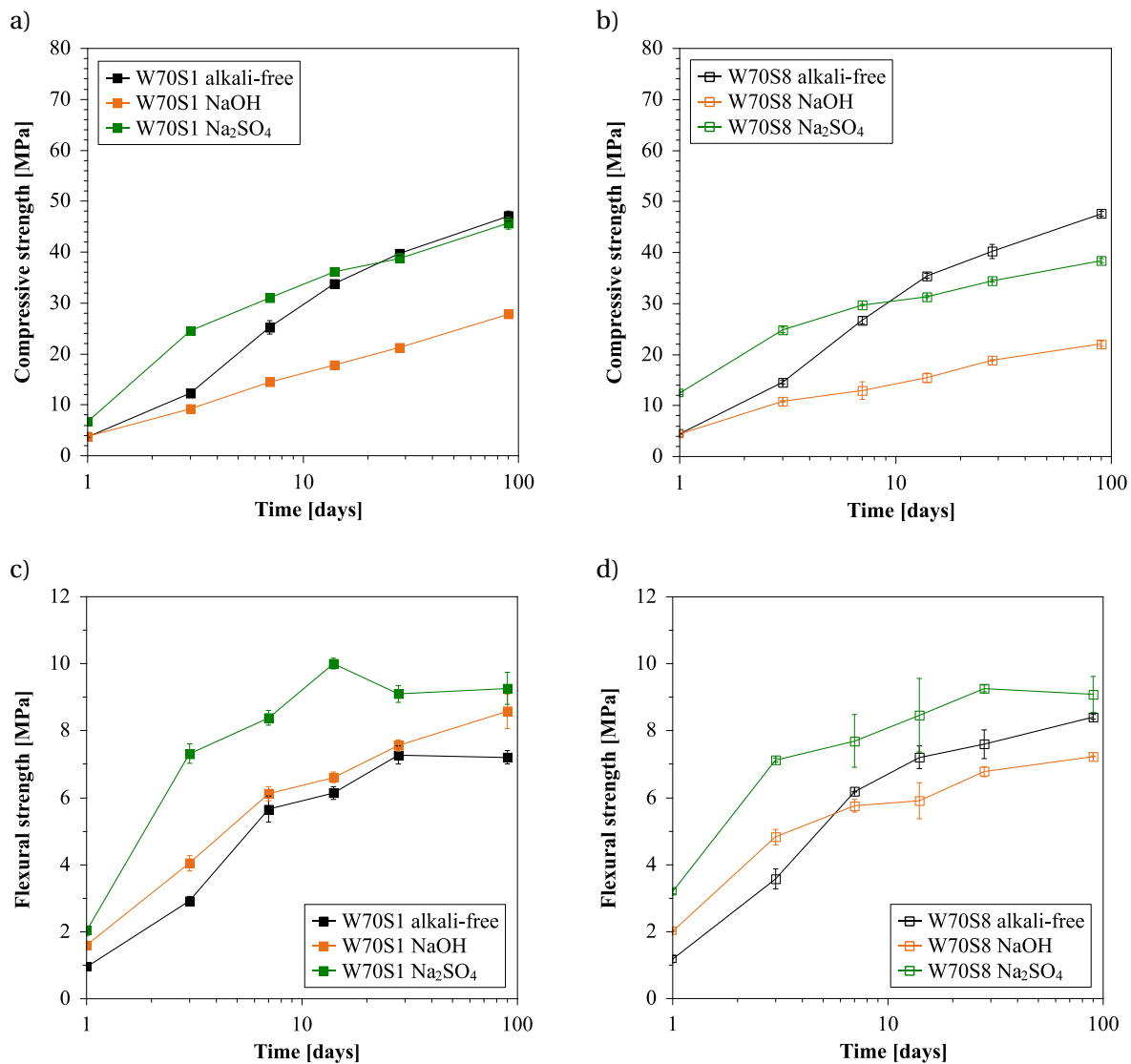


Figure 6.2. Evolution of the compressive and flexural strength in the presence of Na₂SO₄ and NaOH for slag 1 (a and c) and slag 8 systems (b and d).

2.3. Kinetics

Figure 6.3 shows the evolution of the cumulative heat release over time for the slag systems. The trends observed with the addition of Na_2SO_4 are quite different for the two slags. The cumulative heat appears to be equal (for slag 8) or higher (for slag 1) compared to the alkali free systems, while in the non-blended systems with Na_2SO_4 it was lower than the alkali free system and more similar to the NaOH system. The addition of NaOH lowers the cumulative heat release, as in the non-blended systems.

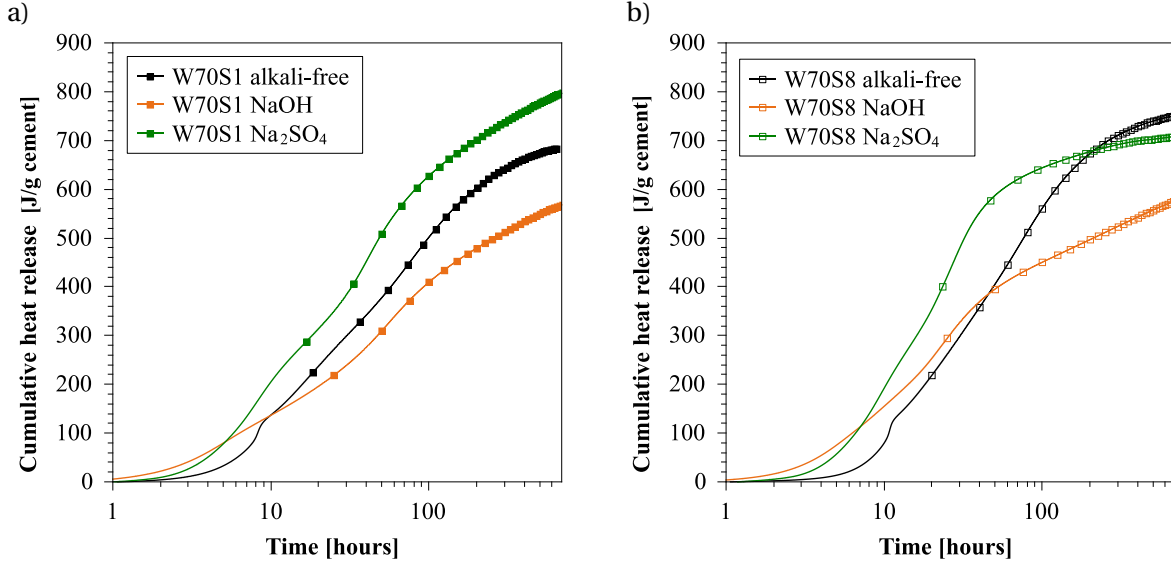


Figure 6.3. Effect of Na_2SO_4 and NaOH on the cumulative heat release up to 28 days for a) slag 1 and b) slag 8 systems.

Degree of hydration of cement

Figure 6.4 shows the evolution of the DoH of cement for each system. For both slags, the presence of Na_2SO_4 increases the DoH of cement at 1 day but afterwards, from 7 days on, it remains constantly 10% lower than in the alkali free systems. In the non-blended systems, the addition of Na_2SO_4 also lowered the DoH of cement a 10% at later ages (see Figure 6.4, where the DoH of cement of slag systems and non-blended systems can be compared) and the DoH of cement is never higher with the presence of alkali. Therefore, the equal or higher cumulative heat release for the Na_2SO_4 system compared to the alkali free system (instead of being 10% lower), suggests that Na_2SO_4 promotes the reaction of slag.

In the non-blended systems, the presence of NaOH lowered the DoH of cement by 10% (as with Na_2SO_4). However, in both slag 1 and 8 systems the presence of NaOH lowers the DoH of cement by ~25% from 3 to 28 days compared to the alkali free systems (see Figure 6.4).

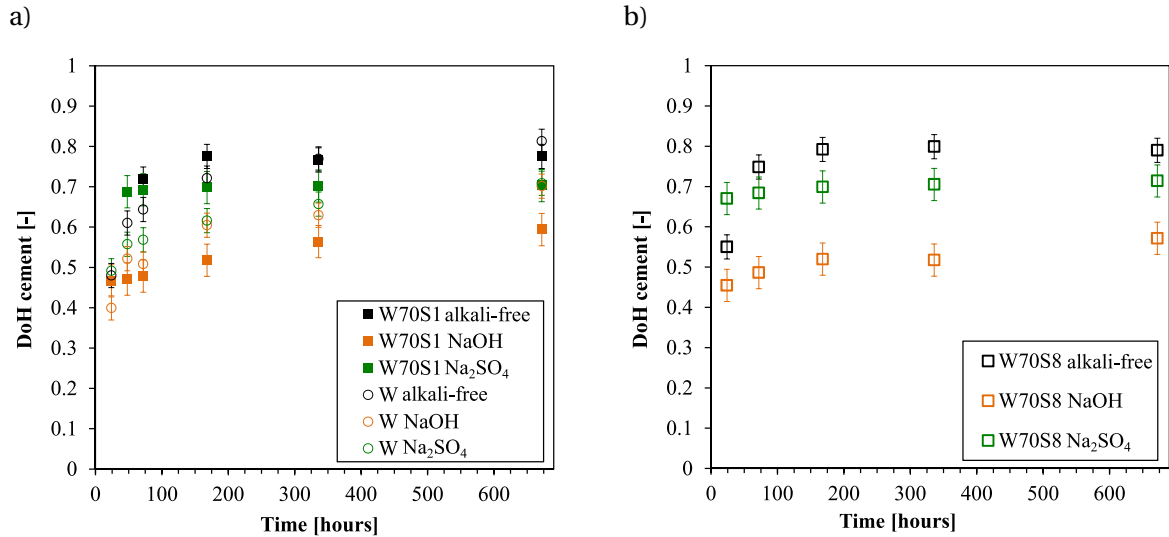


Figure 6.4. Effect of Na₂SO₄ and NaOH on the degree of hydration of cement up to 28 days for a) slag 1 systems (included the DoH of cement in the non-blended systems for comparison) and b) slag 8 systems.

Figure 6.5 and Figure 6.6 show the impact of Na₂SO₄ and NaOH on the DoH of C₃S and C₃A, respectively. The trends of the impact of Na₂SO₄ and NaOH on the DoH of C₃S are the same as the DoH of cement. At 28 days, and for both slag 1 and slag 8 systems, C₃S is fully hydrated in alkali free systems, while it reaches a DoH of 0.85 with Na₂SO₄ and 0.7 with NaOH.

The DoH of C₃A is also lower in the presence of alkali although C₃A in the slag 8 system with Na₂SO₄ tends to be fully hydrated at 28 days. Due to the low amount, the quantification of C₃A is more uncertain.

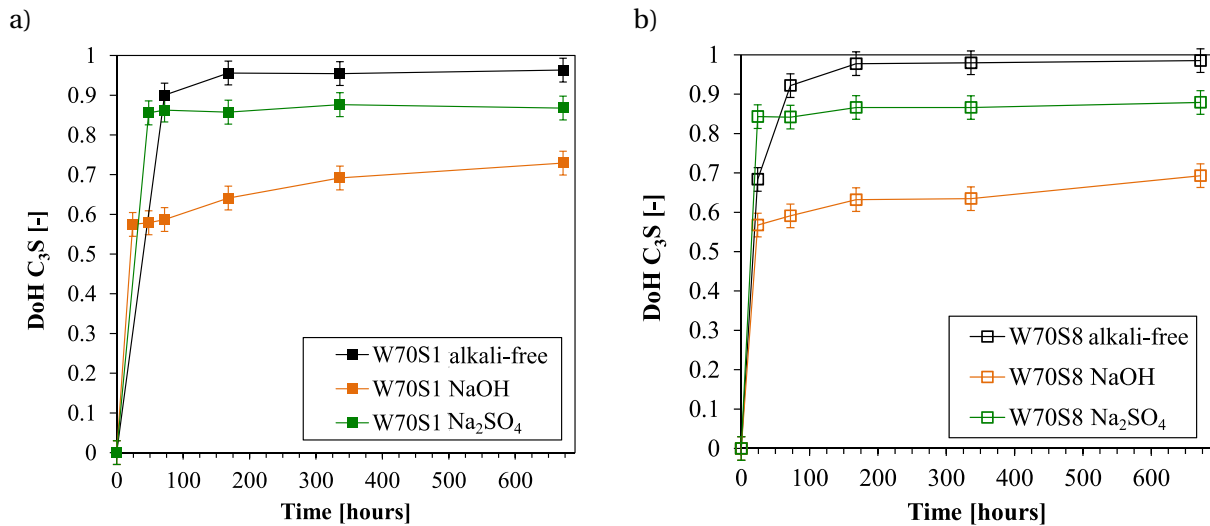


Figure 6.5. Impact of Na₂SO₄ and NaOH on the DoH of C₃S over time for a) slag1 and b) slag 8 systems.

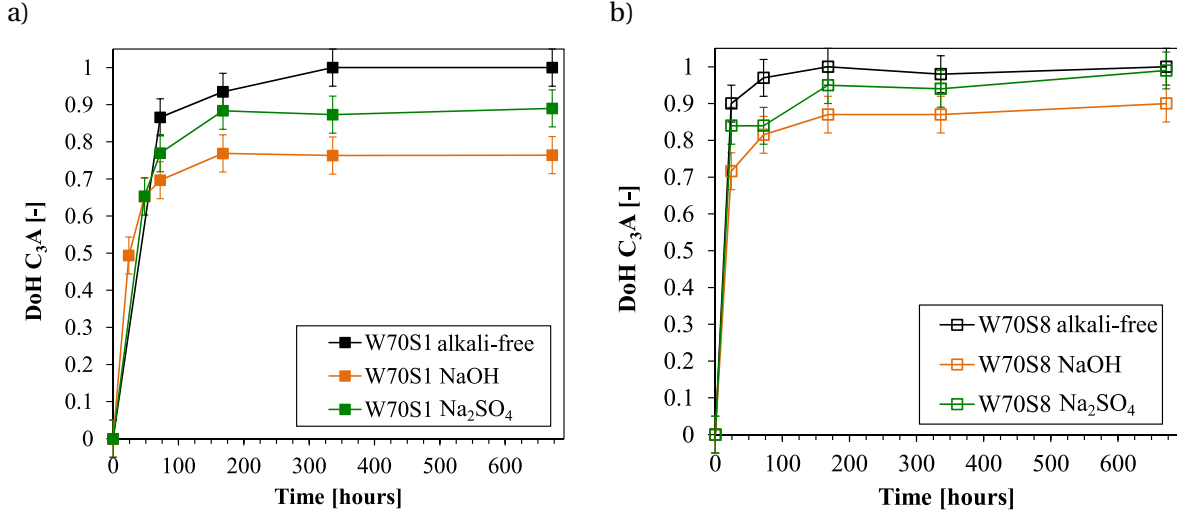


Figure 6.6. Impact of Na_2SO_4 and NaOH on the DoH of C_3A over time for a) slag1 and b) slag 8 systems.

Degree of reaction of slag

Kocaba [110] deduced the effect of slag from the subtraction of a reference calorimetry curve (quartz) from the slag curve. This method assumes that the reaction of the clinker component is the same in the quartz-cement systems with the same replacement level. This method was recently adapted by Berodier [84] after showing that the cement hydration is affected by the replacement of slag. The author estimated the slag reaction based on the heat released from the overall reaction and the degree of hydration of cement previously calculated. The calculated contribution to the heat evolution of the slag is directly proportional to the degree of slag reaction in the blend.

Therefore,

$$H_{slag} = \frac{H_{overall} - H_{cement}}{m_{slag}} \quad [Eq. 6.1]$$

where,

H_{slag} is the heat released from the slag reaction per gram of slag in the blend

$H_{overall}$ is the total heat released from the hydration of the blend. It is determined from the cumulative heat release recorded by isothermal calorimetry.

H_{cement} is the heat released from the hydration of clinker phases.

As a first approximation it was assumed that the alkali salts do not significantly change the enthalpy of reaction and a potential change on the degree of reaction between the two slags for a given enthalpy is not considered. The amount of C_3S , C_2S and C_3A consumed were quantified by XRD-Rietveld analysis and are assumed to react as:

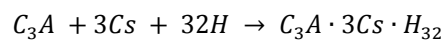
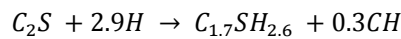
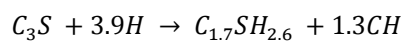


Table 6.2. Enthalpies of the three major reactions in cement hydration [16].

Reaction	H [J/g]
C ₃ S	558
C ₂ S	362
C ₃ A	747

Figure 6.7 shows the contribution of the slag calculated by this method. At 3 days of hydration both alkali salts increase the reaction of slag compared to the alkali free system. From then on, Na₂SO₄ promotes the reaction of slag while NaOH seems to limit its reaction (as well as the degree of hydration of cement, see Figure 6.4). At 28 days, the degree of reaction of slag 1 in the presence of Na₂SO₄ is higher than that of slag 8 (which reaches the same degree of reaction as the alkali free system with slag 8) while in the alkali free and with NaOH systems the degree of reaction of both slags is the same.

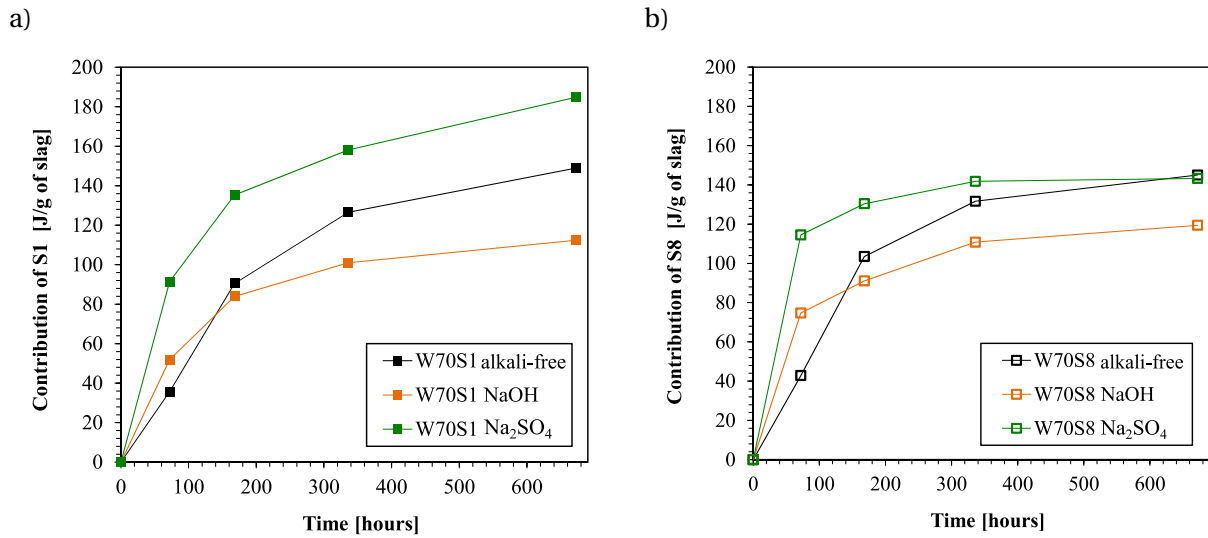


Figure 6.7. Contribution of a) slag 1 and b) slag 8 on the total heat release measured with isothermal calorimetry.

The degree of reaction of slag 1 in the alkali free sample at 28 day was measured with coupled image analysis (IA) of BSE and EDS Mg mappings. The method used is similar to the one described by Kocaba et al. [111] but a new algorithm was written by J. Bizzozero and P. Durdzinski (a detailed description about this technique and the algorithm used can be found in [112]).

The degree of reaction of slag 1 was found to be $25.1 \pm 2\%$. The contribution of slag to the total heat released in the system is proportional to its degree of reaction. Therefore, the degree of reaction of slag in the remaining systems at 28 days can be estimated as follows:

$$DoR\ Slag_x = \frac{Heat_x \times DoR\ Slag_{ref}}{Heat_{ref}} \quad [Eq. 6.2]$$

where,

$Heat_x$ is the heat contribution from slag in the system of interest (x) at 28 days

$DoR\ Slag_{ref}$ is the degree of reaction of slag 1 in the alkali free system at 28 days (25.1±2%)

$Heat_{ref}$ is the heat contribution from slag 1 in the alkali free system at 28 days (148.8 J/g slag 1).

To validate this calculation, the DoR of slag 1 in the system with Na_2SO_4 at 28 days was also measured with the coupled image analysis and mapping technique and compared with the value calculated from the equation above. The degrees of reaction obtained were 35±2% and 33.1±2%, respectively, which shows a good agreement between the two techniques. Table 6.3 shows the DoR of slag for each system at 28 days.

Table 6.3. Degree of reaction of slag (±2%) for each system at 28 days.

	DoR Slag 1 at 28 days		
	Contribution S1 calorimetry [J/g slag]	Calculated from [Eq 6.2] [%]	IA+EDS [%]
W70S1 alkali free	148.8	25.1	25.1 (reference)
W70S1 Na_2SO_4	184.8	33.1	35 (validation)
W70S1 NaOH	112.4	18.9	-

	DoR Slag 8 at 28 days		
	Contribution S1 calorimetry [J/g slag]	Calculated from [Eq 6.2] [%]	IA+EDS [%]
W70S8 alkali free	145.1	24.5	-
W70S8 Na_2SO_4	143.2	24.1	-
W70S8 NaOH	119.3	20.6	-

2.4. Composition of pore solution

Figure 6.8 shows the concentration of sulfate in the pore solution extracted from the first hours until 28 days. The addition of Na_2SO_4 or NaOH increases the amount of sulfate in solution at early (<24 hours). The highest amounts of sulfate correspond to the systems with Na_2SO_4 . Figure 6.9 shows the concentration of aluminate ions in the pore solution. A higher concentration of aluminate ions in solution in the presence of Na_2SO_4 or NaOH could be related to the increased solubility of aluminate in alkali systems.

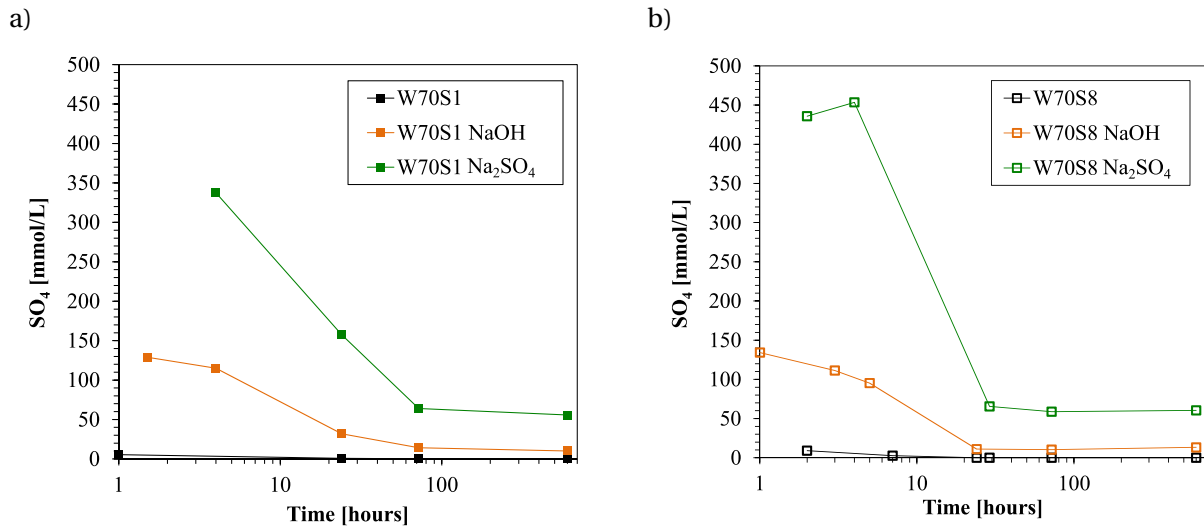


Figure 6.8. Sulfate concentration in pore solution extracted over time for a) slag 1 and b) slag 8 systems.

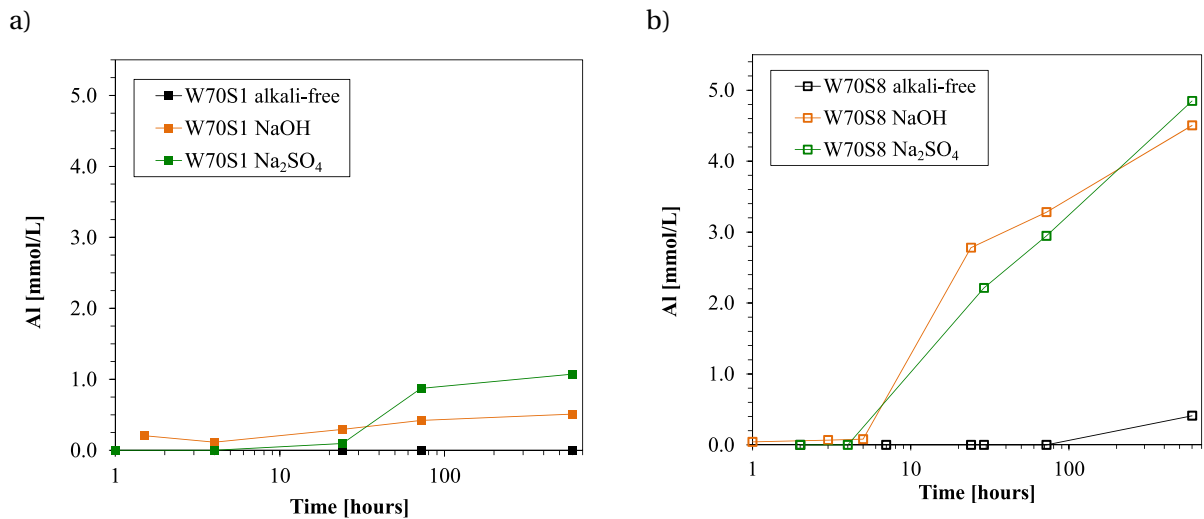


Figure 6.9. Concentration of aluminate ions in pore solution extracted over time for a) slag 1 and b) slag 8 systems. In slag systems, most of aluminate ions in solution comes from the dissolution of slag. Slag 8 has a higher Al₂O₃ content than slag 1. Both slags contain more Al₂O₃ than white cement.

In the previous chapter (Chapter 5) it was proposed that the a slower dissolution of silicate phases in the presence of alkali could be linked to a lower relative humidity (and a lower activity of water) and/or a higher concentration of aluminate ions in solution (due to the increase in the solubility of aluminium in presence of alkali) compared to the alkali free system (see Chapter 5, Figure 5.8). For non-blended systems, the lower DoH of cement was suggested to be more related to a lower relative humidity as they both decreased at the same time.

Figure 6.10 shows the evolution of the RH for slag 1 systems until 28 days. RH does not decrease significantly in the presence of alkali (contrary to non-blended systems where RH decreased since the first day, see Figure 5.8 in Chapter 5). In slag 1 systems with Na₂SO₄ the RH remains at 100% during the first 5 days and then it decreases smoothly reaching ~93% RH around 28 days. NaOH maintains an RH

around 100% until ~10 days and from then on it starts to decrease reaching ~98% RH at about 28 days, which is fairly insignificant.

The RH humidity measurements suggest that the slowdown of the hydration kinetics in the presence of alkali is not directly linked to a lower activity of water. The RH remains around 100% during the first 10 days in the presence of NaOH, but the degree of hydration of C_3S is already much lower at 3 days compared to the alkali free system. The higher RH in slag systems compared to the unblended systems could be explained by the higher dilution of the clinker compared to the unblended systems and the relatively low DoH of slag compared to clinker.

On the other hand, the concentration of aluminate ions in solution appears to be a contributing factor to a lower DoH. The main dissolution of C_3S takes place during the first 24 hours as these are highly diluted systems with slag. The concentration of aluminate ions during the first 24 hours (Figure 6.9) is higher in the systems with NaOH, which agrees with the lower dissolution of C_3S already at 24 hours. It could be that with the addition of Na_2SO_4 , C_3S had more time to continue dissolving at early ages since the concentration is not that high at 24 hours. However, a higher concentration of aluminate ions seemed unlikely to explain the whole of the effect on the slowdown of the hydration kinetics in white cement systems (Chapter 5).

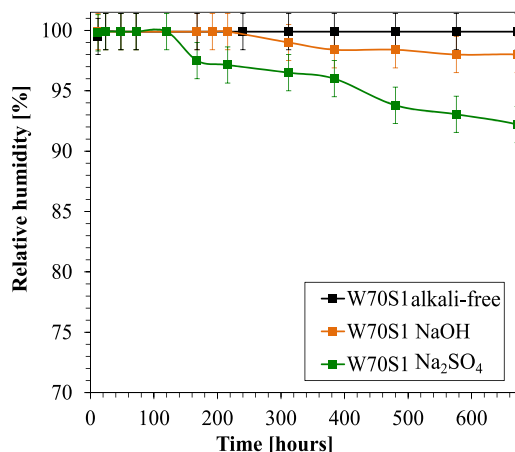


Figure 6.10. Effect of NaOH and Na_2SO_4 on the relative humidity of slag 1 systems over time.

2.5. Phase assemblages

GEMS was used to calculate the phase assemblage for slag systems at 28 days. However, it was used as a mass balance calculation instead of a proper thermodynamic calculation. This was done because in some systems the hydrates precipitated with GEMS did not agree with the hydrates identified with XRD-Rietveld; e.g. with the addition of Na_2SO_4 portlandite was not calculated in GEMS calculations but XRD analysis confirmed its precipitation as shown in Figure 6.11. For this reason, and to ensure that the phase assemblage better approaches the reality, the amounts of ettringite, portlandite and AFm phases measured with XRD-Rietveld were used as input for a mass balance with GEMS. For each calculation, the DoH of each individual anhydrous phase - mainly C_3S and C_3A , as C_2S starts to react from 28 days on- measured from XRD-Rietveld analysis was used as input for the calculation. A new phase corresponding to slag 1 was created in the programme based on the XRF analysis. The amount of slag reacting for the calculation was considered from the DoR previously calculated (see DoR of slags in Table 6.3). The amount of water introduced in GEMS corresponded to a w/s 0.4. As an approximation, the volume of C-S-H was estimated based on the gel density value of 2 g/cm^3 obtained from ^1H NMR analysis in Chapter 5.

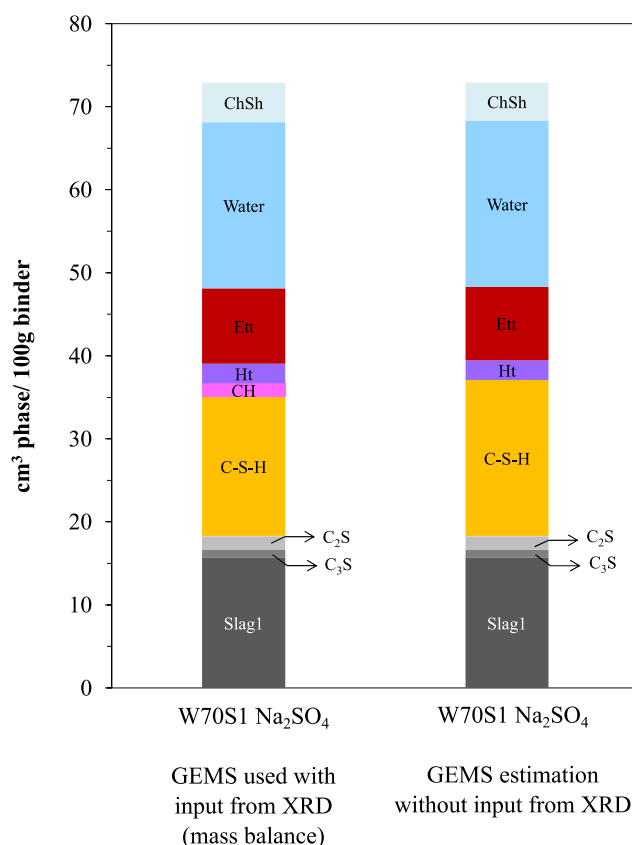


Figure 6.11. Comparison between GEMS and mass balance calculations for the slag system with Na₂SO₄ at 28 days. (CH: portlandite, Ht: Hydrotalcite, Ett: ettringite)

Figure 6.12 shows the volume of each phase at 28 days for slag 1 and Figure 6.13 for slag 8 systems. In the presence of Na₂SO₄ the amount of ettringite is significantly higher compared to the alkali free system (more than three times higher in volume). The same effect was previously observed in the non-blended systems (see Chapter 5). In the presence of NaOH the volume of hydrates is lower than in the alkali free system or with Na₂SO₄. In the slag, alkali free systems at 28 days there is a small precipitation of Hc or Ms (in slag 1 and 8 systems, respectively). Those are absent in the presence of Na₂SO₄, as well as in slag 8 systems with NaOH. But in slag 1 systems, NaOH promotes the precipitation of a solid solution of Hc/Ms⁶ with a volume three times higher than that in the alkali free system.

U-phase (Na-substituted AFm phase) can precipitate in systems with the presence of sodium ions. However, it was not detected from XRD analysis in any of the here studied alkali systems and at any testing time.

⁶ A mix of Ms and Hc was identified in XRD in slag 1 system with NaOH which indicates the presence of a solid solution of both phases already suggested in [113,114]. The diffraction pattern of the solid solution Hc/Ms was centered at 10.63 °2θ (with a broad peak shape between 10.16-11.16 °2θ).

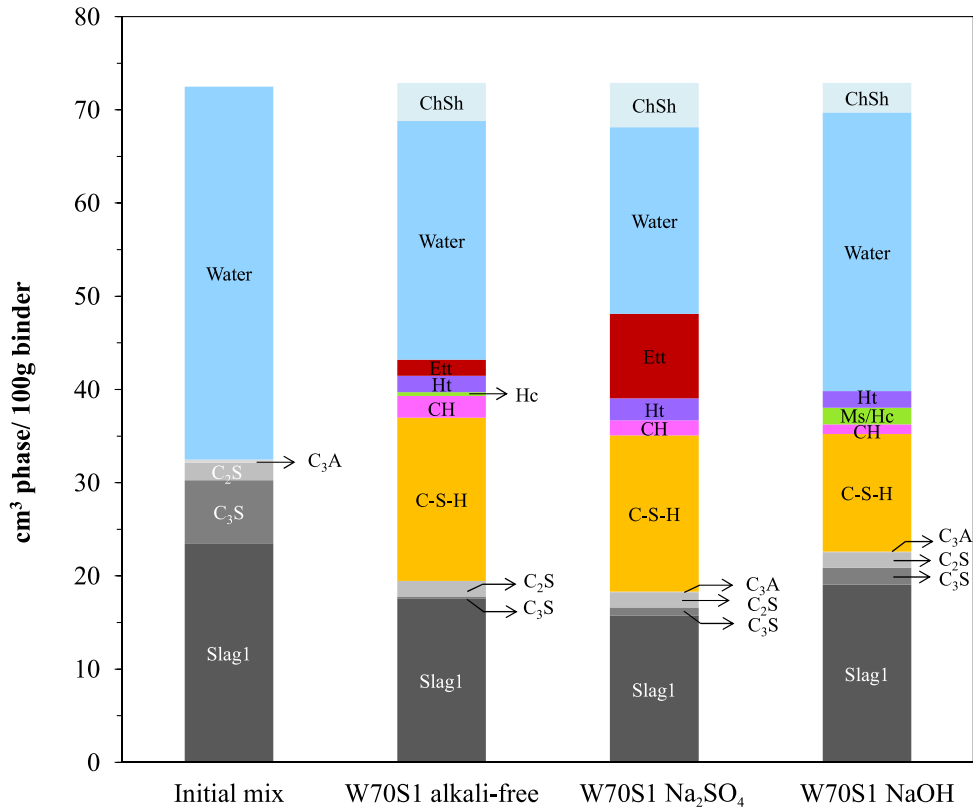


Figure 6.12. Estimation of the phase assemblage for slag 1 systems at 28 days (CH: portlandite, Ht: Hydrotalcite, Ett: ettringite, Hc: hemicarboaluminate, Ms/Hc: Solid solution hemicarboaluminate and monosulfoaluminate).

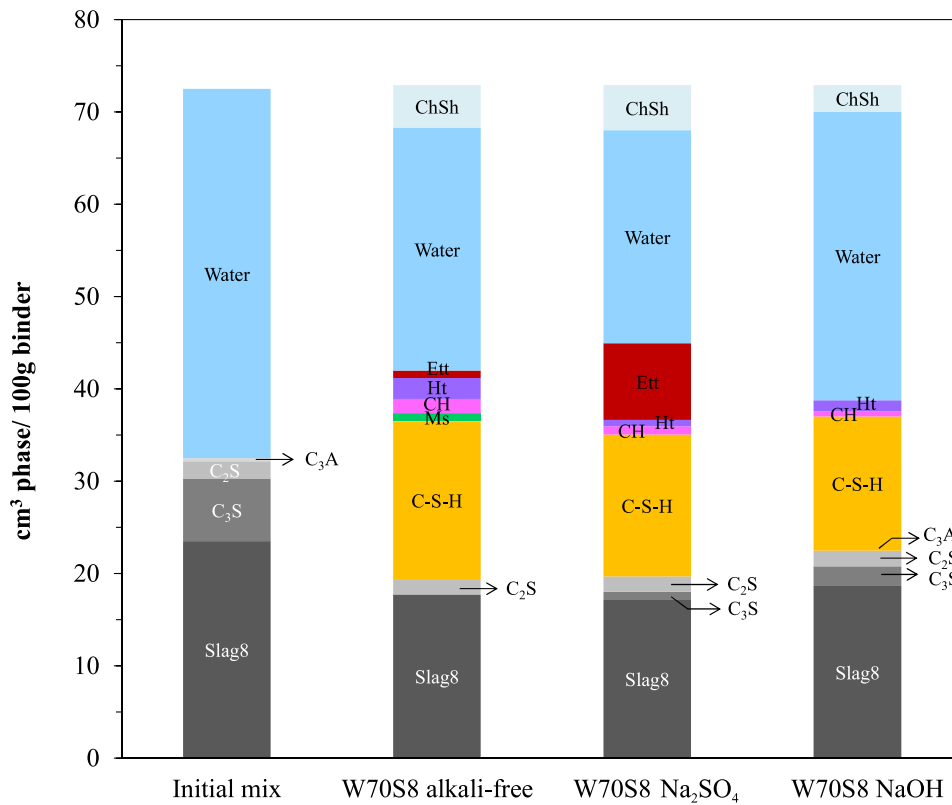
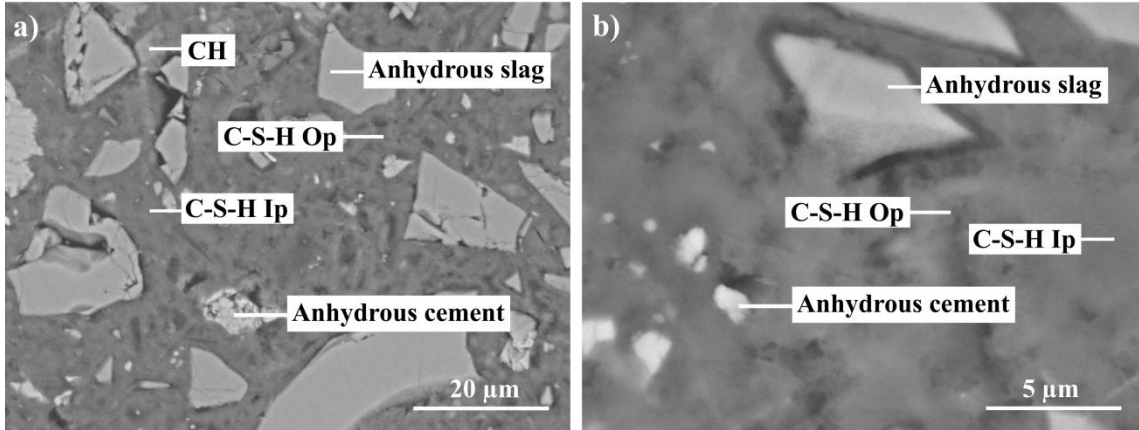


Figure 6.13. Estimation of the phase assemblage for slag 8 systems at 28 days (CH: portlandite, Ht: Hydrotalcite, Ett: ettringite, Ms: monosulfoaluminate).

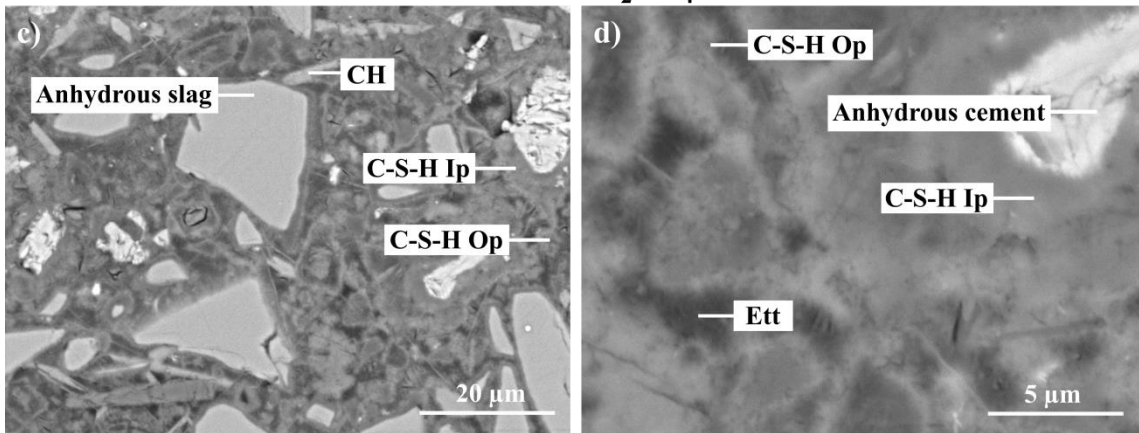
2.6. Distribution of hydrates in the matrix

Figure 6.14 shows the polished sections of slag 1 systems at 28 days. In the absence of alkali (Figure 6.14a and b) the hydrates are well developed and C-S-H appears as the main phase to filling the space between grains. The presence of Na₂SO₄ (Figure 6.14 c and d) clearly shows a lower degree of hydration of cement, which is evident as more anhydrous cement can be identified. C-S-H seems to be less dense than in the alkali free system but it is difficult to judge from the micrographs. Ettringite is easy to identify in the matrix. The addition of NaOH (Figure 6.14e and f) completely changes the appearance of the matrix. It is easy to detect a higher porosity as well as more unreacted small slag grains compared to the alkali free system and the system with Na₂SO₄ (which agrees with the trends observed for the DoR of slag calculated in Table 6.3). Likewise, in the case of non-blended systems, the addition of NaOH results in very little precipitation of outer C-S-H compared to the alkali free system and that with Na₂SO₄. There are some elongated plates that EDS results (Figure 6.15) suggest correspond to portlandite and AFm phases. The two hydrates with an elongated morphology in the presence of NaOH are identified as portlandite (larger crystals) and a mix between Hc and Ms (smaller crystals). This agrees with the phase assemblage quantification based on XRD-Rietveld analysis. EDS analyses in Figure 6.15 strongly support the formation of a solid solution of Hc/Ms also identified with XRD-Rietveld.

W70S1 alkali-free



W70S1 Na₂SO₄



W70S1 NaOH

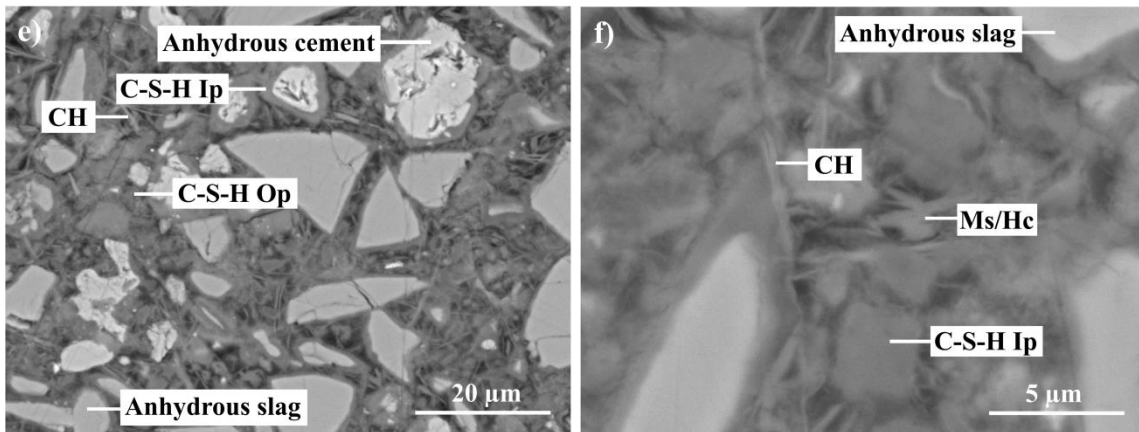


Figure 6.14. Polished sections of slag 1 systems at 28 days of hydration. Lower magnification (images in the left side) and higher magnification (images in the right side). (a and b) Alkali free system, (c and d) with Na₂SO₄ and (e and f) with NaOH.

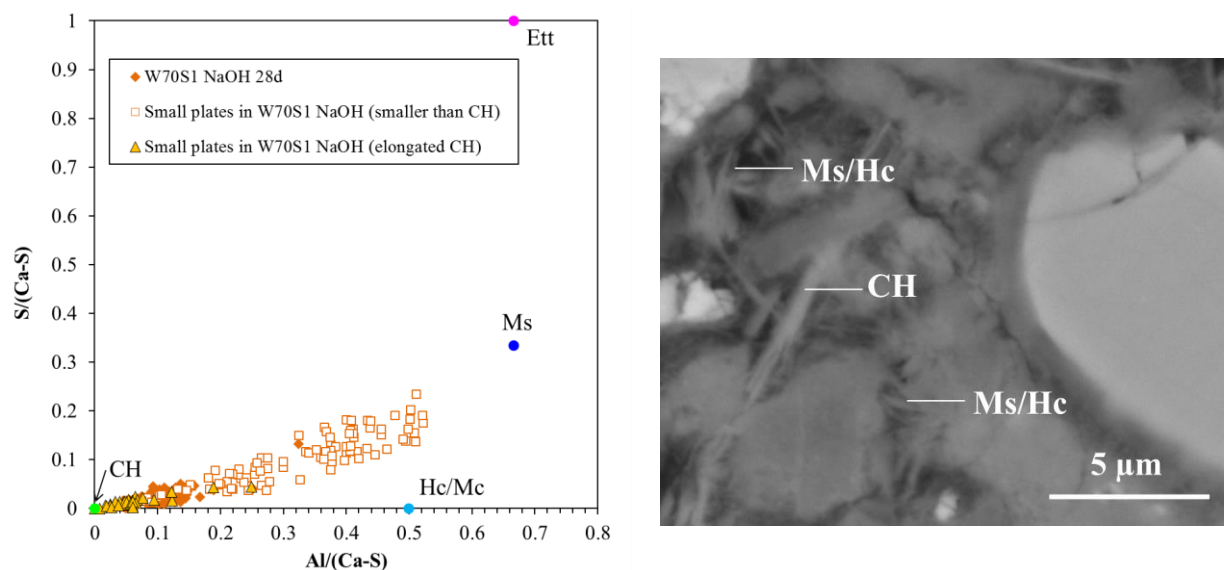


Figure 6.15. $S/(Ca-S)$ versus $Al/(Ca-S)$ ratios for the small plates in the slag 1 system with NaOH at 28 days. Full dots represent the reference composition of ettringite (Ett), monosulfoaluminate (Ms), portlandite (CH) and hemicarboaluminate (Hc). They were used to identify the hydrates with elongated morphology shown in the right SEM-BSE micrograph of the slag 1 system with NaOH at 28 days.

2.7. Porosity

Figure 6.16 shows the total porosity in slag systems at 28 days as a function of the pore radius. The total porosity measured in the presence of Na₂SO₄ is very similar to the porosity in the alkali free system but NaOH increases the porosity, more in the slag 1 system (almost 10% higher) than the slag 8 system (less than 5% higher). MIP results at 28 days agree with the phase assemblage results at 28 days (Figure 6.12 and Figure 6.13). Despite the degree of hydration of C₃S and C₃A being lower in the presence of Na₂SO₄ compared to the alkali free system, the total porosity of both systems is similar because Na₂SO₄ promotes the formation of ettringite which helps to better fill the capillary pores and consequently reduces the total porosity. On the contrary, NaOH inhibits the precipitation of ettringite and consequently the porosity is higher. These observations are similar to those for the non-blended systems⁷.

Figure 6.17 shows the compressive strength against the total porosity measured by MIP for the slag systems. The linear relationship suggests that the compressive strength can be explained by total amount of porosity in the sample, as was shown for the non-blended systems in Chapter 5.

⁷ The impact of Na₂SO₄ and NaOH on the morphology and chemical composition of C-S-H in slag systems has been studied and the same changes as in the non-blended systems were observed. The results are presented in the Appendix B because GEMS analysis for non-blended systems (see Chapter 5) suggested that the differences in compressive strength were not dependent on those.

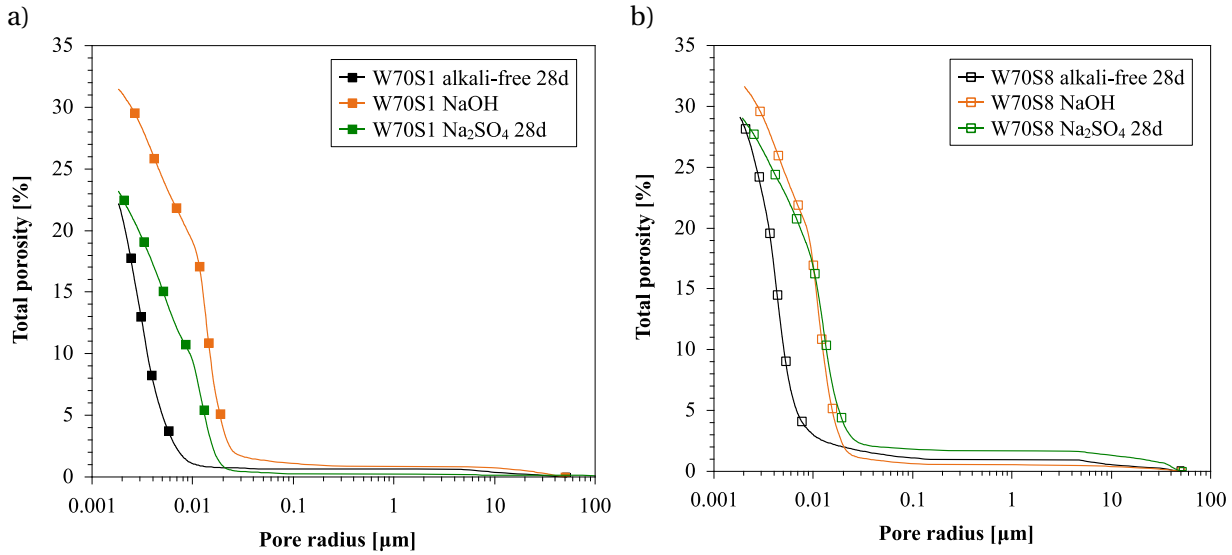


Figure 6.16. Impact of Na_2SO_4 and NaOH on the total porosity of b) slag 1 and d) slag 8 samples at 28 days.

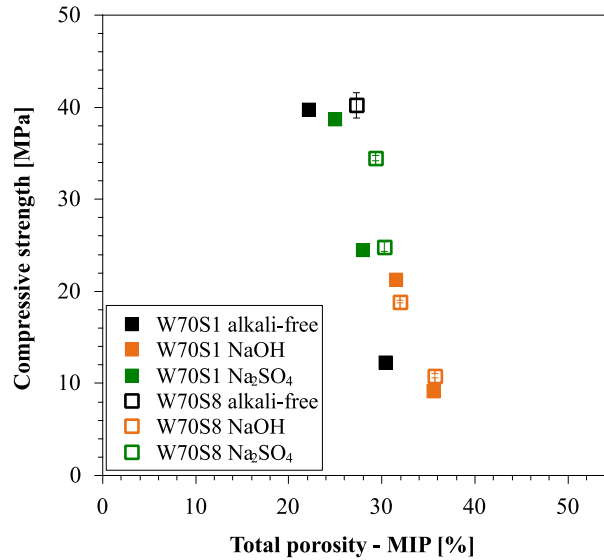


Figure 6.17. Relationship between compressive strength and total porosity (measured by MIP) for slag systems.

The addition of slag (as well as other SCMs) is reported to refine the porosity of blended systems [84]. This is observed in Figure 6.18 for the alkali free systems, where the critical entry radius in the slag systems (Figure 6.16a and b) is lower than in the absence of slag (Figure 6.16c). However, the presence of NaOH or Na_2SO_4 in slag systems (Figure 6.16a and b) does not refine the porosity but rather there is more and coarser porosity.

On the one hand, the addition of Na_2SO_4 leads to some significant differences in the capillary porosity between slag 1 and 8 systems. The capillary porosity in the presence of Na_2SO_4 is much coarser in the system with slag 8 (similar to the NaOH system) than in the system with slag 1. This difference can be related to the higher degree of reaction of slag 1 compared 8 (33.1% and 24.1%, respectively, see Table 6.3). On the other hand, in the systems with NaOH the amount of capillary pores and their coarseness is comparable in slag 1 and slag 8 systems, related to the total absence of ettringite.

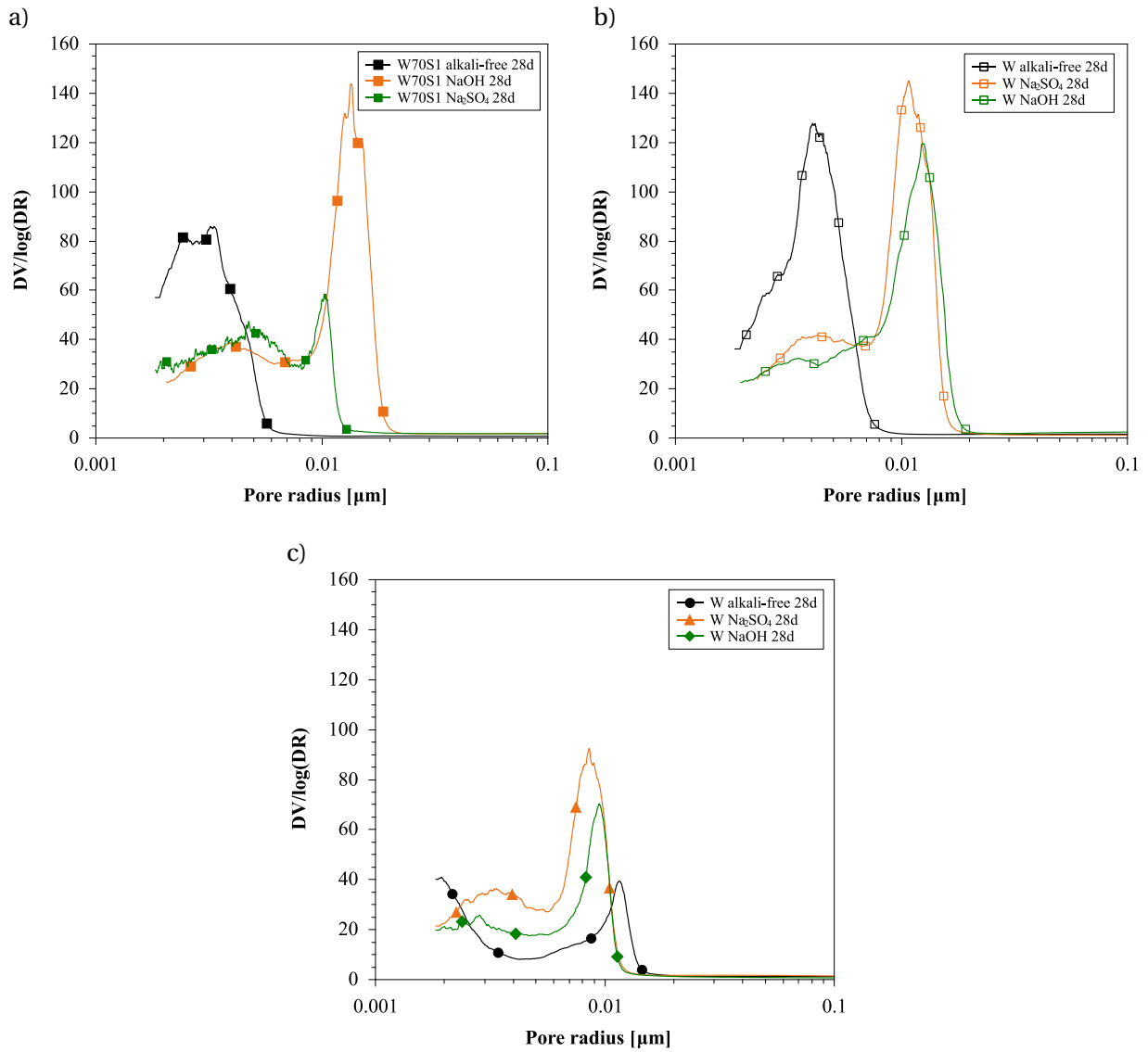


Figure 6.18. Impact of NaOH and Na₂SO₄ on the critical entry radius of a) slag 1 and b) slag 8 samples at 28 days compared to c) the non-blended systems at 28 days.

3. Impact of sodium gluconate on white cement-slag systems with Na_2SO_4

3.1. Reason to study the impact of sodium gluconate

The impact of sodium gluconate is studied because it has been shown to increase the strength development when combined with Na_2SO_4 . To define which is/are the cause/s of this effect, five parameters have been studied:

- Water distribution in capillary and C-S-H porosity
- Kinetics: degree of hydration of cement and degree of reaction of slag
- Phase assemblages
- Distribution of hydrates in the matrix and morphology of C-S-H
- Chemical composition of C-S-H

3.2. Systems studied

The aim is to study the effect of sodium gluconate (GL) when combined with Na_2SO_4 and compare the results with the systems Na_2SO_4 but without gluconate. Figure 6.19 shows the systems studied and Table 6.4 shows further details of the used formulations. Small amounts of sodium gluconate (0.05 wt. % of solids) were mixed with slag and cement previous to adding of water. The compressive and flexural tests as well as the calorimetry and XRD analysis for the systems without sodium gluconate were taken from Chapter 5 since they were already previously studied. The remaining tests presented here were done on a new batch of pastes.

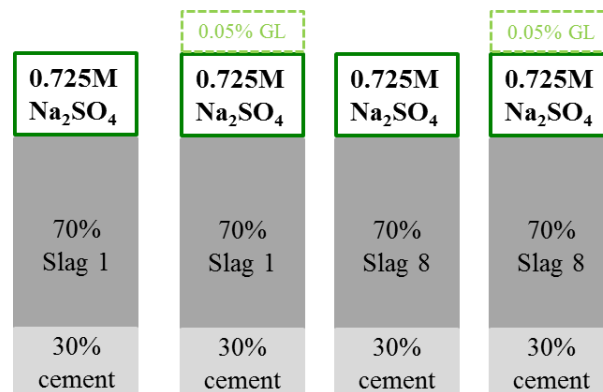


Figure 6.19. Composition of the slag systems studied, with and without gluconate, in wt.%.

Table 6.4. Formulations of slag systems studied with and without gluconate.

	White cement [wt.%]	Slag 1 or 8 [wt.%]	Mixing solution	Nomenclature in figures
Slag 1	30	70	0.725M Na_2SO_4	W70S1 Na_2SO_4
	30	70	0.725M Na_2SO_4	W70S1 Na_2SO_4 +GL
Slag 8	30	70	0.725M Na_2SO_4	W70S8 Na_2SO_4
	30	70	0.725M Na_2SO_4	W70S8 Na_2SO_4 +GL

3.3. Mechanical strength

Figure 6.20 shows the impact of sodium gluconate on the compressive (Figure 6.20a and b) and flexural strength (Figure 6.20c and d) over time for slag 1 and 8 systems with Na₂SO₄. The addition of sodium gluconate in both slag systems with Na₂SO₄ not only (i) maintains or even slightly increases the early compressive strength and (ii) but also increases the compressive strength at later ages (~8 MPa higher in slag 8 system and ~6MPa higher in slag 1 system) compared to the system with only Na₂SO₄. The impact of sodium gluconate on the flexural strength (Figure 6.20c and d) is less clear. Although it seems to increase the flexural strength values from 3- 7 days, the differences are not significant and no further conclusions can be done since only two specimens were tested.

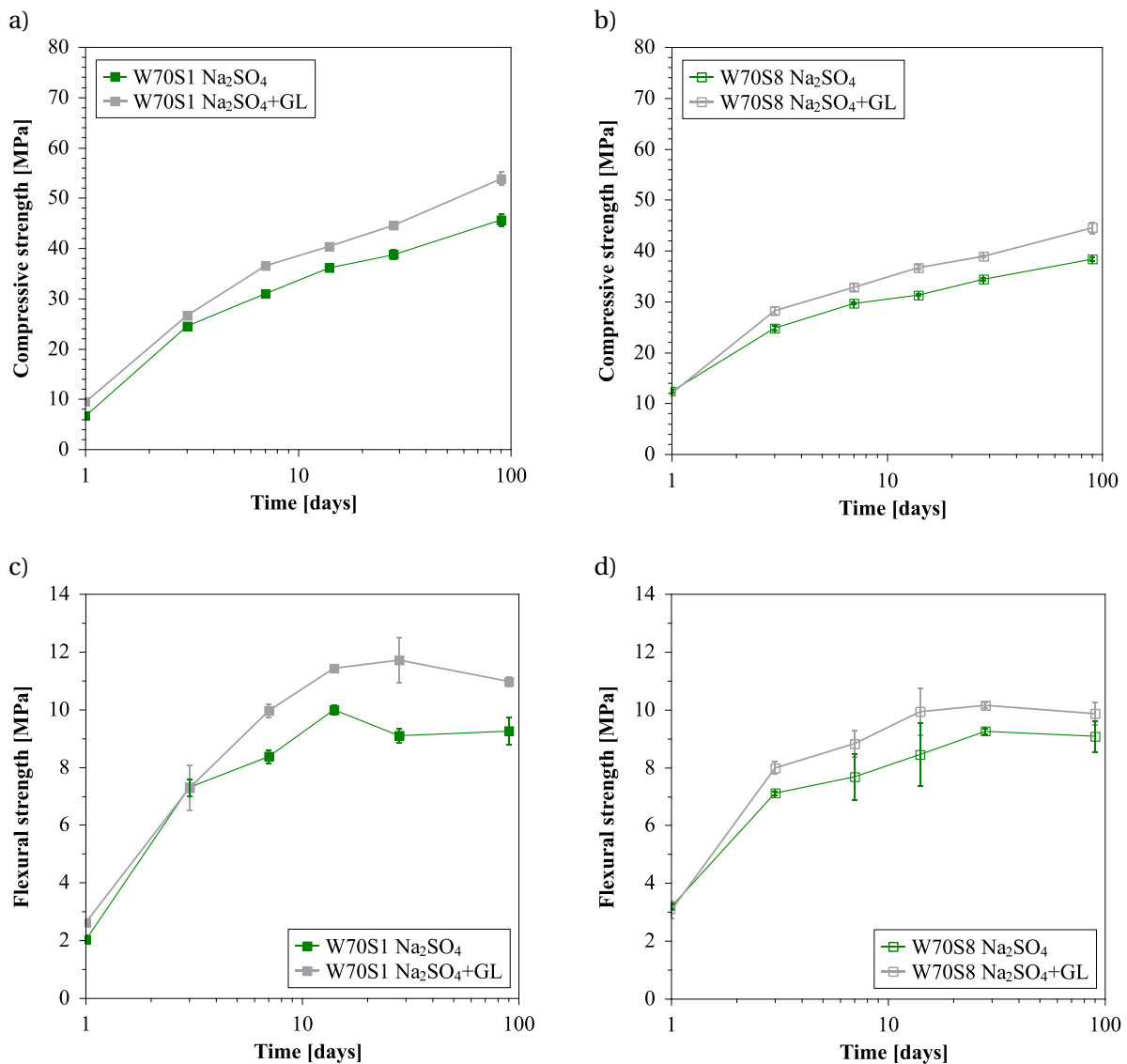


Figure 6.20. Evolution of the compressive and flexural strength in the presence and absence of GL for the slag 1 (a and c) and slag 8 systems (b and d).

3.4. Kinetics

Heat release

Figure 6.21 shows the impact of sodium gluconate on the heat evolution rate during the first days. The addition of sodium gluconate retards the hydration at early ages, delaying both C_3S and C_3A reaction. However, understanding the mechanisms that lie behind this retardation effect is out of the focus of this work. Figure 6.22 shows the impact of sodium gluconate on the cumulative heat release for slag systems until 28 days. The retardation effect is shortlived. One might expect a higher cumulative heat release in the presence of sodium gluconate since it increases the compressive strength. Nevertheless, the cumulative heat release is the same from 1-2 days either with or without gluconate (in slag 1 systems they become equivalent at ~24 hours and in slag 8 systems at ~48 hours). There has been no publication on understanding the cause of the improved strength development with sodium gluconate.

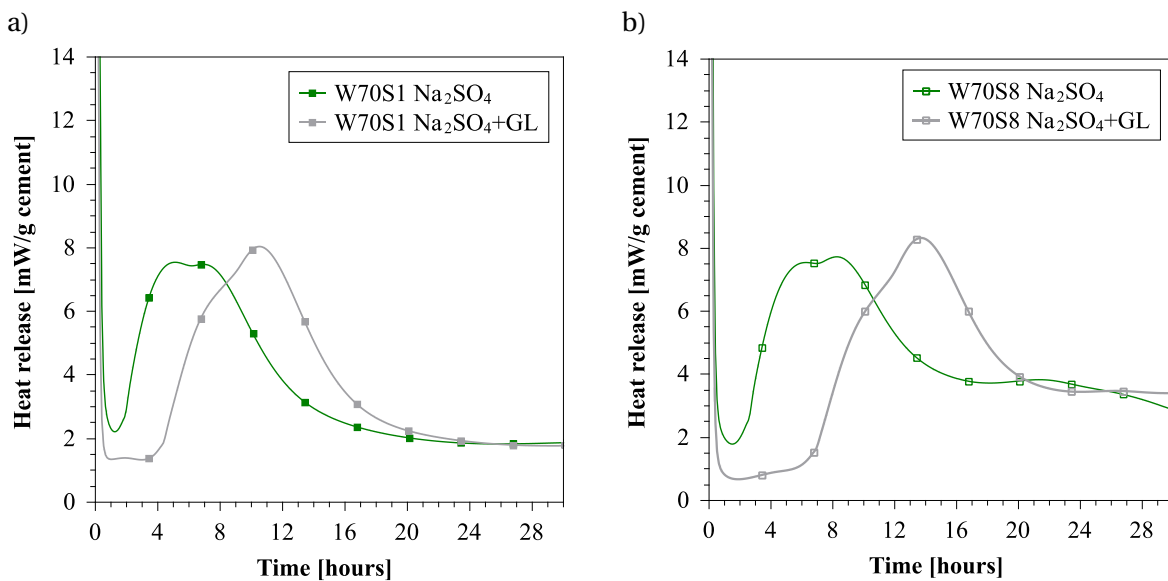


Figure 6.21. Effect of sodium gluconate on the heat evolution rate up to 40 hours for slag systems in the presence of Na_2SO_4 with a) slag 1 and b) slag 8.

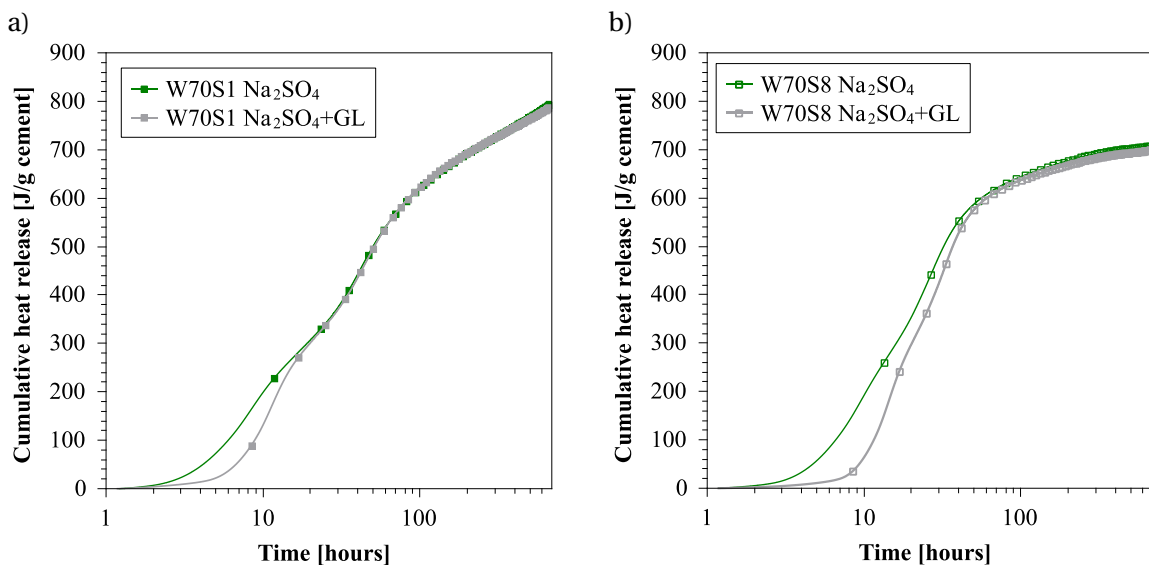


Figure 6.22. Effect of sodium gluconate on the cumulative heat release up to 28 days for slag systems in the presence of Na_2SO_4 with a) slag 1 and b) slag 8.

Degree of hydration of cement

Figure 6.23 shows the effect of sodium gluconate on the DoH of cement up to 28 days for the slag systems with Na₂SO₄. These results agree with the trends for the cumulative heat release, with the same DoH measured with and without gluconate at all ages. The addition of gluconate does not impact the DoH of cement. If the presence of sodium gluconate alters neither the cumulative heat release nor the DoH of cement, this suggests that the degree of reaction of slag will be the same with and without sodium gluconate.

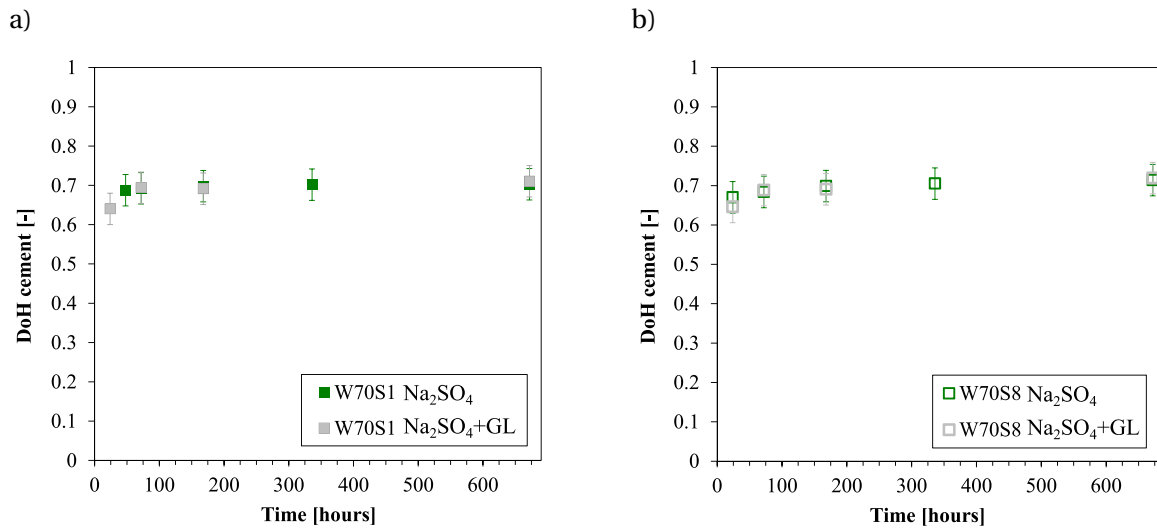


Figure 6.23. Effect of sodium gluconate on the DoH_{cement} up to 28 days for for slag systems in the presence of Na₂SO₄ with a) slag 1 and b) slag 8.

3.5. Phase assemblages

Figure 6.24 shows the volume of ettringite, portlandite and hydrotalcite with XRD-Rietveld in the presence and absence of sodium gluconate. The addition of sodium gluconate does not change the amount these hydrates in the system. Sodium gluconate delays the occurrence of the main aluminate reaction (Figure 6.21) but the amount of Etringite does not change⁸ (Figure 6.24).

⁸ Moreover, most carboxylic acids do not affect the morphology of ettringite [115].

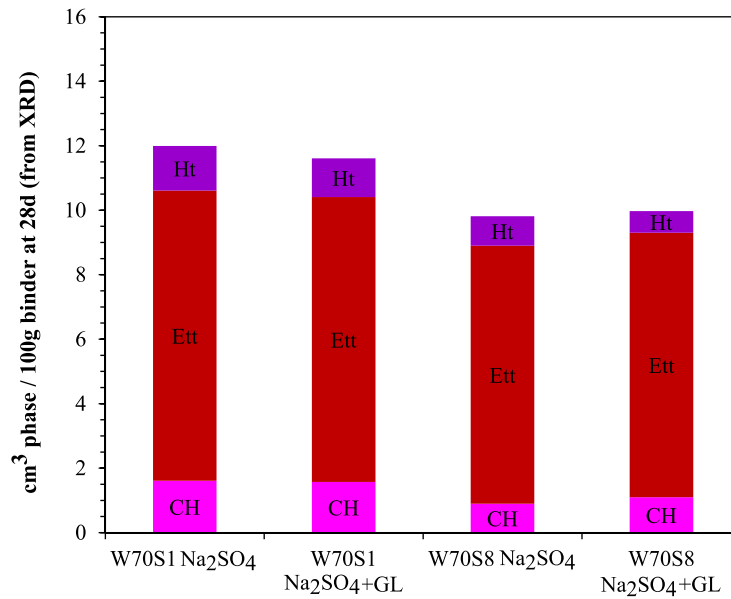


Figure 6.24. XRD-Rietveld quantification of portlandite (CH), ettringite (Ett) and hydrotalcite (Ht) for slag 1 and slag 8 systems with Na₂SO₄ at 28 days, in the absence and presence of sodium gluconate.

3.6. Distribution of hydrates and morphology of C-S-H

Distribution of hydrates

Figure 6.25 and Figure 6.26 show the impact of sodium gluconate on the distribution of hydrates in the matrix at 24 hours and 28 days, respectively. Sodium gluconate does not appear to modify the distribution at early or even later ages. The increase of the compressive strength cannot be explained by a change in the heterogeneity of the sample or a change in the morphology of portlandite crystals. In all the studied systems at higher magnification it is possible to identify numerous crystals of ettringite in the bigger pores. It is fairly uncertain to judge by eye about potential changes in the density of C-S-H with the addition of sodium gluconate from the BSE micrographs in Figure 6.25 and Figure 6.26 since the images have not been adjusted to the same brightness and contrast.

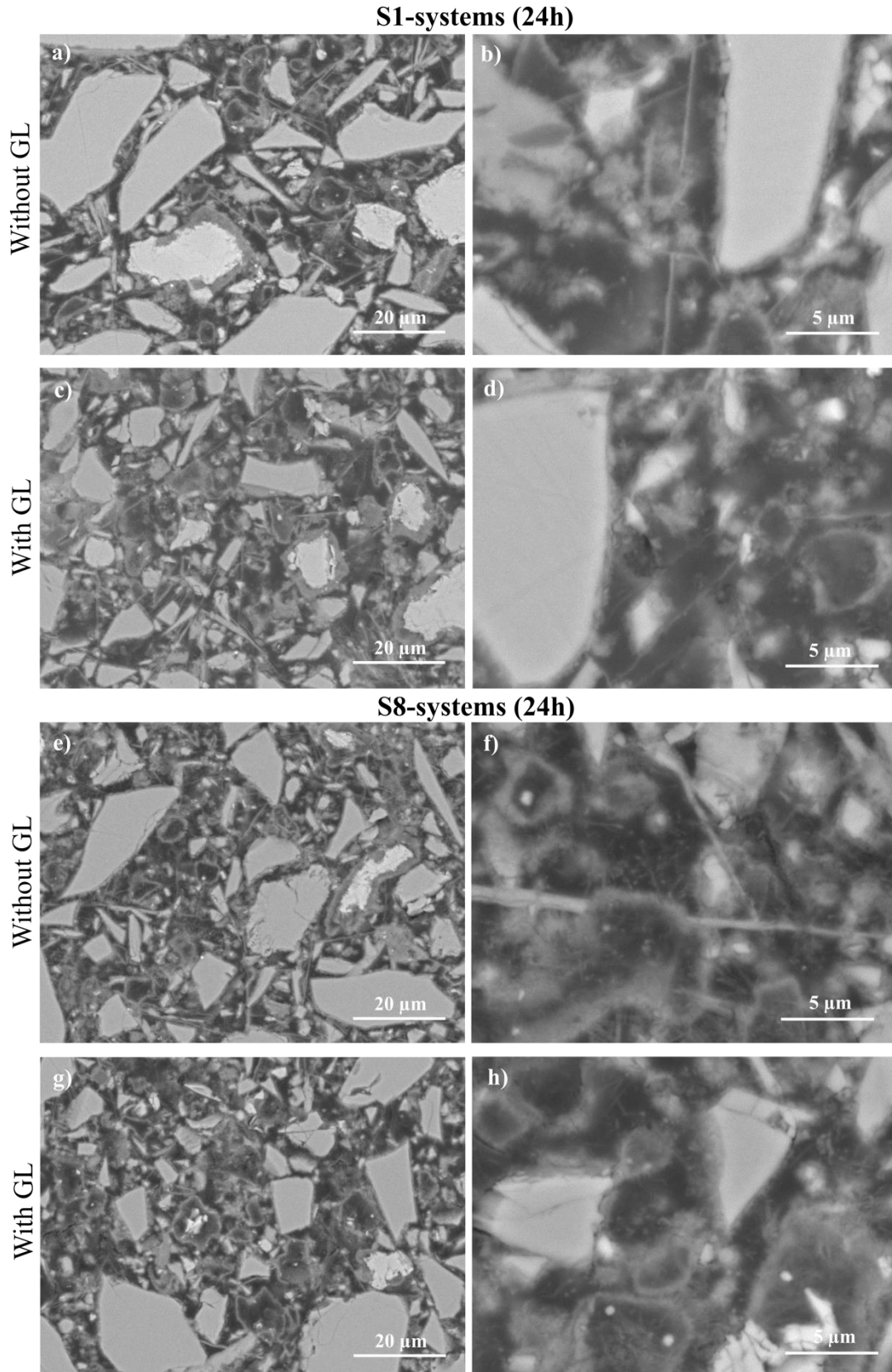


Figure 6.25. Polished sections of slag 1 and slag 8 systems with Na₂SO₄ at 24 hours in the absence (a, b, e, f) and presence (c, d, g, h) of sodium gluconate. Lower magnification (images left side). Higher magnification (images right side).

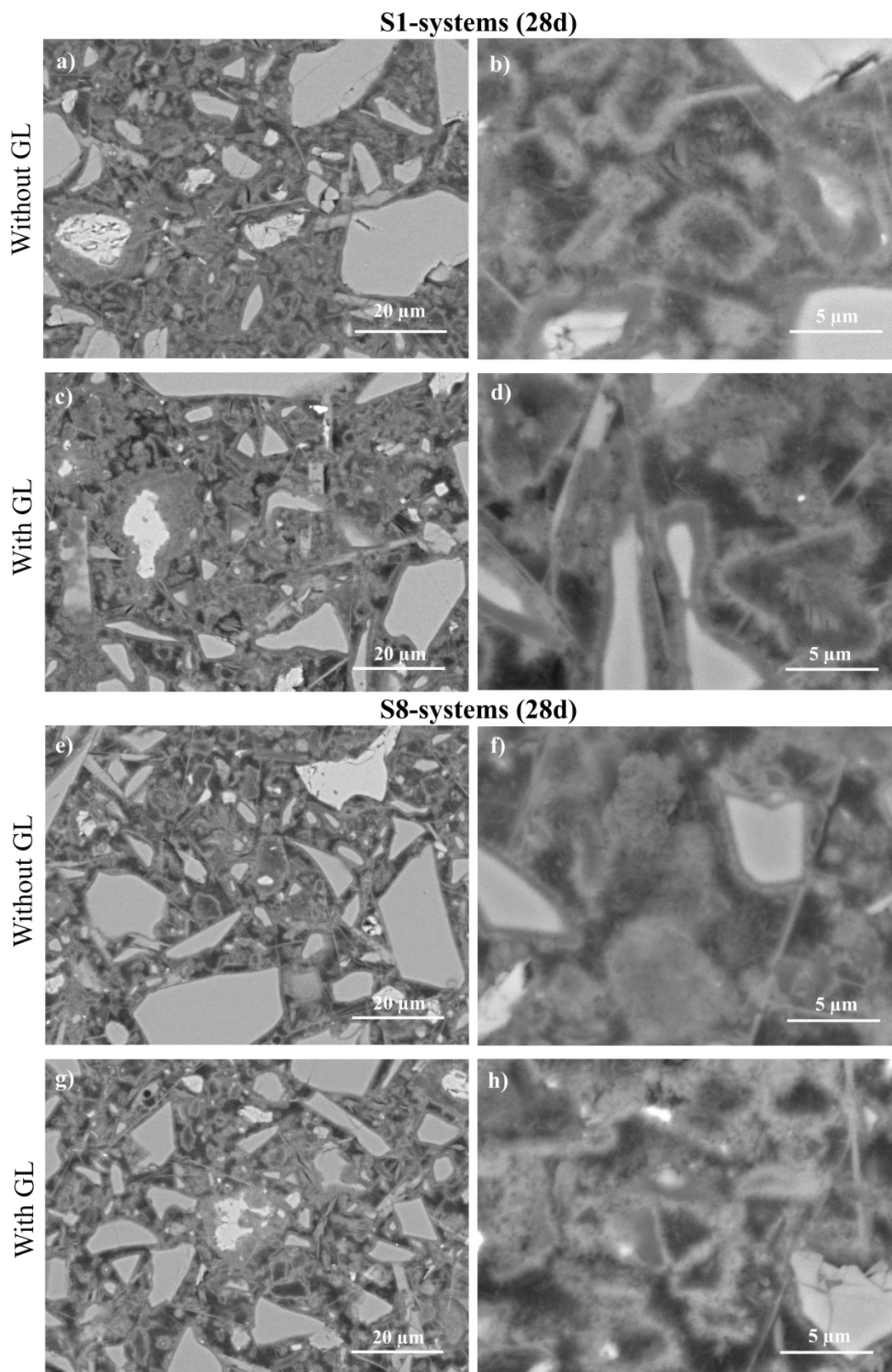


Figure 6.26. Polished sections of slag 1 and slag 8 systems with Na_2SO_4 at 28 days in the absence (a, b, e, f) and presence (c, d, g, h) of sodium gluconate at 28 days. Lower magnification (images left side). Higher magnification (images right side).

The morphology of C-S-H at early age

Figure 6.27 shows the morphology of C-S-H at early ages at the end of the acceleration period for the systems with slag 1. The addition of sodium gluconate (Figure 6.27c and d) does not change the morphology of C-S-H compared to the samples without it (Figure 6.27a and b). In both cases there is a needle-like, divergent C-S-H. This which confirms that the increase in strength induced by sodium gluconate is not related to a change in C-S-H morphology.

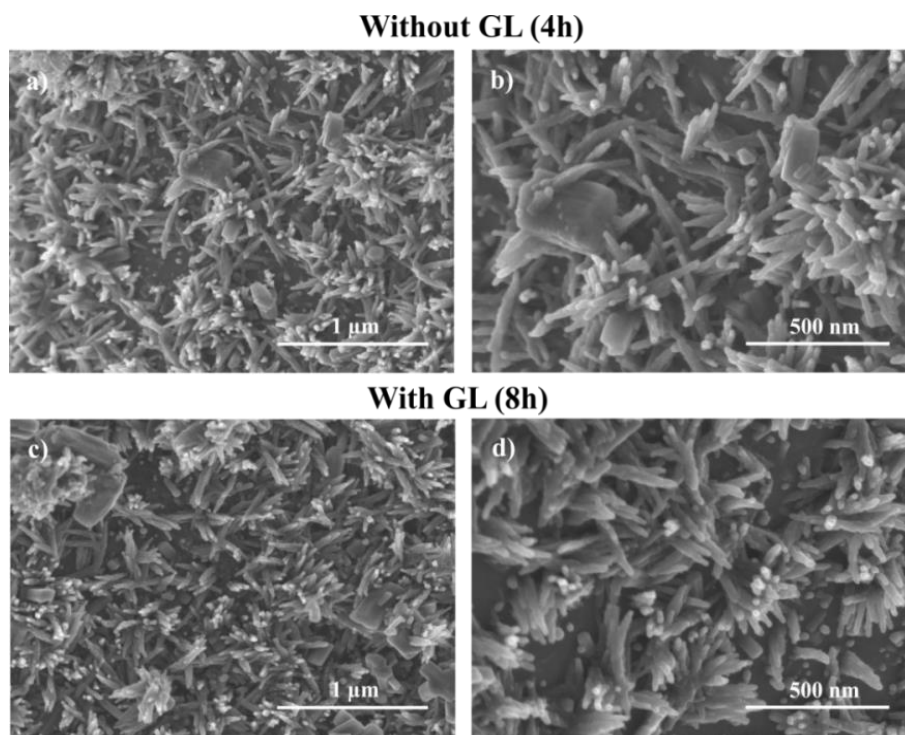


Figure 6.27. C-S-H morphology at the end of acceleration period in systems with slag 1 and Na₂SO₄, (a, b) without and (c, d) with sodium gluconate.

3.7. Chemical composition of C-S-H

(Ca-S)/Si ratio and sulfate uptake

Figure 6.28 shows the impact of sodium gluconate on the (Ca-S)/Si ratio and the uptake of sulfate in C-S-H on slag 1 systems at 24 hours, 7 and 28 days. The (Ca-S)/Si as well as the S/(Ca-S) ratios are not affected with the addition of sodium gluconate. The (Ca-S)/Si ratio over time evolves in the same way in all the systems, reaching a stable value around ~1.5 at 7 days. It is reasonable that the sulfate uptake does not change if the (Ca-S)/Si is the same. This means that the surface of C-S-H will adsorb similar amounts of Ca²⁺ and SO₄²⁻ in the presence or absence of sodium gluconate.

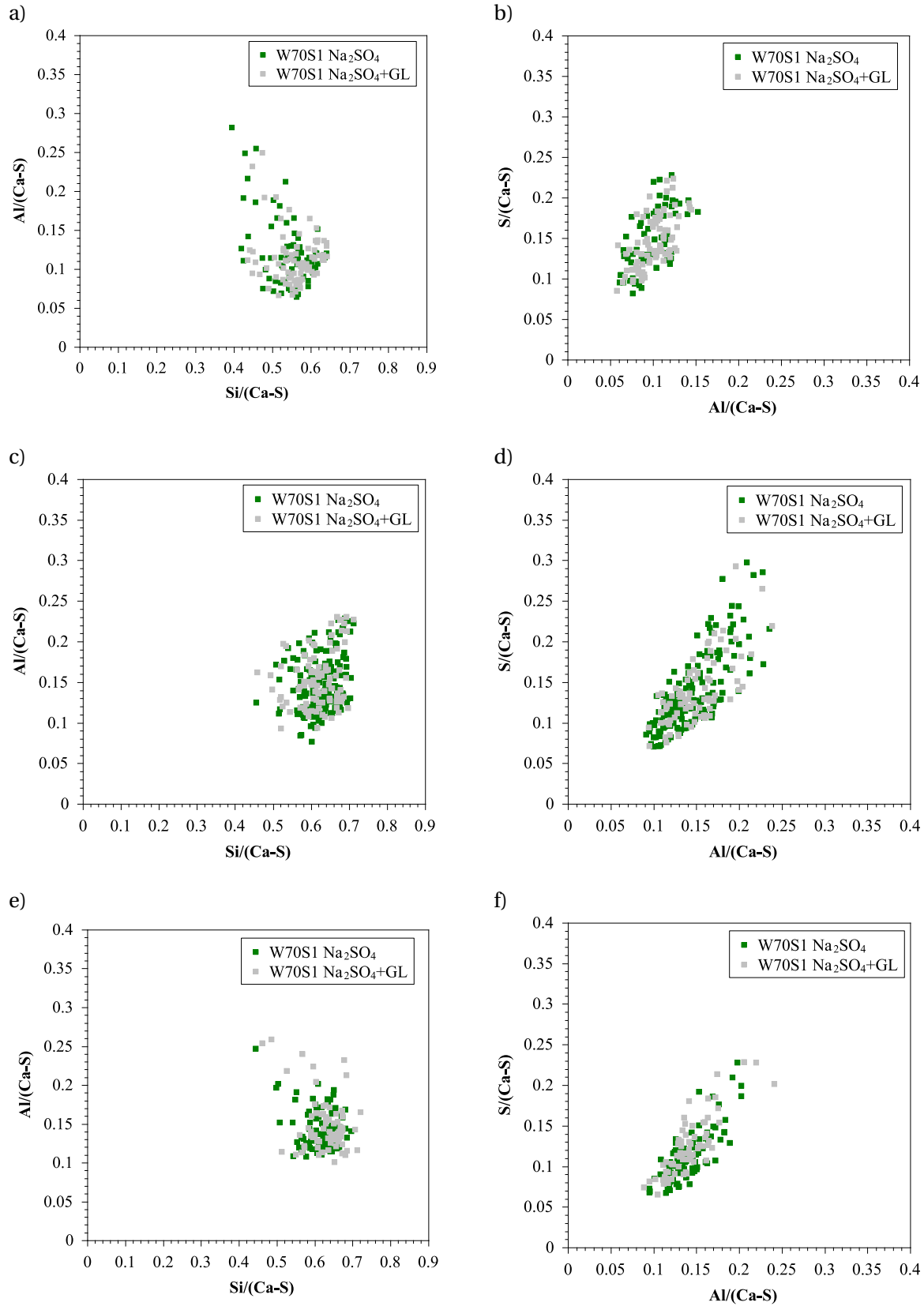


Figure 6.28. Impact of sodium gluconate on the (Ca-S)/Si ratio (left column) and the uptake of sulfate (right column) in C-S-H in slag 1 systems at 24 hours (a and b), 7 days (c and d) and 28 days (e and f).

Table 6.5. Quantification of the (Ca-S)/Si ratio of C-S-H in slag 1 systems in the presence and absence of sodium gluconate at 24 hours (a and b), 7 days (c and d) and 28 days (e and f).

	(Ca-S)/Si		
	24 hours	7 days	28 days
W70S1 Na ₂ SO ₄	1.60	1.47	1.50
W70S1 Na ₂ SO ₄ +GL	1.61	1.48	1.49

Uptake of sodium

Figure 6.29 shows that sodium uptake in C-S-H is also the same in presence or absence of sodium gluconate, which was expected as sodium gluconate does not lower the (Ca-S)/Si ratio of C-S-H and so the replacement of Ca²⁺ by Na⁺ should not vary.

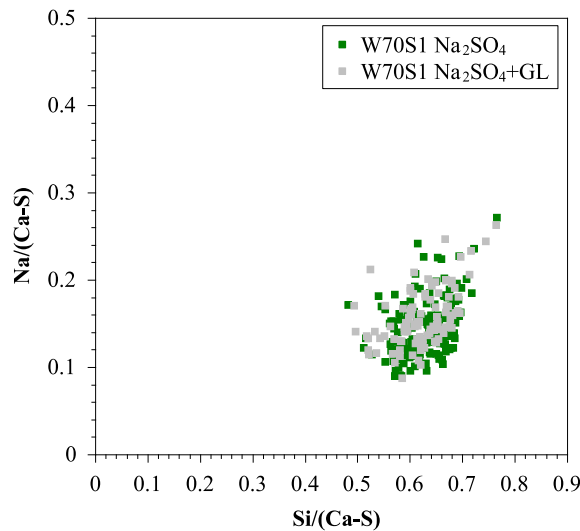


Figure 6.29. Impact of sodium gluconate on the uptake of sodium in C-S-H at 7 days in slag 1 systems with Na₂SO₄.

3.8. Water distribution in capillary and C-S-H porosity

Figure 6.30 shows the impact of sodium gluconate on the amount of mass loss in slag systems with Na₂SO₄ at 28 days. For both slag systems, sodium gluconate increases the mass loss in the range of temperature from 30°C to 350°C. This range of temperatures is mainly related to the decomposition of ettringite, C-S-H [109], gypsum and AFm phases. For the studied systems, (i) the amount of ettringite and hydrotalcite is the same with or without sodium gluconate and (ii) gypsum is absent at all ages after the gypsum depletion. And as sodium gluconate does not affect the DoH of cement, a higher amount of water loss in this range does not suggest a higher precipitation of C-S-H but rather the precipitation of a C-S-H with a higher water content compared to the systems without sodium gluconate.

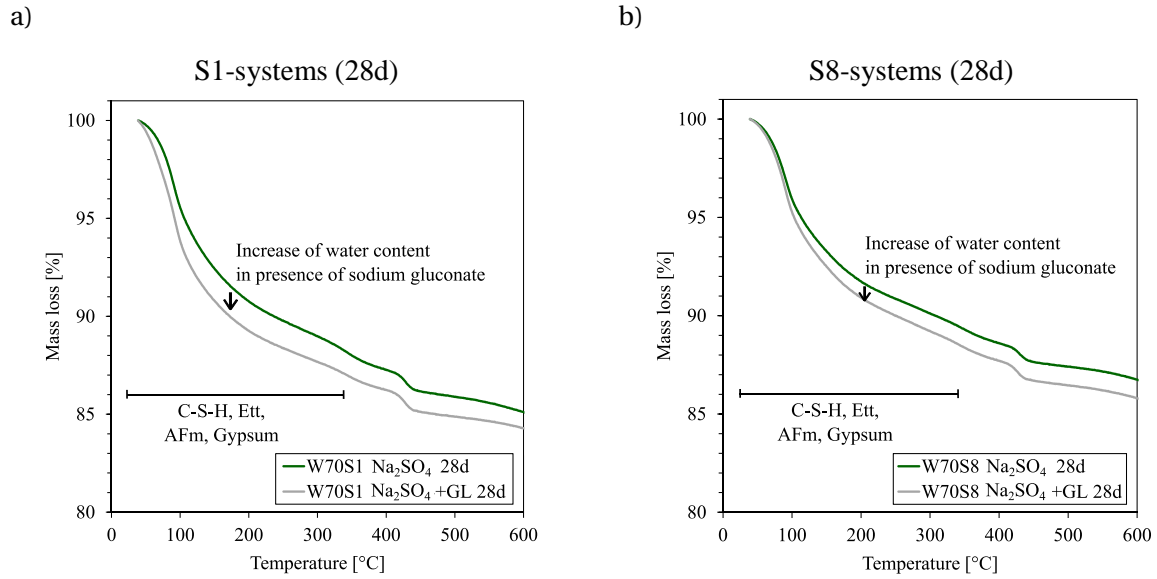


Figure 6.30. Impact of sodium gluconate on the amount of mass loss in slag systems with Na_2SO_4 at 28 days between 30 and 600°C.

^1H NMR measurements

To investigate this difference in weight loss further, the distribution of the water in the sample among the different populations (capillary, gel and interlayer) was analysed by ^1H NMR for the samples at 28 days. Figure 6.31 shows the results for the systems with slag 1. Sodium gluconate lowers the capillary water, but increases the gel and interlayer water; as the solid signal is the same with and without sodium gluconate. This suggests the precipitation of a C-S-H with more water in the presence of sodium gluconate. A lower capillary porosity cannot be explained with a higher precipitation of ettringite because the amount of ettringite has been quantified to be the same in the presence and absence of sodium gluconate (Figure 6.24). A C-S-H with more water would have a lower density. Thus, a less dense C-S-H will fill more space than a denser C-S-H and consequently the capillary porosity will be lower.

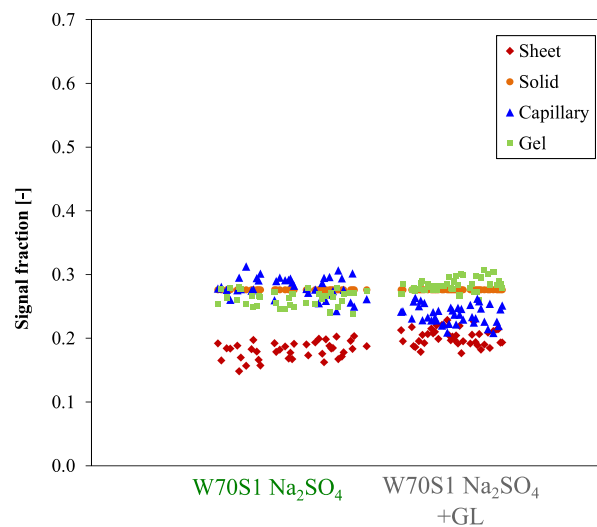


Figure 6.31. Impact of sodium gluconate on the distribution of the water among the different populations of water at 28 days for the systems with slag 1. Repetitive measurements on one sample were taken at 28 days in order to be statistically representative (each point in the figure corresponds to one measurement). The water/solids ratio was adapted at 0.35 for ^1H NMR analysis to avoid bleeding.

C-S-H density measured with image analysis

Image analysis from BSE micrographs allows the quantitative (relative, but not absolute) analysis of the changes in the density of C-S-H. It is based on the different grey levels in the images. Darker phases have a lower density and lighter phases a higher density. The advantage of this method is the possibility to differentiate each type of C-S-H individually⁹ (Figure 6.32 shows the features analysed). Images have to be adjusted with the same brightness and contrast level, previously to start the analysis, taking slag grains and C₂S as reference levels. For representative results, 50 points (average) per phase and per image are required. In the present work, 5 images were studied for each system. The standard deviation of all the measurements is used as error bars.

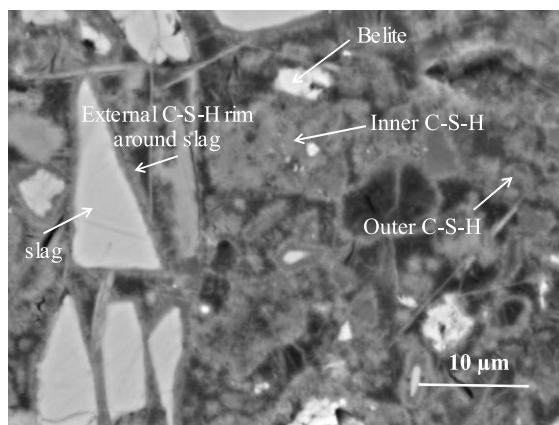


Figure 6.32. Identification of anhydrous phases taken as reference grey levels (belite and slag) and each type of C-S-H to analyse. The closest, darker rim around slag grains was not measured due to intermixing with Strätlingite.

Figure 6.33 shows the impact of sodium gluconate on the evolution of the relative density of outer C-S-H, C-S-H around cement grains and around slag grains in both slag 1 (Figure 6.33a) and slag 8 systems (Figure 6.33b). The good calibration of the brightness and contrast of the images is confirmed by the agreement in the values for slag and C₂S with and without sodium gluconate. The presence of sodium gluconate clearly lowers the density of outer C-S-H as well as the C-S-H around slag grains in both slag systems. On the contrary, although the density of inner C-S-H does show some decrease with sodium gluconate in slag 1 systems, it appears not to be affected in slag 8 systems.

Actually, outer C-S-H is more likely to affect the mechanical properties compared to inner product as it is filling the original water filled space in the matrix (Figure 6.34). Inner product grows around the anhydrous grains. Therefore, a lower density for the outer C-S-H will have more impact on the strength than a lower density for the inner C-S-H.

⁹ ¹H NMR could give an indication of the overall density of C-S-H, i.e., an averaged value for the outer product, the inner product around cement grains and C-S-H around slag grains. However, it would not be possible to distinguish the impact of sodium gluconate on each product individually.

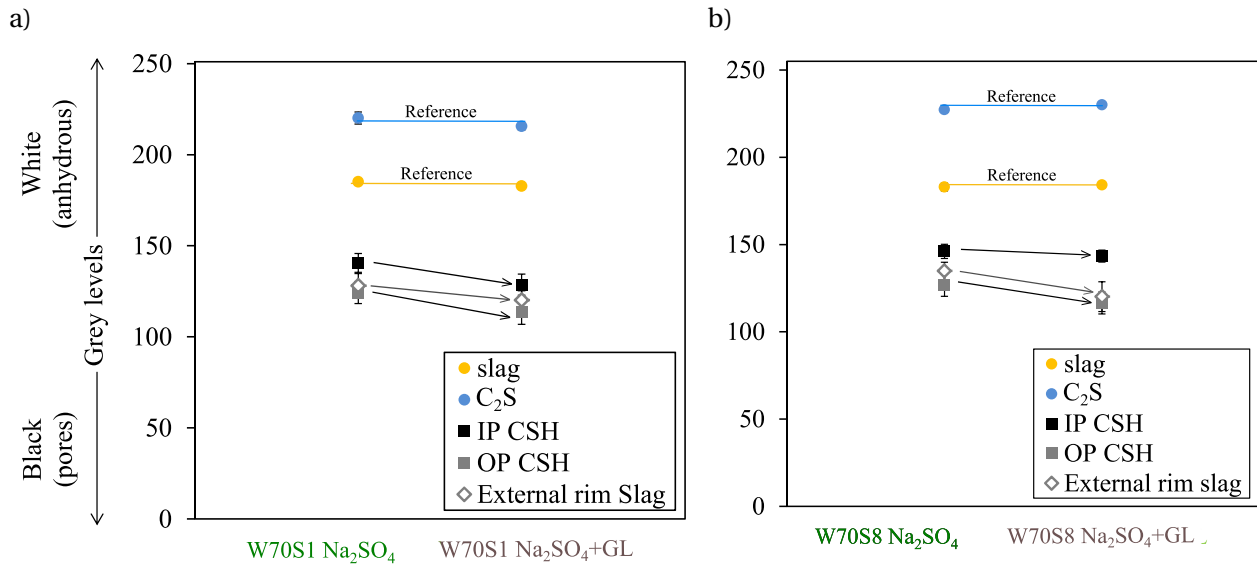


Figure 6.33. Impact of sodium gluconate on the density of inner and outer C-S-H (qualitative comparison) at 28 days for the systems a) with slag 1 and b) with slag 8.

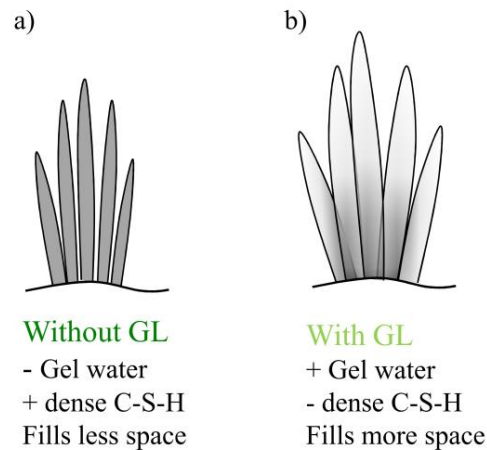


Figure 6.34. Schematic C-S-H representation a) without and b) with sodium gluconate. Lighter grey represents a less dense C-S-H.

3.9. Discussion on the effect of sodium gluconate

Porosity and relation to mechanical strength

Figure 6.35 shows the compressive strength as a function of the total porosity measured with MIP for the slag systems at 28 days in the presence and absence of sodium gluconate. The addition of sodium gluconate lowers the total porosity of both slag systems compared to the alkali free systems and consequently the compressive strength is higher.

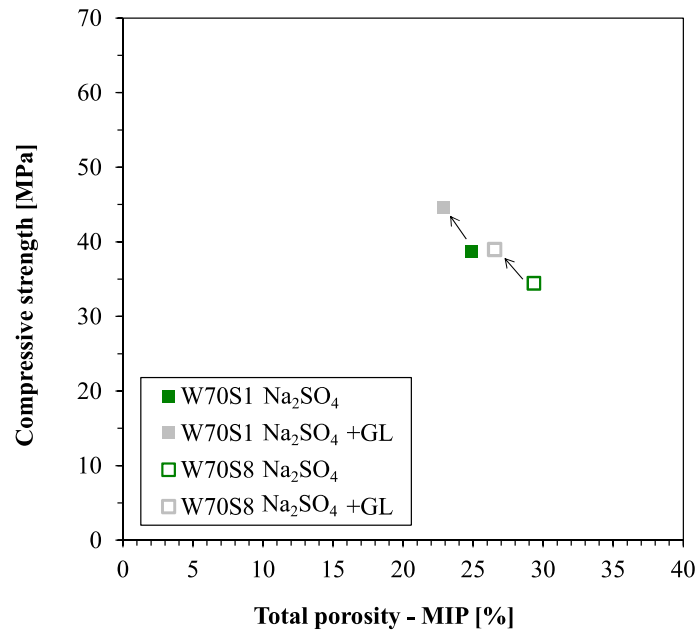


Figure 6.35. Impact of sodium gluconate on the compressive strength of slag systems as a function of the total porosity from MIP.

Figure 6.36 shows the total porosity for slag systems in the presence and absence of sodium gluconate at 28 days measured with MIP. Sodium gluconate decreases the total porosity. In slag 8 systems this decrease is evident while in the slag 1 systems the capillary porosity (>5 nm pore radius) appears to be the same in the presence and absence of sodium gluconate.

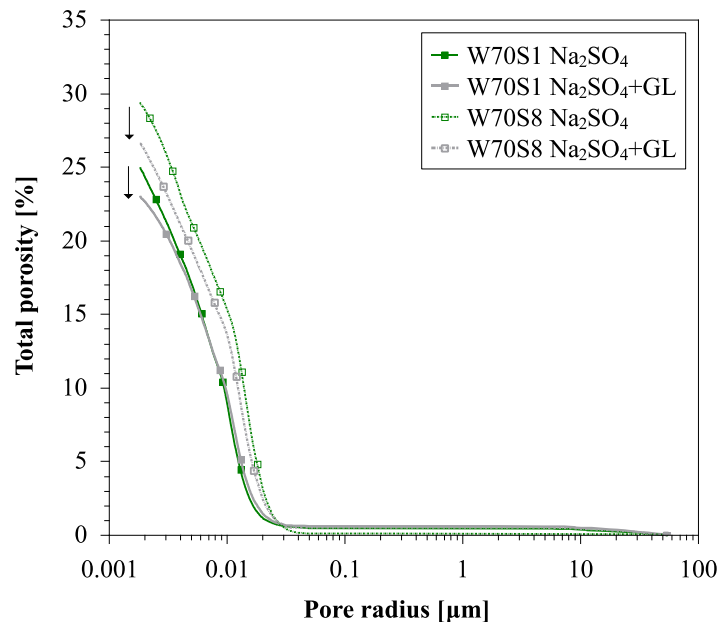


Figure 6.36. Impact of sodium gluconate on the total porosity of slag systems at 28 days measured with MIP.

Three of the main drawbacks of MIP technique are (i) the impossibility to detect interlayer porosity as well as (ii) the depercolated porosity, and (iii) the need to dry the sample before the analysis. On the one hand, the drying process can partially collapse and increase the size of the capillary porosity, which could explain why MIP does not detect any difference in the capillary porosity fraction whereas ^1H NMR does (for ^1H NMR measurements the sample is never dried and so there are no drying artefacts). On the other hand, the porosity net in the absence of sodium gluconate could probably be less percolated, meaning that a fraction of the porosity would not be measured by MIP whereas ^1H NMR would be able to detect the water in depercolated pores. It is worth noting that a recent study reports that MIP can partially detect the gel porosity besides the capillary porosity [15] for white cement pastes (non-blended); however, this has not been verified for blended systems. It will mostly depend on the characteristics of the pores net, which changes between systems. Therefore, in the present white cement-slag systems, it becomes uncertain to compare porosity results from ^1H NMR and MIP.

4. Summary

About the **impact of Na_2SO_4 and NaOH and on white cement-slag systems:**

- The addition of Na_2SO_4 or NaOH accelerates the DoH of cement and the degree of reaction of slag since the first hours compared to the alkali free system. This effect is more extreme in the presence of NaOH. The same observations were done in alite and unblended systems.
- At later ages, Na_2SO_4 or NaOH lower the DoH of cement (as in alite and unblended systems). In the presence of Na_2SO_4 it remains closer to the alkali free system while with the addition of NaOH it is significantly lower. In slag systems, the water activity remains high to much later times than when the differences in DoH occur. This shows that changes in the water activity cannot explain the slowdown in hydration kinetics. A lower DoH of cement could be related to a higher concentration of aluminate ions in solution, which increases with the addition of Na_2SO_4 and NaOH, but seems unlikely to explain the whole of the effect. This suggests that other factors might be responsible for a lower DoH.
- Both Na_2SO_4 and NaOH also increase the degree of reaction of slag during the first 3 days compared to the alkali free system. At later ages, the degree of reaction of slag 1 remains higher with the addition of Na_2SO_4 while that of slag 8 is the same as for the alkali free system. For both slag 1 and slag 8, the presence of NaOH significantly lowers the degree of reaction of slag.
- The strength development is related to the total porosity and so to the total volume of hydrates formed, as observed previously in Chapter 5 for unblended systems. The addition of Na_2SO_4 promotes the precipitation of ettringite as well as outer C-S-H which fill the space and contribute to reduce the porosity. On the contrary, the addition of NaOH inhibits the precipitation of outer C-S-H and moreover ettringite is completely absent. Therefore, a lower volume of hydrates filling the space leads to a higher porosity.
- Although in slag systems the morphology and chemical composition of C-S-H also clearly changes in the presence of Na_2SO_4 or NaOH, these are independent on the strength development.

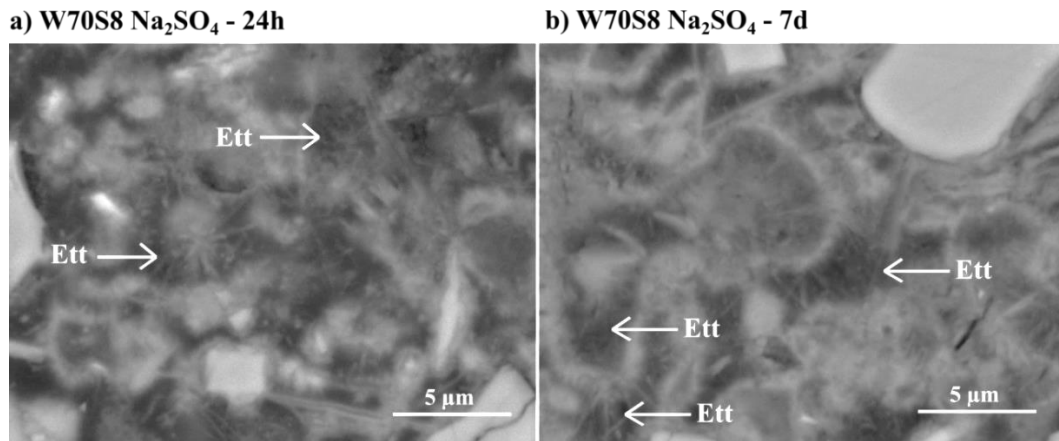


Figure 6.37. Ettringite crystals growing in the capillary pores and helping to reduce the total porosity of slag 8 systems with Na₂SO₄ at a) 24 hours and b) 7 days.

About the **impact of sodium gluconate on white cement-slag systems with Na₂SO₄:**

- The addition of sodium gluconate in cement-slag systems with Na₂SO₄ improves the strength development not only at early but also later ages.
- The following parameters are not affected by the presence of sodium gluconate: the degree of hydration of cement, the degree of reaction of slag, the phase assemblage and the morphology and chemical composition of C-S-H.
- Sodium gluconate promotes the precipitation of C-S-H with more water and the density has been measured to be lower. A less dense C-S-H fills more space. Consequently, the porosity is lower and the strength development is higher compared to the systems without sodium gluconate.

CHAPTER 7. Conclusions and perspectives

Conclusions

The objective of this work was to understand the impact of NaOH and Na₂SO₄, as well as the presence of gypsum, on the kinetics, the microstructure and strength development of alite, cement, and cement-slag systems. The main conclusions from the present work are presented below.

1. The impact of alkali salts on the kinetics

- NaOH and Na₂SO₄ clearly accelerate the hydration at early age, leading to a shorter induction period and a higher slope during the nucleation and growth period.
- At later ages, the degree of hydration in the presence of alkali is lower. From the studies on alite, white cement and white cement-slag systems, it has been observed that a slowdown in hydration kinetics could not be explained by changes in water activity. The increased concentration of aluminate ions could explain some of the slowdown. However, other studies reported that the inhibition effect of aluminate vanishes at high alkali conditions (pH≥13) [99,100]. It appears there are other effects that might explain the lower DoH.

2. The impact of alkali salts on the strength development

- The compressive strength is clearly related to the total porosity in all the studied systems (Figure 7.1a) while there is no direct relationship with the critical entry radius (Figure 7.1b). The differences in the trends between alite and cement systems are related to the lower DoH of alite compared to cement and the lack of fine grains in the case of alite.
- The addition of NaOH increases the total porosity and so decreases the compressive strength (Figure 7.2) compared to the alkali free system and with Na₂SO₄. This is related to the lower volume of hydrates filling the space. With NaOH, ettringite is almost or completely absent and there is less outer C-S-H product. Figure 7.2 shows that the systems with a higher volume of hydrates reach a better strength development.
- The strength development was found to be independent on the morphology of C-S-H, nor its Ca/Si ratio, although the morphology of C-S-H was shown to vary with the composition of the pore solution with the addition of alkalis.

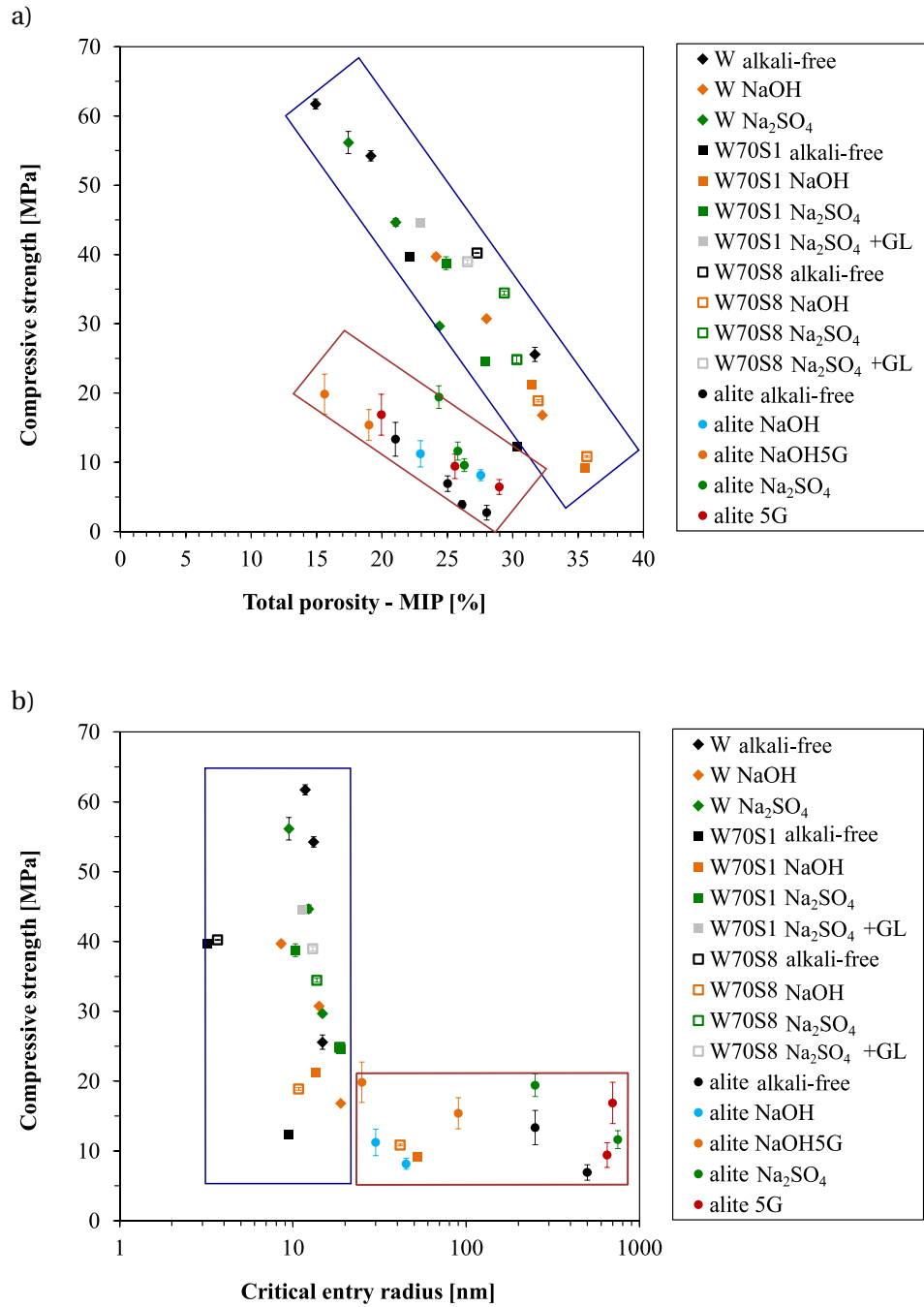


Figure 7.1. a) Total porosity related to the compressive strength and b) evolution of the compressive strength related to the critical entry radius from MIP for all the systems studied in this work. The latest testing time for all the systems is 28 days. Red rectangle mainly groups alite systems and blue rectangle marks non-blended systems and slag systems.

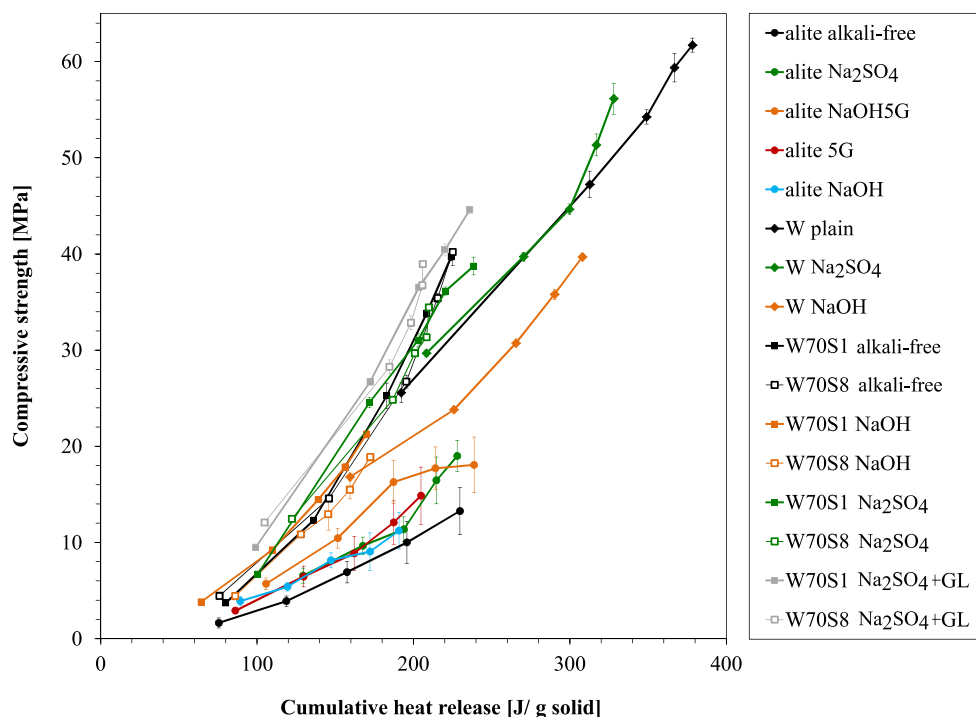


Figure 7.2. Cumulative heat release (J/g solid) related to the compressive strength for all the systems.

3. The impact of alkali salts on C-S-H and portlandite

- The addition of Na₂SO₄ promotes a divergent needled structure due to the uptake of sulfate on C-S-H. NaOH promotes the formation of C-S-H with a foil-like morphology. However, mechanical properties were found not to be dependent on the morphology of C-S-H.
- The addition of Na₂SO₄ or NaOH decreases the Ca/Si ratio from 1.7 in alkali free systems to ~1.4-1.5. However, the differences in strength development are independent on the chemical composition of C-S-H.
- Alkali salts modify the morphology of portlandite from bigger to smaller crystals. This modification of the morphology is more pronounced and clear in alite-based systems than in cement-based or blended systems.

4. ¹H NMR insights on the impact of alkali on C-S-H density

- ¹H NMR results show that the gel water to sheet water ratio of C-S-H is lower in the presence of Na₂SO₄ or NaOH compared to the alkali free system. The amount of sheet water is not affected but the gel water decreases in the presence of Na₂SO₄ or NaOH.
- The solid density of the C-S-H nanocrystalline regions is lower in the presence of Na₂SO₄ or NaOH. This is proposed to be related to an increase of the interlayer space. The uptake of

sodium ions in C-S-H in the presence of alkalis suggests a partial replacement of calcium ions by sodium ions in the interlayer. This would weaken the electrostatic forces (interactions with monovalent Na^+ are weaker compared to divalent Ca^{2+}) and consequently increase the interlayer space.

- However, the gel density remains unchanged due to the lower amount of gel water. The reason for this is still unknown.

5. The impact of sodium gluconate

- The addition of sodium gluconate in slag systems with Na_2SO_4 increases the strength development compared to the systems with only Na_2SO_4 .
- ^1H NMR shows that sodium gluconate increases the amount of water in C-S-H and image analysis confirms the formation of a less dense C-S-H, which can better fill the space. Consequently, the capillary porosity decreases and the strength development increases.

Perspectives

The present study has brought new insights about on the impact of alkali salts on the kinetics and microstructural development of different cementitious systems but also opened some questions for further investigations.

GEMS was used as a mass balance calculation for cement-slag systems, instead of a proper thermodynamic calculation. This was done because in some systems the hydrates precipitated with GEMS were not agreeing with the hydrates identified with XRD-Rietveld. To ensure that GEMS results better approach the reality, it would be interesting to study a C-S-H phase that incorporates sodium and include its thermodynamic properties in the model to improve the calculation of the phase assemblage in alkali conditions. The use of ^{27}Al NMR and ^{23}Na NMR could contribute to better characterize this phase. Indeed, the lower Ca/Si ratio observed in the presence of alkali salts could be considered for GEMS calculations and improve the calculated amounts of portlandite.

The proper analysis of alite pastes with ^1H NMR was impossible due to the absence of Fe^{3+} (paramagnetic ions) in alite [15]. In cement, the primary ^1H relaxation mechanism is interaction with surface Fe^{3+} paramagnetic impurities. The synthesis of alite with a small amount of iron may shorten the relaxation times and the evolution of the different populations of water could probably be measurable from the first weeks. This could allow a comparison between the impact of alkalis on the density of C-S-H in alite and that obtained in Chapter 5 for white cement and probably a better understanding of the mechanisms behind. Indeed, alite could be used to understand why sodium gluconate enhances the gel and interlayer water content.

It has been observed that a slowdown in hydration kinetics could not be explained by changes in water activity. A lower DoH of cement could be related to a higher concentration of aluminate ions in solution, since Na_2SO_4 and NaOH increase the concentration of aluminate ions in solution, but seems unlikely to explain the whole of the effect. Other studies reported that the inhibition effect of aluminate

vanishes at high alkali conditions ($\text{pH} \geq 13$) [99,100]. An extensive study of the impact of aluminate ions in solution on the dissolution of silicate species as a function of the pH (~ 11.5 to 13), considering a wide range of aluminate ions concentrations, would be very useful to clarify its impact on the degree of hydration. An important drawback in this study is that the concentration of aluminate ions in the pore solution could not be quantified by ICP-OES in the non-blended systems because the concentrations were too low. The use of other techniques like ionic chromatography with an ion-exchange column for aluminate ions could probably detect lower concentrations.

Therefore, the question remains open as to what other factors might be responsible. Other changes in the pore solution, for example early concentration of Ca and Si, could be responsible. Figure 7.3 shows the evolution of calcium and silicon concentrations in the pore solution of cement-slag systems from very early to later ages. They suggest that alkalis affect the pore solution from early ages, especially with the addition of NaOH since calcium amounts drop from the very first hours and silicon increases. Na_2SO_4 shows a slightly different behaviour because during the first 24 hours the trends are the same as in the alkali free system while from then become similar to the system with NaOH. This could probably be related to a different distribution of inner and outer C-S-H (it has been observed here that NaOH inhibits the precipitation of outer product).

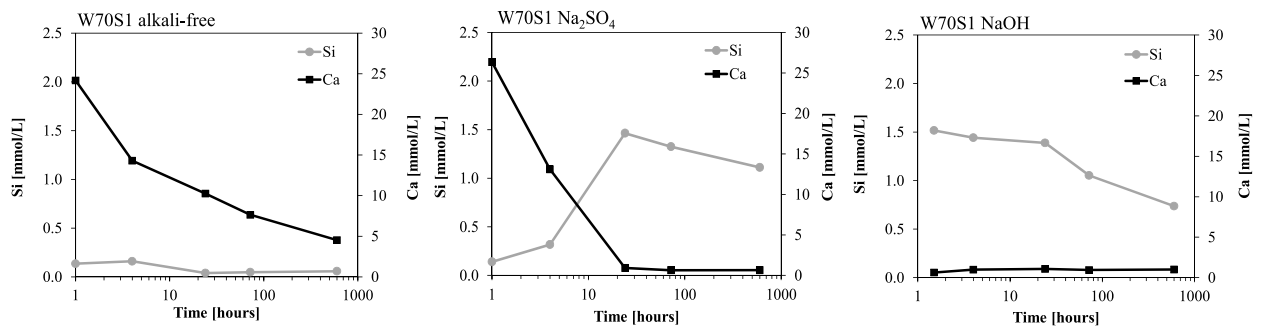


Figure 7.3. Experimental measurements of calcium and silicon concentrations in the pore solution extracted over time for white cement systems with slag 1.

As mentioned in this work, the convergence/divergence of C-S-H needles observed during the nucleation and growth period could find its explanation in the early nucleation of C-S-H (unstable nucleation sites). A potential effect of sulfate on the orientation of the nucleation sites attaching to the surface of alite could probably lead to a differently oriented growth of C-S-H needles. However, the mechanism behind this effect remains speculative. Some of the key questions to answer are: i) what could explain a different orientation of the nucleation sites between the systems without and with sulfate?, ii) does the presence of sulfate change the amounts of Ca and Si of the unstable nucleation sites?, and iii) could sulfate “poison” some growing sites of these nucleation sites and limit the growth direction?

Further work on atomistic simulations could be useful to determine at which moment this mechanism takes place (pre-nucleation, nucleation or very early growth) as well as to identify the parameter promoting a misorientation of the nucleation sites (either unstable or already stabilized): lower silicate concentration, sulfate poisoning, etc.

This study is focused on the effect of sodium salts but potassium salts should be considered for a similar study. This would contribute to clarify the disagreements found in literature regarding the different/similar impact of sodium and potassium.

Appendix A. Comparison between alite and cement

There is a general agreement on considering alite as a simplified system of cement, as alite is the main phase of cement (up to ~75 wt.%). However, the final properties of both pastes differ, i.e. a straightforward comparison is most of the time not appropriate for the following reasons.

Figure A.1a compares the cumulative heat release between alite and cement (alkali free) up to 7 days (both hand mixed for 2 minutes at w/s 0.4 and cured in sealed conditions). The DoH of alite is lower than in typical cement systems. Alite reaches ~10% DoH at the peak while in the case of cement it would be around 30%. This is mainly due to the coarser particle size distribution of alite resulting from the synthesis and grinding in the laboratory. The main difference is the amount of very fine material, which is not well estimated by the $d(50)$. Considering the $d(10)$ as a representation of the finer particles it is estimated to be lower for a standard white cement compared to alite ($d(10)_{\text{white cement}} = 1.0\mu\text{m}$ and $d(10)_{\text{alite}} = 1.7\mu\text{m}$). Therefore, the porosity in alite systems is much coarser (Figure A.1b) and so the strength development is lower.

BSE images in Figure A.2 and Figure A.3 compare the matrix of an alite paste and white cement at 24 hours. Not only the matrix of alite (Figure A.2a) is less hydrated than the matrix of cement (Figure A.2b) but also the distribution of hydrates is different. The morphology of portlandite masses is significantly different between the systems. In cement they are much more elongated, smaller and homogeneously distributed (it is difficult to find large areas without portlandite, contrary to the alite system).

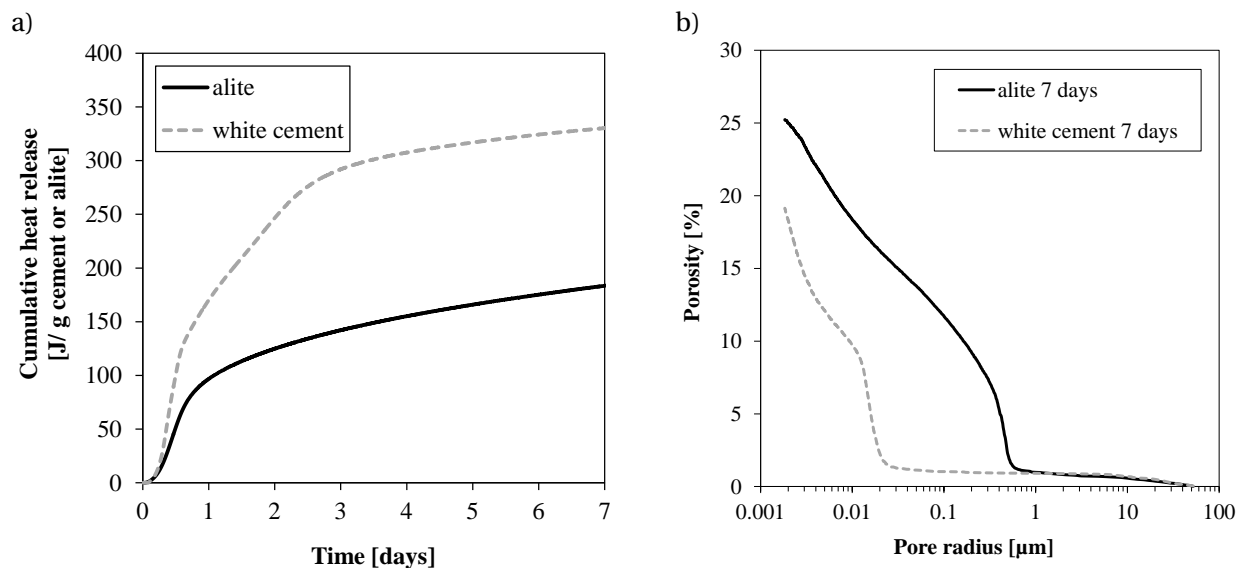


Figure A.1. a) Cumulative heat release and b) total porosity (7 days) for alite and white cement pastes.

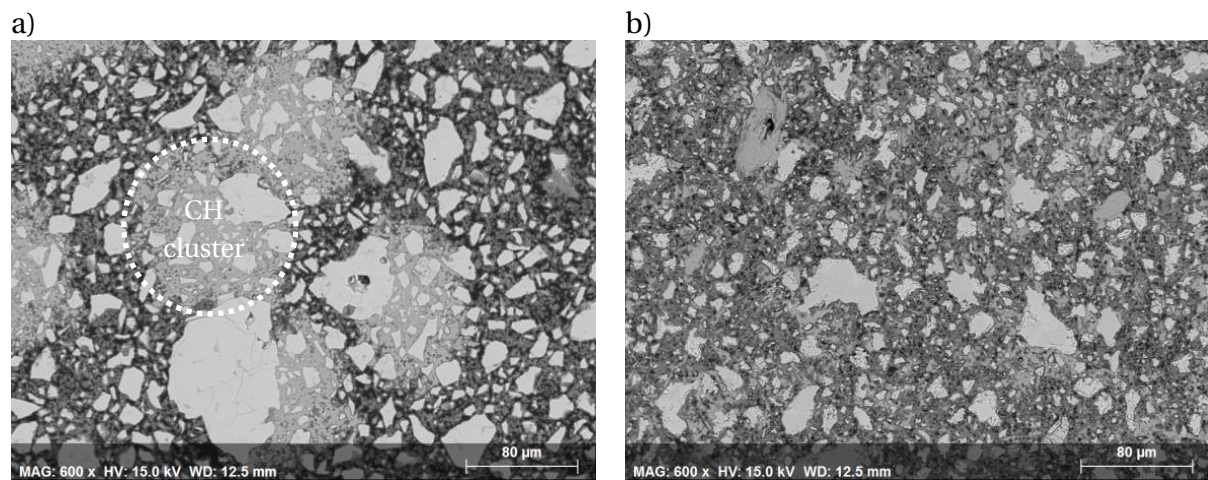


Figure A.2. Polished sections at 24 hours of a) alite and b) cement pastes (lower magnification).

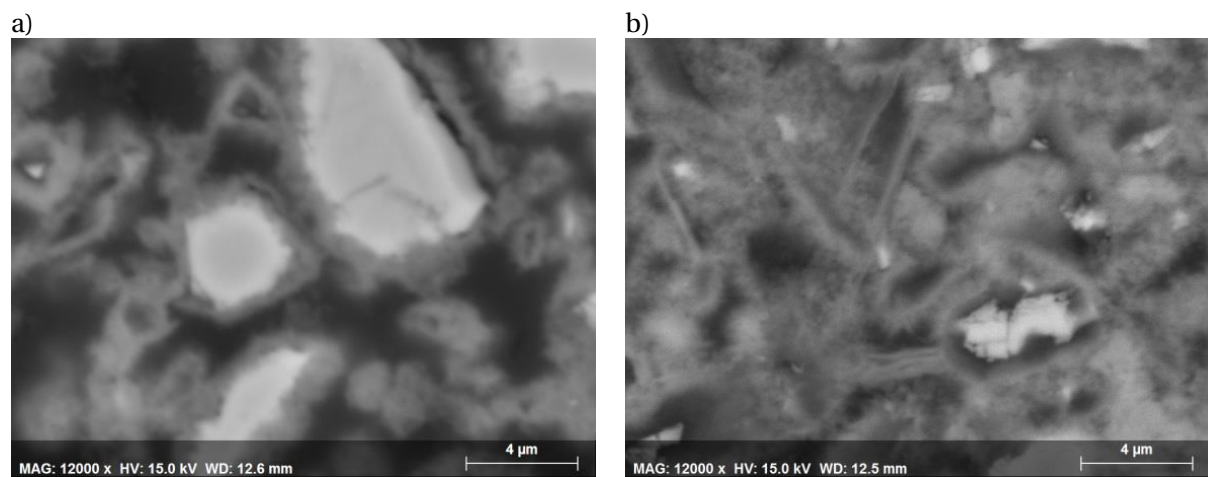


Figure A.3. Polished sections at 24 hours of a) alite and b) cement pastes (higher magnification).

Appendix B. C-S-H characteristics in white cement-slag systems

The morphology and chemical composition of C-S-H in white cement systems blended with slag 1 was also studied to see if the results for blends are comparable to the results for non-blended systems.

The morphology of C-S-H at early ages

Figure B.1 shows the times when the hydration was stopped to analyse the surface of the cement/slag grains. They all correspond to the end of nucleation and growth period as the C-S-H has grown enough to clearly detect if there are any differences in the morphology.

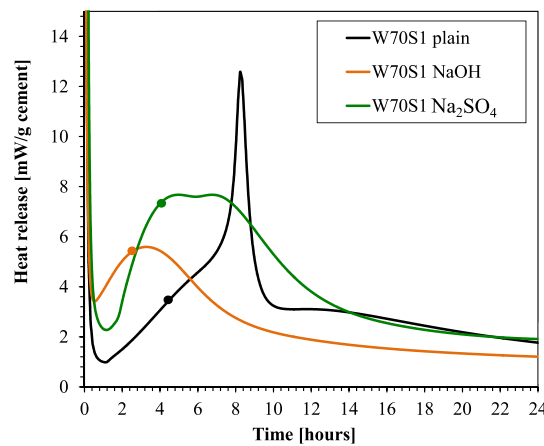


Figure B.1. Times (full points) when hydration was stopped to analyse the surface of cement/slag grains.

Figure B.2 shows the hydrates precipitated in the surface of the grains (mainly C-S-H) at the end of the acceleration period. It was impossible to distinguish the surface of a cement grain from a slag grain. Usually, with BSE mode one can distinguish two materials if their density is different enough. In this case, it was not feasible as the density of slag (2.95g/cm^3 for S1 and 2.91g/cm^3 for S8) is too similar to the density of cement (3.11g/cm^3).

For blended systems the changes in the morphology of C-S-H in the presence NaOH or Na₂SO₄ are reported to be the same as for the non-blended systems:

- Alkali free system (Figure B.2a and Figure B.2b): fibrillar C-S-H with a divergent morphology, growing as individual needles or groups of a few needles.
- System with Na₂SO₄ (Figure B.2c and Figure B.2d): fibrillar and divergent C-S-H, similar to the alkali-free C-S-H. It is easy to identify some fine ettringite crystals intermixed with C-S-H
- System with NaOH (Figure B.2e and Figure B.2f): more planar/foil-like C-S-H, it does not grow outwards from the surface.

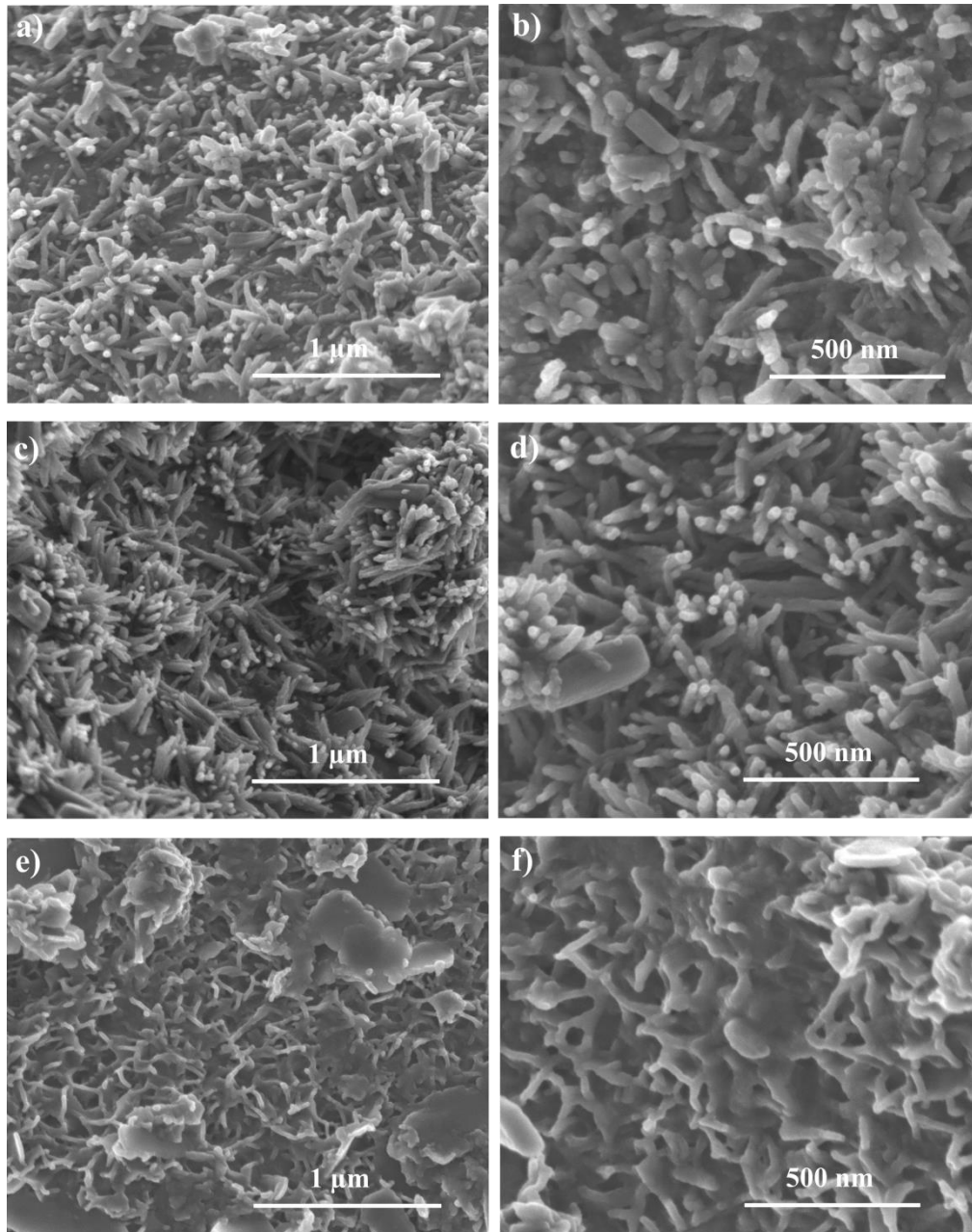


Figure B.2. Hydrates in the surface of the cement/slag grains of slag systems (at the end of the nucleation and growth period). Lower magnification (left side images) and higher magnification (right side images). They correspond to (a and b) alkali free, (c and d) with Na_2SO_4 and (e and f) with NaOH system.

The chemical composition of C-S-H

Figure B.3 and Table B.1 show that the addition of NaOH or Na_2SO_4 in blended systems has the same impact on the chemical composition of C-S-H as in non-blended systems: a decrease of the (Ca-S)/Si ratio.

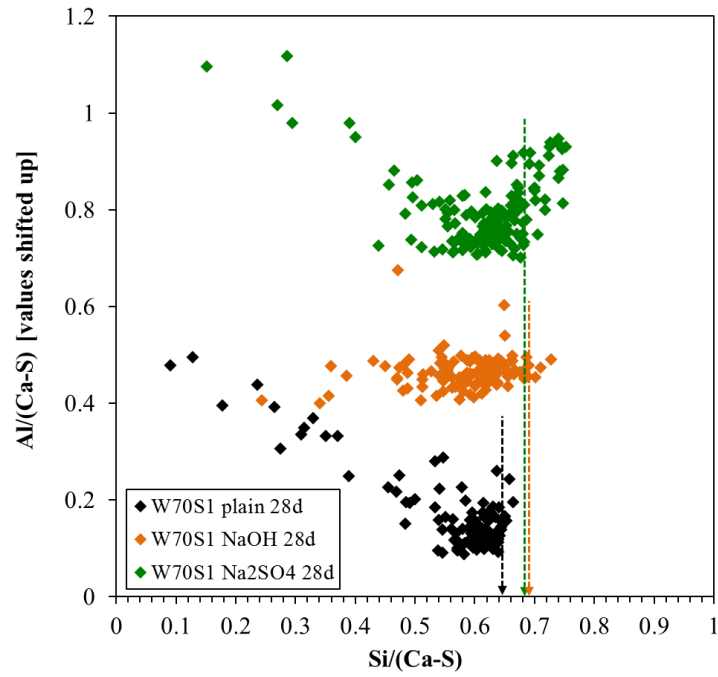


Figure B.3. $Al/(Ca-S)$ ratio against $Si/(Ca-S)$ ratio for slag systems at 28 days.

Table B.1. $(Ca-S)/Si$ ratio for white cement-slag systems at 28 days, calculated from EDX analysis.

System	$(Ca-S)/Si$ at 28 days
W70S1 plain	1.56
W70S1 NaOH	1.44
W70S1 Na_2SO_4	1.47

Appendix C. Calculations for the analysis of ^1H NMR data

The following calculations for the treatment of ^1H NMR data are extracted from the recent work of Muller [15]. The reader is suggested to visit his work for more details.

The interpretation of ^1H NMR relaxation data in cements is based on the observation that the NMR signal can be resolved into 5 discrete populations of water. The first is a fast relaxing component with a ^1H nuclear spin-spin relaxation time T_2 of the order of 10 μs . It is assigned to ^1H chemically combined in the solid crystalline phases calcium hydroxide and ettringite. Two further components have relaxation times of the order 80-120 μs and 300-500 μs . These are attributed to water in C-S-H inter-layers and to gel pore water respectively. The fourth and fifth components are assigned to water in nano-scale inter-hydrate spaces and to water in larger capillary pores and micro-cracks.

Some earlier studies have lacked quantification of signal amplitudes and hence water mass in different environments due to the difficulty of measuring the intensity fraction of chemically combined ^1H . This last difficulty was overcome by use of a quadrature echo pulse sequence method.

With this assignment, mass and volume balance equations can be written for paste:

$$1 + \frac{w}{c} = (1 - \alpha) + \frac{w}{c} [\beta I_{\text{solid}} + \gamma I_{\text{CSH}} + \delta (I_{\text{gel}} + I_{\text{cap}})] \quad [\text{Eq. C.1}]$$

$$\frac{1}{\rho_{uc}} + \frac{w}{c\rho_w} = \frac{(1-\alpha)}{\rho_{uc}} + \frac{w}{c} \left[\frac{\beta I_{\text{solid}}}{\rho_{\text{solid}}} + \frac{\gamma I_{\text{CSH}}}{\rho_{\text{CSH}}} + \frac{\delta (I_{\text{gel}} + I_{\text{cap}} + I_{\text{void}})}{\rho_w} \right] \quad [\text{Eq. C.2}]$$

Here, I are water signal fractions measured in the as prepared material normalised to the total signal intensity before account is taken of chemical shrinkage. The densities are ρ . The subscripts uc , w , solid , CSH , gel , cap and void refer to unreacted cement, water, chemically combined water, C-S-H, gel pore water, capillary pore water and chemical shrinkage respectively. For sealed cured samples, as here, it is the calculated increase in signal arising if the chemical shrinkage volume is filled with water. The parameters α , β , γ and δ are the degree of hydration and the reciprocal water mass fractions of the solid, C-S-H and pore fluid respectively with $\delta = 1$. The solid signal is assumed to comprise two parts, portlandite and ettringite, so that $\beta I_{\text{solid}} = \beta_{\text{CH}} I_{\text{CH}} + \beta_{\text{ett}} I_{\text{ett}}$ and $\beta I_{\text{solid}}/\rho_{\text{solid}} = \beta_{\text{CH}} I_{\text{CH}}/\rho_{\text{CH}} + \beta_{\text{ett}} I_{\text{ett}}/\rho_{\text{ett}}$ with the values of $\beta_{\text{CH}} = 74/18$ and $\beta_{\text{ett}} = 1255/576$ from the known molecular composition of portlandite and ettringite respectively. We take $\rho_{uc,CH,ett,w} = 3.15, 2.24, 1.77$ and 1 g/cm^3 .

The unknowns are α , I_{ett} , ρ_{CSH} and γ . A measurement of α , the degree of hydration and I_{ett} , the mass fraction of water bound in ettringite can be made independently, using, for instance, XRD, so enabling the C-S-H density and water fraction to be found. Assuming $\text{Ca}_z(\text{Si}_y\text{Al}_{(1-y)})\text{O}_{(z+1/2y+3/2)} \cdot (\text{H}_2\text{O})_x$, the reciprocal water fraction of C-S-H, γ , is related to x as

$$x = \frac{56z+9y+51}{18(\gamma-1)} \quad [\text{Eq. C.3}]$$

where $y = n_{\text{Si}}^{\text{CSH}} / (n_{\text{Si}}^{\text{CSH}} + n_{\text{Al}}^{\text{CSH}})$ and $n_{\text{Si,Al}}^{\text{CSH}}$ are the molar content of Si and Al in the C-S-H. The numerical constants derive from the atomic masses of C, S, A and H.

A further conservation equation can be written for the overall Ca/(Si+Al) ratio. If α' is defined as the mass of reacted ($C_3S + C_2S$) divided by the mass of the anhydrous powder, and ignoring minor reactive components other than C_3A , then

$$\frac{3\left(\frac{0.9\alpha'}{C_3S^{AMU}}\right) + 2\left(\frac{0.1\alpha'}{C_2S^{AMU}}\right) + 1.5n_{Al}^{CSH}}{\left(\frac{0.9\alpha'}{C_3S^{AMU}}\right) + \left(\frac{0.1\alpha'}{C_2S^{AMU}}\right) + n_{Al}^{CSH}} = \frac{\frac{I_{CH}n_{Hyd}}{2} + \frac{I_{CSH}n_{Hyd}^z}{2x} + 1.5n_{Al}^{CSH}}{\frac{I_{CSH}n_{Hyd}^y}{2x} + n_{Al}^{CSH}} \quad [Eq. C.4]$$

Here, n_{Hyd} is the molar content of hydrogen in the paste. The further assumptions leading to equation (4) as now stated are as follows. First, it is known that in the hydration reaction, C_3S is consumed much more quickly than C_2S . Hence, we assume a consumption ratio of 9:1 in favour of C_3S until it is been used up. Second, X-ray analysis of samples at different ages, to be described in the next section, shows that ettringite all forms early, at most within the first 3 days. Since the analysis mainly focuses on data acquired after three days, we make the simplifying assumption that the ettringite forms at the start of the process. Third, we assume that the aluminium from the C_3A remaining after ettringite formation is included in the C-S-H from the start. The factors determining the extent of alumina uptake into the C-S-H are not well understood. This hypothesis implies there is a negligible amount of alumina in the pore solution, which is in accord with thermodynamics and experimental results. It follows that $n_{Al}^{CSH} = 2(f_{C_3A} - f_{C_3A}^{Ett})/C_3A^{AMU}$ where f_{C_3A} and $f_{C_3A}^{ett}$ are the mass fractions of C_3A in the anhydrous powder and the C_3A mass fraction used to form ettringite respectively.

Given the above assumptions concerning the formation of ettringite, the Si to (Si+Al) ratio, y , can be expressed as

$$y = \frac{n_{Si}^{CSH}}{n_{Si}^{CSH} + n_{Al}^{CSH}} = 1 - \frac{4x(f_{C_3A} - f_{C_3A}^{Ett})}{I_{CSH}n_{Hyd}C_3A^{AMU}} \quad [Eq. C.5]$$

The alternate C-S-H composition including gel water, $Ca_z.(Si_yAl_{(1-y)})O_{(z+1/2y+3/2)}.(H_2O)_x$ has

$$x' = x(I_{CSH} + I_{gel})/I_{CSH} \quad [Eq. C.6]$$

Bibliography

- [1] J.M. Crow, The concrete conundrum, Chem. World Mag. (2008) 62–66.
- [2] Cement Technology Roadmap 2009: Carbon emissions reductions up to 2050, 2009.
- [3] T. Soubotina, Beyond Economic Growth: An Introduction to Sustainable Development. Chapter 3 - World Population Growth, The World Bank, 2004.
- [4] World Urbanization Prospects: The 2014 Revision, 2015.
- [5] B. Lothenbach, K. Scrivener, R.D. Hooton, Supplementary cementitious materials, Cem. Concr. Res. 41 (2011) 1244–1256.
- [6] I. Jawed, J. Skalny, Alkalies in cement: A review. II. Effects of alkalies on hydration and performance of portland cement, Cem. Concr. Res. 8 (1978) 37–52.
- [7] B. Osbaeck, On the influence of alkalis on strength development of blended cements, The chemistry and Chemically related properties of cement, Br. Ceram. Proc. 35 (1984) 375–383.
- [8] A. Kumar, G. Sant, C. Patapy, C. Gianocca, K.L. Scrivener, The influence of sodium and potassium hydroxide on alite hydration: Experiments and simulations, Cem. Concr. Res. 42 (2012) 1513–1523.
- [9] S.J. Way, A. Shayan, Early hydration of a Portland cement in water and sodium hydroxide solutions: composition of solutions and nature of solid phases, Cem. Concr. Res. 19 (1989) 759–769.
- [10] F. Škvára, Alkali activated materials or geopolymers?, 51 (2007) 173–177.
- [11] S. Garrault-Gauffinet, a Nonat, Experimental investigation of calcium silicate hydrate (C-S-H) nucleation, J. Cryst. Growth. 200 (1999) 565–574.
- [12] A.C.A. Muller, K.L. Scrivener, A.M. Gajewicz, P.J. McDonald, Densification of C–S–H Measured by ^1H NMR Relaxometry, J. Phys. Chem. C. 117 (2013) 403–412.
- [13] I.G. Richardson, The calcium silicate hydrates, Cem. Concr. Res. 38 (2008) 137–158.
- [14] H.M. Jennings, Refinements to colloid model of C-S-H in cement: CM-II, Cem. Concr. Res. 38 (2008) 275–289.
- [15] A. Muller, Characterization of porosity and C-S-H in cement pastes by ^1H NMR, (PhD Thesis) Ecole Polytechnique Fédérale de Lausanne, 2014.
- [16] Taylor, H.F.W., Cement Chemistry, 2nd ed., Thomas Telford, 1997.
- [17] A. Bazzoni, Study of early hydration mechanisms of cement by means of electron microscopy (EPFL thesis), 2014.

- [18] S. Galmarini, Atomistic Simulation of Cementitious Systems, in Faculté des sciences et techniques de l'ingénieur, (PhD Thesis) Ecole Polytechnique Fédérale de Lausanne, 2013.
- [19] P. Yu, R.J. Kirkpatrick, B. Poe, P.F. McMillan, X. Cong, Structure of Calcium Silicate Hydrate (C-S-H): Near-, Mid-, and Far-Infrared Spectroscopy, *J. Am. Ceram. Soc.* 82 (1999) 742–748.
- [20] I. Pochard, C. Labbez, a. Nonat, H. Vija, B. Jönsson, The effect of polycations on early cement paste, *Cem. Concr. Res.* 40 (2010) 1488–1494.
- [21] C. Labbez, I. Pochard, B. Jönsson, A. Nonat, C-S-H/solution interface: Experimental and Monte Carlo studies, *Cem. Concr. Res.* 41 (2011) 161–168.
- [22] B. Lothenbach, A. Nonat, Calcium silicate hydrates: Solid and liquid phase composition, *Cem. Concr. Res.* (2015).
- [23] C. Labbez, A. Nonat, I. Pochard, B. Jönsson, Experimental and theoretical evidence of overcharging of calcium silicate hydrate., *J. Colloid Interface Sci.* 309 (2007) 303–7.
- [24] K. Garbev, M. Bornefeld, G. Beuchle, P. Stemmermann, Cell dimensions and composition of nanocrystalline calcium silicate hydrate solid solutions. Part 1: Synchrotron-based X-Ray Diffraction, *J. Am. Ceram. Soc.* 91 (2008) 3015–3023.
- [25] I.G. Richardson, Tobermorite/jennite- and tobermorite/calcium hydroxide-based models for the structure of C-S-H: applicability to hardened pastes of tricalcium silicate, β -dicalcium silicate, Portland cement, and blends of Portland cement with blast-furnace slag, metakaol, *Cem. Concr. Res.* 34 (2004) 1733–1777.
- [26] B. Mota, T. Matschei, K. Scrivener, The influence of sodium salts and gypsum on alite hydration, *Cem. Concr. Res.* 75 (2015) 53–65.
- [27] E. Berodier, Impact of the supplementary cementitious materials on the kinetics and microstructural development of cement hydration (EPFL Thesis), 2015.
- [28] K. Scrivener, A. Bazzoni, B. Mota, J. Rossen, “Electron microscopy” in A practical guide to the microstructural characterisation of cementitious materials (book submitted for publishing), 2015.
- [29] J. Rossen, Composition and morphology of C-A-S-H in pastes of alite and cement blended with supplementary cementitious materials, Ecole Polytechnique Fédérale de Lausanne, 2014.
- [30] B. Jönsson, a Nonat, C. Labbez, B. Cabane, H. Wennerström, Controlling the cohesion of cement paste., *Langmuir.* 21 (2005) 9211–21.
- [31] I. Odler, M. Rößler, Investigations on the relationship between porosity, structure and strength of hydrated Portland cement pastes. II. Effect of pore structure and of degree of hydration, *Cem. Concr. Res.* 15 (1985) 401–410.
- [32] N. Smaoui, M.A. Bérubé, B. Fournier, B. Bissonnette, B. Durand, Effects of alkali addition on the mechanical properties and durability of concrete, *Cem. Concr. Res.* 35 (2005) 203–212.
- [33] T.C. Powers, Structure and Physical Properties of Hardened Portland Cement Paste, *J. Am. Ceram. Soc.* 41 (1958) 1–6.

-
- [34] B. Pichler, C. Hellmich, J. Eberhardsteiner, J. Wasserbauer, P. Termkhajornkit, R. Barbarulo, et al., Effect of gel–space ratio and microstructure on strength of hydrating cementitious materials: An engineering micromechanics approach, *Cem. Concr. Res.* 45 (2013) 55–68.
- [35] P. Termkhajornkit, Q.H. Vu, R. Barbarulo, S. Daronnat, G. Chanvillard, Dependence of compressive strength on phase assemblage in cement pastes: Beyond gel–space ratio — Experimental evidence and micromechanical modeling, *Cem. Concr. Res.* 56 (2014) 1–11.
- [36] P. Termkhajornkit, R. Barbarulo, G. Chanvillard, Microstructurally-designed cement pastes: A mimic strategy to determine the relationships between microstructure and properties at any hydration degree, *Cem. Concr. Res.* 71 (2015) 66–77.
- [37] H. Mori, K. Minegishi, T. Ohta, T. Akiba, The effect of alkali on the microstructure of hardened $3\text{CaO}.\text{SiO}_2$ paste, *Proc. 25th Gen. Meet. Cem. Assoc. Japan*, 1971, 33–37.
- [38] W. Lerch, The Influence of Gypsum on the Hydration and Properties of Portland Cement Pastes, *Res. Bull. 12, Portl. Cem. Assoc.* (1946) 1–48.
- [39] H. Mori, K. Minegishi, T. Ohta, Early hydration of $3\text{CaO}.\text{SiO}_2$ in the presence of alkali, *Proc. 23rd Gen. Meet. Cem. Assoc. Japan*, 1969, 58–60.
- [40] M.C. Garci Juenger, H.M. Jennings, Examining the relationship between the microstructure of calcium silicate hydrate and drying shrinkage of cement pastes, *Cem. Concr. Res.* 32 (2002) 289–296.
- [41] D.P. Bentz, Influence of alkalis on porosity percolation in hydrating cement pastes, *Cem. Concr. Compos.* 28 (2006) 427–431.
- [42] A. Kumar, Modelling hydration kinetics of cementitious systems, (PhD Thesis) Ecole Polytechnique Fédérale de Lausanne, 2012.
- [43] I. Odler, R. Wonnemann, Effect of alkalies on portland cement hydration I. Alkali oxides incorporated into the crystalline lattice of clinker minerals, *Cem. Concr. Res.* 13 (1983) 477–482.
- [44] Holcim Technology Ltd., Internal communication, (n.d.).
- [45] A. Kumar, G. Sant, C. Patapy, C. Gianocca, K. Scrivener, Influence of alkali metal ions on hydration of cementitious systems, *Intern. Commun.* (2011).
- [46] A. Shayan, I. Ivanusec, Influence of NaOH on mechanical properties of cement paste and mortar with and without reactive aggregate, *8th Int. Conf. Alkali-Aggregate React.* (1989) 715–720.
- [47] R.L. Berger, J.D. McGregor, Influence of admixtures on the morphology of calcium hydroxide formed during tricalcium silicate hydration, *Cem. Concr. Res.* 2 (1972) 43–55.
- [48] E. Gallucci, K. Scrivener, Crystallisation of calcium hydroxide in early age model and ordinary cementitious systems, *Cem. Concr. Res.* 37 (2007) 492–501.
- [49] S. Galmarini, A. Aimable, N. Ruffray, P. Bowen, Changes in portlandite morphology with solvent composition: Atomistic simulations and experiment, *Cem. Concr. Res.* 41 (2011) 1330–1338.
- [50] S. Galmarini, A. Aimable, N. Ruffray, P. Bowen, Erratum to “Changes in portlandite morphology with solvent composition: Atomistic simulations and experiment” [*Cement Concrete Res.* 41 (2011) 1330–1338], *Cem. Concr. Res.* 61–62 (2014) 71.

- [51] A. Gray, Crystal morphology and surface reactivity studies of calcium hydroxide, (PhD Thesis) Brunel University, 1990.
- [52] D.E. Macphee, K. Luke, F.P. Glasser, E.E. Lachowski, Solubility and Aging of Calcium Silicate Hydrates in Alkaline Solutions at 25°C, *J. Am. Ceram. Soc.* 72 (1989) 646–654.
- [53] S. Hong, F.P. Glasser, Alkali binding in cement pastes. Part I: The C-S-H phase, 29 (2000) 1893–1903.
- [54] D.A. Kulik, Improving the structural consistency of C-S-H solid solution thermodynamic models, *Cem. Concr. Res.* 41 (2011) 477–495.
- [55] E. L'Hôpital, Aluminium and alkali uptake in Calcium Silicate Hydrates (EPFL thesis), 2014.
- [56] H. Stade, On the reaction of C-S-H(di, poly) with alkali hydroxides, *Cem. Concr. Res.* 19 (1989) 802–810.
- [57] T.T.H. Bach, E. Chabas, I. Pochard, C. Cau Dit Coumes, J. Haas, F. Frizon, et al., Retention of alkali ions by hydrated low-pH cements: Mechanism and Na⁺/K⁺ selectivity, *Cem. Concr. Res.* 51 (2013) 14–21.
- [58] G. Renaudin, J. Russias, F. Leroux, C. Cau-dit-Coumes, F. Frizon, Structural characterization of C-S-H and C-A-S-H samples—Part II: Local environment investigated by spectroscopic analyses, *J. Solid State Chem.* 182 (2009) 3320–3329.
- [59] I. Lognot, I. Klur, A. Nonat, NMR and Infrared spectroscopies of C-S-H and Al-substituted C-S-H synthesised in alkaline solutions, et al. P. Colombet (Ed.), *Nucl. Magn. Reson. Spectrosc. Cem. Based Mater.*, Springer Berlin Heidelberg, 1998, 189–196.
- [60] I. García-Lodeiro, A. Fernández-Jiménez, A. Palomo, *Eco-Efficient Concrete*, Elsevier, 2013.
- [61] H. Viallis, P. Faucon, J.-C. Petit, A. Nonat, Interaction between Salts (NaCl, CsCl) and Calcium Silicate Hydrates (C-S-H), *J. Phys. Chem. B.* 103 (1999) 5212–5219.
- [62] E. Gartner, J. Young, D. Damidot, I. Jawed, *Hydration of Portland cement*, Struct. Perform. Cem., Taylor and Francis group, 2002, .
- [63] I.G. Richardson, The nature of C-S-H in hardened cements, *Cem. Concr. Res.* 29 (1999) 1131–1147.
- [64] C. Labbez, I. Pochard, B. Jönsson, A. Nonat, C-S-H/solution interface: Experimental and Monte Carlo studies, *Cem. Concr. Res.* 41 (2011) 161–168.
- [65] M. Medala, I. Pochard, C. Labbez, A. Nonat, Investigations of the interacting forces between Calcium Silicate Hydrate (C-S-H) particles : influence of sulphate sorption on C-S-H., *Cem. Concr. Sci. Conf. Leeds.* (2009).
- [66] R. Barbarulo, Comportement des matériaux cimentaires: actions des sulfates et de la température, (PhD Thesis) Université Laval, 2002.
- [67] A. Quennoz, K.L. Scrivener, Interactions between alite and C3A-gypsum hydrations in model cements, *Cem. Concr. Res.* 44 (2013) 46–54.

-
- [68] C. Hesse, F. Goetz-Neunhoeffler, J. Neubauer, A new approach in quantitative in-situ XRD of cement pastes: Correlation of heat flow curves with early hydration reactions, *Cem. Concr. Res.* 41 (2011) 123–128.
- [69] N.B. Singh, Effect of gluconates on the hydration of cement, *Cem. Concr. Res.* 6 (1976) 455–460.
- [70] Available at <http://www.pmpinc.com/documents/concrete-app-color.pdf> (PMP Fermentation Products, Inc.) (last access 30.06.2015).
- [71] V. Dodson, *Concrete Admixtures*, Chapter 5, Van Nostrand Reinhold, 1990.
- [72] J. Cheung, A. Jeknavorian, L. Roberts, D. Silva, Impact of admixtures on the hydration kinetics of Portland cement, *Cem. Concr. Res.* 41 (2011) 1289–1309.
- [73] M. Collepardi, S. Monosi, G. Moriconi, M. Pauri, Influence of Gluconate, Lignosulfonate, and Glucose Admixtures on the Hydration of Tetracalcium Aluminoferrite in the Presence of Gypsum with or without Calcium Hydroxide, *Commun. Am. Ceram. Soc.* 68 (1985) 126–128.
- [74] M. Collepardi, S. Monosi, G. Moriconi, M. Pauri, Influence of gluconate, lignosulfonate or glucose on the C3A hydration in the presence of gypsum with or without lime, *Cem. Concr. Res.* 14 (1984) 105–112.
- [75] R. Myrdal, Retarding admixtures for concrete (SINTEF report), (2007).
- [76] Y. Yamamoto, Retarders for concrete, and their effects on setting time and shrinkage. Joint Highway Research Project, (1972).
- [77] H. Chen, Autogenous and Thermal Deformations and their Interaction in Early Age Cementitious Materials, (PhD Thesis) Ecole Polytechnique Fédérale de Lausanne, 2013.
- [78] J.E. Rossen, Composition and morphology of C-A-S-H in pastes of alite and cement blended with supplementary cementitious materials (EPFL thesis), 2014.
- [79] J.E. Rossen, B. Lothenbach, K.L. Scrivener, Composition of C–S–H in pastes with increasing levels of silica fume addition, *Cem. Concr. Res.* 75 (2015) 14–22.
- [80] J.G. Powles, J.H. Strange, Zero Time Resolution Nuclear Magnetic Resonance Transient in Solids, *Proc. Phys. Soc.* 82 (2002) 6–15.
- [81] S. Meiboom, D. Gill, Modified spin-echo method for measuring nuclear relaxation times, *Rev. Sci. Instrum.* 29 (1958) 688–691.
- [82] A.C.A. Muller, K.L. Scrivener, A.M. Gajewicz, P.J. McDonald, Use of bench-top NMR to measure the density, composition and desorption isotherm of C–S–H in cement paste, *Microporous Mesoporous Mater.* 178 (2013) 99–103.
- [83] L. Venkataramanan, Y.Q. Song, M.D. Hürlimann, Solving Fredholm integrals of the first kind with tensor product structure in 2 and 2.5 dimensions, *IEEE Trans. Signal Process.* 50 (2002) 1017–1026.
- [84] E. Berodier, K. Scrivener, Evolution of pore structure in blended systems, *Cem. Concr. Res.* 73 (2015) 25–35.
- [85] L. Baquerizo, Impact of water activity on the mineralogy of hydrated cement (EPFL thesis), 2015.

- [86] L.G. Baquerizo, T. Matschei, K.L. Scrivener, M. Saeidpour, A. Thorell, L. Wadsö, Methods to determine hydration states of minerals and cement hydrates, *Cem. Concr. Res.* 65 (2014) 85–95.
- [87] D.A. Kulik, T. Wagner, S. V. Dmytrieva, G. Kosakowski, F.F. Hingerl, K. V. Chudnenko, et al., GEM-Selektor geochemical modeling package: revised algorithm and GEMS3K numerical kernel for coupled simulation codes, *Comput. Geosci.* (2012) 1–24.
- [88] T. Wagner, D.A. Kulik, F.F. Hingerl, S. V. Dmytrieva, Gem-selektor geochemical modeling package: TSolMod library and data interface for multicomponent phase models, *Can. Mineral.* 50 (2012) 1173–1195.
- [89] Available at <http://gems.web.psi.ch/> (last access 16.09.2014).
- [90] W. Hummel, U. Berner, E. Curti, F.J. Pearson, T. Thoenen, Nagra/PSI Chemical Thermodynamic Database 01/01, Univers. Publ., 2002.
- [91] B. Lothenbach, T. Matschei, G. Möschner, F.P. Glasser, Thermodynamic modelling of the effect of temperature on the hydration and porosity of Portland cement, *Cem. Concr. Res.* 38 (2008) 1–18.
- [92] T. Matschei, B. Lothenbach, F.P. Glasser, Thermodynamic properties of Portland cement hydrates in the system $\text{CaO-Al}_2\text{O}_3\text{-SiO}_2\text{-CaSO}_4\text{-CaCO}_3\text{-H}_2\text{O}$, *Cem. Concr. Res.* 37 (2007) 1379–1410.
- [93] Available at <http://www.empa.ch/cemdata/> (last access 31.05.2015).
- [94] P. Juilland, E. Gallucci, R. Flatt, K. Scrivener, Dissolution theory applied to the induction period in alite hydration, *Cem. Concr. Res.* 40 (2010) 831–844.
- [95] A. Kumar, S. Bishnoi, K.L. Scrivener, Modelling early age hydration kinetics of alite, *Cem. Concr. Res.* 42 (2012) 903–918.
- [96] P.W. Brown, C.L. Harner, E.J. Prosen, The effect of inorganic salts on tricalcium silicate hydration, *Cem. Concr. Res.* 16 (1985) 17–22.
- [97] F. Begarin, S. Garraut, A. Nonat, L. Nicoleau, Hydration of alite containing aluminium, 29th Cem. Concr. Sci. Congr. Cem. Concr. Sci. Congr., 2010, 9–12.
- [98] T. Chappex, K.L. Scrivener, The influence of aluminium on the dissolution of amorphous silica and its relation to alkali silica reaction, *Cem. Concr. Res.* 42 (2012) 1645–1649.
- [99] P. Suraneni, R.J. Flatt, Use of micro-reactors to obtain new insights into the factors influencing tricalcium silicate dissolution, *Cem. Concr. Res.* 78 (2015) 208–215.
- [100] L. Nicoleau, E. Schreiner, A. Nonat, Ion-specific effects influencing the dissolution of tricalcium silicate, *Cem. Concr. Res.* 59 (2014) 118–138.
- [101] Available at http://wwwbrr.cr.usgs.gov/projects/GWC_coupled/phreeqc/ (last access 16.09.2014).
- [102] D. Jacques, Benchmarking of the cement model and detrimental chemical reactions including temperature dependent parameters, NIRONd-TR Rep. 2008–30 E, SCK-BEN. (2009).

-
- [103] L. Nicoleau, A. Nonat, D. Perrey, The di- and tricalcium silicate dissolutions, *Cem. Concr. Res.* 47 (2013) 14–30.
- [104] S. Diamond, Calcium hydroxide in cement paste and concrete-a microstructural appraisal in: Skalny, J. Gebauer, J. Odler (Eds.). *Material Science of Concrete, Special Volume: Calcium Hydroxide in Concrete*, Am. Ceram. Soc. (2001) 37–58.
- [105] C. Labbez, B. Jönsson, M. Skarba, M. Borkovec, Ion–Ion Correlation and Charge Reversal at Titrating Solid Interfaces, *Langmuir*. 25 (2009) 7209–7213.
- [106] J. Bizzozero, C. Gosselin, K.L. Scrivener, Expansion mechanisms in calcium aluminate and sulfoaluminate systems with calcium sulfate, *Cem. Concr. Res.* 56 (2014) 190–202.
- [107] R. Chamrova, Modelling and measurement of elastic properties of hydrating cement paste (EPFL thesis), 2010.
- [108] S.-Y. Hong, F. Glasser, Alkali sorption by C-S-H and C-A-S-H gels. Part II: Role of alumina, *Cem. Concr. Res.* 32 (2002) 1101–1111.
- [109] E. L'Hôpital, B. Lothenbach, G. Le Saout, D. Kulik, K. Scrivener, Incorporation of aluminium in calcium-silicate-hydrates, *Cem. Concr. Res.* 75 (2015) 91–103.
- [110] V. Kocaba, Development and evaluation of methods to follow microstructural development of cementitious systems including slags (EPFL thesis), (2009).
- [111] V. Kocaba, E. Gallucci, K.L. Scrivener, Methods for determination of degree of reaction of slag in blended cement pastes, *Cem. Concr. Res.* 42 (2012) 511–525.
- [112] J. Bizzozero, Hydration and dimensional stability of calcium aluminate cement based systems, (PhD Thesis) Ecole Polytechnique Fédérale de Lausanne, 2014.
- [113] F. Deschner, F. Winnefeld, B. Lothenbach, S. Seufert, P. Schwesig, S. Ditttrich, et al., Hydration of Portland cement with high replacement by siliceous fly ash, *Cem. Concr. Res.* 42 (2012) 1389–1400.
- [114] T. Matschei, B. Lothenbach, F.P. Glasser, The AFm phase in Portland cement, *Cem. Concr. Res.* 37 (2007) 118–130.
- [115] A.M. Cody, H. Lee, R.D. Cody, P.G. Spry, The effects of chemical environment on the nucleation, growth, and stability of ettringite $[\text{Ca}_3\text{Al}(\text{OH})_6]_2(\text{SO}_4)_3 \cdot 26\text{H}_2\text{O}$, *Cem. Concr. Res.* 34 (2004) 869–881.

Curriculum Vitae

Berta Mota Gassó

Date of birth: 4th April 1987

Nationality: Spanish

Professional experience

- | | | |
|-------------|--|------------------------------|
| 2011 - 2015 | Research Assistant
<i>Laboratory of Construction Materials (LMC), Ecole Polytechnique Fédérale de Lausanne (EPFL). Financial support from HOLCIM</i>
“Impact of alkali salts on the kinetics and microstructural development of cementitious systems”
Supervisor: Prof. Karen Scrivener / Co-supervisor: Thomas Matschei <ul style="list-style-type: none">- Supervised master students for the semester projects.- Assistant of “General chemistry” and practical works for civil engineering and material science students. | Lausanne, Switzerland |
| 2010 - 2011 | Laboratory Trainee
<i>Center for Research in NanoEngineering, Universitat Politècnica de Catalunya (UPC)</i>
“Retention mechanisms of oxyanions in cementitious materials”
Supervisor: Prof. Ignasi Casanova and Patricia Pardo | Barcelona, Spain |
| 2008 - 2009 | Laboratory Assistant
<i>External Geodynamics Department, Universitat de Girona (UdG)</i>
“Regional vulnerability of water sources to climate change”
Supervisor: Dr. Josep Mas-Pla | Girona, Spain |

Education

- | | |
|-------------|---|
| 2011 - 2015 | PhD Thesis in Material Sciences and Engineering
Laboratory of Construction Materials, Ecole Polytechnique Fédérale de Lausanne (EPFL) – Switzerland |
| 2009 - 2011 | Master in Environmental Engineering
Civil Engineering School, Universitat Politècnica de Catalunya (UPC) – Spain |
| 2005 - 2009 | Bachelor in Environmental Sciences
Faculty of Sciences, Universitat de Girona (UdG) – Spain |

Languages

- Spanish: Native
- Catalan: Native
- English: Fluent
- French: Fluent
- German: Beginner

Technical skills and competences

Experimental and characterization techniques

- Scanning electron microscopy (SEM)
- Energy dispersive analysis (EDS)
- ¹H NMR
- Isothermal calorimetry
- Polishing
- X-ray diffraction (XRD)
- Cement and mortar design/mixing
- Thermogravimetric analysis (TGA)
- Mechanical tests
- Chemical shrinkage
- Pore solution extraction
- Mercury intrusion porosimetry (MIP)

Computer skills

- GEMS (geochemical thermodynamic modelling software)
- PhreeqC
- X'Pert HighScore Plus

Publications

- Mota, B., Matschei, T., Scrivener, K. *The influence of sodium salts and gypsum on alite hydration*, Cement and Concrete Research, 2015, p. 53-65
- Scrivener, K., Bazzoni, A., Mota, B. and Rossen, J. *Chapter 8: Electron microscopy*, in *A practical guide to microstructural characterization of cementitious materials*, book submitted to the publisher
- Mota, B., Matschei, T., Scrivener, K. *The effect of alkali salts on the morphology of C-S-H*, Proceedings of the 15th Euroseminar of Microscopy applied to Building Materials, Delft 2015
- Mota, B., Matschei, T., Scrivener, K. *The impact of alkalis on cement hydration*, Proceedings of the 34nd Annual Conference on Cement and Concrete Science, Sheffield 2014
- Matschei, T., Scrivener, K., Mota, B. *The impact of alkalis on cement hydration*, Workshop on Cement hydration. Villars 2014
- Mota, B., Matschei, T., Scrivener, K. *The effect of sodium salts on alite hydration*, Proceedings of the 32nd Annual Conference on Cement and Concrete Science, Belfast 2012

Other interests

- TEDxLausanne 2015: Registration team (volunteer)
- TEDxLausanne 2014: Finance & Fundraising team (volunteer)
- European Youth Parliament Girona 2013: Chair member